Geologisch-Paläontologisches Institut und Museum
Christian-Albrechts-Universität
Kiel, Deutschland

Berichte — Reports

Nr. 68

Editors: Sarnthein, M. (Chief Scientist);
Pflaumann, U.; Wang, P. X.; Wong, H. K. (Senior Scientists):

PRELIMINARY REPORT ON SONNE-95 CRUISE "MONITOR MONSOON" TO THE SOUTH CHINA SEA

Vorläufiger Bericht über SONNE-Fahrt 95 „Monitor Monsoon"
in die Südchina-See.

Manila - Guangzhou - Hongkong - Kota Kinabalu - Hongkong
16 April - 8 June 1994
(funded by the BMFT Bonn)

Berichte — Reports, Geol.-Paläont. Inst. Univ. Kiel, Nr. 68,
225 S., 200 Figs., 24 Tabs., Kiel, (Juli) 1994

ISSN 0175-9302

PRELIMINARY REPORT ON SONNE-95 CRUISE "MONITOR MONSOON" TO THE SOUTH CHINA SEA

Manila - Guangzhou - Hongkong - Kota Kinabalu - Hongkong

16 April - 8 June 1994

(funded by the BMFT Bonn)

Editors: M. Sarnthein (Chief Scientist)
U. Pflaumann, P.X. Wang, and H.K. Wong (Senior Scientists)

Berichte - Reports, Geol. - Paläont. Inst. Univ. Kiel, Nr. 68,
225 S., 200 Figs., 24 Tabs., Kiel (Juli) 1994

ISSN 0175-9302

Shipboard Party on SONNE-95 cruise, leg 2 (from left to right): L.J. Wang, J. Lu, L.F. Chen, H.Y. Zhou, Z.M. Jian, B. Lu, P.X. Wang, E. Heinrich, M. Staubwasser, M. Kienast, H. Lüskow, M. Sarnthein, B. Haupt, S. Hess, U. Pflaumann, H.L. Lin, H.K. Wong, S. Heilig, M. Wollschläger.

Shipboard Party on SONNE-95 cruise, leg 3 (in front, from left to right): S. Hess, S. Heilig, E. Heinrich, H.Y. Zhou, P.X. Wang, M. Sarnthein, Z.M. Jian, K. Kißling; (in the rear, from right to left:) M. Staub wasser, R. Botz, U. Pflaumann, M.P.Ph. Chen, L.J. Wang, W. Kuhnt, W. Rehder, P. Jöhrend, M. Wiesner.

List of Contents

Participants of SONNE Cruise 95

Botz, Rainer, Dozent Dr.	Geochemistry	GPI	3-4
Calvert, Steve, Professor	Isotopic chemistry	DOV	1
Chen JF, Research Scientist	Organ.Geochemistry	SOA	2
Chen MP-Ph. Professor	Paleoceanographie	NTU	3-4
Haupt, Berndt, Dipl.Ozeanogr.	Oceanography, Modelling	GPI	1-2
Heilig, Stephanie, cand.geol.	Sedimentology	GPI	1-4
Heinrich, Elke, cand.geol.	Sedimentology, Logging	GPI	1-4
Hensch, Heidrun, TA	Micropaleontology	GPI	1-2
Heß, Sylvia, Dipl.Geol.	Micropaleontology	GPI	1-4
Jian, Zhimin, Dr.	Micropaleontology	TJU	2-4
Jöhrendt, Peter, TA.	Sediment traps	IfBM	3-4
Kienast, Markus, cand.geol.	Sedimentology	GPI	1-4
Kißling, Karin, TA	Sedimentology	GPI	3-4
Kuhnt, Wolfgang, Professor	Micropaleontology	GPI	3-4
Lin Hui-Ling, Professor	Marine Sedimentology	IMG	1-2
Lu, Bo, Research Scientist	Physical Properties	SCSI	2
Lu, Jun, Research Scientist	Micropaleontology	SCSI	2
Lüdmann, Thomas, Dipl.Geol.	Geophysics	IfBM	1-2
Lüskow, Heike, cand.geol.	Seismics	IfBM	1-2
Mühlhan, Norbert, TA	Geology	GPI	1-4
Pflaumann, Uwe, Dr.	Micropaleontology	GPI	1-4
Rehder, Wilma, TA	Marine geology	GPI	1-4
Sarnthein, Michael, Professor	Chief Scientist, Paleocean.	GPI	1-4
Staubwasser, Michael, cand.geol.	Geology	GPI	1-4
Villanueva, J. Dr.	Organ.Geochemistry	CID-CSIC	1
Wang, Pinxian, Professor	Paleoceanogr., Micropal.	TJU	1-4
Wang, Lüjiang, Dr.	Sedimentology, Isotopes	GPI	1-4
Wang, Yubo, Dipl.Geophys.	Sedimentology	IfBM	3-4
Wiesner, Martin G., Dr.	Sedimentology	IfBM	1-4
Wollschläger, Markus, Dipl.Geoph.	Geophysics	IfBM	1-3
Wong, How-Ken, Professor	Marine Geology	IfBM	1-2
Zheng, Lianfu, Sen. Res. Scientist	Sedimentology	SOA	1
Zhou, H.Y., Dr.	Isotopes	SOA	2-4

Participating Institutions

CID-CSIC
Centre d'investigacio i desenvolupament
Consell Superior d'Invest. Cientifiques
Barcelona/ Spain
FAX: 0034-3-204 5904
e-mail: jgoqam @cid.csic.ES

DOV
Department of Oceanography
University of British Columbia
Vancouver, B.C./ Canada V6T 1Z4
FAX: 001 604 822 6091
e-mail: calvert@unixg.ubc.ca

GPI
Geologisch-Paläontologisches Institut
Universität Kiel,
Olshausenstr. 40,
D-24118 Kiel/ Germany
FAX: 049 431 880 4376
e-mail: ngl43@rz.uni-kiel.de

IfBM
Institut für Biochemie und Meereschemie
der Universität Hamburg
Bundesstraße 55,
D-20146 Hamburg/ Germany
FAX: 49 40 4123 6347
e-mail: fg3a507@GEOMAT.math.uni-hamburg.de

IMG
National Sun Yat-Sen University
Institute of Marine Geology
Kaohsiung, Taiwan 804, ROC
FAX 886-7-532-6863
e-mail: hllin@cc.nsysu.edu.tw

NTU
Institute of Oceanography
National Taiwan University
Taipei 10764, Taiwan/ China
FAX 00886.2.391.4442 (or 392.5294)

SOA
Second Institute of Oceanography
SOA (State Oceanography Administration)
P.O.Box 1207
Hangzhou, Zhejiang 310012/ China
FAX: 0086. 571 8071 539

TJU
Dept. of Marine Geology,
Tongji University
Shanghai 200092/ China
FAX (0086) 21 54 58 965

Crew SONNE 95

1	Kapitän	Bruns
2	1. Offizier	Kalthoff/Öllerich
3	2. Offizier	Berkenheger
4	Funkoffizier	Sturm
5	Schiffsarzt	Dr.Eubisch
6	1. Ingenieur	Neve
7	2. Ingenieur	Guzman Navarrete
8	2. Ingenieur	Neumann
9	2. Ingenieur	Beyer
10	Elektriker	Freitag/Bekaan
11	Elektroniker	Duthel
12	Elektroniker	Vöhrs
13	System-Operator	Dr. Schlaak
14	System-Operator	Tank
15	Deckschlosser	Rossmeyer
16	Motorenwärter	Meyer, Helmut
17	Motorenwärter	Sonowski
18	Motorenwärter	Koch
19	Koch	Grün
20	Kochsmaat	Pade/Cwienk
21	1. Steward	Bronn
22	2. Steward	Slotta/Hammoor
23	2. Steward	Müller,W.
24	Bootsmann	Hartwig
25	Matrose	Reichmacher
26	Matrose	vom Berg
27	Matrose	Stängl
28	Matrose	Röpti
29	Matrose	Mahlmann
30	Matrose	Krüger

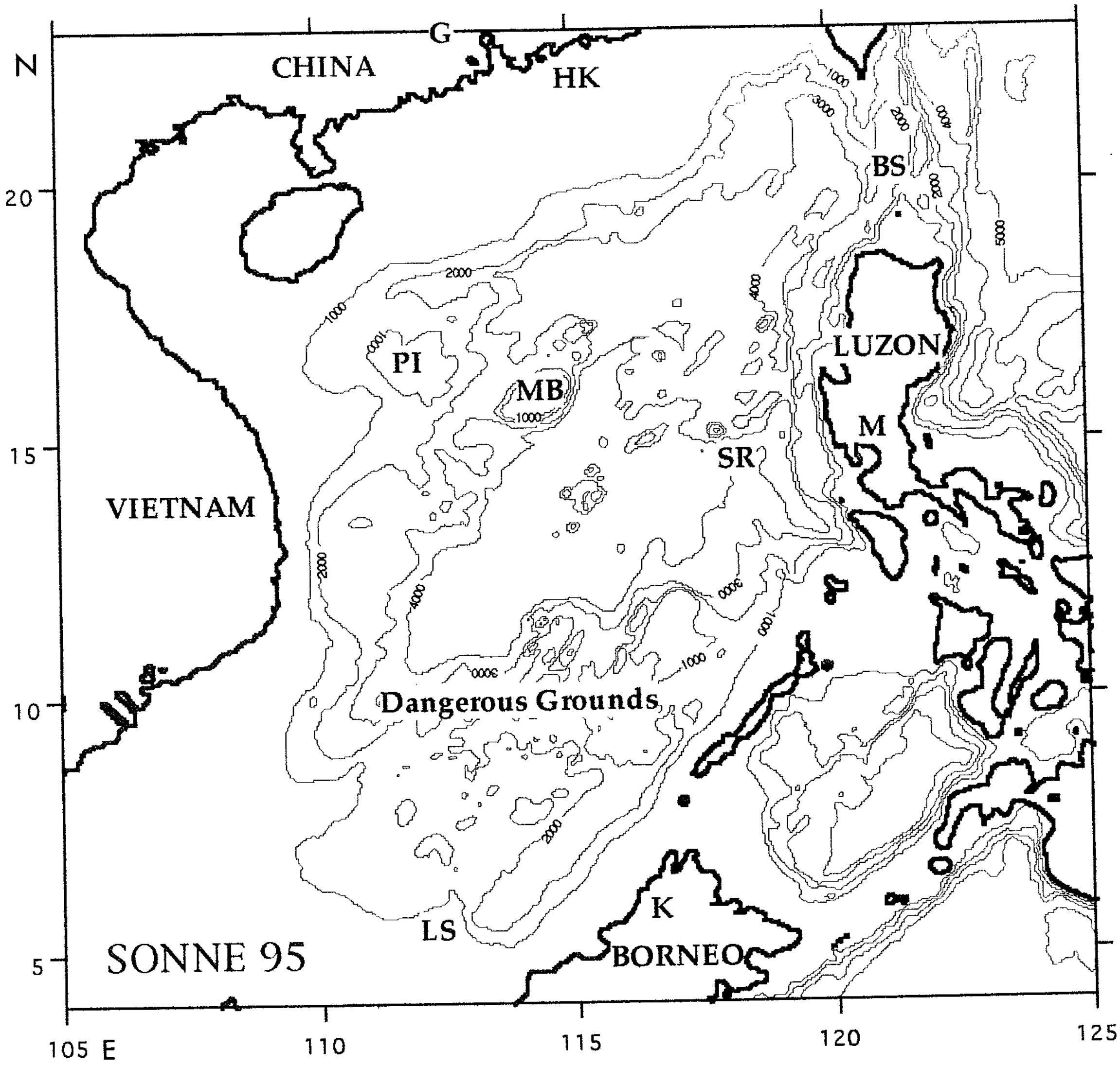

Index map of the South China Sea

G = Guangshou, HK = Hong Kong, K = Kota Kinabalu, M = Manila

BS = Bashi Strait, LS = Luconia Shoals, MB = Macclesfield Bank,

PI = Paracel Islands, SR = Scarborough Reef

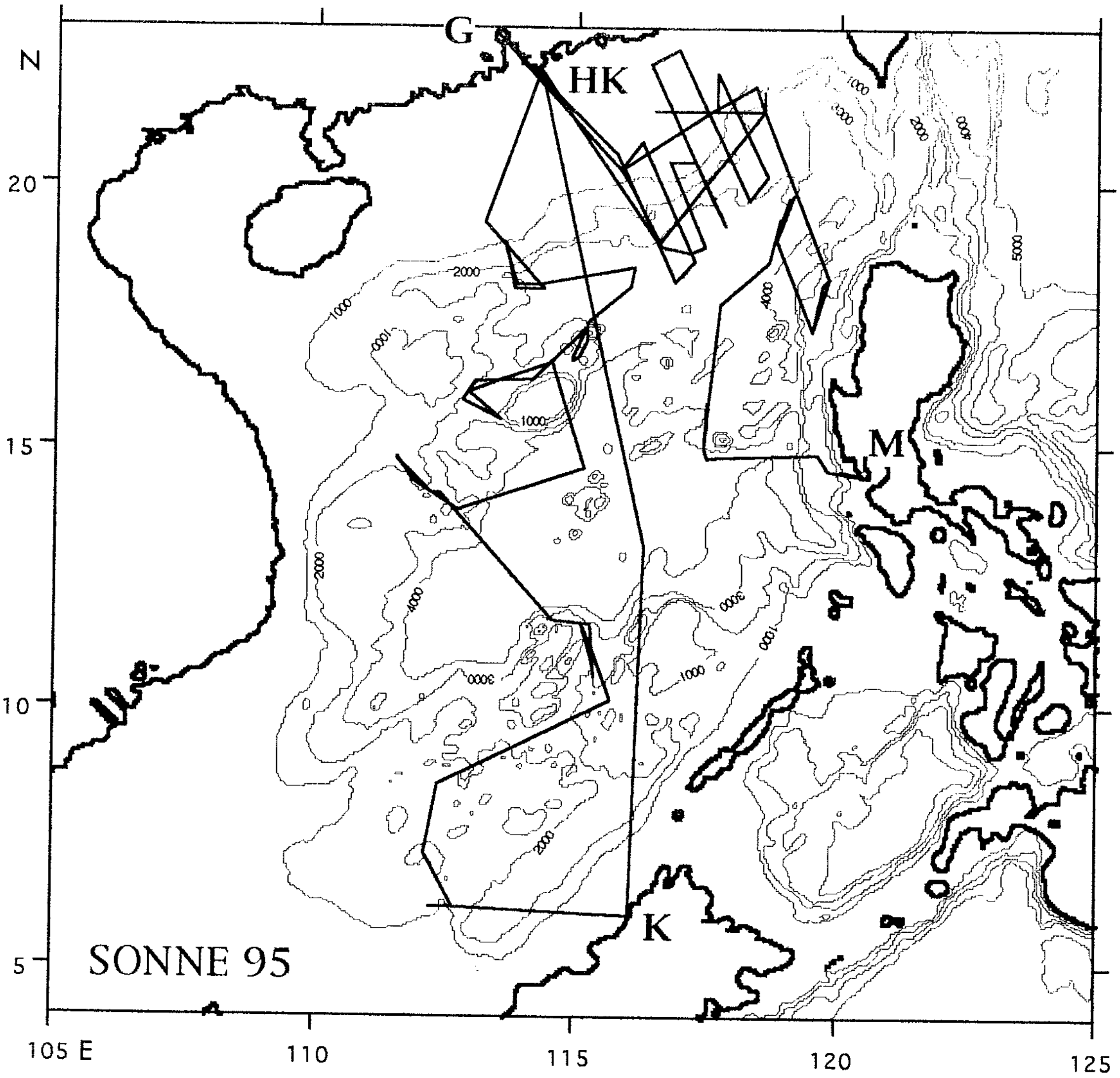

Index map of the South China Sea showing the ship's track of SONNE cruise 95

G = Guangshou, HK = Hong Kong, K = Kota Kinabalu, M = Manila

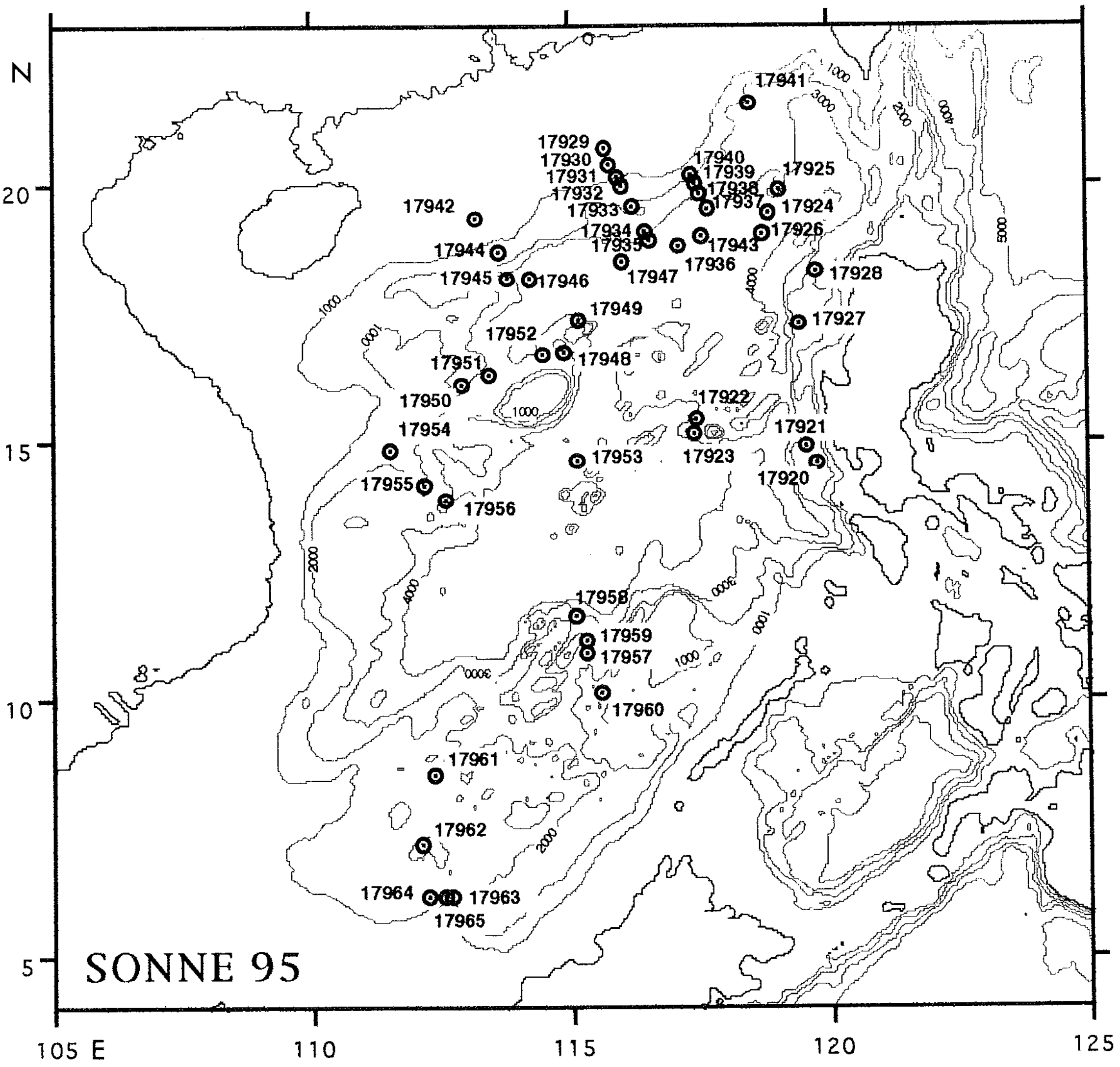

Index map of the South China Sea showing locations of Sonne 95 core sites

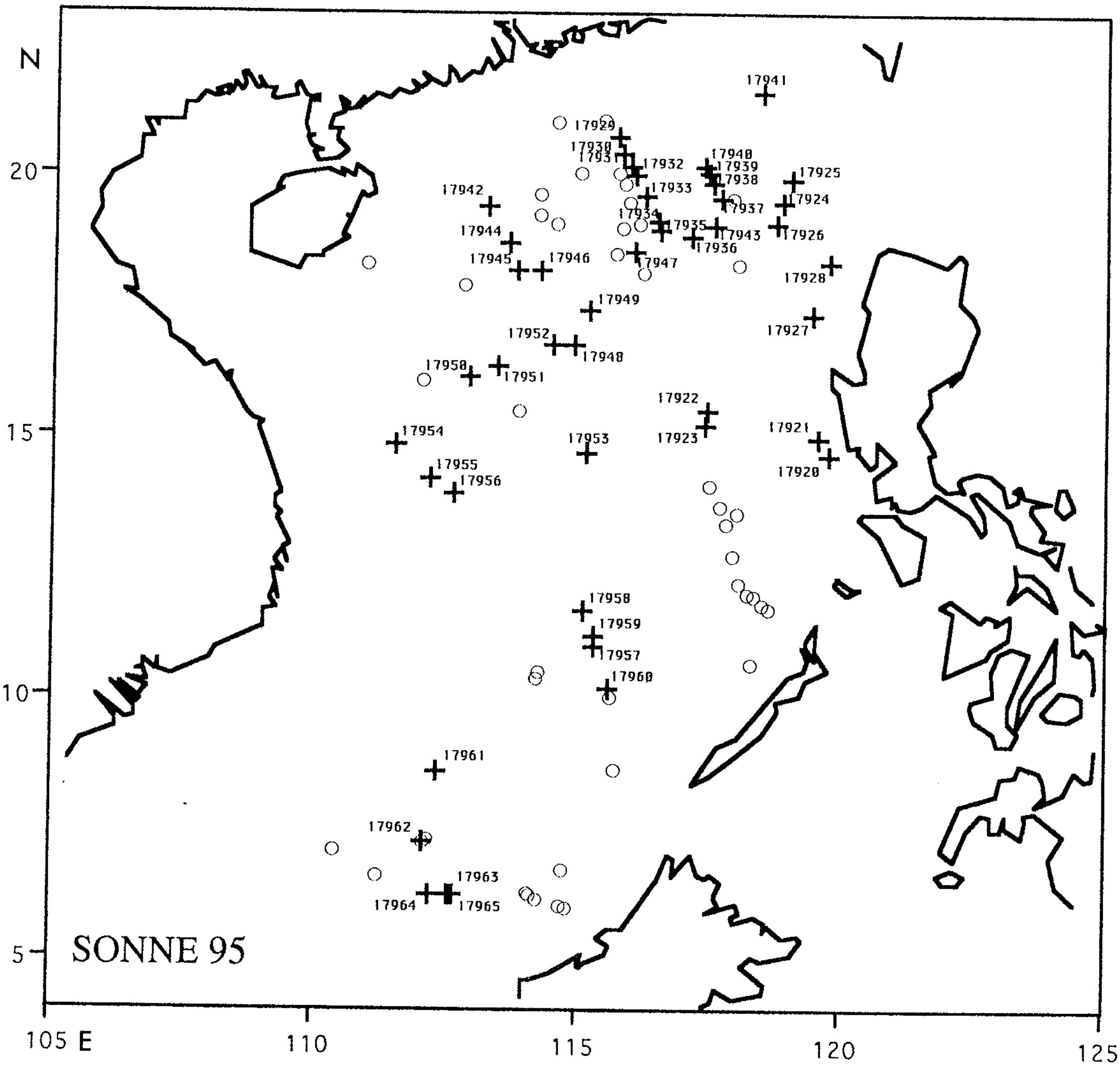

Core locations of SONNE-95 cruise (+) and various previously published key sites (o)

TABLE OF STATIONS

Date	SONNE Station	start (L.T.)	w.d. (m)	Latitude (N)	Longitude (E)	GIK Nr.	Recovery (m)	Instrument deployed
16.4.94	1	18h00	2507	14°35.1	119°45.1	17920-1	0.43	Spade box core
	2	22h15	2507	14°54.7	119°32.3	17921-1	0.40	Spade box core
17.4.94	3	18h00	4221	15°25.0	117°27.5	17922-1	0.46	Spade box core
			4224	15°25.0	117°27.5	17922-2	6.63	Gravity core
18.4.94	4	02h45	1839	15°08.3	117°25.2	17923-1	0.00	Spade box core
			1839	15°08.3	117°25.2	17923-1	0.00	Spade box core
19.4.94	5	10h55	3438	19°24.7	118°50.8	17924-1	0.47	Spade box core
			3440	19°24.7	118°50.9	17924-2	11.50	Gravity core
			3436	19°24.6	118°50.8	17924-3	19.89	Piston core
20.4.94	6	02h35	2979	19°51.2	119°02.8	17925-1	2400	Multinet haul
			2980	19°51.1	119°02.8	17925-2	0.36	Spade box core
			2980	19°51.2	119°02.8	17925-3	12.42	Gravity core
20.4.94	7	14h55	3758	19°00.0	118°44.0	17926-1	3769.8	CTD (hydrography)
			3761	19°00.0	118°44.0	17926-2	0.42	Spade box core
			3760	19°00.0	118°44.0	17926-3	10.06	Gravity core
21.4.94	8	09h43	2800	17°15.0	119°27.2	17927-1	0.52	Spade box core
			2804	17°15.1	119°27.2	17927-2	5.58	Gravity core
21.4.94	9	20h45	2480	18°16.3	119°44.7	17928-1	1201.1	CTD (hydrography)
			2486	18°16.3	119°44.7	17928-2	0.45	Spade box core
			2484	18°16.3	119°44.7	17928-3	3.30	Gravity core
27.4.94	10	03h38	371	20°40.9	115°42.0	17929-1	0.36	Spade box core
30.4.94	11	16h12	629	20°20.0	115°46.9	17930-1	0.46	Spade box core
			629	20°20.0	115°46.9	17930-2	5.34	Gravity core
30.4.94	12	20h40	1005	20°06.0	115°57.8	17931-1	0.41	Spade box core
			1003	20°06.0	115°57.8	17931-2	3.00	Gravity core
			1001	20°06.0	115°57.8	17931-3	4.31	Gravity core
01.5.94	13	01h25	1365	19°57.0	116°02.3	17932-1	0.49	Spade box core
			1360	19°57.1	116°02.2	17932-2	7.56	Gravity core
01.5.94	14	07h35	1970	19°31.5	116°13.9	17933-1	1600	Multinet haul
			1972	19°32.0	116°13.6	17933-2	0.44	Spade box core
			1970	19°32.0	116°13.6	17933-3	12.48	Gravity core
			1970	19°32.0	116°13.6	17933-4	19.75	Piston core
02.5.94	15	00h15	2665	19°01.9	116°27.7	17934-1	0.46	Spade box core
			2665	19°01.9	116°27.7	17934-2	11.87	Gravity core
02.5.94	16	06h08	3143	18°52.7	116°31.6	17935-1	3140.6	CTD (hydrography)
			3143	18°52.7	116°31.6	17935-2	0.42	Spade box core
			3138	18°52.7	116°31.6	17935-3	12.27	Gravity core
02.5.94	17	16h15	3809	18°46.0	117°07.2	17936-1	0.48	Spade box core
			3809	18°46.0	117°07.2	17936-2	13.33	Gravity core
05.5.94	18	02h00	3428	19°30.1	117°40.0	17937-1	0.41	Spade box core
			3428	19°30.0	117°39.9	17937-2	12.92	Gravity core
05.5.94	19	08h55	2835	19°47.2	117°32.3	17938-1	0.41	Spade box core
			2840	19°47.2	117°32.3	17938-2	11.78	Gravity core

Date	SONNE Station	time (L.T.)	w. d. (m)	Latitude (N)	Longitude (E)	GIK Nr.	Recovery (m)	Instrument deployed
05.5.94	20	15h00	2473	19°58.2	117°27.3	17939-1	0.50	Spade box core
			2474	19°58.2	117°27.3	17939-2	12.74	Gravity core
05.5.94	21	20h45	1728	20°07.0	117°23.0	17940-1	0.56	Spade box core
			1727	20°07.0	117°23.0	17940-2	13.30	Gravity core
13.5.94	22	02h09	2201	21°30.9	118°28.9	17941-1	0.39	Spade box core
			2200	21°31.0	118°29.0	17941-2	9.90	Gravity core
18.5.94	24	07h04	329	19°20.0	113°12.1	17942-1	0.47	Spade box core
19.5.94	25	12h46	917	18°57.0	117°33.2	17943-1	0.48	Spade box core
			919	18°57.0	117°33.2	17943-2	11.74	Gravity core
19.5.94	26	17h34	1219	18°39.5	113°38.3	17944-1	0.44	Spade box core
			1217	18°39.5	113°38.2	17944-2	8.92	Gravity core
19.5.94	27	23h21	2404	18°07.6	113°46.6	17945-1	0.45	Spade box core
20.5.94			2403	18°07.6	113°46.6	17945-2	10.21	Gravity core
			2404	18°07.6	113°46.6	17945-3	15.68	Piston core
	28	12h00	3465	18°07.5	114°15.0	17946-1	0.41	Spade box core
			3464	18°07.5	114°15.0	17946-2	11.34	Gravity core
21.5.94	29	02h45	3761	18°28.0	116°01.7	17947-1	3700	CTD (hydrography)
			3765	18°28.0	116°01.7	17947-2	0.47	Spade box core
				18°28.1	116°02.8	17947-3		Sediment trap depl.
22.5.94	30	09h35	2841	16°42.5	114°53.8	17948-1	0.49	Spade box core
			2855	16°42.3	114°53.8	17948-2	13.09	Gravity core
22.5.94	31	17h18	2195	17°20.9	115°10.0	17949-1	0.45	Spade box core
			2197	17°20.9	115°10.0	17949-2	13.34	Gravity core
24.5.94	32	01h30	1868	16°05.6	112°53.8	17950-1	0.44	Spade box core
			1865	16°05.6	112°53.8	17950-2	9.91	Gravity core
24.5.94	33	07h12	2340	16°17.3	113°24.6	17951-1	0.47	Spade box core
			2341	16°17.3	113°24.6	17951-2	11.97	Gravity core
24.5.94	34	14h47	2864	16°40.0	114°28.4	17952-1	1600	Multinet haul
			2882	16°40.0	114°28.4	17952-2	0.49	Spade box core
			2883	16°40.0	114°28.4	17952-3	12.04	Gravity core
25.5.94	35	09h40		14°36.2	115°07.1	17953-1		Sediment trap rec.
			4309	14°35.8	115°08.6	17953-2	--	Spade box core
			4307	14°33.0	115°08.6	17953-3	0.62	Spade box core
			4306	14°33.0	115°08.6	17953-4	12.49	Gravity core
26.5.94		00h25	4306	14°36.0	115°07.0	17953-5	4000	CTD (hydrography)
				14°36.2	115°07.1	17953-6		Sediment trap depl.
27.5.94	36	12h14	1517	14°45.5	111°31.6	17954-1	0.46	Spade box core
			1520	14°47.8	111°31.5	17954-2	11.52	Gravity core
			1515	14°47.7	111°31.5	17954-3	11.49	Gravity core
28.5.94	37	00h05	2404	14°07.3	112°10.6	17955-1	0.45	Spade box core
			2393	14°07.3	112°10.6	17955-2	11.66	Gravity core
28.5.94	38	08h05	3387	13°50.9	112°35.3	17956-1	0.48	Spade box core
			3388	13°50.9	112°35.3	17956-2	13.56	Gravity core

Date	SONNE Station	time (L.T.)	w.d. (m)	Latitude (N)	Longitude (E)	GIK Nr.	Recovery (m)	Instrument deployed
29.5.94	39	16h37	2197	10°53.9	115°18.3	17957-1	0.42	Spade box core
			2195	10°53.9	115°18.3	17957-2	13.84	Gravity core
30.5.94	40	00h00	2581	11°37.1	115°04.9	17958-1	0.47	Spade box core
			2581	11°37.3	115°04.9	17958-2	10.73	Gravity core
30.5.94	41	06h29	1957	11°08.3	115°17.2	17959-1	0.43	Spade box core
			1959	11°08.3	115°17.2	17959-2	13.93	Gravity core
	42	16h00	1707	10°07.2	115°33.5	17960-1	0.45	Spade box core
31.5.94	43	10h33	1795	08°30.4	112°19.9	17961-1	0.49	Spade box core
			1795	08°30.4	112°19.9	17961-2	10.30	Gravity core
	44	22h13	1970	07°10.9	112°04.9	17962-1	0.47	Spade box core
01.6.94			1968	07°10.9	112°04.9	17962-2	8.29	Gravity core
			1969	07°10.9	112°04.9	17962-3	8.81	Gravity core
			1969	07°10.9	112°04.9	17962-4	14.80	Piston core
01.6.94	45	13h05	1232	06°10.0	112°40.0	17963-1	1151	Multinet haul
			1233	06°10.0	112°40.0	17963-2	0.56	Spade box core
			1232	06°10.0	112°40.0	17963-3	8.57	Gravity core
01.6.94	46	20h00	1556	06°09.5	112°12.8	17964-1	0.59	Spade box core
			1556	06°09.5	112°12.8	17964-2	13.04	Piston core
02.6.94			1556	06°09.5	112°12.8	17964-3	9.12	Gravity core
02.6.94	47	06h20	889	06°09.4	112°33.1	17965-1	0.66	Spade box core
			890	06°09.4	112°33.1	17965-2	6.83	Gravity core

TABLE OF CORES

(SPADE BOX CORE)

GIK Nr.	w.d. (m)	Lat. (N)	Long. (E)	recov. (cm)
17920-1	2507	14°35.1	119°45.1	43
17921-1	2507	14°54.7	119°32.3	40
17922-1	4221	15°25.0	117°27.5	46
17923-1	1839	15°08.3	117°25.2	0
17923-2	1839	15°08.3	117°25.2	0
17924-1	3438	19°24.7	118°50.8	40-47
17925-2	2980	19°51.1	119°02.8	36
17926-2	3761	19°00.0	118°44.0	42
17927-1	2800	17°15.0	119°27.2	52
17928-2	2486	18°16.3	119°44.7	26-45
17929-1	371	20°40.9	115°42.0	36
17930-1	629	20°20.0	115°46.9	46
17931-1	1005	20°06.0	115°57.8	41
17932-1	1365	19°57.0	116°02.3	49
17933-2	1972	19°32.0	116°13.6	44
17934-1	2665	19°01.9	116°27.7	46
17935-2	3143	18°52.7	116°31.6	41.5
17936-1	3809	18°46.0	117°07.2	38-48
17937-1	3428	19°30.1	117°40.0	41
17938-1	2835	19°47.2	117°32.3	41
17939-1	2473	19°58.2	117°27.3	50
17940-1	1728	20°07.0	117°23.0	56
17941-1	2201	21°30.9	118°28.9	39
17942-1	329	19°20.0	113°12.1	45-47
17943-1	917	18°57.0	117°33.2	48
17944-1	1219	18°39.5	113°38.3	44
17945-1	2404	18°07.6	113°46.6	45
17946-1	3465	18°07.5	114°15.0	39-41
17947-2	3765	18°28.0	116°01.7	46-47
17948-1	2841	16°42.5	114°53.8	46-49
17949-1	2195	17°20.9	115°10.0	45
17950-1	1868	16°05.6	112°53.8	43-44
17951-1	2340	16°17.3	113°24.6	45-47

TABLE OF CORES

(SPADE BOX CORE)

GIK Nr.	w.d. (m)	Lat. (N)	Long. (E)	recov. (cm)
17952-2	2882	16°40.0	114°28.4	49
17953-2	4309	14°35.8	115°08.6	--
17953-3	4307	14°33.0	115°08.6	62
17954-1	1517	14°45.5	111°31.6	46
17955-1	2404	14°07.3	112°10.6	45
17956-1	3387	13°50.9	112°35.3	48
17957-1	2197	10°53.9	115°18.3	42
17958-1	2581	11°37.3	115°04.9	47
17959-1	1957	11°08.3	115°17.2	43
17960-1	1707	10°07.2	115°33.5	45
17961-1	1795	08°30.4	112°19.9	47-49
17962-1	1970	07°10.9	112°04.9	47
17963-2	1233	06°10.0	112°40.0	56
17964-1	1556	06°09.5	112°12.8	59
17965-1	889	06°09.4	112°33.1	66

TABLE OF CORES

(GRAVITY CORE)

GIK Nr.	w.d. (m)	Lat. (N)	Long. (E)	penetr. (m)	recov. (m)
17922-2	4224	15°25.0	117°27.5	n.d.	6.63
17924-2	3440	19°24.7	118°50.9	>13.50	11.50
17925-3	2980	19°51.2	119°02.8	~17.00	12.42
17926-3	3760	19°00.0	118°44.0	17.45	10.06
17927-2	2804	17°15.1	119°27.2	±6.00	5.58
17928-3	2484	18°16.3	119°44.7	~6.00	3.30
17930-2	629	20°20.0	115°46.9	575	5.34
17931-2	1003	20°06.0	115°57.8	~3.00	3.00
17931-3	1001	20°06.0	115°57.8	4.70	4.31
17932-2	1360	19°57.1	116°02.2	~9.00	7.56
17933-3	1970	19°32.0	116°13.6	15.50	12.48
17934-2	2665	19°01.9	116°27.7	16.50	11.87
17935-3	3148	18°52.7	116°31.6	14.70	12.27
17936-2	3809	18°46.0	117°07.2	~15.00	13.33
17937-2	3428	19°30.0	117°39.9	16.50	12.92
17938-2	2840	19°47.2	117°32.3	14.50	11.78
17939-2	2474	19°58.2	117°27.3	~15.00	12.74
17940-2	1727	20°07.0	117°23.0	n.d.	13.30
17941-2	2200	21°31.0	118°29.0	14.50	9.90
17943-2	919	18°57.0	117°33.2	12.50	11.74
17944-2	1217	18°39.5	113°38.2	±13.00	8.92
17945-2	2403	18°07.6	113°46.6	14.75	10.21
17946-2	3464	18°07.5	114°15.0	15.50	11.34
17948-2	2855	16°42.3	114°53.8	> 12.70	13.09
17949-2	2197	17°20.9	115°10.0	14.50	13.34
17950-2	1865	16°05.6	112°53.8	14.50	9.91
17951-2	2341	16°17.3	113°24.6	14.40	11.97
17952-3	2883	16°40.0	114°28.4	14.40	12.04
17953-4	4306	14°33.0	115°08.6	19.50	12.49
17954-2	1520	14°47.8	111°31.5	14.35	11.52
17954-3	1515	14°47.7	111°31.5	14.40	11.49

TABLE OF CORES

(GRAVITY CORE)

GIK Nr.	w.d. (m)	Lat. (N)	Long. (E)	penetr. (m)	recov. (m)
17955-2	2393	14°07.3	112°10.6	14.40	11.66
17956-2	3388	13°50.9	112°35.3	15.00	13.56
17957-2	2195	10°53.9	115°18.3	14.40	13.84
17958-2	2581	11°37.3	115°04.9	14.40	10.73
17959-2	1959	11°08.3	115°17.2	14.40	13.93
17961-2	1968	08°30.4	112°19.9	15.00	10.30
17962-2	1968	07°10.9	112°04.9	15.00	8.29
17962-3	1969	07°10.9	112°04.9	15.50	8.81
17963-3	1232	06°10.0	112°40.0	15.50	8.57
17964-3	1556	06°09.5	112°12.8	15.00	9.12
17965-2	890	06°09.4	112°33.1	15.30	6.83

TABLE OF CORES

(PISTON CORE)

GIK Nr.	w.d. (m)	Lat. (N)	Long. (E)	penetr. (m)	recov. (m)
17924-3	3436	19°24.6	118°50.8	>24.00	19.89
t.w. core					1.32
17933-4	1970	19°32.0	116°13.6	26.00	19.75
t.w. core					1.47
17945-3	2404	18°07.6	113°46.6	23.30	15.68
t.w. core				1.80	1.77
17962-4	1969	07°10.9	112°04.9	23.65	14.80
t.w. core				1.70	1.39
17964-2	1556	06°09.5	112°12.8	22.00	13.04
t.w. core					1.15

TABLE OF PARASOUND PROFILES

Profile Nr.		latitude (N)	longitude (E)	date	time (UTC)
#001	start	14°48.0	117°27.8	17.4.94	04h42
	turn	14°59.8	117°24.0	17.4.94	06h18
	end	15°52.5	117°27.6	17.4.94	09h30
#002	start	17°48.0	117°42.0	18.4.94	14h20
	turn	18°35.0	118°36.0	18.4.94	21h16
	end	19°24.6	118°50.9	19.4.94	02h28
	start	19°24.6	118°50.9	19.4.94	15h26
	turn	19°50.0	118°58.2	19.4.94	18h00
	end	19°50.0	119°03.1	19.4.94	18h30
#---	start	17°15.0	119°27.0	21.4.94	06h00
	turn	18°08.0	119°39.0	21.4.94	11h05
	end	18°17.1	119°45.3	21.4.94	12h39
#003	start	21°28.0	118°30.0	22.4.94	11h30
	end	21°28.0	117°30.0	22.4.94	23h55
#004	start	21°28.0	117°30.0	22.4.94	23h55
	end	20°20.0	115°47.0	24.4.94	01h46
#005	start	20°41.0	115°42.0	26.4.94	21h33
	break	20°13.2	115°54.8	27.4.94	04h25
	continue	20°14.6	115°54.1	27.4.94	06h43
	end	18°12.4	116°50.0	28.4.94	12h06
#006	start	18°12.4	116°50.0	28.4.94	12h06
	end	18°36.6	117°10.8	28.4.94	19h20
#007	start	18°36.6	117°10.8	28.4.94	19h20
	end	20°53.1	116°10.0	30.4.94	04h24
#008	start	18°52.0	117°25.0	02.5.94	14h55
	end	20°30.0	116°42.0	03.5.94	14h26
#009	start	20°30.0	116°42.0	03.5.94	14h26
	end	20°30.0	117°13.0	03.5.94	21h40
#010	start	20°30.0	117°13.0	03.5.94	21h48
	end	19°17.0	117°46.0	04.5.94	15h30
#011	start	20°31.3	117°12.4	05.5.94	18h41
	end	22°23.0	116°22.0	06.5.94	21h30
#012	start	22°23.0	116°22.0	06.5.94	21h30
	end			06.5.94	21h45
#013	start	22°39.0	116°53.0	07.5.94	01h40
	end	19°47.4	118°12.1	08.5.94	19h37
#014	start	19°47.4	118°12.1	08.5.94	19h37
	end	20°13.2	118°34.1	09.5.94	02h58
#015	start	20°13.0	118°34.1	09.5.94	06h51
	end	22°12.0	117°37.0	10.5.94	12h00
#016	start	22°12.0	117°37.0	10.5.94	12h00
	end	21°28.0	117°37.0	11.5.94	05h50
#017	start	21°28.0	116°25.0	11.5.94	07h03
	end	21°28.0	117°30.0	11.5.94	20h37
#018	start	21°28.0	117°30.0	11.5.94	20h37
	end	21°59.0	118°19.0	12.5.94	08h46
#019	start	21°59.0	118°19.0	12.5.94	08h46
	end	21°28.0	118°30.0	12.5.94	16h28
#020	start	21°28.0	118°30.0	12.5.94	05h00
	end	18°54.0	116°31.0	14.5.94	23h12

Profile Nr.		latitude (N)	longitude (E)	date	time (UTC)
#021	start	19°19.8	113°12.0	17.5.94	23h32
	end	18°05.0	114°19.0	18.5.94	14h49
#022	start	18°05.0	114°19.0	18.5.94	14h49
	end	18°05.0	114°45.0	18.5.94	19h53
#023	start	18°05.0	114°45.0	18.5.94	19h53
	end	18°56.0	113°35.0	19.5.94	04h12
#024	start	18°27.2	116°03.1	21.5.94	04h00
	end	18°06.9	115°59.5	21.5.94	06h55
#025	start	18°06.9	115°59.5	21.5.94	06h55
	end	17°24.0	115°10.0	21.5.94	15h29
#026	start	17°24.0	115°10.0	21.5.94	15h29
	end	17°03.0	115°10.0	21.5.94	19h04
#027	start	17°03.0	115°10.0	21.5.94	19h04
	end	16°45.0	115°00.0	21.5.94	22h27
#028	start	16°45.0	115°00.0	21.5.94	22h27
	end	16°41.8	114°52.1	21.5.94	23h50
#029	start	17°20.9	115°10.0	22.5.94	12h21
	end	16°20.0	114°08.0	22.5.94	19h38
#030	start	16°20.0	114°08.0	22.5.94	19h38
	end	16°16.0	113°00.0	23.5.94	03h50
#031	start	16°16.0	113°00.0	23.5.94	03h50
	end	15°54.0	112°47.5	23.5.94	06h57
#032	start	15°54.0	112°47.5	23.5.94	06h57
	end	15°34.0	113°31.5	23.5.94	12h45
#033	start	15°34.0	113°31.5	23.5.94	12h58
	end	16°05.6	112°53.8	23.5.94	17h30
#034	start	16°05.4	112°54.0	23.5.94	20h02
	end	16°17.4	113°24.6	23.5.94	23h08
#035	start	16°17.4	113°24.6	24.5.94	02h14
	end	16°40.0	114°28.4	24.5.94	06h47
#036	start	13°47.5	112°40.5	26.5.94	15h43
	end	14°22.4	111°48.0	26.5.94	23h20
#037	start	14°22.4	111°48.0	26.5.94	23h20
	end	14°50.0	111°30.0	27.5.94	03h22
#038	start	14°47.7	111°31.5	27.5.94	08h36
	end	14°07.3	112°10.6	27.5.94	15h43
#039	start	14°07.3	112°20.6	27.5.94	21h36
	end	13°50.9	112°35.3	27.5.94	23h37
#040	start	11°42.0	114°32.0	28.5.94	18h28
	end	11°36.0	115°15.0	28.5.94	23h30
#041	start	11°36.0	115°15.0	28.5.94	23h30
	end	10°34.9	115°19.9	29.5.94	06h42
#042	start	10°28.9	115°31.9	30.5.94	04h44
	end	10°10.0	115°39.0	30.5.94	07h01
#043	start	08°30.4	112°19.9	31.5.94	04h56
	end	07°11.0	112°05.0	31.5.94	13h53
#044	start	07°11.0	112°05.0	31.5.94	22h22
	end	06°10.0	112°40.0	01.6.94	05h05
#045	start	06°10.0	112°40.0	01.6.94	08h48
	end	06°09.5	112°12.8	01.6.94	11h38

SEDIMENT TRAPS University of Hamburg				
GIK Nr.	w.d. (m)	Lat. (N)	Long. (E)	deployment
17947-3		18°28.0	116°03.2	failure of 1-trap system depl.
17953-1	4310	14°35.8	115°03.2	recovery of 2 traps
17953-6	4306	14°36.2	115°07.1	deployment of 3 traps

MULTINET HAULS					
GIK Nr.	w.d. (m)	Lat. (N)	Long. (E)	w.d. (m)	
				start	closures
17925-1	2979	19°51.2	119°02.8	2400	1600, 800, 400, 200
17933-1	1970	19°31.5	116°13.9	1600	800, 400, 200, 100
17952-1	2882	16°39.9	114°28.3	1600	800, 400, 200, 100
17963-1	1232	06°10.0	112°40.0	1151	800, 400, 200, 100

CTD HYDROGRAPHY PROFILES				
GIK Nr.	w.d. (m)	Lat. (N)	Long. (E)	profile length (m)
17926-1	3758	19°00.0	118°44.0	3769.8
17928-1	2480	18°16.3	119°44.7	1201.1
17935-1	3143	18°52.7	116°31.6	3140.6
17947-1	3761	18°28.0	116°01.7	3700.0

1.1 GENERAL RESEARCH PROGRAM OF SONNE-95 CRUISE

M. Sarnthein and U. Pflaumann (University of Kiel), Wang, P.X. (Tongji University, Shanghai), and H.K. Wong (University of Hamburg)

Climate and hydrography in the South China Sea region are largely controlled by the monsoonal wind system which is characterized by its pronounced seasonality. Strong southwesterly winds during summer and northeasterly winds during winter are driving a semi-annual reversal in surface-water circulation from roughly clockwise to anticlockwise (Tchernia, 1980). As off Somalia and Arabia, monsoonal winds lead to seasonal coastal upwelling off Vietnam, a process that may have occurred also off southern China during glacial times when large shelf regions were dried up. Moreover, an enhanced glacial northeasterly monsoon may trigger upwelling west off Luzon during winter.

The sediments in the South China Sea contain medium to high concentrations of carbonate and are deposited at high rates (Broecker et al., 1988 a and b; Miao et al., 1993 and 1994; Schönfeld und Kudrass, 1993; Thunell et al., 1992; Wang CH et al., 1986; Wang PX et al., 1994; Winn et al., 1990/92) thus offering an unique opportunity to unravel the Quaternary history of the monsoonal climate system at high time resolution, moreover, to reconstruct the regional patterns of oceanic circulation. With the SONNE 95 project, we intend to contribute significantly to a better understanding of both the climatic change in Southeast Asia and the hydrological and carbon cycles in the South China Sea. To achieve these aims, we sampled modern, Holocene, and Pleistocene sedimentation patterns through shallow reflection seismics, sediment traps and a number of core transects extending from the upper continental slope down to the deep sea. Based on these data we head for reconstructing paleoceanographic and paleoclimatic time series with special emphasis on the following three objectives:

1) To decipher *glacial-to-interglacial changes in monsoonal climate*, in particular to test still controversial models on past changes in atmospheric circulation (Sirocko et al., 1991, 1993; Bigg and Jiang, 1993) and to reveal the potential sedimentological structures resulting from extremely swift fluctuations in sea level and ocean currents, and their influence on sedimentation and the reworking of shelf and basin deposits. These themes will be approached by means of various groups of proxy data:

a) Variations in the character and accumulation rates of riverine sediments and pollens as a function of changes in temperature and rainfall in Southeast Asia and the Indonesian Archipelago.

b) Variations in temperature, salinity, and density of the surface water. These data may serve as direct signal of i) the monsoonal hydrological cycle, ii) the degree of its seasonality, and iii) the various degrees in spatial isolation of the South China Sea due to Quaternary sea level changes.

c) Paleoproductivity records based on various parameters such as accumulation rates of organic carbon and the species communities of diatoms, planktonic and benthic foraminifers.

d) A detailed tephrochronology for which numerous volcanic ash layers provide a unique opportunity in the South China Sea, especially in the central and eastern parts.

2. To reconstruct the *history of deep-water circulation* and ventilation in the South China Sea as a product of variations in both local intermediate-water formation and varying age of North Pacific Upper Deepwater. Based on previous studies, the present estuarine mode largely persisted (Johnson et al., 1993; Wang LJ, 1992).

3. To study the *variability of the regional marine and ambient terrestrial carbon cycles* as resulting from the fluctuations in monsoon climate.

Besides these studies of the history of monsoonal climate, the SONNE-95 cruise serves for a second goal, the *reflection seismic profiling of the Pearl River Mouth Basin at the South China continental margin*. By means of this seismic profiling the Hamburg University group wants to contribute to the following questions (see Wong et al., this vol.):

1. To characterize the depo-environment and to establish a seismic sequence stratigraphy at the South China margin in continuation of previous studies on SONNE-50B and SONNE-72A cruise.

2. To map a regional fault system and its influence on sedimentation patterns.

The outlined objectives of the SONNE-95 cruise are closely related to various ongoing paleoceanographic projects of the investigators in the Atlantic, Indian, and North Pacific Oceans. They supplement the endeavour of other research projects in Germany (National Climate Project: Terrestrial Palaeoclimatology; the SCOPE project at Hamburg University, and studies at the Geological Survey of Germany (BGR) in Hannover). The proposed cruise falls within the framework of a successful and longstanding scientific collaboration between the Kiel and Hamburg Institutes with the Chinese colleagues from Tongji University, Shanghai, the 2nd Institute of Oceanography (SOA) in Hangzhou, and the South China Institute of Oceanography in Guangzhou. Last not least, this cruise may serve as a "Pre-Site-Survey" for planning a future expedition of the drilling vessel JOIDES Resolution within the Ocean Drilling Program (ODP).

REFERENCES

Bigg, G.R. and D. Jiang (1993): Modelling the late Quaternary Indian Ocean circulation. - Paleoceanogr., 8, 23-46.

Broecker, W.S., M. Andree, G. Bonani, W. Wolfli, M. Klas, A. Mix and H. Oeschger (1988): Comparison between radiocarbon ages obtained on coexisting planktonic foraminifers. - Paleoceanogr., 3, 647-657.

Broecker, W.S., M. Andree, M. Klas, G. Bonani, W. Wolfli and H. Oeschger (1988): New evidence from the South China Sea for an abrupt termination of the last glacial period. - Nature, 333, 156-158.

Johnson, G. C. and J. M. Toole (1993): Flow of deep and bottom water in the Pacific at 10° N. - Deep-Sea Res. I, 40, 371-394.

Miao, Q. and R. Thunell (1993): Recent deep-sea benthic foraminiferal distributions in the South China and Sulu Seas. - Marine Micropaleont., 22, 1-32.

Miao, Q., R. Thunell and D.M. Anderson (1994): Glacial-Holocene carbonate dissolution and sea surface temperatures in the South China and Sulu seas. - Paleoceanogr., 9, 269-290.

Schönfeld, J. and H.-R. Kudrass (1993): Hemipelagic sediment accumulation rates in the South China Sea related to late Quaternary sea level changes. - Quat. Res., 40, 368-379.

Sirocko, F., M. Sarnthein, H. Lange and H. Erlenkeuser (1991): The atmospheric summer circulation and coastal upwelling in the Arabian Sea during the Holocene and the last glaciation. - Quaternary Research, 36, 72-93.

Sirocko, F., M. Sarnthein, H. Erlenkeuser, H. Lange, M. Arnold and J. C. Duplessy (1993): Century-scale events in monsoonal climate over the past 24,000 years. - Nature, 364, 322-324.

Tchernia, P. (1980): Descriptive Regional Oceanography. - Pergamon Marine Series, 3, Pergamon Press, Oxford/Frankfurt, pp.253.

Thunell, R.C., Q. Miao, S.E. Calvert, and T.F. Pedersen (1992): Glacial-Holocene biogenic sedimentation patterns in the South China Sea: Productivity variations and surface water pCO_2. - Paleoceanogr., 7, 143-162.

Wang, C.-H., M.-P. Chen, S.-C. Lo and J.-C. Wu (1986): Stable isotope records of late Pleistocene sediments from the South China Sea. - Bull. Inst. Earth Sci., Acad. Sin. Taipei, 6, 185-195.

Wang, L.-J. (1992): The late Quaternary oxygen isotope record and its implications for the ventilation state of the South China Sea. - In: Ye, Z. and P.X. Wang (eds), Contributions to late Quaternary paleoceanography of the South China Sea, 195-205.

Wang, P.-X., L.-J. Wang, and Z.-M. Jian (1994): Late Quaternary Paleoceanography of the South China Sea: Surface circulation and carbonate cycles. - Mar. Geol., in press.

Winn, K., L. Zheng, H. Erlenkeuser, and P. Stoffers (1992): Oxygen/carbon isotopes and paleoproductivity in the South China Sea during the past 110,000 Years. - In: Xianglong, J., Kudrass, H.-R. and Pautot, G. (eds), Marine Geology and Geophysics of the South China Sea. Proceedings of the Symposium on the Recent Contributions to the Geological History of the South China Sea, 154-166.

1.2 SUMMARY: SCIENTIFIC HIGHLIGHTS OF SONNE-95 CRUISE

M. Sarnthein (University of Kiel)

The cruise logo 'MONITOR MONSOON' outlines the main objectives of the SONNE-95 cruise:

- To collect samples for reconstructing the short-term Quaternary variability of monsoonal climate in Southeast Asia, that is a region which houses one third of mankind, and to investigate the factors governing global climatic change.
- To investigate the long-term Neogene history of monsoon-controlled sedimentation on the continental margin of South China by means of seismic stratigraphy.

Thanks to optimum weather conditions and the extreme efforts of the Shipboard Scientific Party the outlined targets of the cruise were reached by more than 100 %, an outstanding result:

- In total, 515 m of gravity and piston cores (up to 20 m 'long cores') and 46 box cores were recovered at 46 stations.
- Continuous magnetic susceptibility records were measured for all cores. Grey-code curves were measured from six cores.
- More than 30,000 subsamples were removed from the cores to provide abundant material for a joint stratigraphic and paleoclimatic/paleoceanographic evaluation of the sediment record by various scientific groups in Germany and China, Canada, Holland, Spain, and on Taiwan.
- A set of sediment traps was successfully retrieved and again deployed in the central South China Sea, thereby continuing a long-term trap experiment of Hamburg University. Unfortunately, we did not succeed to deploy a second mooring of sediment traps in the northern South China Sea.
- Almost 3000 km of shallow reflection seismic profiles were obtained between Pratas Island and Taiwan Banks from the northeastern Pearl River Mouth Basin at the South China continental margin.
- In addition, almost 5000 km of PARASOUND subbottom profiles were obtained to assess sediment transport and deposition processes and to select coring stations with undisturbed hemipelagic sedimentation.

The shipboard observations led already to a number of important discoveries and preliminary conclusions:

- Based on sediment sections that are up to 23 m (composite depth) long, it will be possible to reconstruct detailed time series of the variations in monsoonal climate, sea level, and sediment input over the last 350,000 years. A preliminary core carbonate stratigraphy, tephrochronology, and maps of sedimentation rates were already developed on board.

- Both off southern China and off the Sunda Shelf we discovered extremely high sedimentation rates that lead to a rare time resolution of 15-20 years per cm sediment. These rates will enable us to reconstruct with great detail the impact of monsoonal climate on the Chinese political and cultural history.
- Extremely high hemipelagic sedimentation rates (60 cm/ky during glacial times) in front of the Sunda Shelf provide strong evidence for a major Amazon-style tropical 'Moolengraaf River' during glacial times, as proposed by Dutch colleagues. This river collected the abundant runoff from the Sunda continental platform which was dried-up during glacial times, and entered the South China Sea north of western Borneo. The sediment discharge of this river led to the fast burial of the southern Dangerous Ground carbonate platform.
- On the other hand, PARASOUND subbottom profiles indicate that large parts of the South China continental slope southeast of Pratas Island have been subject to persistent sediment erosion by contour currents.
- Shallow seismic reflection profiles demonstrate a recent tectonic activity with Tertiary strata being folded and intersected by strike-slip faults that strike perpendicular to the continental margin of South China west of Taiwan.
- The recent eruptions of the Philippine volcano Pinatubo produced a volcanic ash layer which extends up to the continental slope of Vietnam. Based on a number of further prominent ash layers extending across most core profiles of the South China Sea it will be possible to develop a detailed tephrochronology of this region.
- The recent ash deposition caused mass mortality among benthic foraminifers over large parts of the deep-sea floor in the South China Sea. Thus, the ash layer forms the base for a unique natural experiment on the resettlement of benthic life in a widespread empty deep-sea region within a few years.

Further important findings were made in the fields of sediment diagenesis, the distribution of planktonic and benthic foraminifers, and of the paleotemperature regime during glacial times. In summary, cruise SONNE 95 is considered as a great success for the study of global change.

2. METHODS AND STRATEGIES IN SEDIMENTOLOGY, MICROPALEONTOLOGY, STRATIGRAPHY, PALEOCLIMATOLOGY, AND PALEOCEANOGRAPHY

2.1 PARASOUND PROFILING ON SONNE-95 CRUISE

M. Sarnthein (University of Kiel)

Acoustic sediment profiling has become generally established over the last three decades as an important tool for both mapping sedimentation patterns in the deep sea and selecting appropriate sites for sediment cores.

On board of FS SONNE the high-resolution acoustic profiling of deep-sea sediments is based on the PARASOUND parametric echosounder system of Krupp-Atlas Elektronik GmbH., Bremen (Spiess, 1992). Conventional 3.5-kHz recorder systems suffer from interference signals of rough morphologies, resulting from their broad acoustic radiation cone reaching 20-35°. In contrast, the PARASOUND system is based on two high-frequency p-wave signals of finite amplitudes that produce a "new" differential frequency signal of about 4 kHz, where the acoustic energy is focussed to a beam as narrow as 4°. Based on this narrow focus the hyperbolic echoes are largely suppressed, and the vertical resolution is increased. On the other hand, the narrow acoustic cone implies that the PARASOUND system is uncapable to record at marine slopes steeper than 4°, a fact that may cause problems at many sites. The sediment penetration depth strongly varies with sediment composition and slope angle, in ideal cases it may reach more than 100 m.

High-quality PARASOUND records were obtained at speeds up to 8 knots, many useful records also at speeds up to 12 knots, depending on both the roughness of the sea floor and the sea surface.

The PARASOUND records (hard copies and pertinent log books) of the SONNE-95 cruise are stored at the Geologisch-Paläontologisches Institut of Kiel University. However, no digital recordings were made. The PARASOUND records of all site locations and various other PARASOUND records are discussed in Section 3: Preliminary Results.

Reference

Spiess, V. (1992): PARADIGMA, Handbuch zum Programmsystem Digitalisierung von Parasound-Seismogrammen, Version 3.1, Fachbereich Geowissenschaften Universität Bremen, Bremen.

2.2 MULTINET HAULS ON SONNE-95 CRUISE

U. Pflaumann (University of Kiel)

Three plankton hauls (see Table) were run for obtaining informations on the distribution and frequency of planktonic foraminifera and radiolarians within various water depths of the South China Sea. We deployed the multinet equipment of Hydrobios (Kiel) using a collecting frame with an opening of 50 x 50 cm and plankton nets with a mesh size of 100 mm and is fitted with 5 plankton cups.

The collected material was preserved and stained in a methanol-Rose Bengal solution. A preliminary inspection of some samples from the last station showed very rare foraminifers, pteropods, and radiolarians among a mass of nectonic organisms. Further evaluations of the hauls in Kiel will require more sophisticated preparation methods, especially methods to concentrate calcareous and siliceous microfossils in the samples.

2.3 BOX CORING, GRAVITY AND PISTON CORING ON SONNE-95 CRUISE

N. Mühlhan, M. Sarnthein, M. Kienast, and M. Staubwasser
(University of Kiel)

The following gear was deployed for sediment sampling on board of SONNE-95 cruise:

1. **(Spade) Box Corer (GKG)**:
   Size of sample box: 50x50 in square, 60 cm high.
   Net weight: about 1100 kg (deep-sea version).
   Producer: Wuttke, Henstedt-Ulzburg, near Hamburg.

2. Combined **Gravity Corer (SL)** and **Piston Corer (KOL)** System, Type 446:
   Weight stand: 2 metric tons
   Steel tubes: 14 cm outer diameter
   Length of tubes: 5.75 m
   Plastic liners: 12 cm inner diameter
   Longest SL section recovered: 13.93 m
   Longest KOL section recovered: 19.89 m
   Producer: Hydrowerkstätten, Kiel-Hassee.

The coring systems were described in detail by Sarnthein et al. (1983) and Wefer (1986). Excellent weather conditions that lasted over large parts of the SONNE-95 cruise enabled us to deploy and retrieve the sediment coring systems with great care. Only in rare cases steel tubes were distorted because of too hard sandy sediments and/or a too slow lowering of the corer (GIK St. no. 17927-2, 17931-2 and 17944-2). - The total length of gravity and piston cores recovered at SONNE-95 cruise amounts to 515 m.

No problems were encountered with the deployment of the GKG box corer, except for too deep penetration in the carbonate-free sediments of GIK Station 17953.

As recognized on many previous cruises, the sediment within the top 5 m of most piston cores was strongly disturbed. This may be caused by difficulties with adjusting the shear piston with sufficient precision. On the other hand, also long gravity cores are known to produce disturbed sediment sections that are significantly compacted near their bottom end. Based on both the continuous magnetic susceptibility records and carbonate curves produced on board of SONNE-95 cruise we were able to precisely estimate for the first time the actual bias in core length at sites with duplicate SL and KOL coring. The comparison of these records revealed that about 2.0-2.5 m of sediment were lost and further portions of the section were heavily distorted in the top 5-6 m of piston cores. On the other hand, in gravity cores the lowermost 2.0-2.5 m core length turned out as compacted by 0.5-1.0 m as compared to the adjacent piston core sections (see section on Coring Sites, Core Logs, and Initial Core Descriptions; sites 17924, 17933, 17945, 17962, and 17964; and section on Composite Depth).

REFERENCES

Sarnthein, M., F. C. Kögler and F. Werner, (1983): Forschungsschiff "Meteor", Reise Nr. 65. Äquatorialer Ostatlantik - GEOTROPEX '83, Juni-August 1983, Bericht der wissenschaftlichen Leiter.- Ber.-Rep. Geol.-Pal. Inst. Univ. Kiel, 2, 1-90.

Wefer, G., (1986): Allgemeines zur geologischen Probennahme.-, In: Gersonde, R. (ed), Die Expedition Arktis III mit F.S. "Polarstern" 1985, Berichte zur Polarforschung, 28, 63-70.

2.4 MEASURING MAGNETIC SUSCEPTIBILITY ON SONNE-95 CRUISE

U. Pflaumann (University of Kiel) and
M.P.Ph. Chen (National University Taipei)

Objectives

Over the last 20 years (Poutiers, 1975; Robinson, 1985; Bloemendal, 1988) magnetique susceptibility logs became a standard technique for producing a rapid shipboard stratigraphy of marine sediment cores. The marine susceptibility signal depends on the abundance of magnetic minerals in the sediment such as magnetite and titanomagnetite. These minerals may be contained in (1) the input of volvanic ashes from the Philippines as common in the South China Sea (Wiesner et al., 1994) and (2) the fluvial and eolian input of siliciclastic sediment from land, that is primarily a climatic and sea-level signal which may be subject to rapid change. (3) Moreover, a magnetic signal is contained in pyrite that formed during early diagenesis usually linked to layers enriched in organic carbon, i.e., a rather incidental signal the stratigraphy has to be corrected for prior to stratigraphic interpretation. On the other hand, both non-magnetic carbonates and the water content of the sediment are lowering the magnetic signal. In many cases the magnetic susceptibility signal turned out to record more sensitively any slight changes in the sediment input than visual core description was able to detect.

Technique

The magnetic susceptibility was measured on board of RV SONNE using the Multi-Sensor Core Logger (MSCL/016) designed and built by GEOTEC, Haslemere, UK. This system enabled us to determine the amount of magnetic material present in the sediment of unsplit sediment cores encased in cylindrical plastic liners.

We measured magnetic susceptibility at core sections of 12 cm diameter, each up to 110 cm long and closed by plastic caps of 12.5 cm diameter. The sediment core was placed on rails of a conveyor system and aligned to the start position. A core pusher moved the core section in increments of choice along the rail track through the BARTINGTON MS2C sensor loop. The system was operated by a Macintosh 180 Powerbook.

A low intensity (ca. 80 A/m RMS) non-saturating, alternating magnetic field (0.565 kHz) is produced by an oscillator circuit in the sensor. Any magnetic material in the near vicinity of the sensor will cause a change in the oscillator frequency, which is electronically converted into (artifical) magnetic susceptibility values.

Based on several test runs, measuring conditions were defined as 1 sec, 1 Hz, 1 cm increments, and a starting position at 3 cm in front of the sensor loop.

Data Management

The data were collected and stored on a Macintosh Powerbook 180, using the MSQB1.BAS program of GEOTEC, then edited by FREDITOR, EXCEL, McDRAW software to provide the magnetic susceptibility curves. To eliminate artificial susceptibility minima near the core section breaks (possibly produced by a higher water and/or air content), the first and last 4 measured values of every core section were deleted from the plots.

During the SONNE 95 cruise more than 520 m of sediment cores were analyzed. The procedure revealed as a quick and robust method, multiple measurements of the same core as well as on different gravitity and piston cores from the same site showed a high reproducibility and close correlation (see Section on Core Logging Records, Fig. 17962; this vol.).

REFERENCES

Bloemendal, J. and P. de Menocal (1989): Evidence for a change in the periodicity of tropical climate cycles at 2.4 Myr from whole core magnetic susceptibility measurements.- Nature, 342, 897-900.

Poutiers, J. and J.P. Rehaut (1975): La susceptibilite magnetique, parametre sedimentologique; application a l'etude de sediments marins du golf de Genes (Italie) (The magnetic susceptibility, sedimentologic parameters; application to the study of marine sediments of the Gulf of Genoa, Italy).- Acad. Sci. Paris, C. R. Ser. D., 278, 3169-3172.

Robinson, S. G. (1986): The late Pleistocene paleoclimatic record of North Atlantic deep-sea sediments revealed by mineral-magnetic measurements. - Physics of the Earth and Planetary Interiors, 42, 22-47

Wiesner, M.G., Y. Wang, L. Zheng, H.K. Wong and K. Airkas (1994): Massive fallout of Volcanic dust to the deep South China Sea, Deep-Sea Res. (subm.)

2.5 COLOR CODE / GRAY CODE LOGGING ON SONNE-95 CRUISE

L.J. Wang, U. Pflaumann and M. Sarnthein (GPI, Kiel University)

Color logging should replace the time consuming and imprecise conventional color description by a continuous high resolution record. This was accomplished by image acquisition and digitization of the sediment cores.

The equipment used includes a high resolution video-camera (HITACHI HV-C10A CCD) with a FUJINON TV zoom lens 1.4/7.5-90 mm, a Neotech Color Adaptor Module, an image capturing card (32-bit, 256 gray/color video image capturing board, Image Grabber Macintosh II NuBus), and a Macintosh IIcx desktop system with color monitor. Image Grabber®2.1 was used for image capturing. Lighting was provided by a pair of Multiblitz® Variolite 250 lamps. Polarization filters were mounted on both lamps and the camera lens to avoid reflections. For increased light intensity, two halogen lamps were used in the photolab.

The archive half of each sediment core was scratched to get a plain sediment surface before taking pictures. A frame of 25x35cm was set for image capturing with a distance of about 70-75cm between the camera and sediment surface. This setup produces a resolution of 20-21 pixel/cm of the image files in gray/color TIFF format. The captured image of about 34 cm core length was transformed into a gray scale/color code curve (density plot) using NIH Image 1.55b5. The density values were calculated as as a mean gray/color code of a defined small horizontal core section (one pixel wide), with a dimension depending on the resolution of the image. Disturbed signals caused by unequalized light conditions were compensated using a statistical function calculated for each core.

With this setup grayscale curves with an amplitude in the range of 0 (white) to 255 (black) density values were obtained. Gray scale values generally reflect the carbonate content of the sediment and thus should be a first approximation of a carbonate curve. The advantage of the image digitizing method is a continuous high resolution record, that could be obtained with conventional carbonate analyses only with tremendous manpower and laboratory costs. The preliminary results of our gray scale logging of five gravity cores are given in Fig. 1-3. Within five cores the grayscale curves closely match and significantly improve the low resolution shipboard carbonate curves shown in the section 'Coring Sites, Core Logs, and Initial Core Descriptions at SONNE-95 Cruise' (this vol.).

The attempt to produce a color logging curve failed due to non-reproducibility of color images under the system conditions. Reynaud (1992) used only a single color channel, which was defined using a color separation software such as Adobe Photoshop. This method can be applied to digitize monochrome signals (red-green-blue) which may provide further information on composition and oxygenation state of the sediments.

REFERENCE:

Reynaud, J.-Y., 1992. Mesures de Reflectance des carottes Paleocinat II Methode et Perspectives. In: Labeyrie, L. (ed): PALEOCINAT II, Rapport Préliminaire, (CNRS).

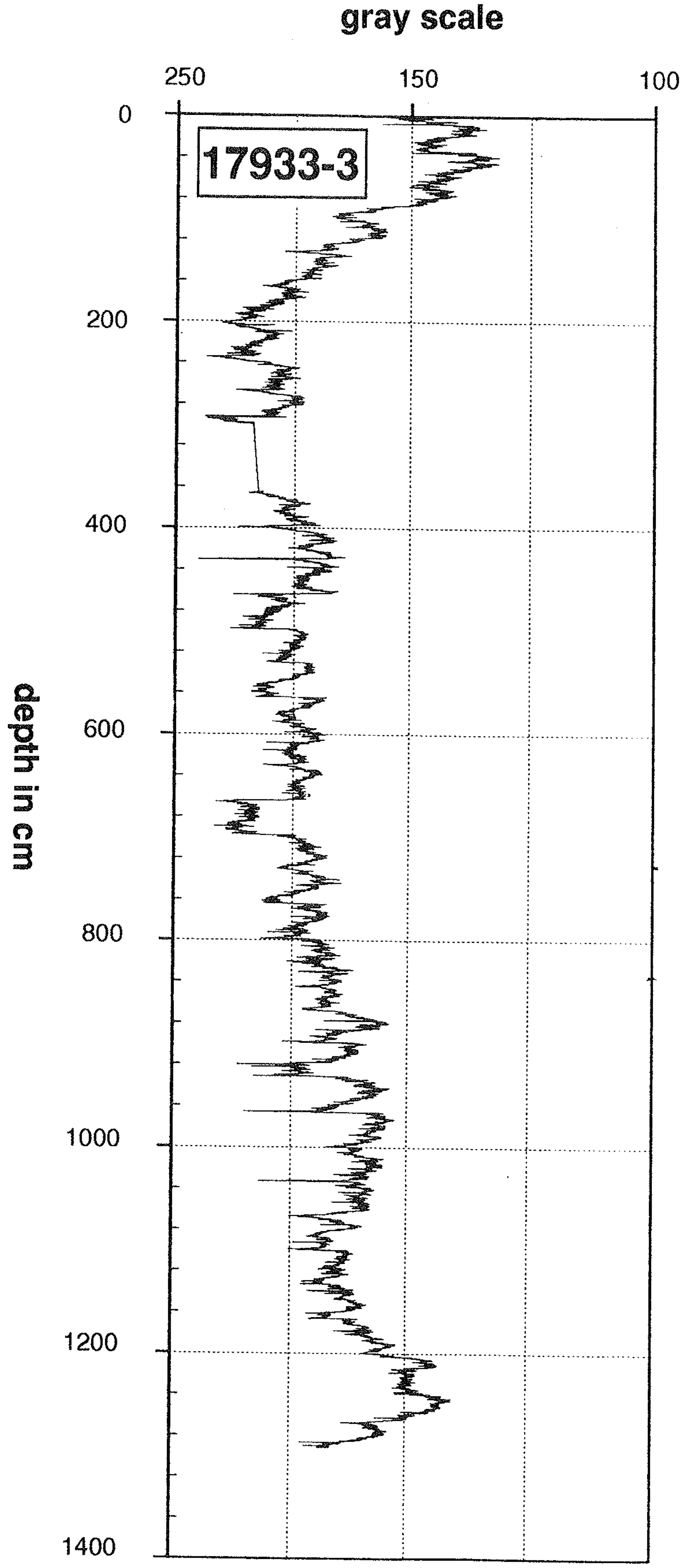

Figure 1a-c. Gray scale curves of cores 17933-3, 17936-2, 17937-2, 17940-2, and 17941-2. Gray code plotted as density values. Low values largely correspond to high carbonate concentrations.

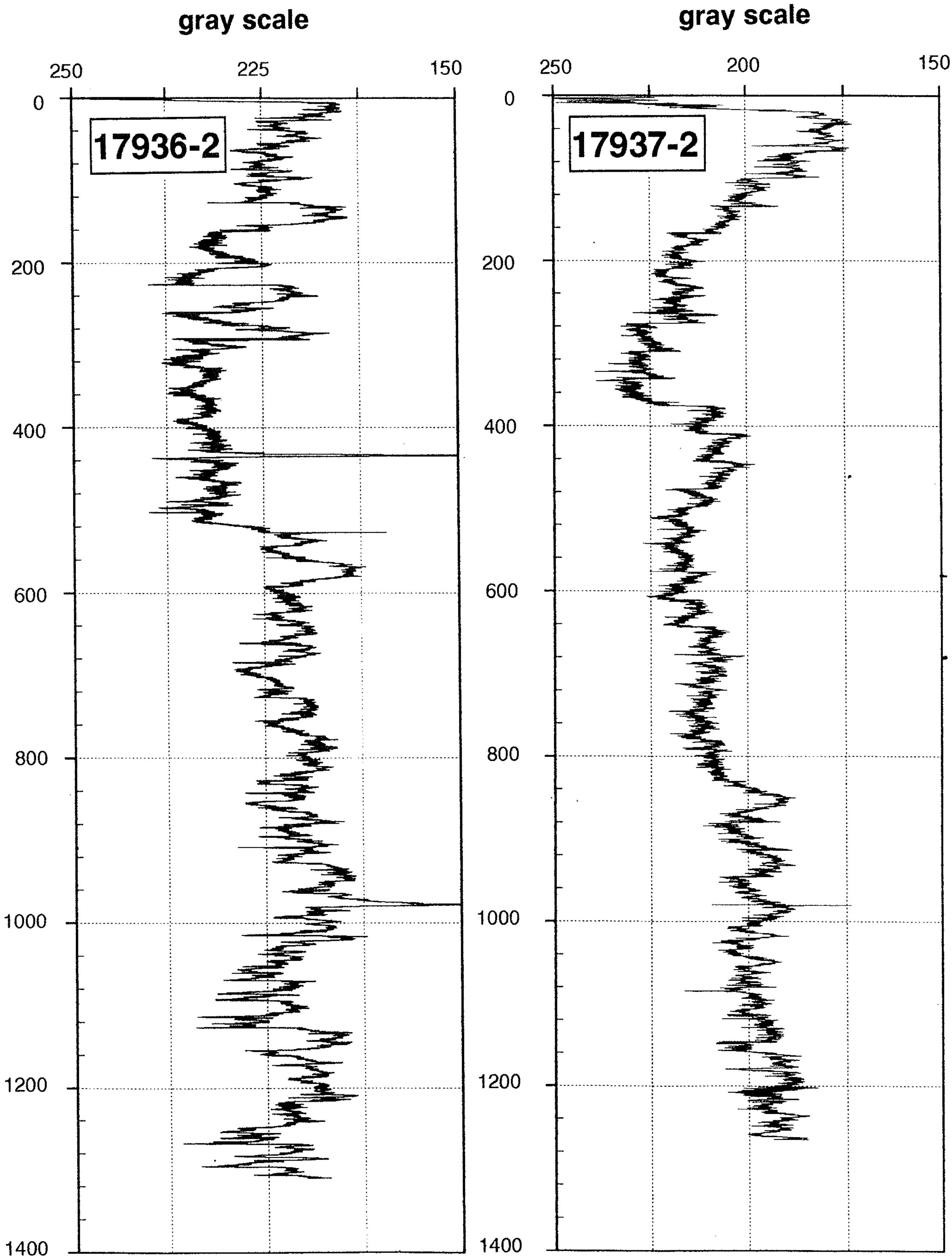

Figure 1a-c. Continued

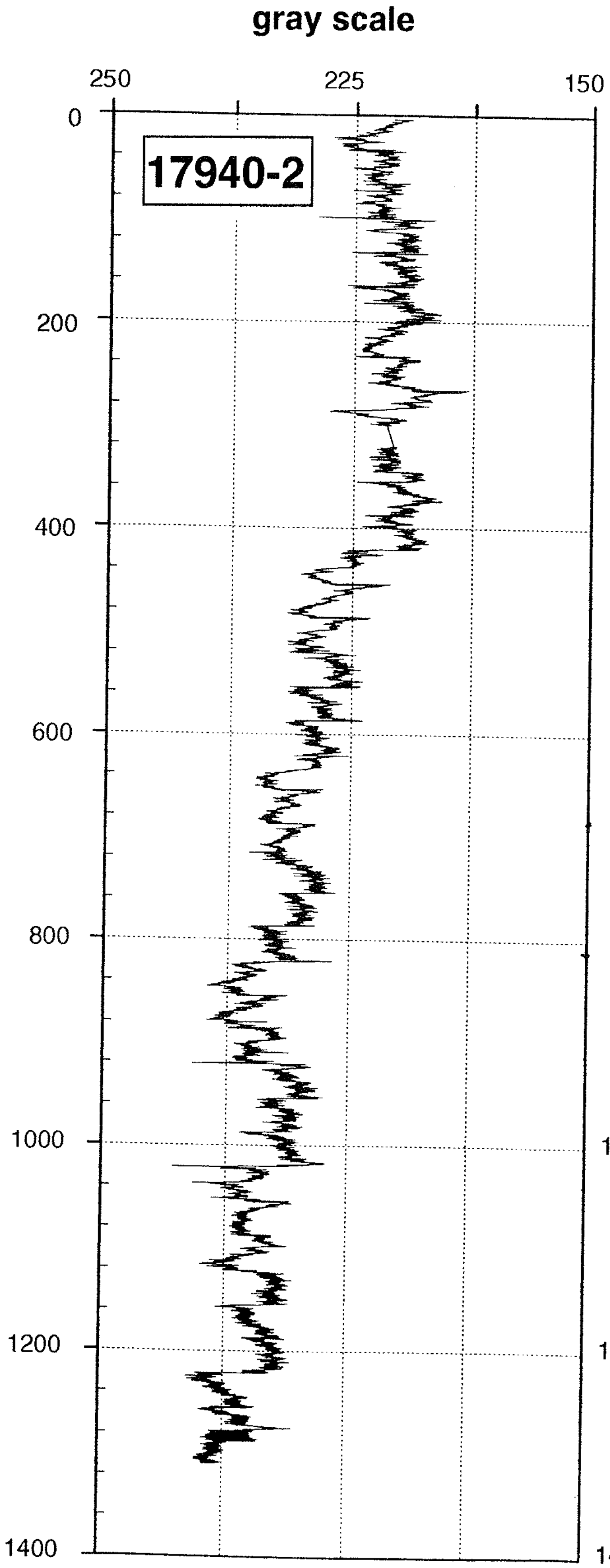

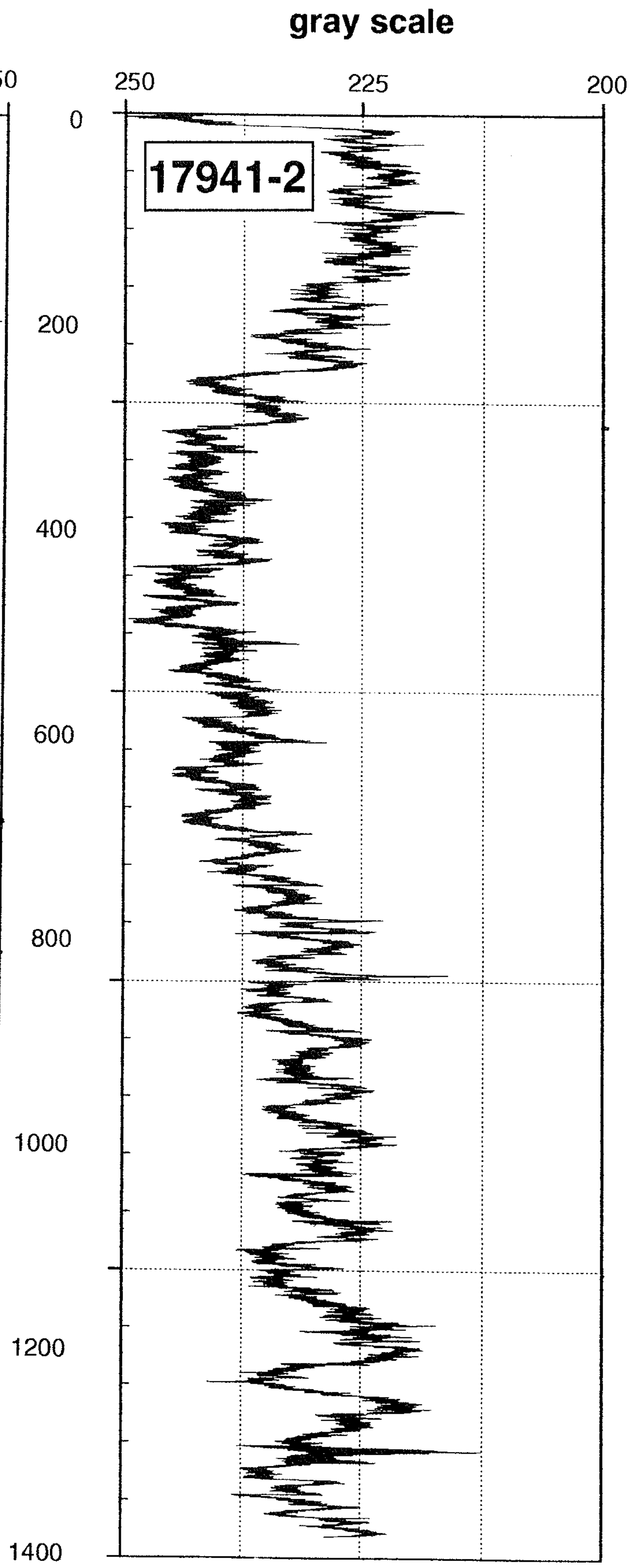

Figure 1a-c. Continued

2.6 BOX CORE HANDLING AND SAMPLING ON SONNE-95 CRUISE

W. Kuhnt[1], R. Botz[1], S. Heilig[1], E. Heinrich[1], H. Hensch[1], S. Hess[1], Z. Jian[2], K. Kißling[1], B. Lu[3], J. Villanueva[4], P.X. Wang[2], and L. Zheng[5]

([1] GPI Kiel, [2] TJU Tongji, [3] SCSI Guangzhou, [4] CID-CSIC Barcelona, [5] SOA Hangzhou)

Immediately after the box cores arrived on the deck of RV Sonne, temperature of the sediment 5 cm below surface and of the seawater in the box corer were measured using an AMA-digit AD 30TH precision digital thermometer with a 0.1 °C precision. The sediment temperatures were generally consistent and provided a reasonable estimate of bottom water temperatures. However, the water temperatures in the box corer were strongly fluctuating and generally at least 10°C higher than the sediment temperatures, indicating a significant water flow into the closed box corer during the hauling.

After the temperature measurement the sediment surface was fixed with a plastic frame and the sediment box removed from the coring device. Seawater was carefully sucked off and filtered over a 63µm sieve to save floating epifaunal organisms such as small komokiaceans (fragile agglutinating foraminifera living at the water-sediment interface) and benthic foraminifera that live within the fluffy layer above the sediment surface.

The morphology and composition of the sediment surface was described and the fluffy organic material in the remaining seawater above the sediment surface was sampled. The sediment surface was carefully surveyed for epifaunal benthic foraminifera. Large agglutinating forms were sampled, counted, examined, and partly photographed on board ship. Especially the occurrence of suspension feeding erect agglutinating foraminifers in life position such as *Saccorhiza ramosa* is regarded as a useful indicator of lateral transport of organic material by bottom currents.

The subsamples listed in Table1 were removed from the sediment surface.

The sampling of box cores was carried out according to the scheme of Fig. 1.

Sampling the surface distribution of benthic foraminifera:

Four metal frames of 10 x 10 cm size (A-D in the sampling scheme) were placed on the sediment surface according to morphologic and sedimentologic features to obtain subsamples of as many varieties of substrates as possible. Position of the frames was noted in a small sketch map and peculiarities of the different sample positions were noted if appropriate.

Selection criteria of the sampling positions included surface morphology (samples from small elevations, mounds, and "pools"), substrate (muddy depressions vs. winnowed areas on small scale sediment ridges), and areas with and without concentrations of organic fluff.

Table 1. Subsamples removed from the sediment surface (*samples were kept cool, ** samples were immediately preserved in a seawater - methanol - Rose Bengal solution)

working group	*amount*	*purpose*
Calvert*	5cc	geochemistry
Villanueva*	3cc	organic tracers (sampled in glass phials with aluminum tops)
Tang	2x5cc	organic tracers
Wang, LJ/Sarnthein**	100cc	stable isotopes
Lin, HL	10cc	CdCa, orbulinas, opal
Lu Jun	5cc	diatoms
Pflaumann	5cc	planktic foraminifers
Wiesner*	100cc	sedimentology
Wang, PX/Liang JM**	100cc	foraminifers and pteropodes
Zheng, LF/Zhou HY	50cc	clay minerals, trace elements
Hess/Kuhnt**	4x100cc	benthic foraminiferal distribution
v.d.Paverd	10cc	radiolarians
Wang LJ/Sarnthein	20cc	sedimentology
Sun, XJ	25cc	pollen
Calvert*	3cc	fluff sample

Downcore sampling:

Pushcores of 10 (benthic foraminifera) and 12 cm diameter (archive) were pushed into the sediment, using a hand-hold piston to avoid extreme compaction. Compaction was measured at the sediment surface (difference of the position of the sediment surface within the push core and the box corer) to allow a better correlation of the downcore distribution of benthic foraminifera to the observed sedimentological features at the opened side of the box corer. At each core transect one 5 cm tube was collected for physical properties studies at SOA Guangzhou (working group Lu Bo).

Downcore sampling:

Pushcores of 10 (benthic foraminifera) and 12 cm diameter (archive) were pushed into the sediment, using a hand-hold piston to avoid extreme compaction. Compaction was measured at the sediment surface (difference of the position of the sediment surface within the push core and the box corer) to allow a better correlation of the downcore distribution of benthic foraminifera to the observed sedimentological features at the opened side of the box corer. At each core transect one 5 cm tube was collected for physical properties studies at SOA Guangzhou (working group Lu Bo).

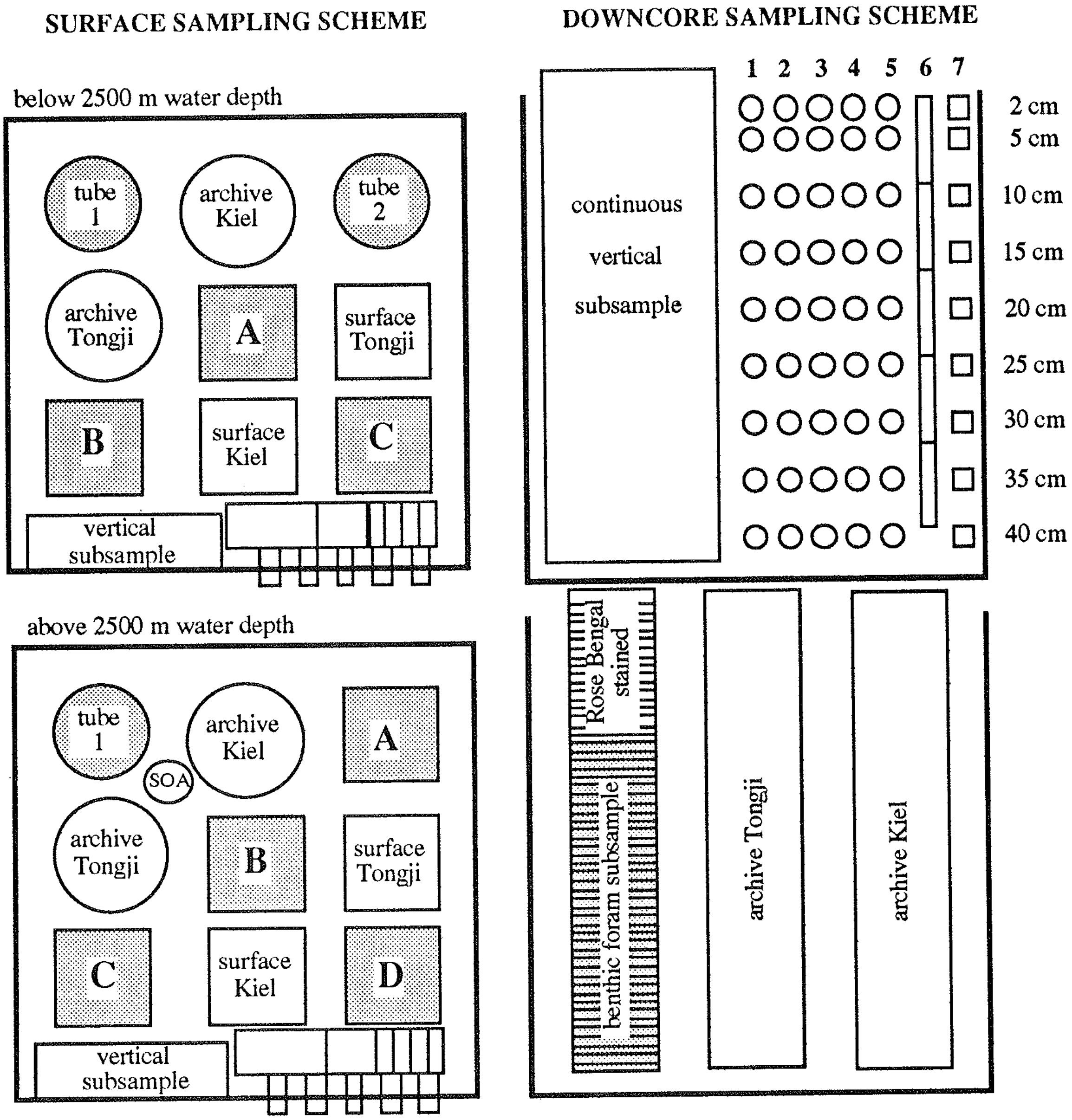

Fig. 1: Box core sampling scheme during cruise Sonne 95 (for explanation of numbers and capital letters see text):

The pushcores taken for examination of the downcore distribution of living/dead benthic foraminifera were cut into 1 cm thick slices immediately after sampling. Each 80cc subsample was immediately preserved in a methanol-seawater solution and samples from the uppermost 15 cm of the sediment column were treated with Rose Bengal to stain organisms that were alive at the time of collection. A number of samples were washed over a 63µm sieve in the shipboard laboratory for rapid examination and split into equal parts for representative counts using the "Scott and Hermelin" wet-splitter.

After surface and push core sampling of the box cores the front of the metal frame was removed and the sediment profile was photographed and described. Special attention was given to changes in sediment colors, position of the redox boundary, and bioturbation features. After description the vertical profile was sampled in 5cm intervals using 5cc and 10cc syringes and glas phials for organic tracer samples. A set of homogenized continuous samples for U/Th analyses was collected in 7.5cm increments using a half tube of 2 cm diameter. Part of the vertical profile was cut out with a brick-shaped plastic box (50 x 20 x 10 cm) as an additional archive core that will be used for X-ray photographs of bioturbational structures.

Sets of vertical samples are used for the following investigations (samples with an asterisk were kept cool):

working group	*amount*	*purpose*
1. Calvert*	5cc	geochemistry
2. Wang, LJ/Sarnthein	10cc	physical properties, stable isotopes
3. Lu Jun	5cc	diatoms
4. Pflaumann	5cc	planktic foraminifers
5. Chen, MP	10cc	biochem. tracers, nannoplankton
6. Botz	7.5 cm half-tubes	U/Th
7. Villanueva*	5cc	organic tracers (sampled in glass phials with aluminum tops)

2.7 GRAVITY AND PISTON CORES: DESCRIPTION AND SAMPLING SCHEMES ON SONNE-95 CRUISE

M. Sarnthein, Univ. of Kiel, and the Shipboard Scientific Party *

* Botz, R.[1], Calvert, S.[2], Chen MP Ph[3], Heilig, S.[1], Heinrich, E.[1], Hensch, H.[1], Hess, S.[1], Jian, Z.[4], Kienast, M.[1], Kissling, K.[1], Kuhnt, W.[1], Lu, B.[5], Mühlhan, N.[1], Pflaumann, U.[1], Rehder, W.[1], Staubwasser, M.[1], Villanueva, J.[6], M., Wang, LJ[1], Wang, PX[4], Wiesner, M.[7], Zheng, L.[8]

1 GPI Kiel, 2 DOV Vancouver, 3 NTU Taiwan, 4 TJU Shanghai, 5 SCSI Guangzhou, 6 CID-CSIC Barcelona, 2 IfBM Hamburg, 8 SOA Hangzhou

The processing of gravity and piston cores was accomplished by following the procedures established on numerous international cruise projects, in particular, the guidelines and procedures developed by the international Ocean Drilling Program (ODP). The various steps of core processing are outlined in the following text:

- As soon as cores were retrieved on deck and had warmed to air temperature, they were carefully labelled and cut into sections of 1 m length or less. Each section was sealed at the top and bottom by a plastic cap. Core catcher samples were carefully packed separately.

- Magnetic susceptibility logging at uncut core sections (see separate section).

- Longitudinal splitting of cores sections by a duplicate vibration saw and a catgut into "working" and "archive" halves, the latter halves serving for all kinds of future continuous downcore measurements and future sampling once the working halves will be used up.

- Gray code / color code logging of the archive halves (see separate section).

- Short visual description of core disturbancies, sediment structures, etc. in the working halves (S. Calvert, U. Pflaumann, L.J. Wang).

- The working half of each core section was sampled by means of 5cc and 10 cc syringes (with cut-up frontal parts) at 5 and 10-cm intervals for numerous specific scientific projects that were proposed by the members of the Shipboard Scientific Party for each core site. Additional samples were removed for a number of projects proposed by shore-based colleagues (Table 1). Standard sampling of each core comprised samples for physical properties (5 cc/10cm) and stable isotope stratigraphy (10cc/10 cm) to provide a common stratigraphic framework for the scientific party. Special samples of ash layers were removed by small plastic boxes taking half the diameter of a working half. Altogether, more than 30,000 syringe samples were removed, labelled, catalogued, and stored on board of SONNE-95 cruise. Records of all samples are kept at the Geologisch-Paläontologisches Institut of Kiel University.

- Only few cores remained unsampled. These cores belong to sites where duplicate cores were recovered for Tongji University (sites 17931, 17954, 17962) and to the last sites of the cruise, where no more sampling containers were left on board (sites 17963-17965).

- Working and archive halves were preserved in D-tubes and are stored at the core repository of the Geologisch-Paläontologisches Institut of Kiel University.

- Additional and more closely spaced sampling of the cores (working halves) is restricted to the Shipboard Scientific Party until the end of September 1995.

Table 1. Samples removed from gravity and piston cores

CF	Benth. and pla.forams, nannos and Pteropods (occasionally plus further 5 cc)	**10 cc**	at 5 cm spacings	Shanghai /Hangzhou
IO	Inorg. geochem. isotopes	**10 cc**	10cm	Vancouver
	Cores in areas 1-4, 2 cores in areas 5-7 and 9-11 each, below 3000 m w.d.			
KE	Ketones, etc. biochem. tracers	**5 cc**	10cm	Barcelona
OP	Cd/Ca and biogenic opal	**10 cc**	10cm	Kaoshiung
	Cores in areas 1-4 and one core in area 7			
TAI	Geochem, nannos	**10 cc**	10cm	Taipeh
	Cores in areas 9-10-11			
PF	Planktonic forams	**5 cc**	10cm	Kiel
PL	Pollen and phytoplankton	**20 cc**	10cm	Beijing
	Core 17945			
RD	Rads.,	**5/10 cc**	10cm	Amsterdam
	In areas 1-4: at >2000 m w.d., 1 core in areas 5-11 each			
SE	Grain-sizes and clay mins.	**10cc**	10cm	Kiel
	Few reference cores near river mouths			
TE	Clays and trace elems	**2x5 cc**	10cm	Hangzhou
	2-3 cores below 2500 m in areas 4, 6, 7 each			
CH	Organic geochem.	**2x5 cc**	10cm	Hangzhou
	2-3 cores below 2500 m in areas 4, 6, 7 each			
DI	Diatoms	**5 cc**	10cm	Guangzhou
	Selected cores in areas 4, 6, 7, 11			
UT	U/Th dating	**vert. u-rails**		Kiel
	1 selected core at >3500 m w.d.			
MIN	Diagenesis of hard layers	**spec. profiles**		Kiel
	Few selected cases		(2 cm wide)	

3. PRELIMINARY RESULTS OF SONNE-95 CRUISE

3.1 SEISMIC REFLECTION PROFILING AT THE NORTHERN CONTINENTAL MARGIN OF THE SOUTH CHINA SEA (SONNE-95 CRUISE)

H. K. Wong, T. Lüdmann and M. Wollschläger (Institute of Biogeochemistry and Marine Chemistry, Hamburg University)

1. METHODS AND STRATEGY

Introduction

Within the framework of the Project "Sedimentation processes in the South China Sea: seismic stratigraphy and sediment trap experiments" funded by the German Federal Ministry of Research and Technology (BMFT Project 03G0095A) 2972 km of shallow reflection seismic profiles (Table S1) were obtained at the northern continental margin of the South China Sea by the Institute of Biogeochemistry and Marine Chemistry of Hamburg University during legs 1 and 2 of cruise SO-95 of the R/V Sonne (April-May, 1994). The area studied is located between Pratas Island and the Taiwan Banks and includes parts of the continental shelf, slope and abyssal plain (Figure S1). Structurally, it belongs to the northeastern margin of the Pearl River Mouth Basin, which is a southwest-northeast striking feature extending from Hainan Island to the southwestern extremity of the Strait of Taiwan. This basin is also part of a system of uppermost Mesozoic oil- and gas-bearing sedimentary basins on the Chinese continental margin, to which the Beibu Gulf, Zingge and Southwest Taiwan Basins also belong. It is approximately 800 km x 100-300 km in dimension, being elongated in its direction of strike. It covers an area of 147,000 km^2 (Guong et al., 1989), and can be divided into three subbasins (Zhu 1, Zhu 2 and Zhu 3 respectively) separated by local highs (Hainan, Wanshan, Shengu, Central and Weitan Highs; Yu, 1990). The sediment thickness reaches 10 km within the deepest parts of the basins.

The Pearl River Mouth Basin is an epicontinental rift basin. It developed largely on continental crust except in the vicinity of the continent-ocean transition zone (Guong et al., 1989; Li, 1984; Wang et al., 1992). The crustal thickness of the northern continental margin of the South China Sea decreases from north to south. It ranges from 28-30 km in the Guangdong coastal area, 24-26 km in the Zhu 1 and Zhu 3 basins, 16-20 km in the Zhu 2 depression, 20-24 km at the Dongsha High, to 5-9 km typical of the oceanic crust at the abyssal plain (Feng and Miao, 1982). 23 boreholes have been drilled into granite, diorite and quartz porphyry with isotopic ages between 70-130 m.y., documenting that emplacement of these rocks occurred during the late Yenshanian movements (Feng and Zheng, 1983; Guong et al., 1989; Qiu et al., 1991). They are part of the Yenshanian igneous zone which strikes northeast along the continental margin (Zhu 1-Central

Uplift-Zhu 3) and lie to the northeast of the Yenshan fold belt (Weitan Uplift-Zhu 2-Shenghu Uplift; Jin et al., 1992).

The geological evolution of the Pearl River Mouth Basin can be divided into three major episodes (Feng and Zheng, 1983; Guong et al., 1989):

(1) the formation of a rift valley in the Early Tertiary;
(2) faulting and subsidence (sagging) from the Late Oligocene to the Early Miocene; and
(3) subsidence since the Middle Miocene.

The purpose of the reflection seismic profiling work during cruise SO-95 is fourfold:

(1) characterisation of the depo-environment (deposition, non-deposition, sediment reworking and redistribution, and erosion) of the northwestern continental margin of the South China Sea;

(2) examination of the distribution of sedimentary units as well as their thickness, external geometry and internal configuration by means of seismic sequence analysis, and reconstruction of the paleo-depositional environment by means of seismic facies analysis. In particular, the facies units mapped during cruises SO-50B and SO-72A should be extended in the northeasterly direction;

(3) mapping of the regional fault system in order to estimate the influence of tectonic processes (in particular those that lead to sea level changes) on sedimentation; and

(4) evaluation of the role of the different mechanisms of sedimentation and sediment transport, including mass transport processes (e.g., sliding, slumping and turbidity flows due to sediment instabilities) and pelagic sedimentation, as well as their controlling factors.

Methods

A basic tool for the interpretation of seismic data is the concept of seismic stratigraphy. Reflections from the subsurface generated at sedimentary or structural interfaces with a significant change in acoustic impedance can be classified according to their external geometries, termination patterns (onlap, offlap etc.) and internal reflection configurations. Each succession of relatively conformable reflectors bounded at its top and base by unconformities or their correlative conformities is interpreted to correspond to a depositional sequence. Such a sequence is chronostratigraphically significant because it is deposited during a given interval of geologic time defined by ages of the sequence boundaries. Differences in internal reflection configuration, amplitude, continuity and frequency content between sequences suggest changes in the seismic facies, and these are attributed to changes in the depo-environment. Thus, seismo-stratigraphic interpretations provide an important tool for the reconstruction of the paleo-environment of an area.

The high-resolution reflection seismic system used during cruise SO-95 to obtain profiles for seismo-stratigraphic analysis consisted of:

(1) three Geco Prakla air guns and one S.S.I. GI-gun with a total volume of 8.7 *l* (1.2, 1.6, 2.5 and 3.4 *l* respectively). This array was towed behind the ship and triggered at 25 m intervals along the profile with pulses generated by the ship's Krupp-Atlas integrated navigation system;

(2) a Geco Prakla 8-channel mini-streamer for the reception of the seismic signal. Each active channel had a length of 12.5 m. The source-, receiver- and CMP-pattern is shown in Fig. S2;

(3) a multi-channel digital data aquisition system, and

(4) two single-channel recording systems for quality control.

On the one hand, signals from the eight channels were separately digitised via a PC-based A/D converter board, multiplexed, and written onto high capaticy Exabyte tapes. In the laboratory, the data will be demultiplexed and rewritten in the standard SEGY format. They will then be processed using our SEISTRIX 3 seismic processing software. The processing steps include sorting, digital filtering, muting, trace editing, NMO-correction, stacking, deconvolution and migration. On the other hand, the incoming analog signals from the different channels of the streamer were summed, amplified, bandpass filtered (15-500 Hz), and are recorded on a DAT-tape for further processing as well as displayed online on a EPC 4800 graphic recorder.

The shipboard high resolution sediment echosounder system (Parasound) operated concomitantly with our reflection seismic profiling system. The data were recorded on a graphic recorder and will be used for a seismo-stratigraphic interpretation of the uppermost sedimentary layers.

Strategy

The seismic profiles were planned to run across strike, i.e., in a generally northwest-southeast direction. They extend the survey area of Sonne cruise SO-72A to the northeast with an overlap so that the new profiles can be correlated to the old data. As many strike-parallel profiles as time permitted were also run to permit a correlation of the across-strike profiles and to enable a crude 3-dimensional view of the sedimentary structures.

2. PRELIMINARY RESULTS

Because processing of our 8-channel digital seismic data can only take place after our equipment is shipped back to Hamburg and because of the lack of time, the following discussion on preliminary results is based solely on a cursory inspection of the (summed) single-channel registration for quality control and must be considered speculative.

Most of the Tertiary sequences in the Pearl River Mouth Basin are terrigenous clastics. The fault-bounded, synrift megasequence below the breakup unconformity is non-marine, and the overlying postrift megasequence grades upward from fluvial deposits to deltaic and marine sequences. Preliminary results of the cruises SO-50B and SO-72A show that recent sedimentation here is dominated by the accumulation of fluvial sediments on the inner shelf and estuary of the Pearl River (Gaedicke et al., 1992; Wong, 1993). The outer shelf and upper slope are regions of sediment bypass and erosion triggered by strong bottom currents. Mass wasting processes such as slumping and sliding characterise the lower slope.

A preliminary interpretation of our seismic data indicates that the observations of the previous cruises apply to the overlapping area of the SO-95 cruise.

A part of profile 7 (Figure S3) penetrated a thick column of folded and faulted strata located on the transition zone between the upper and lower slopes within a water depth of 1,300 to 1,600 m. Here the uppermost layers terminate with offlap at the seafloor. This could be due to subsidence of the slope and tilting of the upper strata, accompanied by erosion of the topmost layers.

Profile 8 (Figure S4) shows the transition between the slope and the basin floor where pelagic sediments alternate with turbiditic material from the slope to form a thick basin fill megasequence. This alternation is evidenced by contrasting reflection configurations, parts of which are subparallel and continuous, while other parts exhibit subparallel, discontinuous to hummocky configurations. A nearly seismically transparent region within the basin may be attributed to a magmatic intrusion. Circulation of hydrothermal water might have infiltrated the surrounding strata, changing the acoustic properties of the material. The upper layers of the basin floor terminate with basinward offlap. They are partly eroded by deepsea currents or may be truncated by sediment sliding. A small basin is trapped behind a faulted basement block.

Profile 20 (Figures S5 and S6) striking parallel to the continental slope within a water depth of 1,500 to 2,000 m shows abrupt facies changes across faults (Figure S5). Blocks of rotated and tilted strata (Figure S6) suggest that these faults are strike-slip in character. Profile 20 also suggests a compressional stress regime with a compressional direction parallel to the continental margin. Most of the strata are folded in the northeast-southwest direction. Canyons are incised across the continental slope (Figure S5) forming pathways for a rapid basinward transport of the sediments where they accumulate as thick sequences of turbiditic layers.

A first compilation of the preliminary results of cruise SO-95 and the previous cruises (SO-50 and SO-72A) suggests the following basic trends:

(1) Within the study area strong bottom currents have led generally to sediment reworking and erosion on the continental slope and deep basin. Therefore most of the outer shelf and upper slope is covered by relict sediments without or with only a thin veneer of Holocene deposits.

(2) The number of channels cut into the slope increases in northeasterly direction. This is accompanied by an obvious increase in transpressional stress within the slope sediments.

(3) In the northeastern part of the study area, the strata are folded and are intersected by strike-slip faults striking perpendicular to the continental margin.

REFERENCES

Feng, Z. and W. Miao (1982): The geological structures and the oil and gas potential of Zhujiangkou basin, the South China Sea. - Exp. Petr. Geol., 4(1), 19-25.

Feng, Z. and W. Zheng (1983): Tectonic evolution of Zhujiangkou (Pearl River Mouth) basin and origin of South China Sea. - Acta Geologica Sinica, 3, 212-222.

Gaedicke, C., H. K. Wong and Y. Liang (1992): Seismic stratigraphy and Holocene sedimentation at the northern margin of the South China Sea. In: Jin, X. L. , H. R. Kudrass and G. Pautot (eds.) Marine Geology and Geophysics of the South China Sea. - Proc. Symposium on Recent Contributions to the Geological History of the South China Sea (China Ocean Press), 21-37.

Guong, Z., Q. Jin, Z. Qui, S. Wang and J. Meng (1989): Geology, tectonics and evolution of the Pearl River Mouth basin. In: Zhu, X. (ed.) Chinese Sedimentary Basins. (Elsevier), 181-196.

Jin, X., H. R. Kudrass and G. Pautot, G. (1992): Marine Geology and Geophysics of the South China Sea. - Proc. Symp. Recent Contributions to the Geological History of the South China Sea. (China Ocean Press, Hangzhou), 266 pp.

Li, Z. (1984): A discussion on the crustal nature of the central and northern parts of South China Sea. - Acta Geophysica Sinica, 27 (2), 153-166.

Qui Y., Q. Wu, X. Ji, J. Li,H. Zhong and Z. Sheng (1991): Meso-Cenozoic taphrogeny and dispersion in the continental margin of southeast China and adjacent seas. - Tectonophysics, 197, 257-269.

Wang, S., T. Xie, S. Wang and L. Liu (1992): Geological characteristics and petroleum potential of sedimentary basins of the China continental shelf. In: Watkins, J. et al. (eds.): Geology and Geophysics of Continental Margins. - Am. Assoc. Petr. Geol. Memoir, 53, 3-16.

Wong, H. K. (ed.) (1993): Quaternary Sedimentation Processes in the South China Sea. - Final Report on Cruise SO-72A of the R/V Sonne. 171 pp.

Yu, H. S. (1990): The Pearl River Mouth Basin: A rift basin and its geodynamic relationship with the southeastern Eurasian margin. - Tectonophysics, 183, 177-186.

Profile #	Point #	Date dd.mm.yy	Time hh:mm	Latitude °:' N	Longitude °:' E	Total Time hh:mm	Total Distance nm	km
03, start	E	22.04.94	11:30	21:28.01	118:30.02	12:15	57	105
03, end	F	22.04.94	23:45	21:28.00	117:30.78			
04, start	F	22.04.94	23:55	21:27.99	117:30.02	25:51	117	217
04, end	G	24.04.94	01:46	20:20.09	115:47.04			
05, start	H	26.04.94	21:33	20:41.04	115:41.96	37:49	160	296
05, end	I	28.04.94	11:22	18:15.04	116:48.63			
06, start	I	28.04.94	13:11	18:15.61	116:53.02	06:12	28	52
06, end	J	28.04.94	19:23	18:36.93	117:10.90			
07, start	J	28.04.94	19:30	18:37.37	117:10.84	32:54	148	274
07, end	K	30.04.94	04:24	20:53.00	116:10.02			
08, start	L	02.05.94	14:57	18:53.10	117:24.96	22:54	104	192
08, end	M	03.05.94	13:51	20:28.07	116:42.88			
09, start	M	03.05.94	16:11	20:30.00	116:46.12	05:37	24	44
09, end	N	03.05.94	21:48	20:30.00	117:12.91			
10, start	N	03.05.94	22:00	20:29.34	117:13.29	17:30	79	147
10, end	O	04.05.94	15:30	19:16.99	117:46.01			
11, start	N	05.05.94	18:40	20:31.19	117:12.46	26:48	123	228
11, end	P	06.05.94	21:28	22:22.84	116:22.06			
12, start	P	06.05.94	21:40	22:23.38	116:22.49	00:33	3	6
12, disruption due to fishing boat activity		06.05.94	22:13	22:23.12	116:23.77			
13, start	Q	07.05.94	01:50	22:38.42	116:48.73	41:41	192	355
13, end	R	08.05.94	19:31	19:47.67	118:11.69			
14, start	R	08.05.94	19:37	19:47.42	118:12.04	07:18	33	61
14, end	S	09.05.94	02:55	20:12.97	118:33.95			
15, start	S	09.05.94	06:40	20:12.20	118:34.44	29:20	132	245
15, end	S'	10.05.94	12:00	22:11.95	117:37.03			
16, start	S'	10.05.94	12:03	22:11.96	117:36.90	17:46	81	150
16, end	T'	11.05.94	05:49	21:28.02	116:25.03			
17, start	T'	11.05.94	07:05	21:28.00	116:24.92	13:32	61	113
17, end	U'	11.05.94	20:37	21:28.00	117:29.99			
18, start	U'	11.05.94	20:37	21:28.00	117:29.99	12:09	58	108
18, end	V'	12.05.94	08:46	21:58.94	118:18.92			
19, start	V'	12.05.94	08:55	21:58.78	118:19.14	07:32	33	61
19, end	E	12.05.94	16:27	21:28.07	118:29.96			
20, start	E	13.05.94	09:40	21:10.83	118:16.67	37:32	72	318
20, end	W	14.05.94	23:12	18:54.00	116:31.00			
					total:	**355:13**	**1605**	**2972**

Table S1: Listing of all Seismic Profiles during Sonne cruise SO-95. The profile and point numbers refer to the cruises track shown in Figure S1. The positions and all relating data were obtained from the ships' GPS.

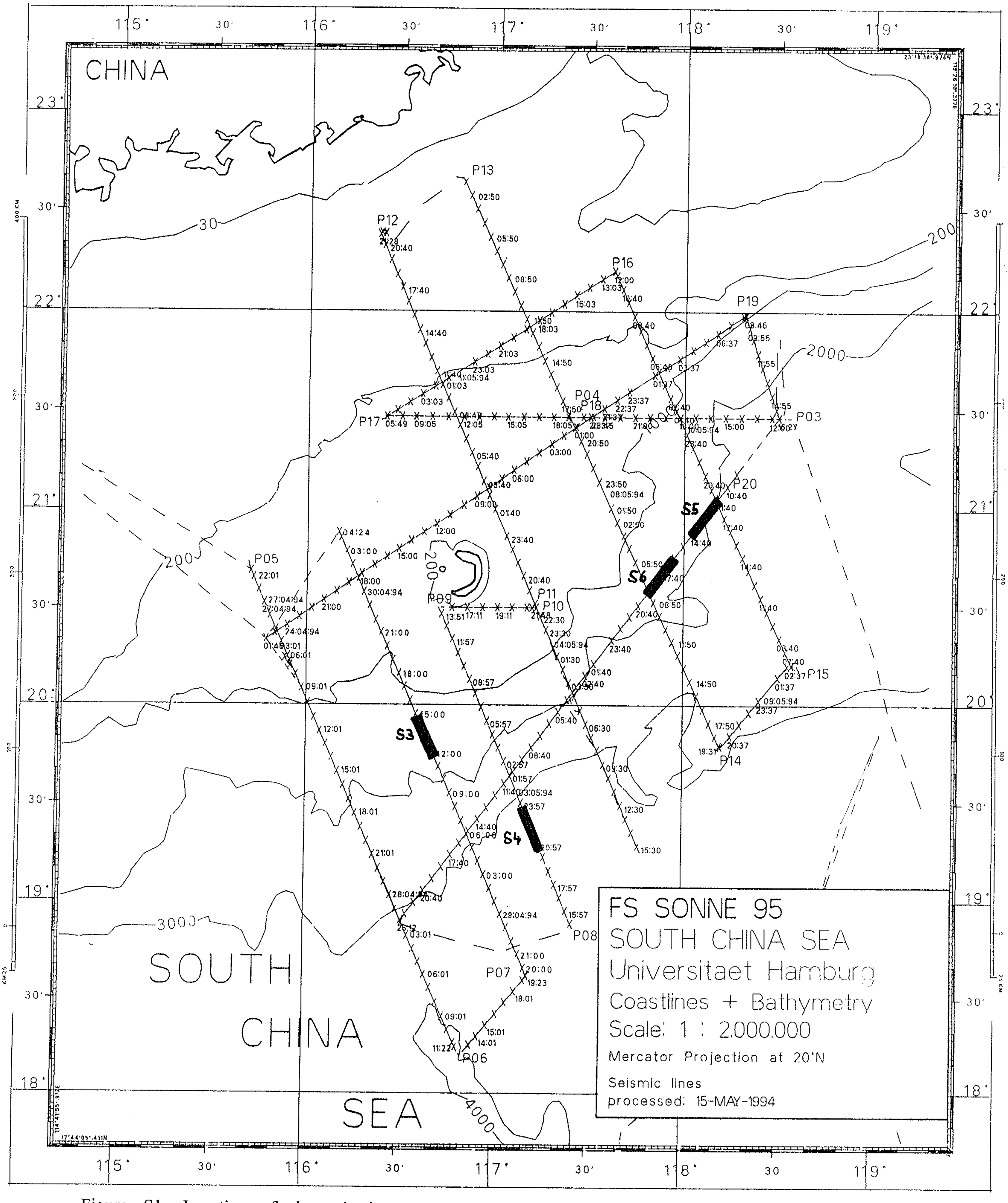

Figure S1: Location of the seismic survey area of cruise SO-95. Profilenumbers are marked at the start of each profile. The examples S3-S6 of this report are marked with bold lines and the relating figure number. The small numbers indicate the UTC-times of the survey.

Station #	**1**	**2**	**3**	**4**	**5**	**6**	**7**	**8**	**9**	**10**	**11**	**12**	**13**	**14**	**15**	**16**	**17**	**18**	**19**	**20**	**21**	**22**	**23**	**24**
Distance (m)	**0**	**12.5**	**25**	**37.5**	**50**	**62.5**	**75**	**87.5**	**100**	**112.5**	**125**	**137.5**	**150**	**162.5**	**175**	**187.5**	**200**	**212.5**	**225**	**237.5**	**250**	**262.5**	**275**	**287.5**
1. Record Channel #	8	7	6	5	4	3	2	1								Shot 1								
CMP #										1 2	3 4	5 6	7 8											
2. Record Channel #			8	7	6	5	4	3	2	1								Shot 2						
CMP #												5 6	7 8	9 10	11 12									
3. Record Channel #					8	7	6	5	4	3	2	1								Shot 3				
CMP #														9 10	11 12	13 14	15 16							
4. Record Channel #							8	7	6	5	4	3	2	1								Shot 4		
CMP #																13 14	15 16	17 18	19 20					
5. Record Channel #									8	7	6	5	4	3	2	1								Shot 5
CMP #																		17 18	19 20	21 22	23 24			

etc

Figure S2: The shot-, receiver- and Common-Mid-Point (CMP) -pattern of the seismic survey. The shot-to-shot-distance was 25 m, the receiver-to-receiver-distance 12.5 m and the CMP-to-CMP-distance 6.25 m. The whole system was moving with a speed of 4.5 knots (8.3 km/h) hence a seismic record was taken every 11 seconds. The coverage of the profiles CMPs is 2-fold.

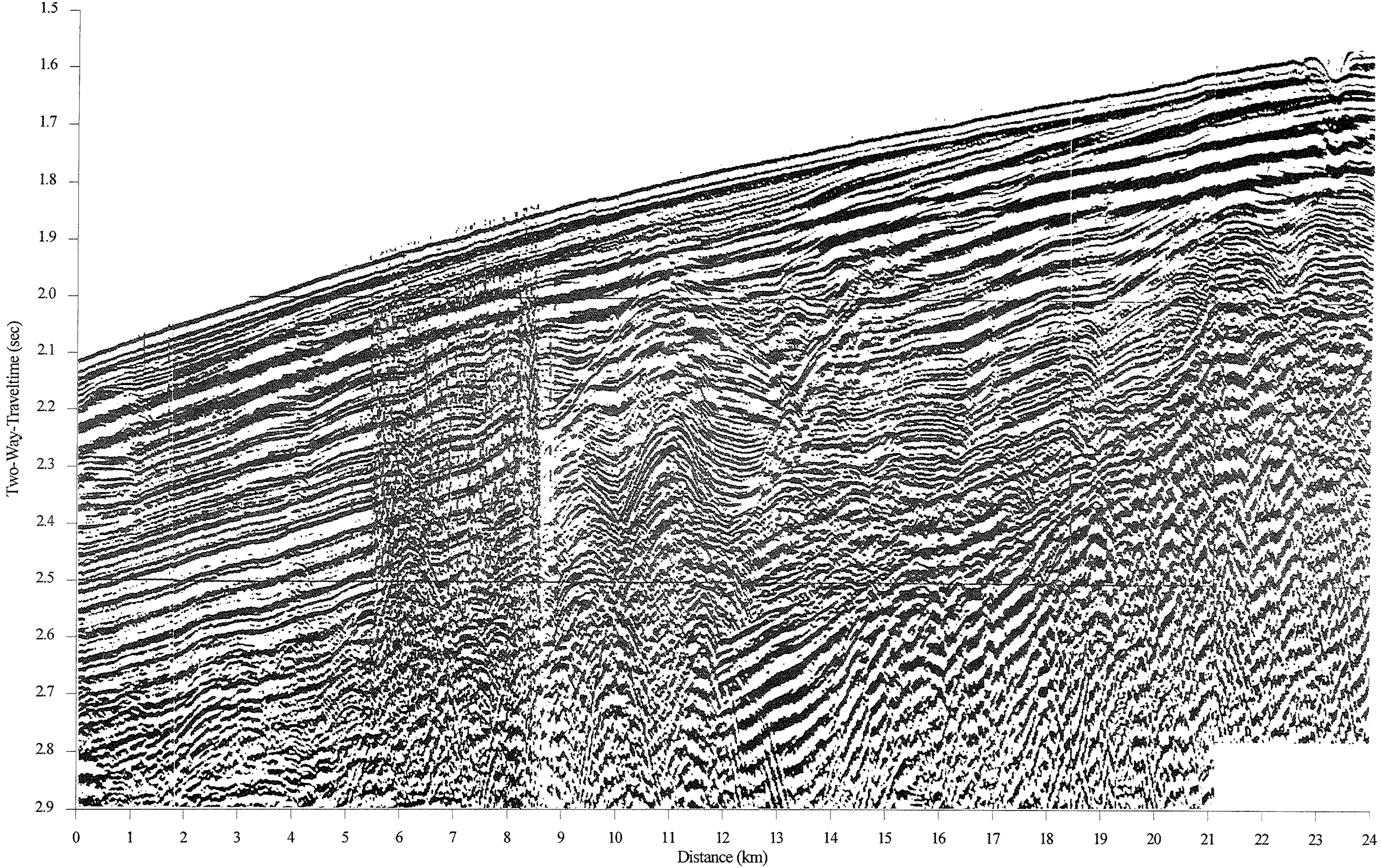

Figure S3: Part of profile P07 showing a thick column of folded and faulted sediments. Waterdepth at 2 sec TWT is 1500 m (see figure S1 for location).

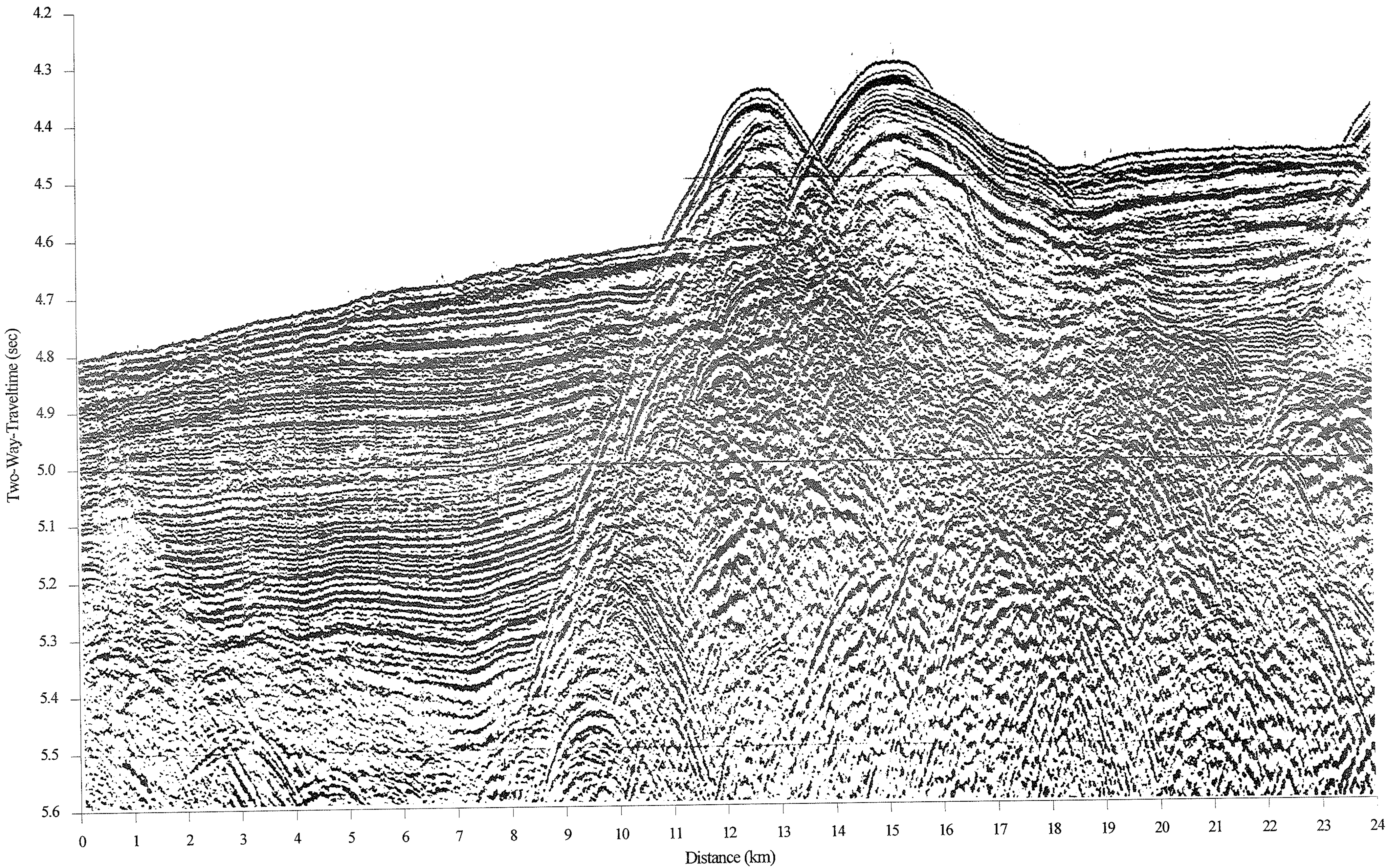

Figure S4: Part of profile P08 showing pelagic sediments alternating with turbiditic material at the transition between slope and basin floor. Waterdepth at 4.5 sec TWT is 3375 m (see figure S1 for location).

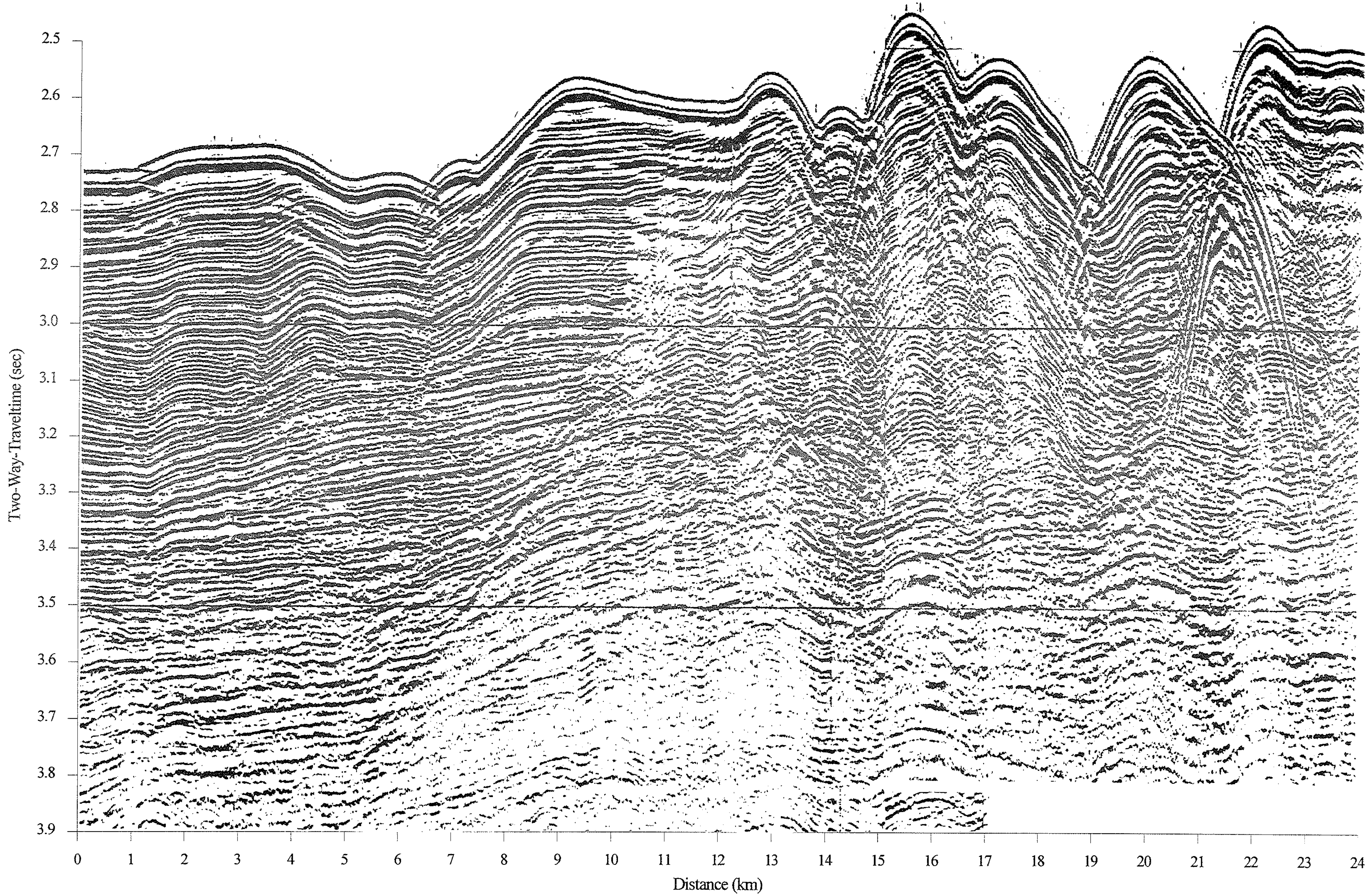

Figure S5: Part of profile P20 showing abrupt facies changes and incised canyons across the continental slope. Waterdepth at 2.5 sec TWT is 1875 m (see figure S1 for location).

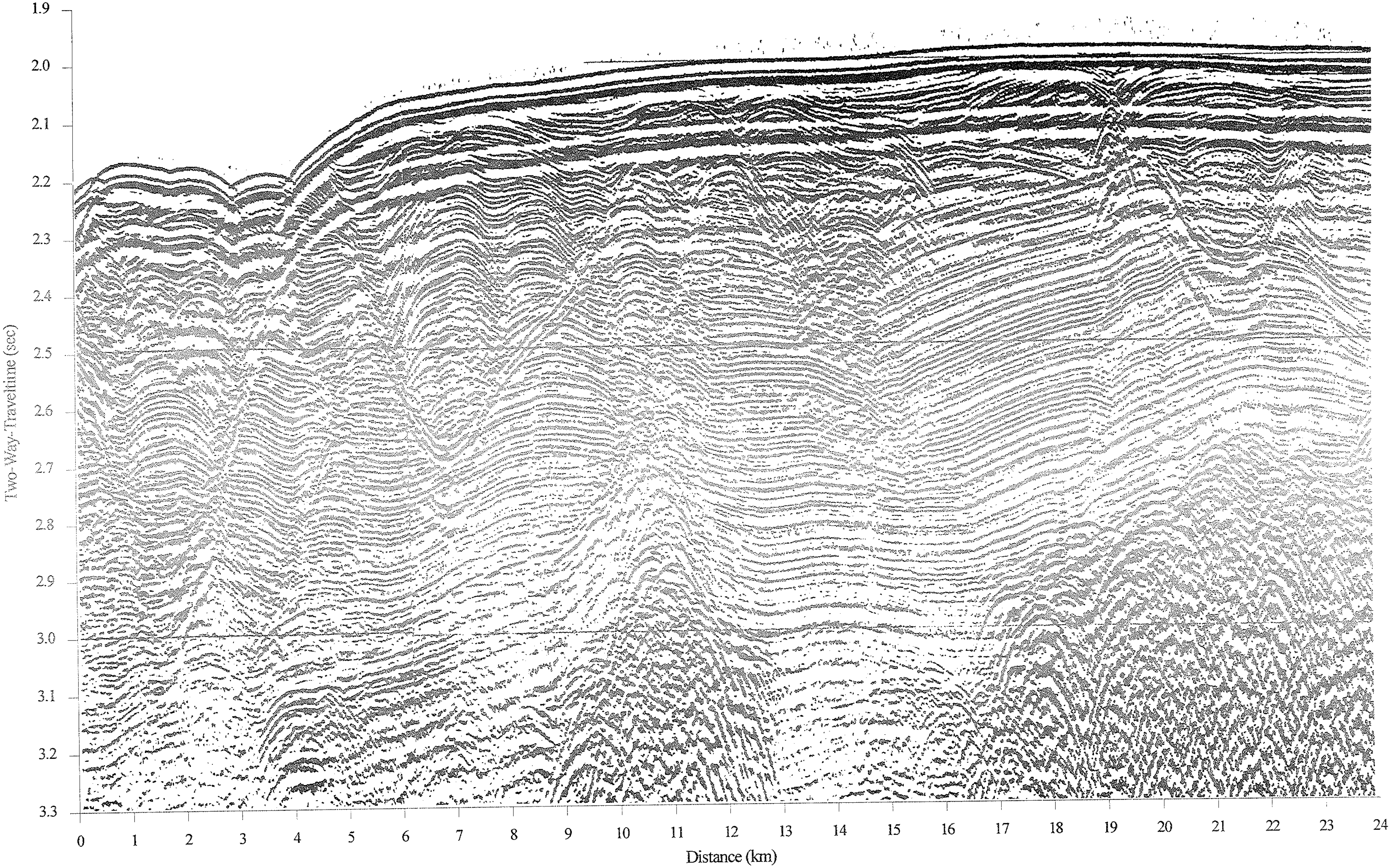

Figure S6: Part of profile p20 showing blocks of rotated and tilted strata on the continental slope. Waterdepth at 2 sec TWT is 1500 m (see figure S1 for location).

3.2 HYDROSWEEP BATHYMETRIC CHARTS FROM SONNE-95 CRUISE

M. Sarnthein (University of Kiel)

HYDROSWEEP is an electronic 3D bathymetric mapping system established on board of RV SONNE (Krupp-Atlas Elektronik GmbH., Bremen). This system is important for the positioning of the RV SONNE at small-scale core locations, moreover, for a careful selection of the trap positions. No systematic bathymetric survey of the South China Sea was run on this cruise. Only in few areas (listed below) did the track lines result in a more coherent bathymetric pattern of general interest:

1. In the seismic survey area along the continental margin of South China (not depicted in this report; for track lines see Wong et al., this volume).

2. The continental slope south of Hongkong, near 18° 15'N (Fig. 1). This chart depicts the narrow channel that connects the small deep-sea basin north of the Paracel Isles with the South China Sea abyssal plain. The channel is 8.5 km wide and more than 3200 m deep near station 17945.

3. The northern slope of the Dangerous Grounds carbonate platform, near GIK stations 17958-17960 (Fig. 2). This area is dominated by very small-scale morphology of drowned reefal structures and slumps between 2000 and 3000 m water depth. Of particular interest is the deep-sea canyon running south-north at about 115° 30'E: The flat canyon floor is about 2850 m deep, 15-25 km wide, in part, confined by rock walls up to more than 1000 m high, and filled by carbonate turbidites and small slumps near the channel margins (section PARASOUND Profiles; Sarnthein et al., this volume). In total, the canyon and its fillings strongly resemble the famous "Tongue of the Ocean" in the Bahama platform.

4. At the ridge north of the Luconia Shoals, near GIK station 17965 (see figure in section Coring Sites, Core Logs, and Initial Core Descriptions; Pflaumann et al., this volume). Based on the parasound records this ridge system seems to be a relic feature, composed of thick and undisturbed hemipelagic sediments originating from the Sunda Shelf. Today this ridge is intensively intersected from all sides by slumps cutting steep V-shaped channels, about 200 m deep.

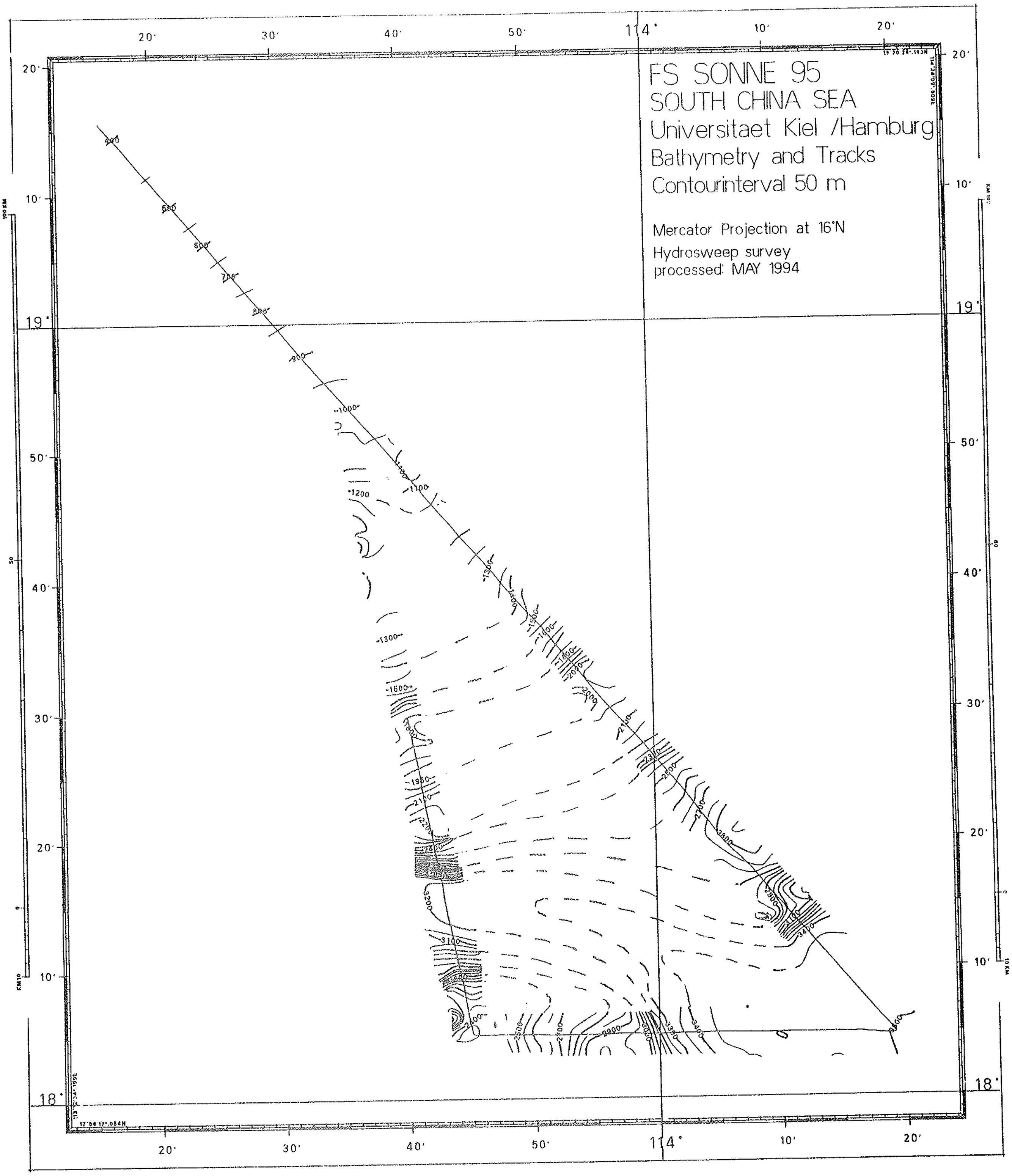

Figure 1. Bathymetric tracks across the South Chinese continental margin south of Hongkong, near GIK stations 17943-17946, showing the channel connecting the small deep-sea basin north of the Paracel Islands with the South China Sea abyssal plain.

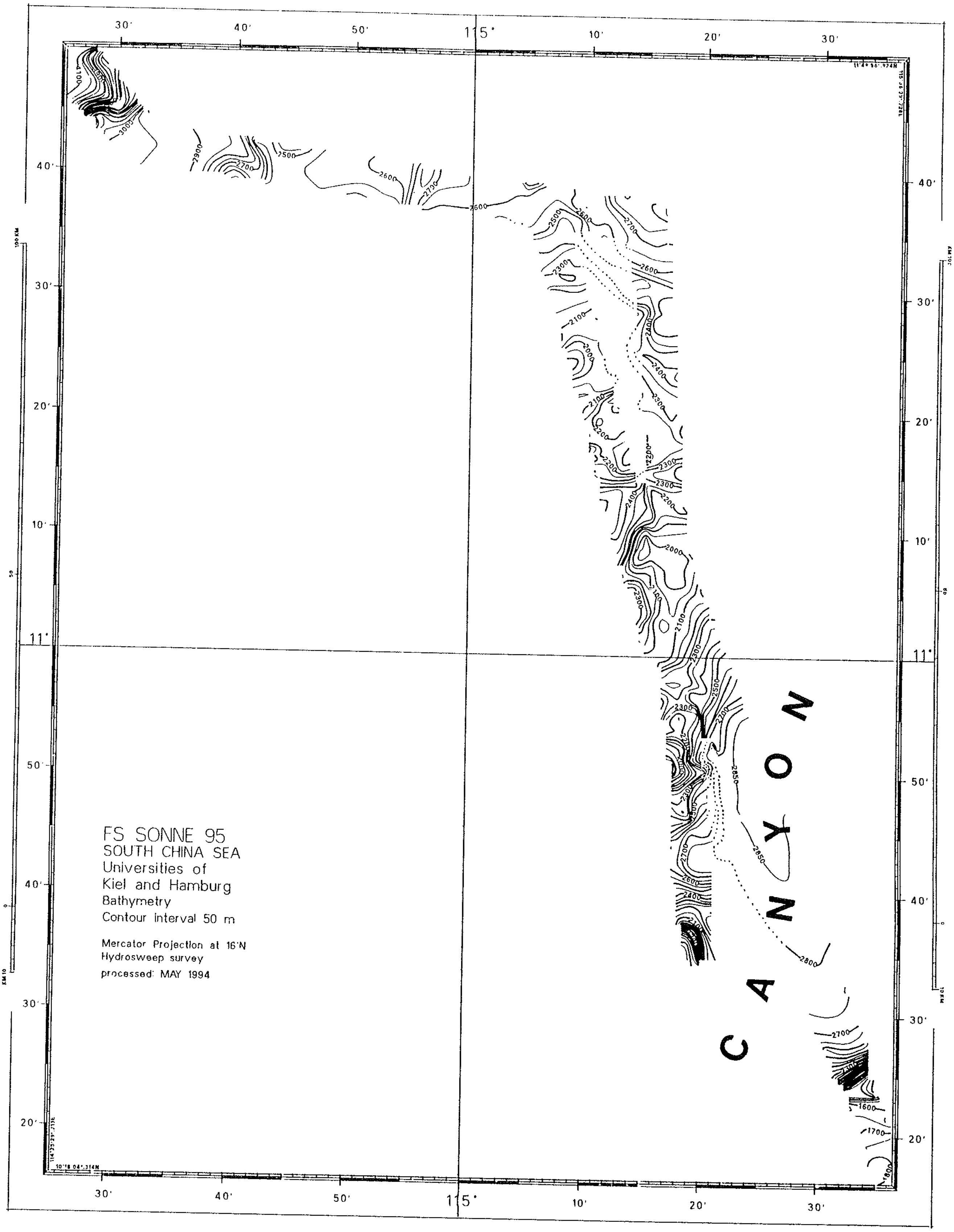

Figure 2. Bathymetric map of the northern slope of the Dangerous Grounds platform, including a channel at about 115°30'E

3.3 IMPORTANT TYPES OF ECHO CHARACTER IN SEDIMENTS OF THE SOUTH CHINA SEA (SONNE-95 CRUISE)

M. Sarnthein[1], P.-X. Wang [2], R. Botz,[1], M.-P. Ph. Chen[3], B. Haupt[1], S. Heilig,[1], E. Heinrich[1], Z.-M. Jiang[2], M. Kienast[1], H.-L. Lin[4], U. Pflaumann[1], and M. Staubwasser[1]

[1] GPI Kiel, [2] TJU Shanghai, [3] NTU Taiwan, [4] IMG Taiwan.

Introduction

In total the PARASOUND echo-sound records of the SONNE cruise 95 comprise profiles extending over more than 2500 nautical miles. The profiles were especially useful for the ad-hoc selection of appropriate coring sites in undisturbed hemipelagic sediments (see section on Coring Sites, Core Logs, and Initial Core Descriptions; Pflaumann et al., this volume). Moreover, the records form a base for both the stratigraphic correlations between cores and future mapping and balancing of sediment accumulation and erosion. PARASOUND echo records, i.e., the micromorphology and reflectivity characteristics of sediments in PARASOUND sub-bottom profiles can be classified and interpreted largely analogous to 3.5 kHz records, following the classification schemes proposed by Damuth (1975), Jacobi and Hayes (1982), and Mienert (1986). In general, however, the echo-character classification system of PARASOUND records appears more simple than that of conventional 3.5 kHz records, mainly because of the reduced occurrence of hyperbolae in the PARASOUND records.

PARASOUND Echo Types

(A) Draping sediment echo types are the most promising evidence of undisturbed hemipelagic deposition (Fig. 1), especially the echo type of *standing and migrating sediment waves* (Fig. 2 and record at GIK site 17936). Based on the fact that the highly focussed PARASOUND echo beam is largely devoid of hyperbolic echos, the record of Fig. 2 provides rare and partly new insights into the mechanisms of sediment-wave migration: (1) The waves generally move obliquely upslope and in particular, upstream, i.e. against the contour current of upper Pacific Deepwater which debouches from the Philippine Basin across the Bashi Strait and along the lower South Chinese continental margin to the west (Wang L.J., 1992). (2) The migration of wave ridges (about 60 m/1-2 M.y.) is linked to thin-rhomboidal sediment wedges that occur in the sediment pile at the lower end of the leeward slope of the waves at frequent and possibly regular intervals. Clearly the sediment wedges record discontinuous rates of deposition and current action.

(B) Fig. 3 depicts a *thick sediment drape* covering the southern Dangerous Grounds carbonate platform in front of the synglacial Sunda river. Based on the preliminary shipboard stratigraphy (see section on

Preliminary Sedimentation Rates; Sarnthein et al., this volume) the first outstanding reflector near 15 m below sea floor may correspond to stage 5.5 (Eemian). Further below, various prominent reflectors may be linked to antecedent extreme sealevel highstands such as during stages 7.7, 9.3, and 11.3, when the Sunda shelf was flooded and the Sunda River did not exist as today. Many delicate reflectors that occured in between the major reflectors on the color image of the PARASOUND monitor, were not preserved on the paper copy of Fig. 3. The first major reflector can be traced over more than 200 km all over the deltaic hemipelagic sediment pile in front of the Sunda shelf up to GIK station 17965.

(C) *Sediment slumps* are clearly recognized in PARASOUND echograms as thick transparent layers that may cut across underlying sediment beds and carry acoustic reverberations and a rough morphology near the surface (Fig. 4 and parts of echogram at GIK station 17953).

(D) Slight *current erosion of hemipelagic sediments* is obviously a widespread feature on the margins of the South China Sea as documented by extensive fields of solitary or bundled hyperbolae that 'cut' into the sea floor in the PARASOUND records from the continental slope of South China (Fig. 5a and b). Because of the narrow PARASOUND beam we surmise that these hyperbolae result from small-scale (0.1->1.0 m) and steep shaped erosional furrows. In some cases these furrows are linked to turbidite currents, where they are clearly confined to the inner ('*gleithang*') slope of curved turbidite channels. In most cases, however, the erosional marks probably originate from large-scale contour currents as deduced from the widespread and continuous distribution of the hyperbola marks reaching from the lower to the upper continental slope (e.g., southeast of Pratas Atoll, about 117°E) .

(E) *Intensive erosion on the upper slope* resulted in a widespread dentate relief up to ten meters high and partly burried by subsequent (Holocene?) sedimentation (Figure 6). Here the erosional activity is further supported by pinch outs of layered Tertiary sediments (compare Wong et al., this volume).

(F) *Turbidites* are marked in PARASOUND records by coarse acoustic layering, mostly separated by thin transparent layers with characteristic small-scale discontinuities and unconformities as a result of braided turbidite channels. In contrast to hemipelagic sediments, turbidites generally do not drape but fill the pre-existing sea-floor morphology and thus can be easily distinguished in PARASOUND records, except for rare cases of very distal turbidites (echograms at GIK stations 17952 and 17953).

There are various PARASOUND echo types not depicted in this section: those associated with sediment waves on the shelf, these with hemipelagic sediments on the upper continental slope (at about 600-1000 m depth), sediments which carry signs of weak downslope winnowing, and cases of extreme sediment transport resulting in slight unconformities.

REFERENCES

Damuth, J.E. (1975): Echo character of the western equatorial Atlantic floor and its relationship to the dispersal and distribution of terrigenous sediments. - Marine Geology, 18, 17-45.

Jacobi, R.D. and D.E. Hayes (1982): Bathymetry, microphysiography, and reflectivity characteristics of the West African margin between Sierra Leone and Mauritania. - In: U. von Rad et al. (eds.) Geology of the Northwest African continental margin (Springer Verlag, Berlin), 545-604.

Mienert, J. (1986): Akustostratigraphie im äquatorialen Ostatlantik: Zur Entwicklung der Tiefenzirkulation der letzten 3,5 Millionen Jahre. - "Meteor" Forschungserg., C 40, 19-86.

Wang, L.-J. (1992): The late Quaternary oxygen isotope record and its implications for the ventilation state of the South China Sea.-, In: Ye, Z. and P.X. Wang, P. (eds), Contributions to late Quaternary Paleoceanography of the South China Sea (Qingdao Ocean Press, Qingdao), 195-205.

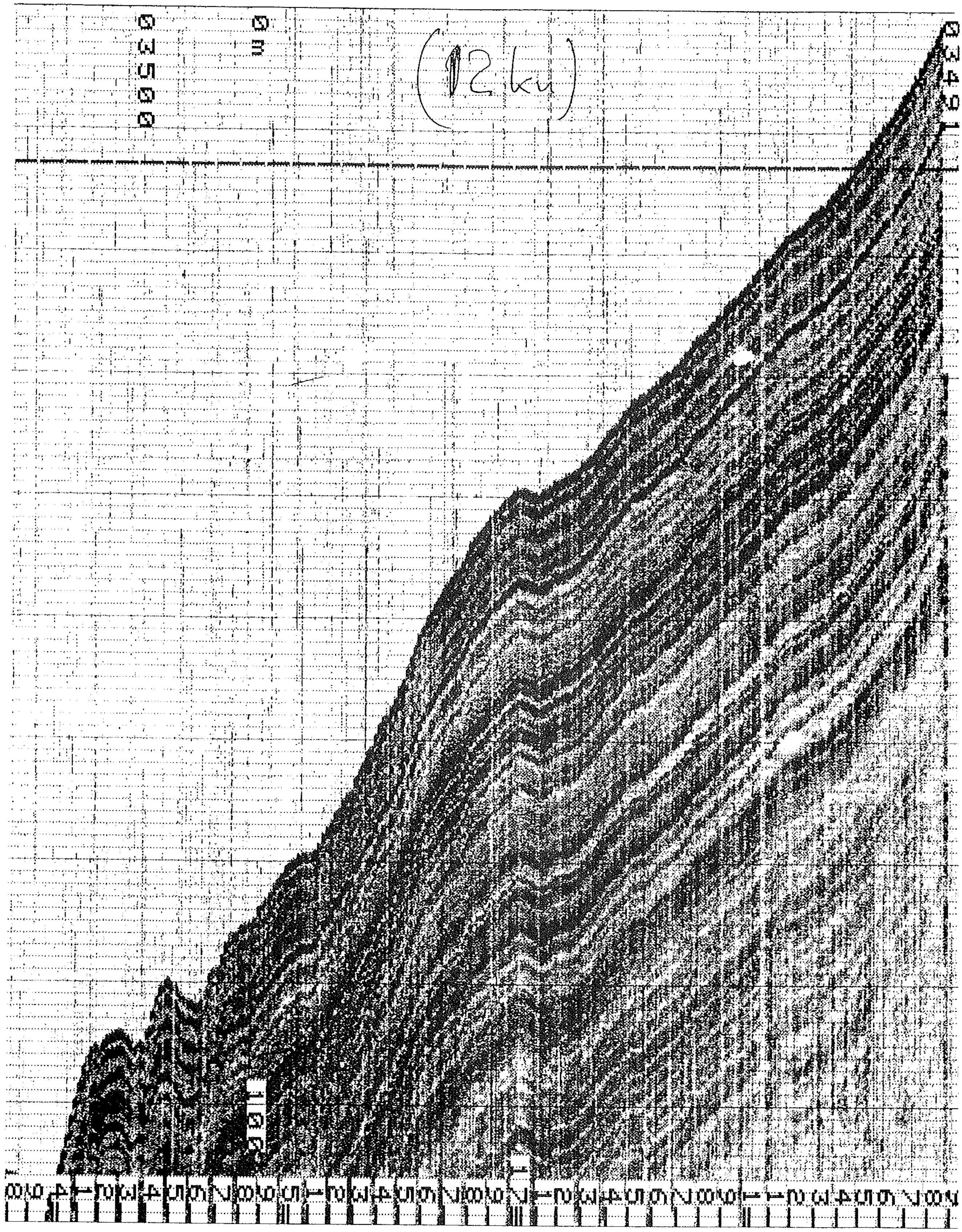

Figure 1. Sediment drape upslope of a field of sediment waves (near GIK site 17936)

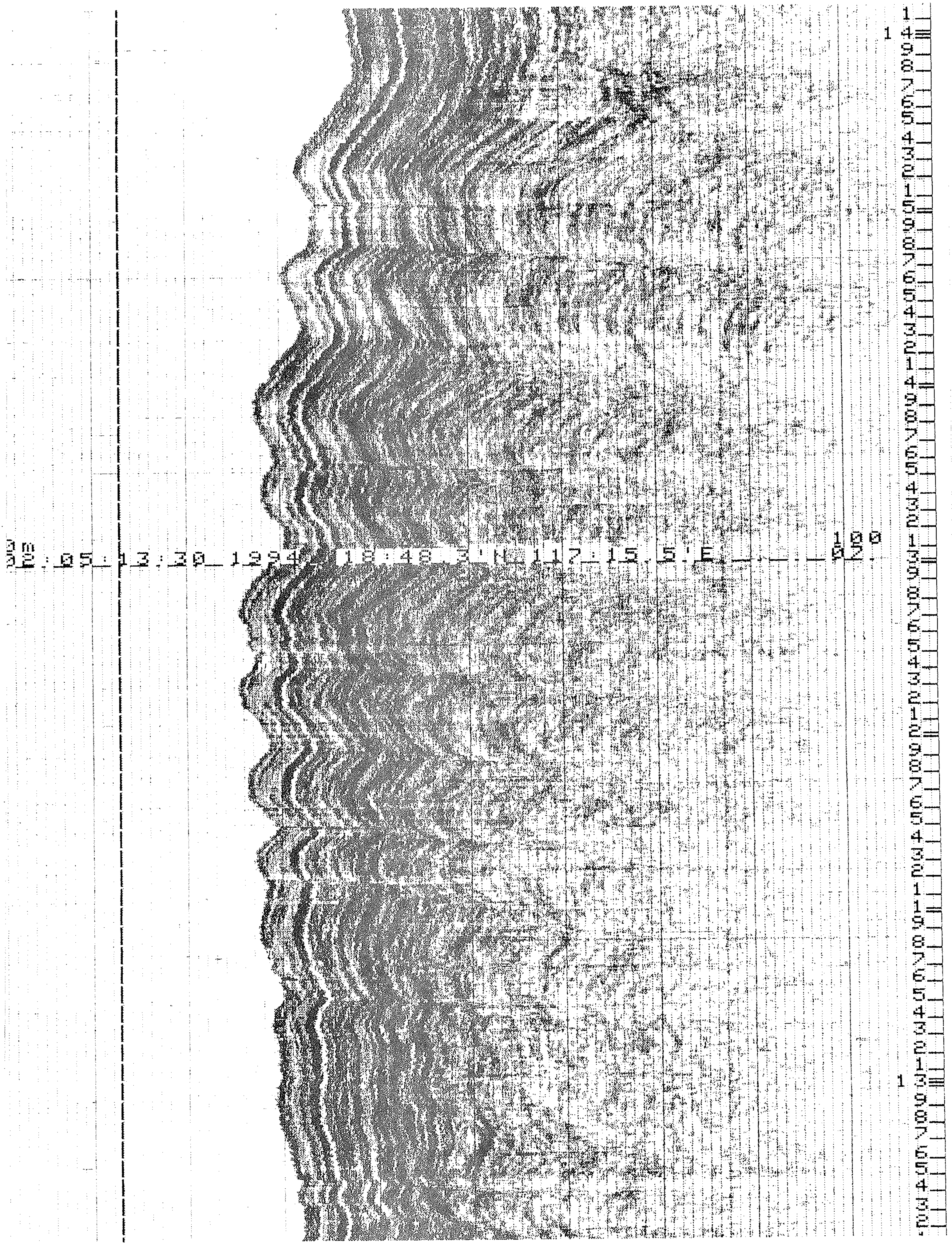

Figure 2. Migrating sediment waves near GIK station 17936

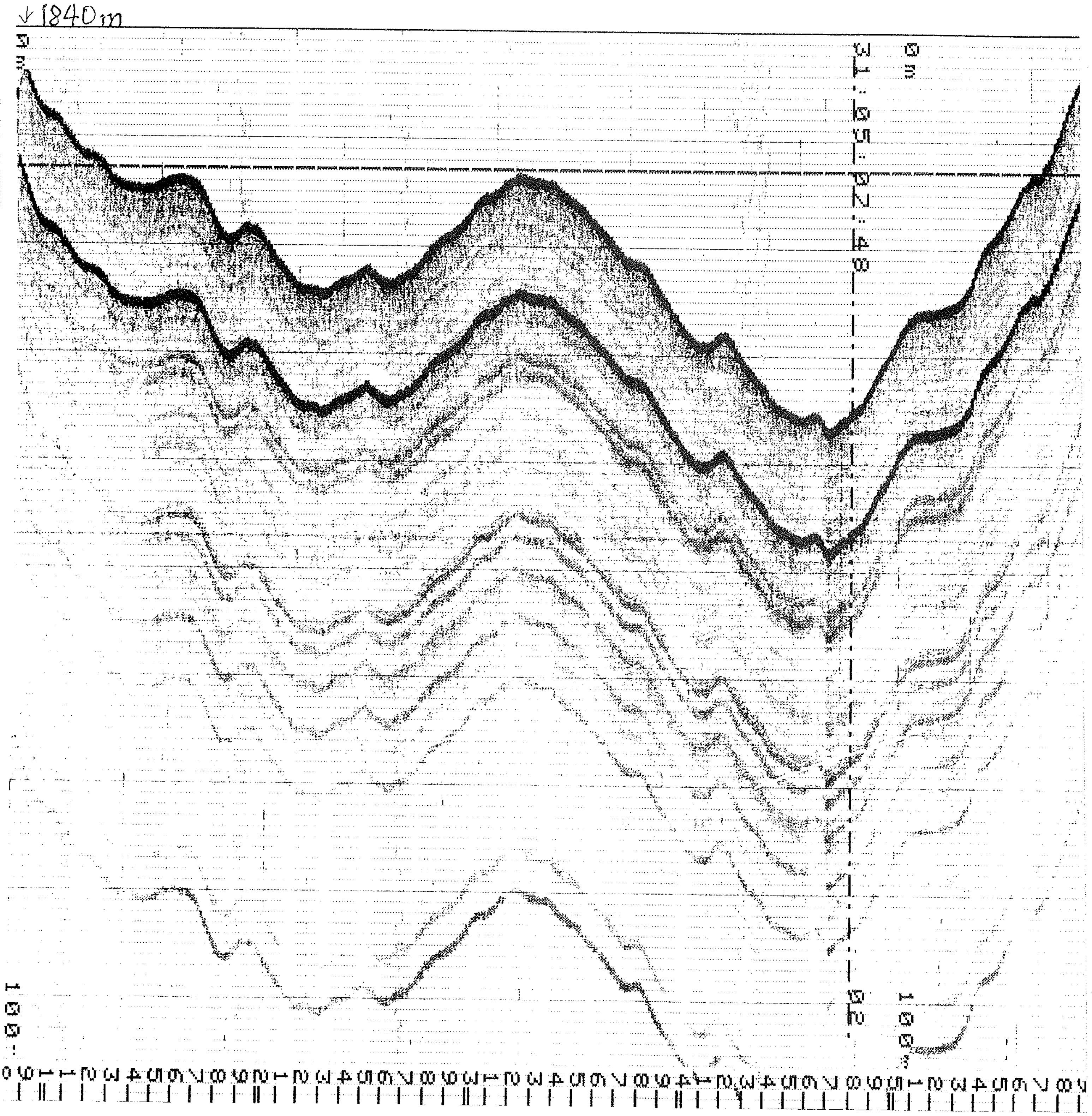

Figure 3. Sediment drape on top of the southern Dangerous Grounds carbonate platform, in front of the glacial Sunda river, near GIK stations 17961-17962.

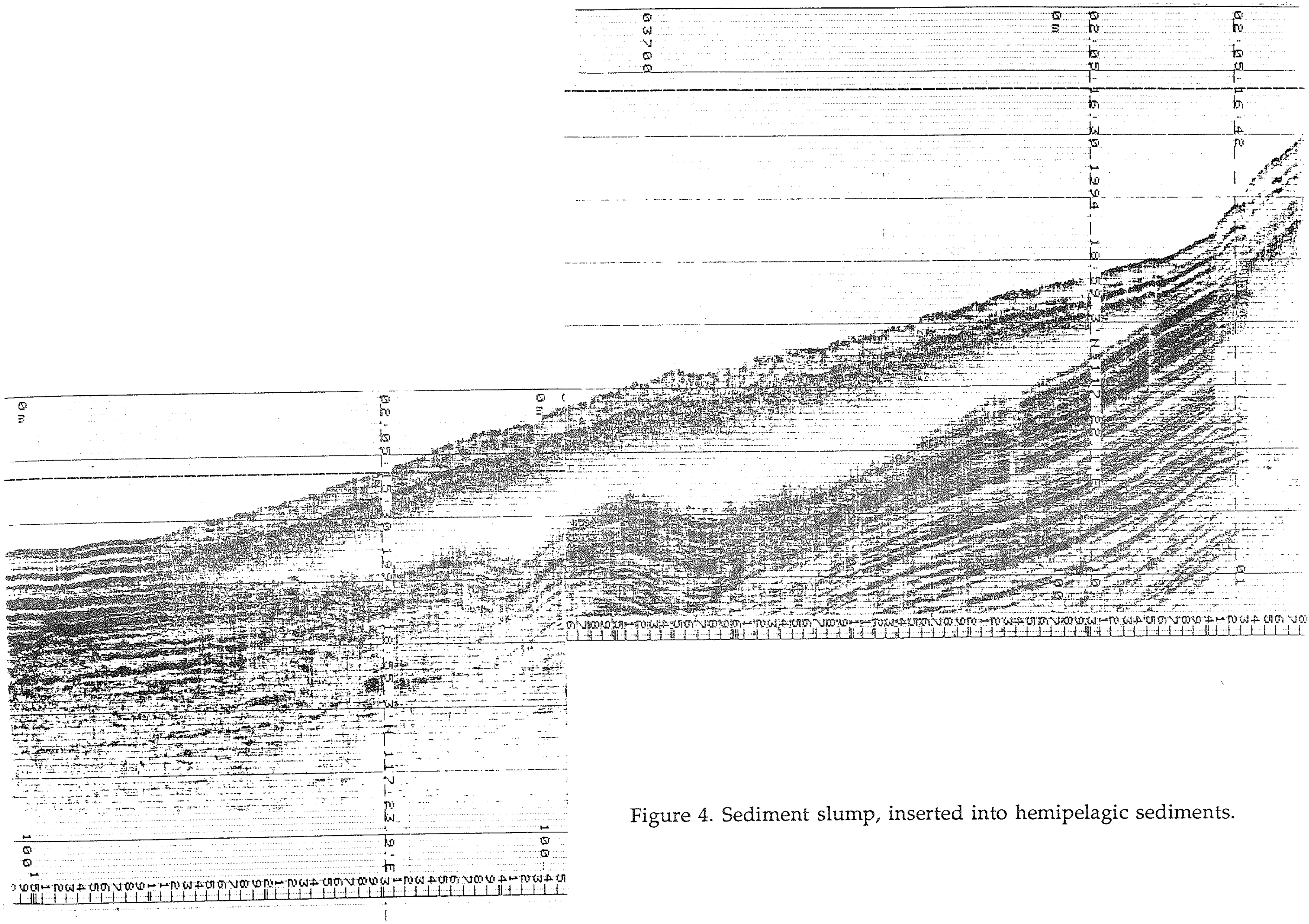

Figure 4. Sediment slump, inserted into hemipelagic sediments.

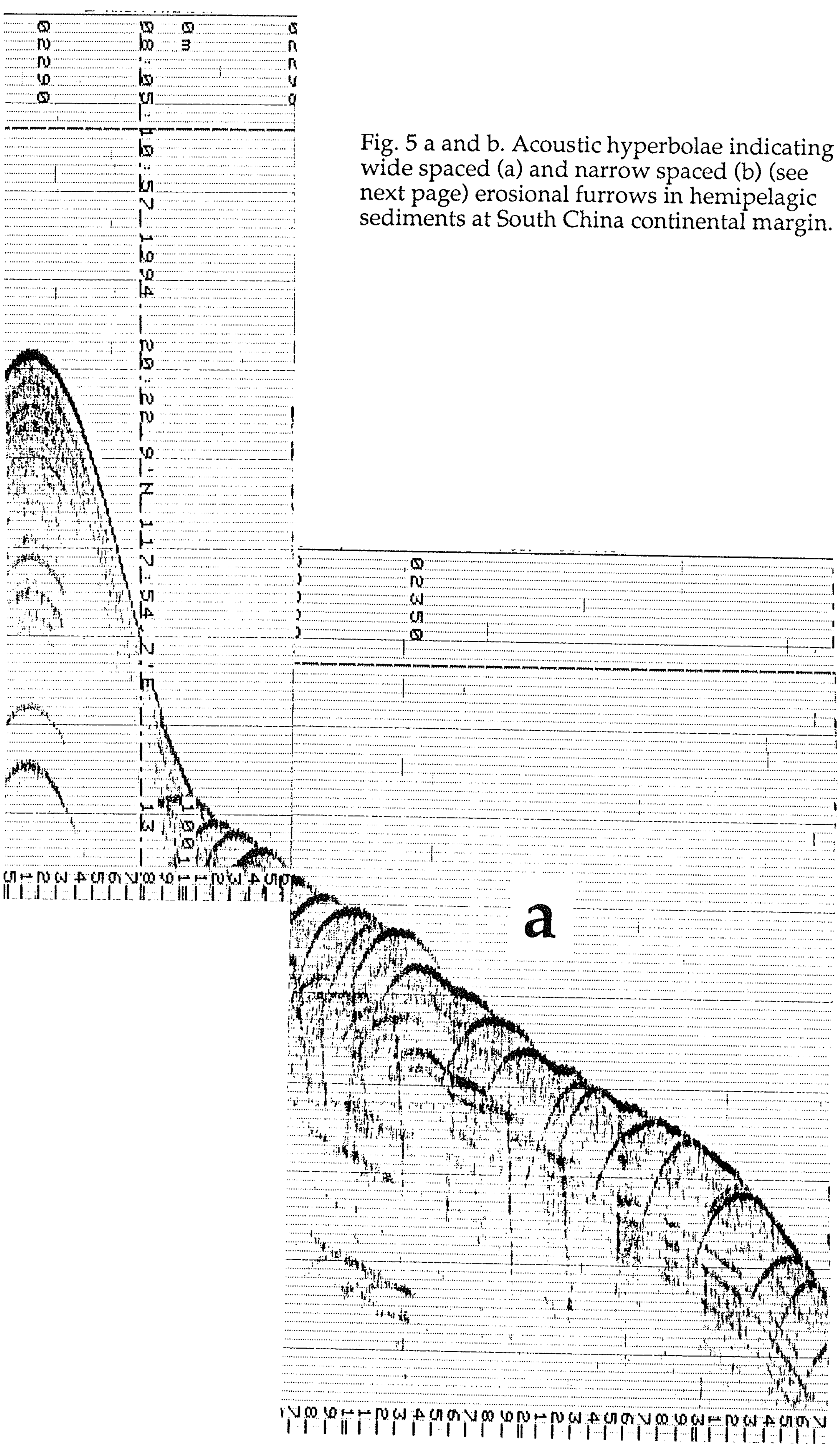

Fig. 5 a and b. Acoustic hyperbolae indicating wide spaced (a) and narrow spaced (b) (see next page) erosional furrows in hemipelagic sediments at South China continental margin.

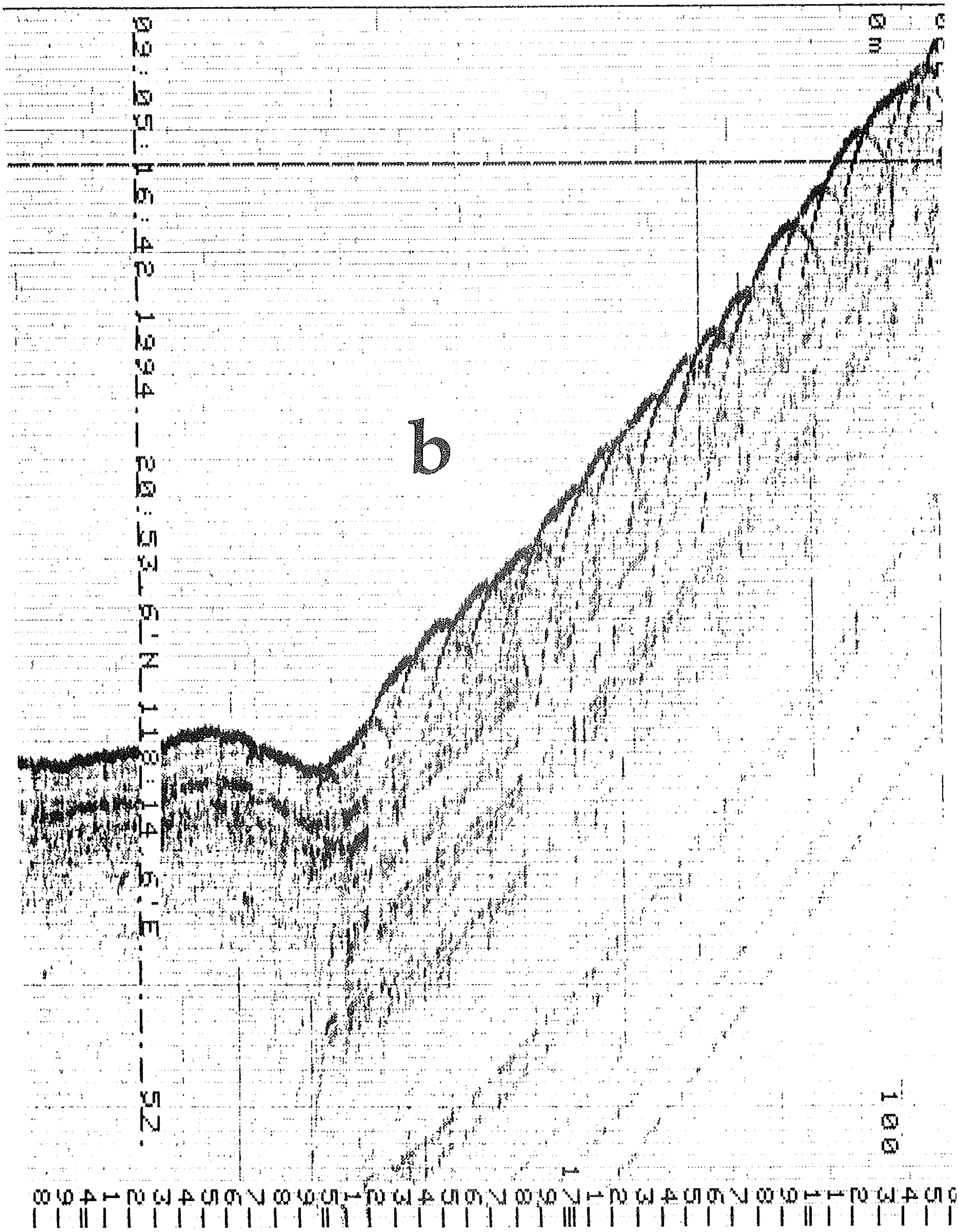

Fig. 5 (continued)

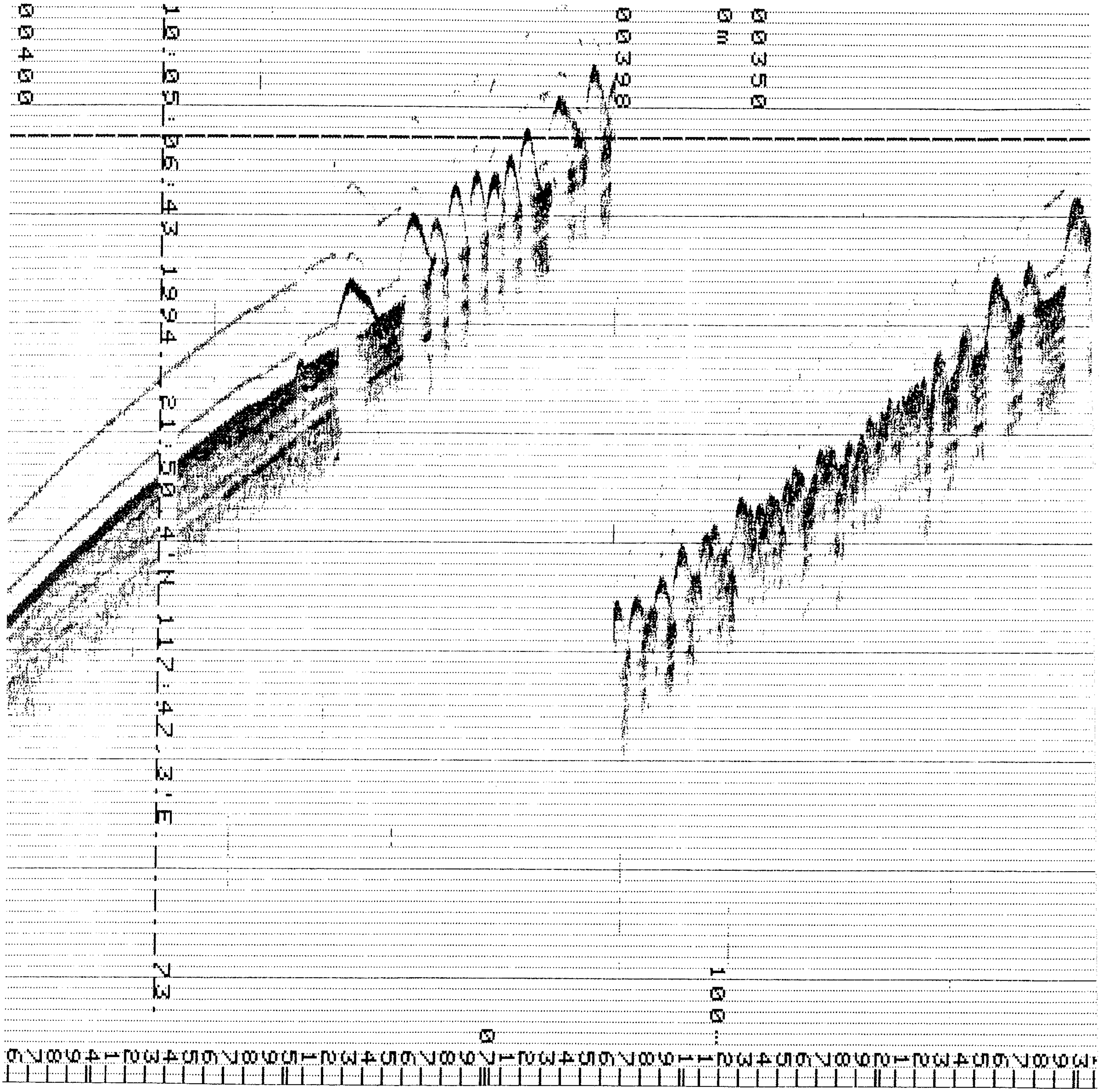

Figure 6. Erosion marks in sediments on the uppermost slope (about 350-450 m water depth), partly burried by subsequent sedimentation.

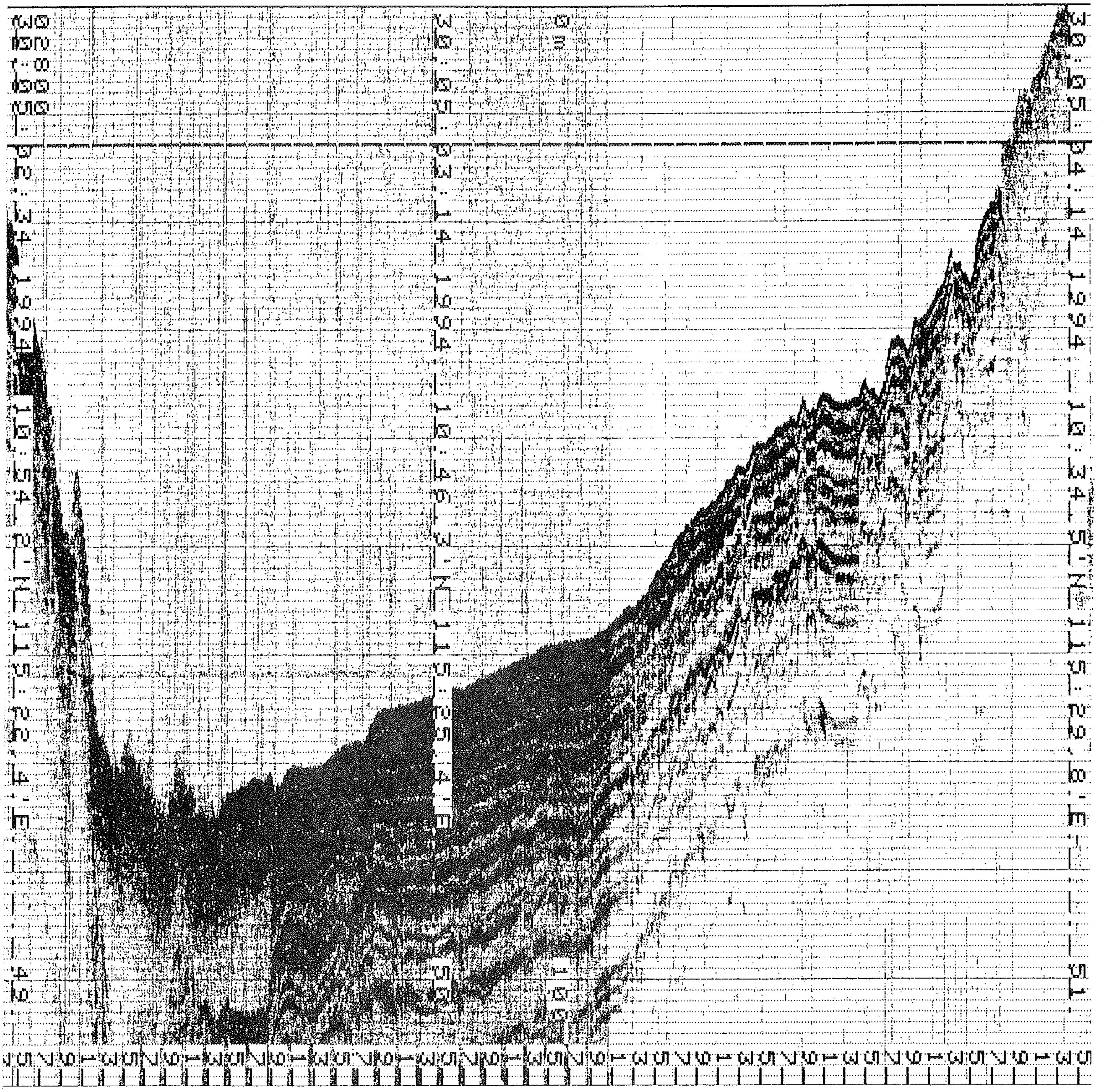

Figure 7. High-speed (12-kn) record of turbidite layers and marginal slumps in the deep-water channel cutting across the Dangerous Grounds carbonate platform similar to the 'Tongue of the Ocean' (for bathymetry see Fig. 2 in section Hydrosweep Bathymetric Records, this volume).

3.4 GENERAL OBSERVATIONS AT BOX CORES ON SONNE-95 CRUISE

W. Kuhnt[1], S. Hess[1], P-X. Wang[2], S. Heilig[1], E. Heinrich[1], R. Botz[1], H. Hensch[1], Z. Jian[2], K. Kißling[1], B. Lu[3], J. Villanueva[4], and L. Zheng[5]

[1] GPI Kiel, [2] TJU Shanghai, [3] SCSI Guangzhou, [4] CID-CSIC Barcelona, [5] SOA Hangzhou

SURFACE DESCRIPTION

The distance of the sediment surface to the top of the box corer was measured at the corners of the metal box to calculate the average recovery and to recognize a potential tilt of the corer during penetration. The penetration depth also provides preliminary information on water content, compaction and grain composition of the sediment.

The surface of the box corer was examined for the following features:

1. presence and abundance of organic fluff at sediment-water interface
2. grains size of sediment, winnowing
3. type of sediment (carbonate, foraminiferal ooze, mud)
4. presence of volcanic ash and thickness of ash layer
5. sediment color
6. biogenic structures: worm tubes, borrows, epifaunal agglutinated foraminifers
7. macroscopically visible tests of foraminifera (large planktics, miliolids such as *Pyrgo murrhina*) and pteropodes: rough estimate of the degree of carbonate dissolution at the sediment surface
8. morphology of the surface (flat, sloped, small scale hills and valleys)

A short compilation of these sediment surface observations is given in the following table.

VERTICAL SECTIONS

The vertical section of each core was described at the opened front side of the box corer. Generally four distinct layers were distinguished (figs. 1-4):

1. A brown oxidation zone at the surface of the box corer reaches down to a normally sharp and distinct redox line. The thickness of this layer is variable between 0 and 33 cm. and may be controlled by the organic matter flux to the seafloor, the oxygenation of bottom waters and the porosity of the sediment. Fluctuations in bottom water oxygenation are not very significant in the South China Sea (Haupt et al., this volume) and the sediments encountered at our stations appear fairly uniform, with the exception of an increased carbonate

Table 1: Observations on box cores surfaces. Abundance of epifaunal agglutinated foraminifera was only estimated during Leg 3 (box cores 17942 - 17965)

GIK station	water depth	sediment temp.	max./min. depth of sediment surface	water	surface morphology	fluff	volcanic ash	biogenic structures	visible microfauna	agglutinated foraminifers (epifauna)	sediment type
17920	2503 m	3,3 °C	13 cm	cloudy	disturbed	few	6,5 cm thick layer	-	-	n.d.	silty clay
17921	2506 m	4,3 °C	16 cm	cloudy	slightly disturbed	yes	4 cm below surface	-	-	n.d.	clay
17922	4226 m	3,5 °C	10 cm	cloudy	disturbed (cracks)	yes (1mm)	1,9 cm thick layer	-	-	n.d.	silty clay
17924	3440 m	2,4 °C	16 cm / 9 cm	clear	wavy structures	yes	-	worm tubes	planktic forams	n.d.	clay
17925	2978 m	3,1 °C	20 cm	clear	smooth	yes	-	echinodermata	planktic forams	n.d.	clay
17926	3761 m	2,3 °C	14 cm	clear	smooth	yes	-	worm tubes	planktic forams	n.d.	clay
17927	2804 m	2,7 °C	4 cm	clear	smooth	yes	-	worm tubes	planktic forams	n.d.	silty clay
17928	2476 m	2,4 °C	30 cm / 11 cm	clear	slumped (washed out)	yes	-	-	planktic forams	n.d.	clay
17929	371 m	11,8 °C	20 cm	cloudy	smooth	no	-	worm tubes, echinodermata	shell fragments	n.d.	sandy clay
17930	628 m	7,3 °C	10 cm	clear	wavy structures	few	-	worm tubes,burrows 5 cm Ø	planktic forams, shell fragments	n.d.	silty clay
17931	1002 m	4,5 °C	15 cm	clear	smooth	yes (+)	-	worm tubes	pteropodes, planktic forams	n.d.	clay
17932	1365 m	3,2 °C	7 cm	clear	smooth	yes (++)	-	worm tubes	pteropodes, planktic forams	n.d.	clay
17933	1972 m	2,6 °C	12 cm	cloudy	smooth	yes (++)	-	-	planktic forams	n.d.	clay
17934	2665 m	2,4 °C	10 cm	cloudy	wavy structures	yes (++)	-	worm tubes,burrows	planktic forams	n.d.	cay
17935	3144 m	2,4 °C	14.5 cm	clear	smooth	yes (++)	-	worm tubes	planktic forams	n.d.	clay
17936	3809 m	2,3 °C	8 cm	clear	wavy structures	yes (+++)	-	-	few planktic forams	n.d.	clay
17937	3423 m	2,4 °C	18 cm / 15 cm	cloudy	disturbed, wavy structures	yes (++)	-	-	planktic forams	n.d.	clay
17938	2839 m	2,4 °C	15 cm	cloudy	disturbed	yes (++)	-	large pellet 1 cm Ø	few planktic forams	n.d.	clay
17939	2474 m	2,5 °C	6 cm	cloudy	disturbed	yes	-	worm tubes	few planktic forams	n.d.	clay
17940	1729 m	2,6 °C	0	no water	soupy	yes	-	worm tubes	pteropodes, planktic forams	n.d.	clay
17941	2200 m	2,5 °C	17 cm	cloudy	smooth	yes	-	worm tubes	pteropodes, planktic forams	n.d.	clay
17942	329 m	11,9 °C	11 cm / 9 cm	clear	wavy structures	no	-	worm tubes, crustacean	planktic forams, shell fragments	few	silty clay
17943	915 m	5,1 °C	6 cm	cloudy	disturbed (washed out)	yes (++)	-	worm tubes	planktic forams, shell fragments	few	clay
17944	1217 m	3,7 °C	12 cm	cloudy	disturbed (washed out), winnowing	yes (+)	-	worm tubes	planktic forams, pteropodes	few	clay
17945	2406 m	2,5 °C	11 cm	cloudy	smooth	yes (++)	-	worm tubes	planktic forams	few	clay
17946	3465 m	2,4 °C	17 cm /15 cm	cloudy	disturbed (washed out)	few	-	worm tubes	planktic forams	common	clay
17947	3766 m	2,4 °C	9 cm	cloudy	disturbed (washed out), winnowing	yes (++)	-	worm tubes		common	clay
17948	2833 m	2,4 °C	10 cm / 7 cm	clear	elevated areas	yes (+)	-	worm tubes,burrows		common	clay
17949	2198 m	2,5 °C	11 cm	clear	smooth	yes (++)	-	-	planktic forams	few	clay
17950	1867 m	2,6 °C	13 cm / 12 cm	clear	smooth, elevated wall of box core	few	-	worm tubes,burrows	pteropodes, planktic forams	few	clay
17951	2340 m	2,5 °C	9 cm / 11 cm	clear	smooth	yes (++)	-	worm tubes	pteropodes, planktic forams	rare	calcareous ooze
17952	2885 m	2,4 °C	7 cm	clear	smooth	few	-	-	planktic forams	few	clay
17953	4308 m	2,3 °C	6 cm above top	no water	disturbed, soupy	no	thin patches, fine-grained	-	-	-	clay
17954	1518 m	3,1 °C	10 cm	cloudy	disturbed (washed out)	yes (++)	-	-		abundant	clay
17955	2404 m	2,4 °C	11 cm	cloudy	with elevated areas	yes (++)	thin patches, fine-grained	-		few	clay
17956	3386 m	2,4 °C	8 cm	cloudy	disturbed (washed out)	no	1 mm ash layer	worm tubes		few	clay
17957	2198 m	2,5 °C	14 cm	clear	smooth	yes (+)	-	abundant worm tubes	large pteropodes, planktic forams	few	clay
17958	2585 m	2,5 °C	9 cm	clear	smooth	few	thin patches, fine-grained	worm tubes, burrows, pellets	planktic forams, shell fragments	common	calcareous ooze
17959	1959 m	2,5 °C	13 cm	clear	smooth	yes (+)	-	worm tubes	planktic forams, shell fragments	common	calcareous ooze
17960	1711 m	2,8 °C	11 cm	clear	mound	few	-	large worm burrow	abundant planktic forams	rare	calcareous sand
17961	1794 m	2,7 °C	9 cm / 7 cm	clear	wavy structures, soupy	yes (++)	-	-	planktic forams, pteropodes, spiculae	common	clay
17962	1967 m	2,7 °C	9 cm	clear	smooth	yes (++)	-	worm tubes	planktic forams, pteropodes	abundant	clay
17963	1232 m	3,6 °C	0	no water	disturbed (cracked)	yes	-	many worm tubes	pteropodes	common	clay
17964	1557 m	3,1 °C	3cm above top / 4 cm	no water	disturbed with elevated corner	yes (++)	-	echinodermata	pteropodes	common	clay
17965	890 m	5,2 °C	10 cm above top	no water	disturbed, soupy	yes	-	worm tubes, spines with epifauna	planktic forams	common	clay

content and probably increased pore volume along the 'Dangerous Grounds' carbonate platform. We interprete the depth of the redox line within the sediment mainly as a function of organic matter (OM) flux and try to use this depth as a proxy of OM flux rates. This interpretation well agrees with the fairly good correlation between the depth of the redox line and water depth (figs. 5-9).

2. A thin (normally 1-3cm thick) dusky brown reduction zone.
3. A variable transition zone rich in biotubation structures, diffuse layers and mottles of brownish oxidized sediment and discontinous dusky layers and patches. Occasionally open worm tubes were observed in this zone.
4. A homogenous gray clay unit is observed at the bottom of most box cores. This unit occasionally exhibited small nodular carbonate and/or manganese-iron early diagenetic concretions.

The varying thickness of these four sedimentary units within each box core are compiled for the Sunda slope, the Vietnamese margin and northern slope (Chinese margin) transects of the South China Sea (figs. 1-4).

Figs. 1-4: Vertical sections of box cores along the Sunda Slope, Dangerous Grounds - Central Carbonate Platforms, Vietnamese Margin and Northern Slope transects. Thickness of oxidation zone and bioturbate transitional zone may indicate differences in organic matter flux rates.

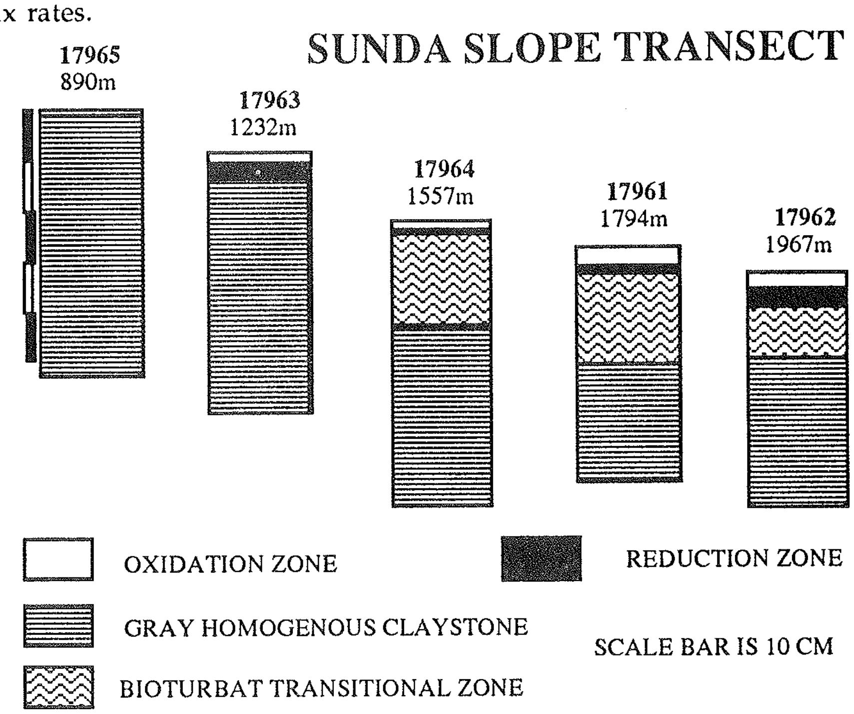

Fig. 1

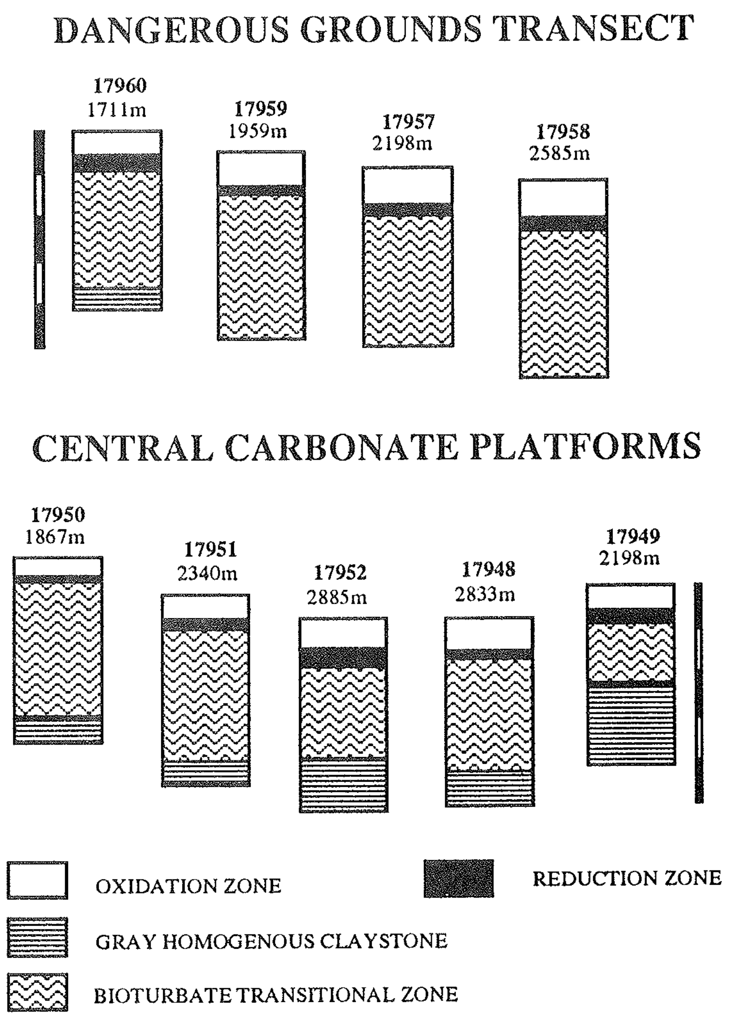

Fig. 2

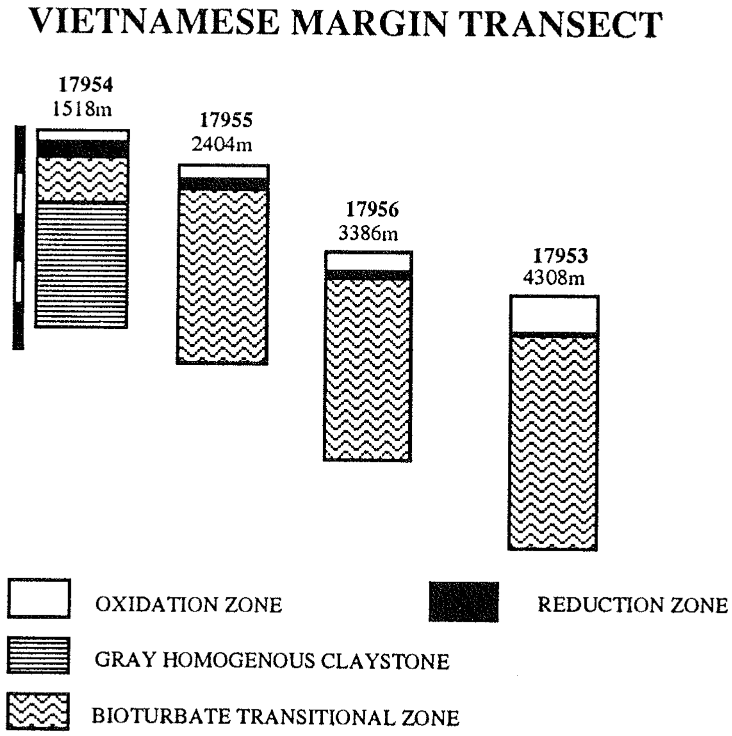
VIETNAMESE MARGIN TRANSECT
17954
1518m
17955
2404m
17956
3386m
17953
4308m
OXIDATION ZONE
REDUCTION ZONE
GRAY HOMOGENOUS CLAYSTONE
BIOTURBATE TRANSITIONAL ZONE

Fig. 3

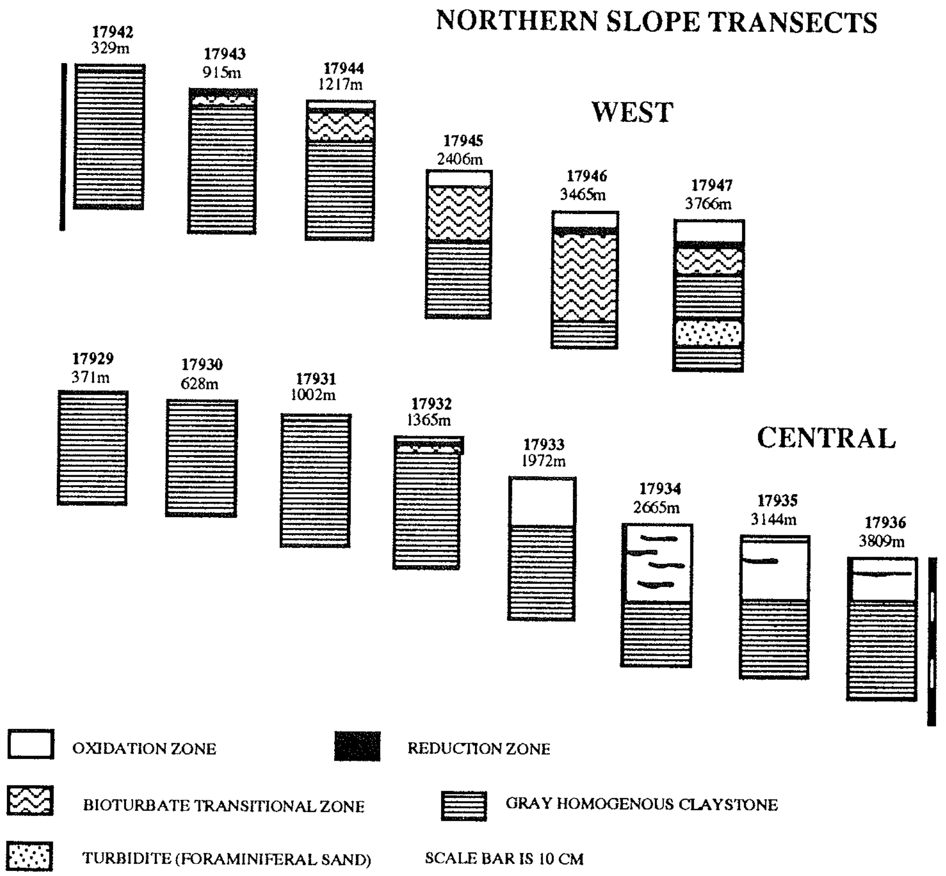
NORTHERN SLOPE TRANSECTS
WEST
17942
329m
17943
915m
17944
1217m
17945
2406m
17946
3465m
17947
3766m
CENTRAL
17929
371m
17930
628m
17931
1002m
17932
1365m
17933
1972m
17934
2665m
17935
3144m
17936
3809m
OXIDATION ZONE
REDUCTION ZONE
BIOTURBATE TRANSITIONAL ZONE
GRAY HOMOGENOUS CLAYSTONE
TURBIDITE (FORAMINIFERAL SAND)
SCALE BAR IS 10 CM

Fig. 4

Tab. 2: Positions of the redox line. Water depth, sediment temperature and the relation of the thickness of the oxigenated zone to the water depth are given for comparison. Stations that may have somewhat increased surface productivity and export flux of organic matter are indicated in bold letters.

GIK station	water depth	depth of redox line	sediment temperature	redox/depth ratio
17920	2503 m	18 cm	3,3 °C	0,007
17921	2506 m	37 cm	4,3 °C	0,015
17922	4226 m	33 cm	3,5 °C	0,008
17924	3440 m	10 cm	2,4 °C	0,003
17925	2978 m	8,5 cm	3,1 °C	0,003
17926	3761 m	11 cm	2,3 °C	0,003
17927	2804 m	6 cm	2,7 °C	0,002
17928	2476 m	17 cm	2,4 °C	0,007
17929	**371 m**	**0 cm**	**11,8 °C**	**0,000**
17930	**628 m**	**0 cm**	**7,3 °C**	**0,000**
17931	1002 m	2 cm	4,5 °C	0,002
17932	1365 m	5 cm	3,2 °C	0,004
17933	1972 m	15 cm	2,6 °C	0,008
17934	2665 m	22 cm	2,4 °C	0,008
17935	3144 m	20 cm	2,4 °C	0,006
17936	3809 m	13 cm	2,3 °C	0,003
17937	3423 m	12 cm	2,4 °C	0,004
17938	2839 m	18 cm	2,4 °C	0,006
17939	2474 m	7 cm	2,5 °C	0,003
17940	1729 m	5 cm	2,6 °C	0,003
17941	2200 m	14 cm	2,5 °C	0,006
17942	329 m	2 cm	11,9 °C	0,006
17943	915 m	5 cm	5,2 °C	0,005
17944	1217 m	3 cm	3,7 °C	0,002
17945	2406 m	5 cm	2,5 °C	0,002
17946	3465 m	6 cm	2,4 °C	0,002
17947	3766 m	16 cm	2,4 °C	0,004
17948	2833 m	8 cm	2,4 °C	0,003
17949	2198 m	9 cm	2,5 °C	0,004
17950	1867 m	4 cm	2,6 °C	0,002
17951	2340 m	6,5 cm	2,5 °C	0,003
17952	2885 m	11 cm	2,4 °C	0,004
17953	4308 m	9 cm	2,3 °C	0,002
17954	1518 m	2,5 cm	3,1 °C	0,002
17955	**2404 m**	**3 cm**	**2,4 °C**	**0,001**
17956	**3386 m**	**4 cm**	**2,4 °C**	**0,001**
17957	2198 m	9 cm	2,5 °C	0,004
17958	2585 m	9 cm	2,5 °C	0,003
17959	1959 m	8 cm	2,5 °C	0,004
17960	1711 m	6 cm	2,8 °C	0,004
17961	1794 m	4 cm	2,7 °C	0,002
17962	1967 m	3 cm	2,7 °C	0,002
17963	**1232 m**	**1 cm**	**3,6 °C**	**0,001**
17964	**1557 m**	**2 cm**	**3,1 °C**	**0,001**
17965	**890 m**	**1 cm**	**5,2 °C**	**0,001**

Regression plots of the depth of the redox line and water depth show a significant correlation of these two parameters within single transects, where the surface productivity can be regarded as fairly constant (e.g. along the Sunda slope, the Vietnam margin and the Chinese (northern) slope of the South China Sea) (figs. 5-9).

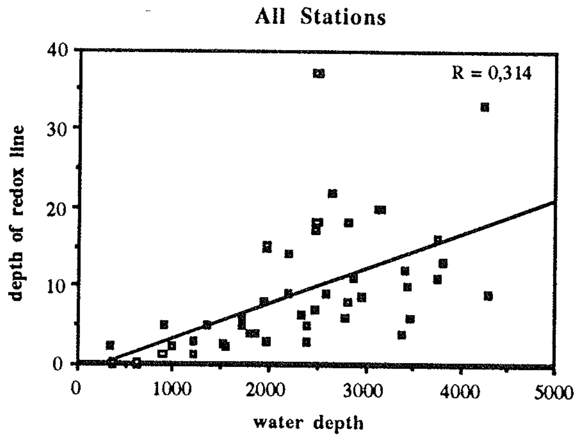

Fig.5

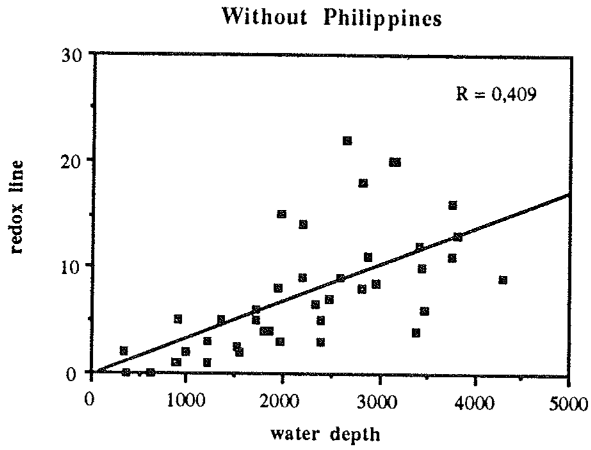

Fig.6

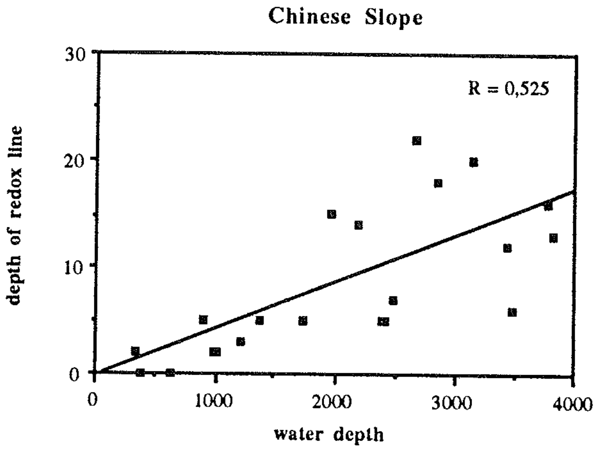

Fig.7

Along the Vietnamese transect stations 17955 and 17956 show an unusually thin oxigenation zone possibly because of locally enhanced organic matter fluxes (upwelling?) (fig. 8).

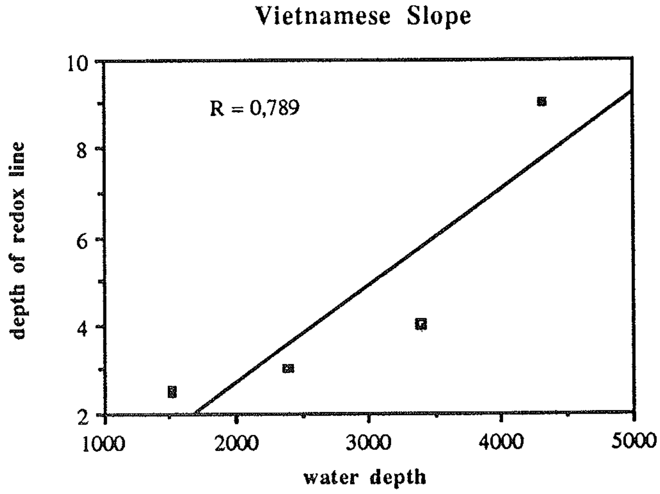

Fig.8

The stations along the Sunda slope transect and the Reed bank carbonate platform stations were combined in one plot (fig. 9). The comparatively good correlation of these stations along one regression line may indicate fairly uniform water masses and surface productivity within the southern part of the South China Sea

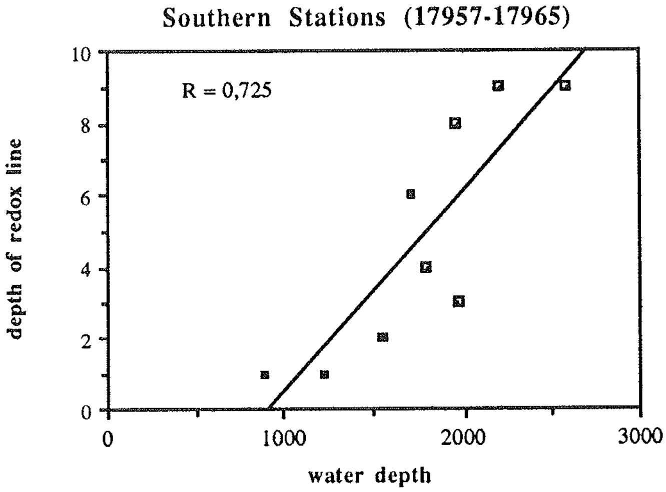

Fig.9

A plot of the ratio between depth of the redox line and water depth is used to identify possible areas of increased surface productivity (HPR). Virtually no such areas were observed within the northeastern South China Sea, which seems to be characterized by prevailing oligotrophic conditions. Areas of possibly enhanced surface productivity may occur along the Northern slope (GIK stations 17929 and 17930 , possibly also stations 17944, 17945, and 17946), along the Vietnamese slope (stations 17955 and 17956) and most commonly along the Sunda Slope (GIK stations 17962 to 17965). The carbonate platforms (Macclesfield Bank and Reed Bank) show a significantly thicker oxigenation zone which may partly be caused by different (carbonate-rich) surface sediments with higher pore volumes partly by lower OM fluxes. Thickest oxigenation zones are observed along the Philippine margin (northeastern South China Sea), where oligotrophic water masses prevail (fig. 10).

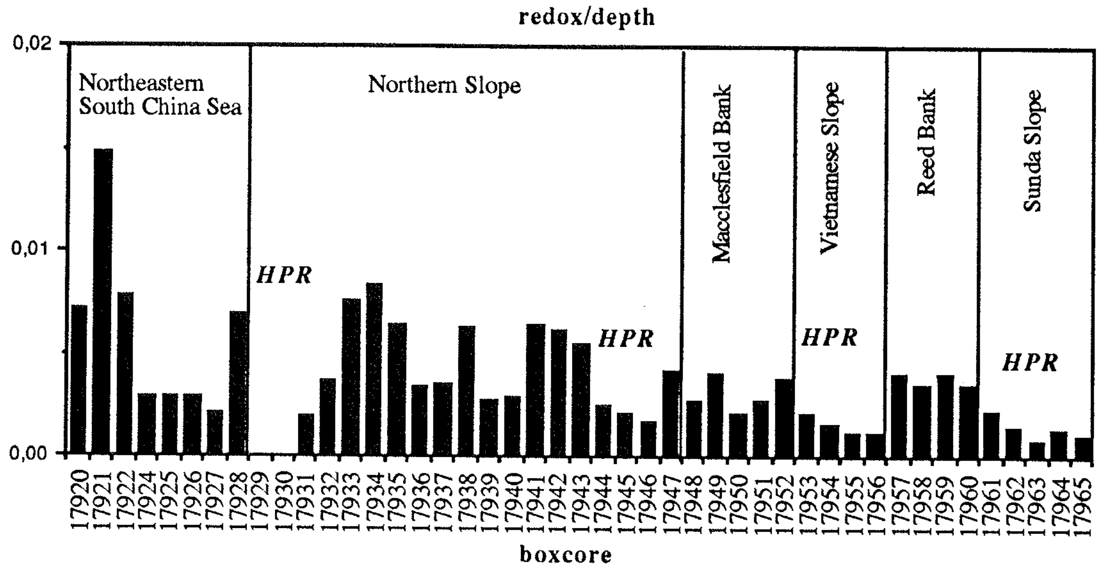

Fig. 10: Depth of redox line / water depth ratio for box core stations in the South China Sea.

3.5 CORING SITES, CORE LOGS, AND INITIAL CORE DESCRIPTIONS AT SONNE-95 CRUISE

Pflaumann, U., Sarnthein, M., Wang, L.J. (University of Kiel)

$CaCO_3$ concentrations (%)

Magnetic susceptibility: values expressed as S.I.$\times 10^{-6}$

Sediment composition:

A = Ash layer or spot
C = Clayey
F = Forams
M = Clayey mud
P = Pteropods
S = Silt, silty
SA = Sand, sandy
SH = Shells

Modifying characteristics:

/ = alternating
b = brown, brownish
d = dark
f.l. = faint layering
g = gray, grayish
gr = green, greenish
l = light
m = mottled, bioturbated
o = olive
r = red, reddish
s = sharp boundary
y = yellow, yellowish

Sediment recovery:

full recovery; section boundary; artificial coring gap; coring disturbance

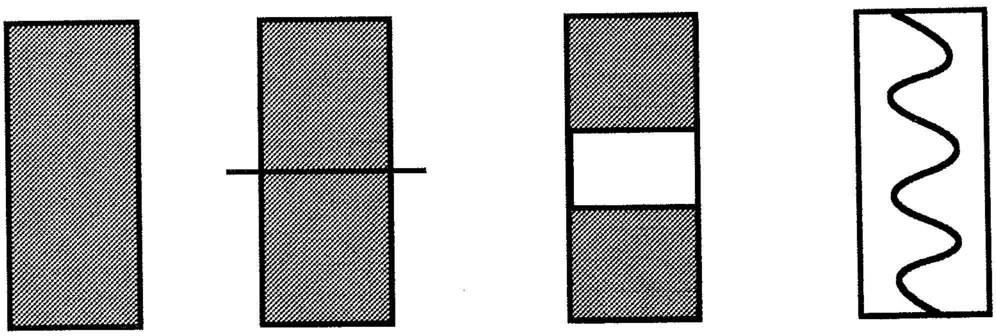

Core 17922-2

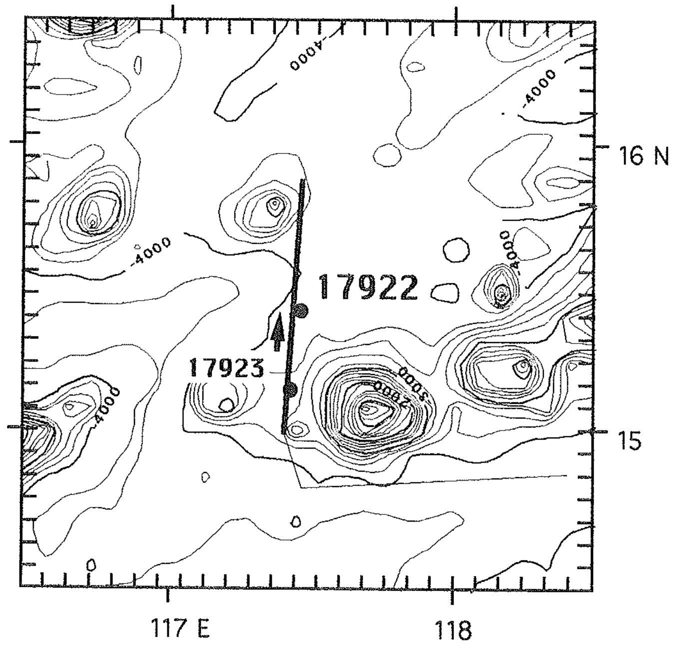

Scarborough Reef

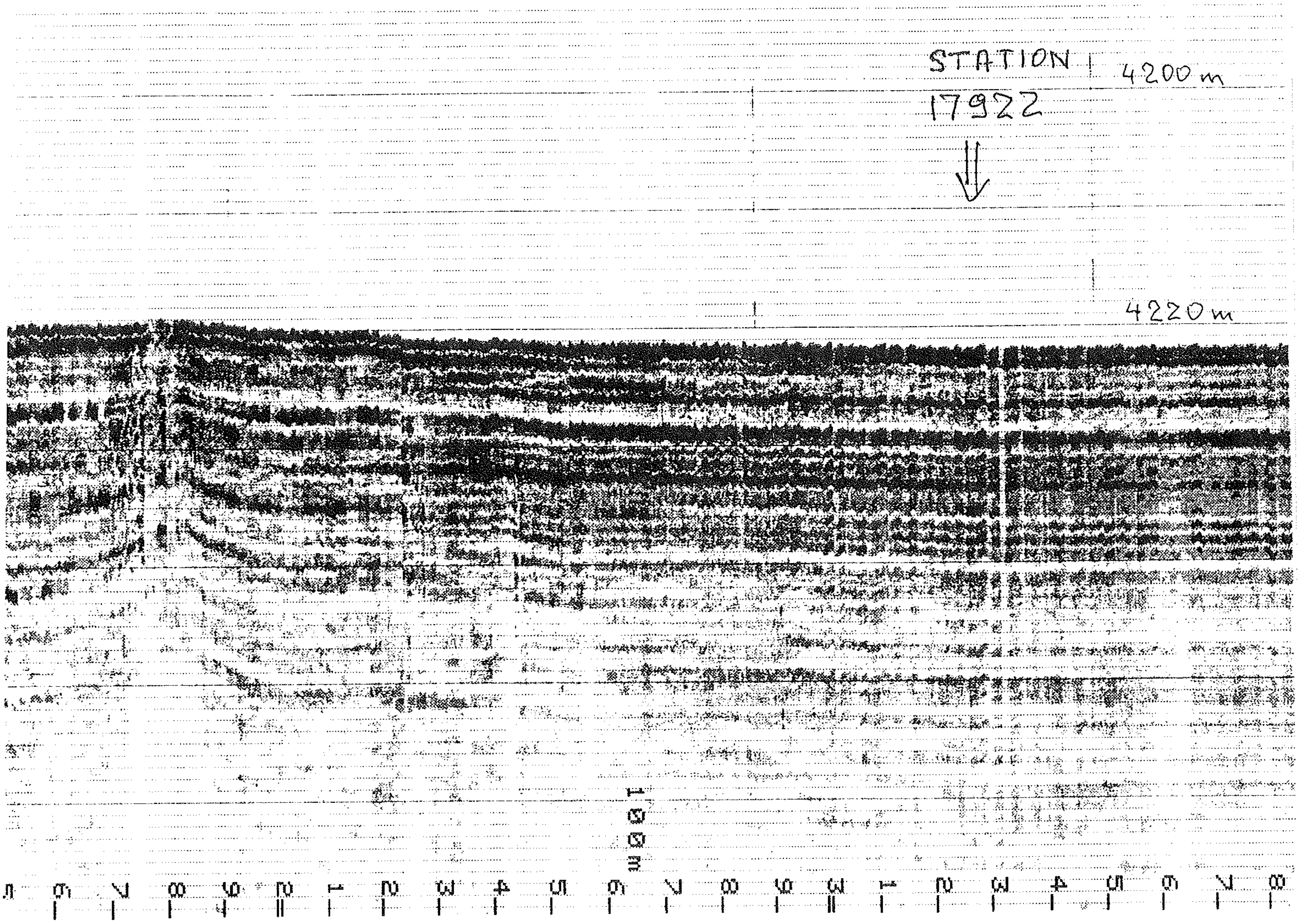

17922-2 15°25.0 N 117°27.5 E, 4224 m w.d., core length 6.63 m

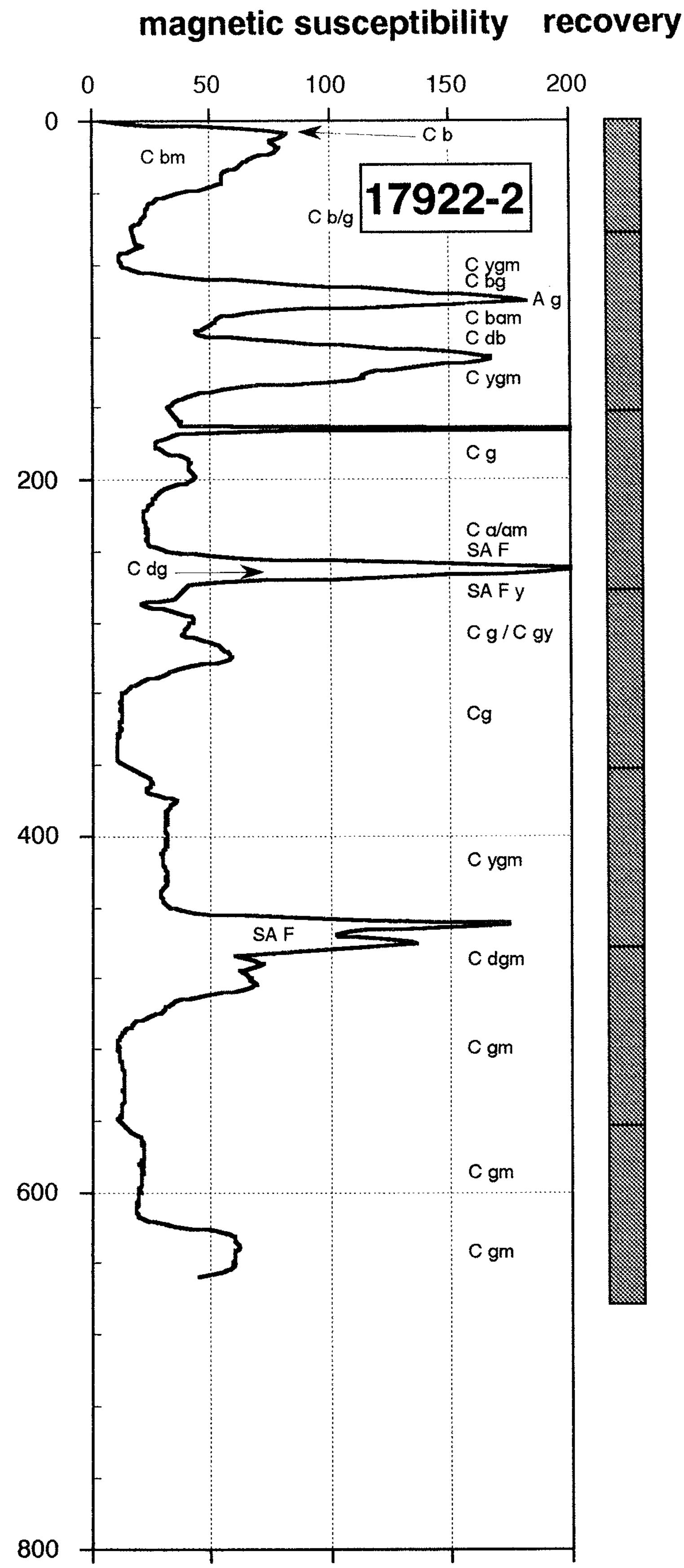

Core 17924-2
and
Core 17924-3

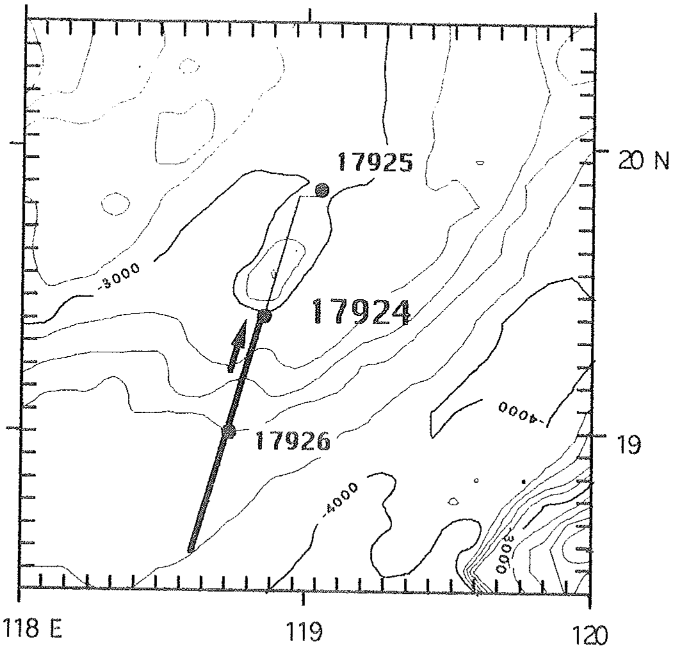

North Eastern South China Sea

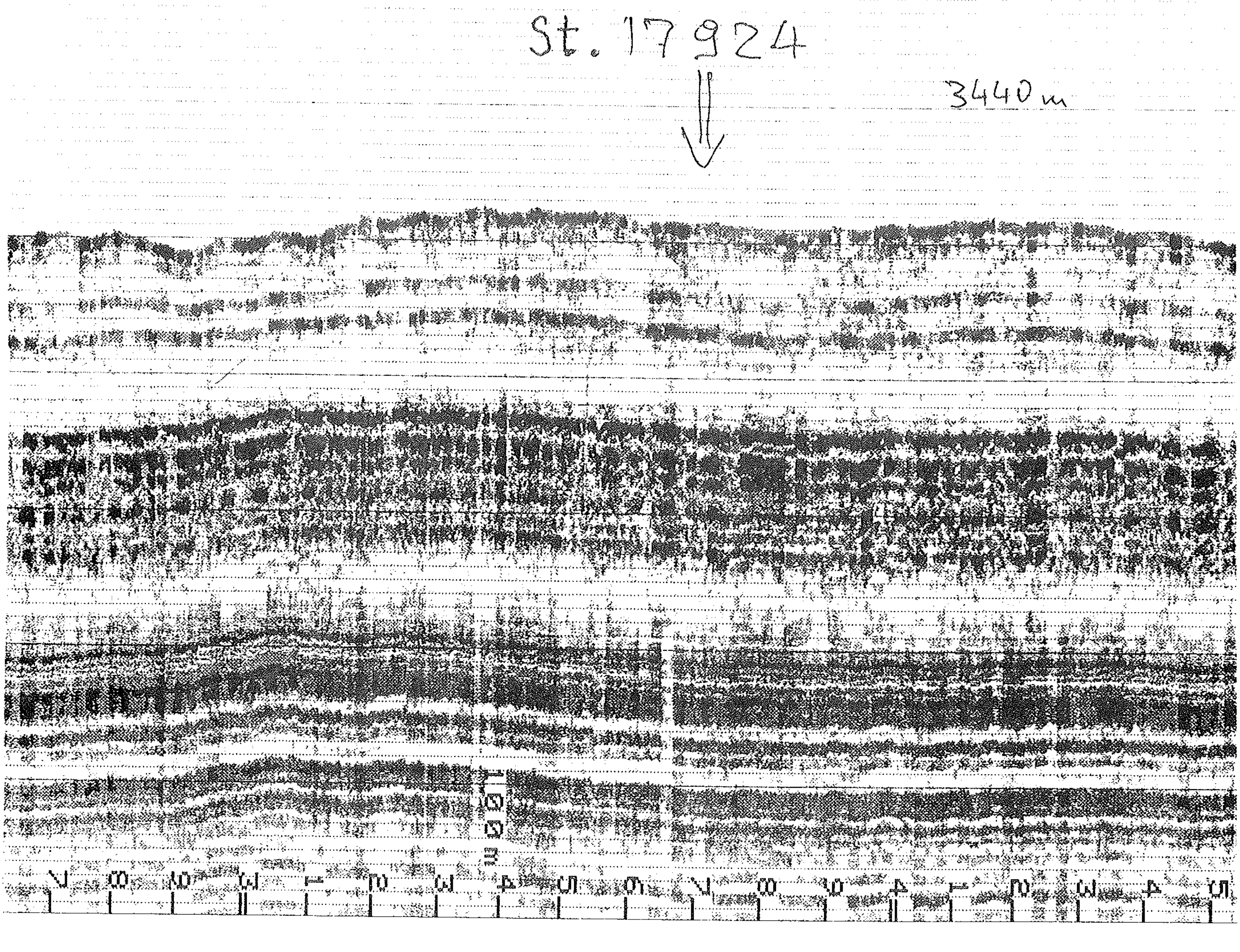

17924-2/3 19°24.7 N 118°50.9 E, 3440/36 m w.d., core length 11.50/19.89 m

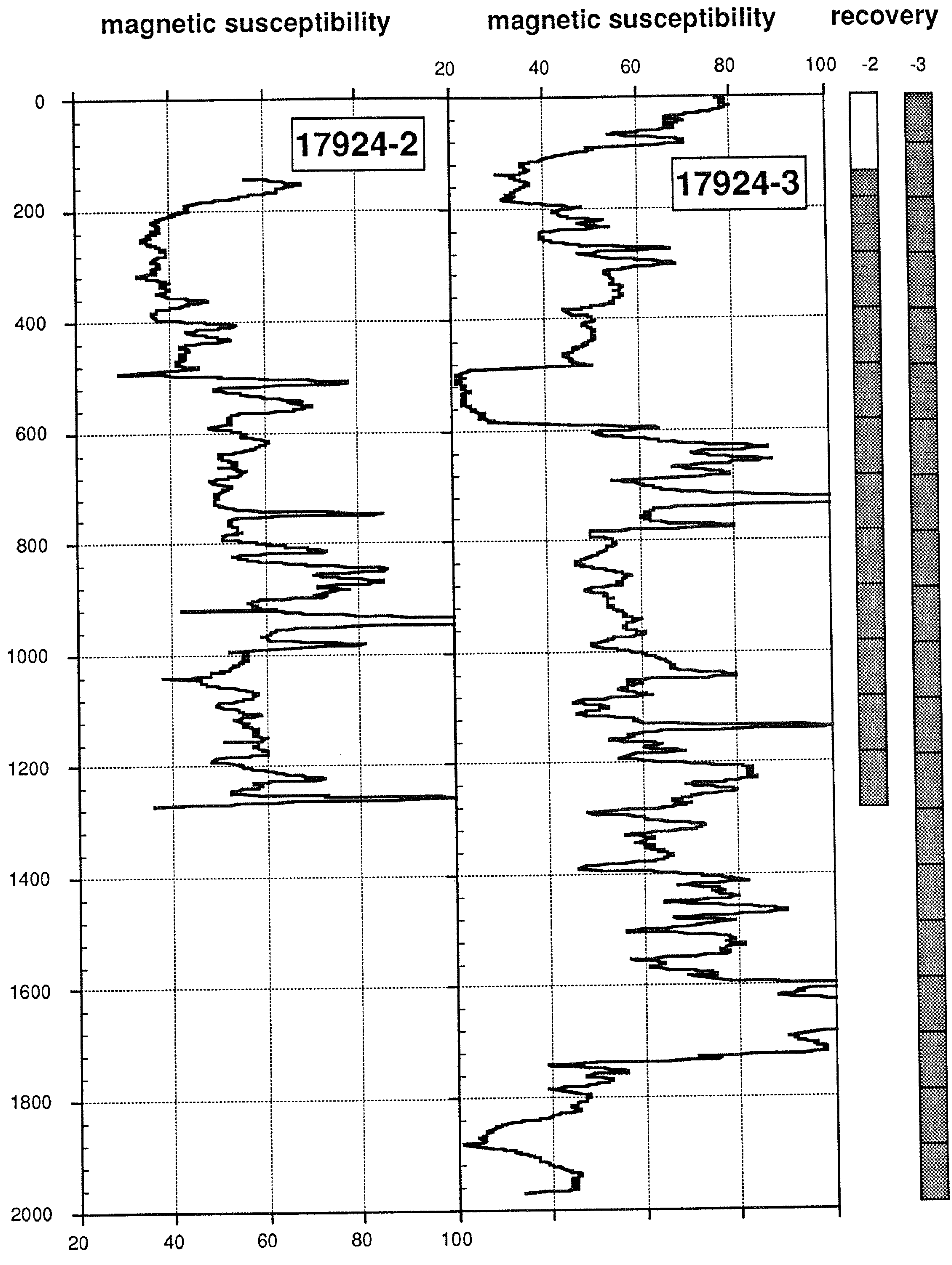

Core 17925-3

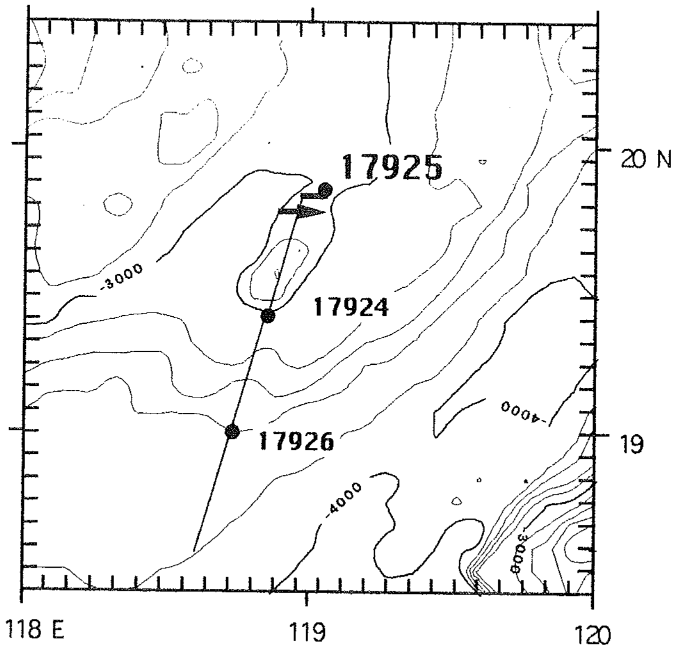

North Eastern South China Sea

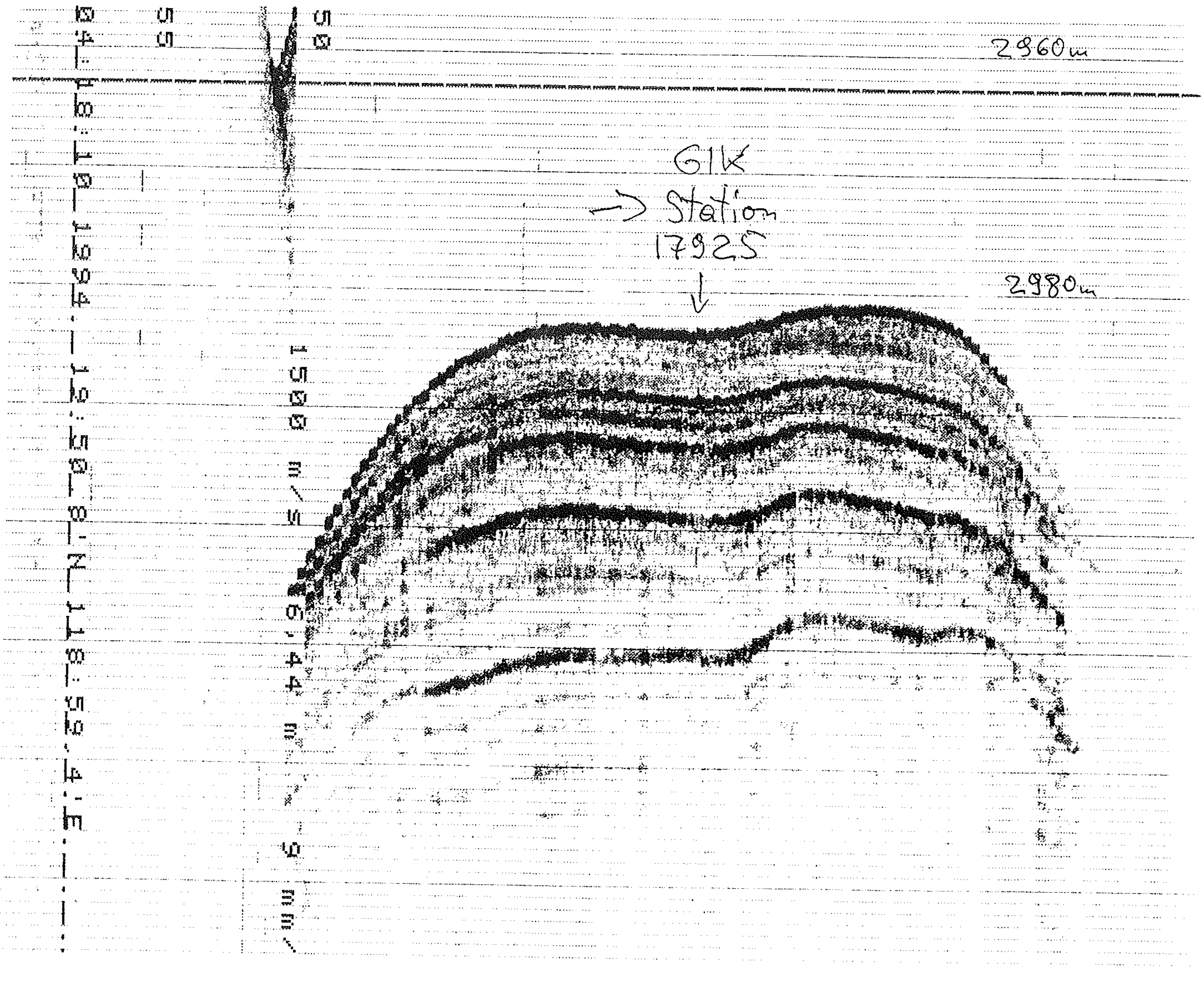

17925-3 19°51.2 N 119°02.8 E, 2980 m w.d., core length 12.42 m

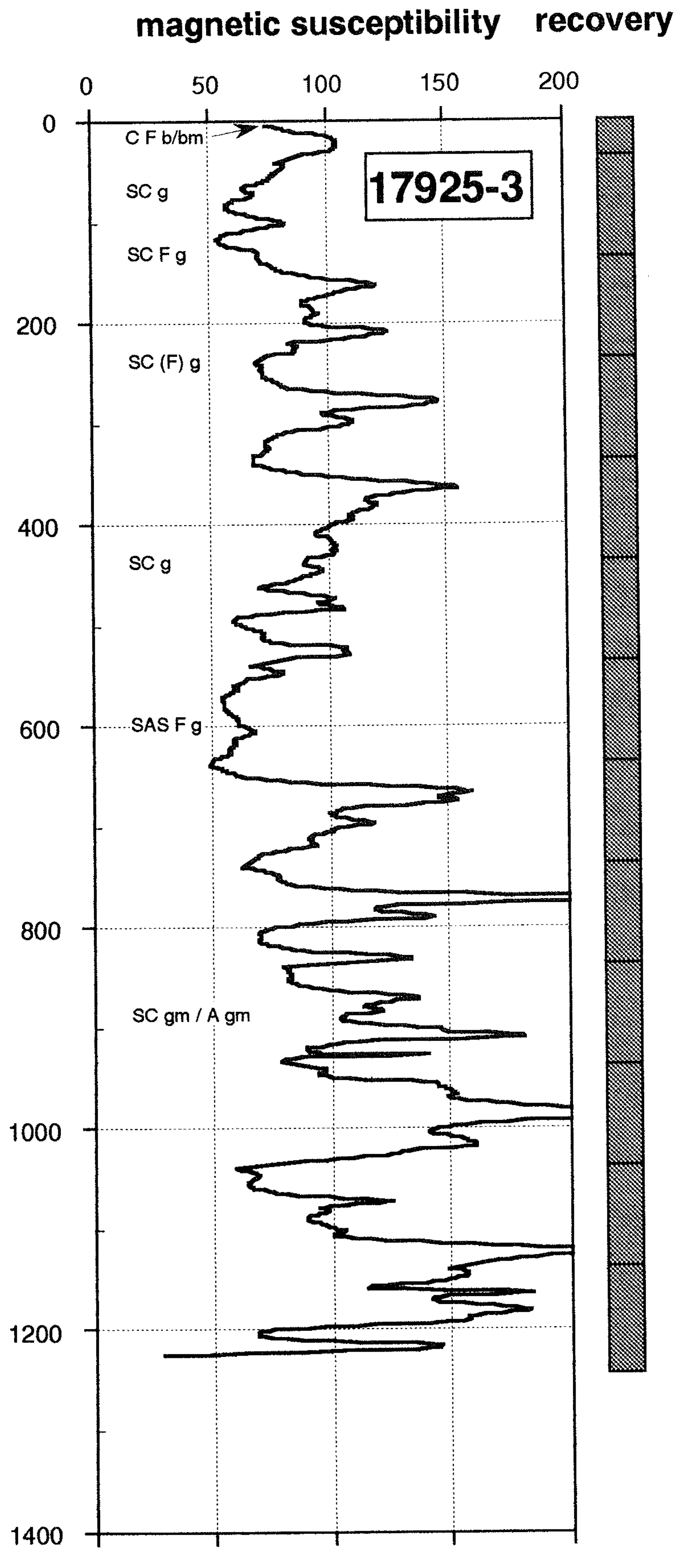

Core 17926-3

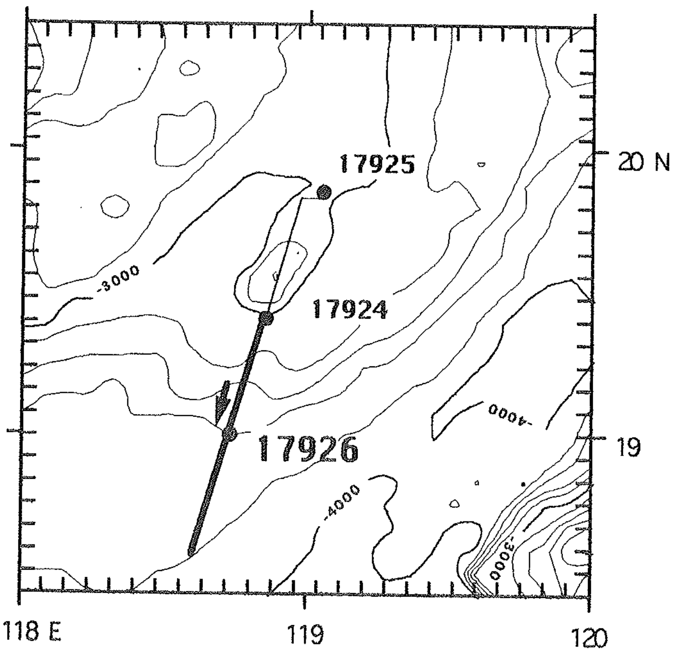

North Eastern South China Sea

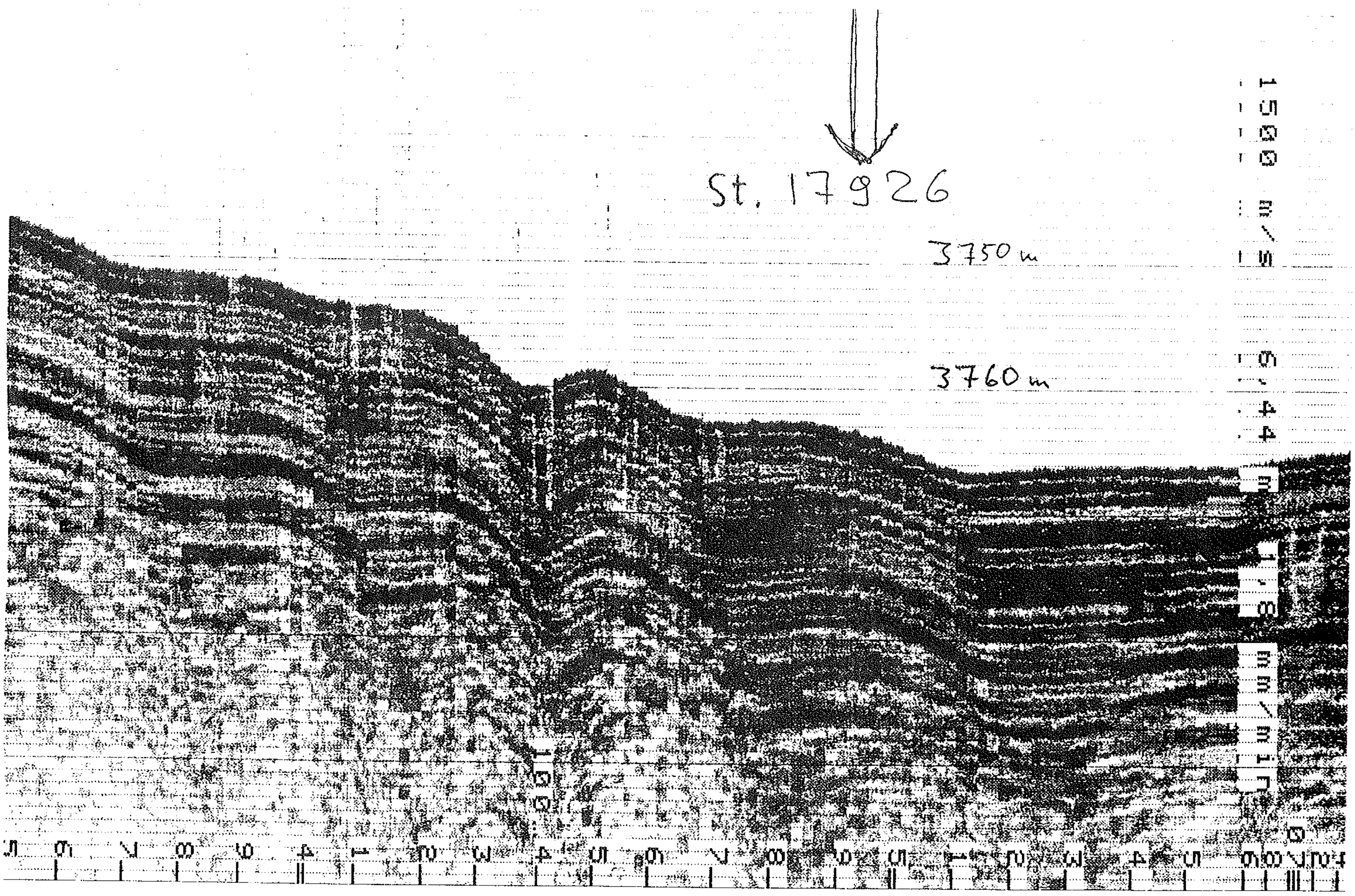

17926-3 19°00.0 N 118°44.0 E, 3760 m w.d., core length 10.06 m

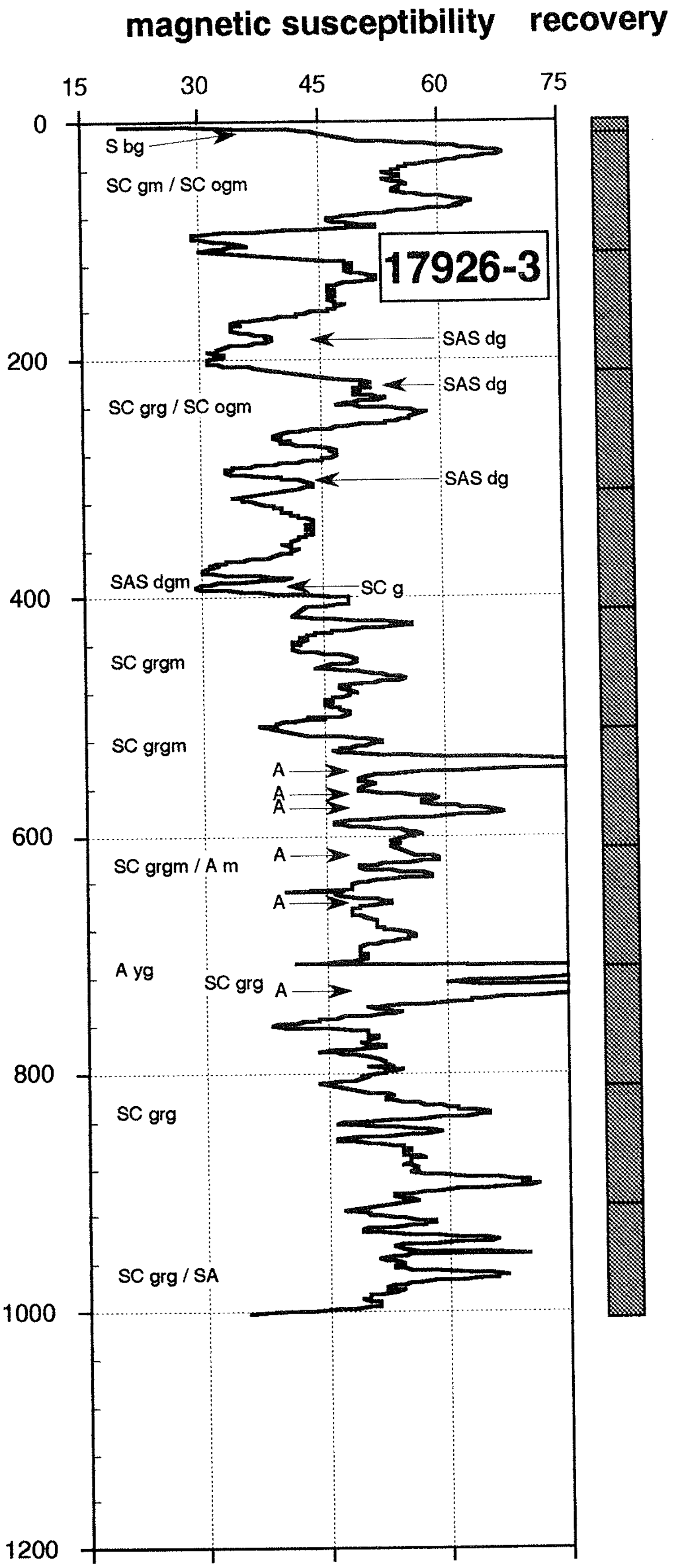

Core 17927-2

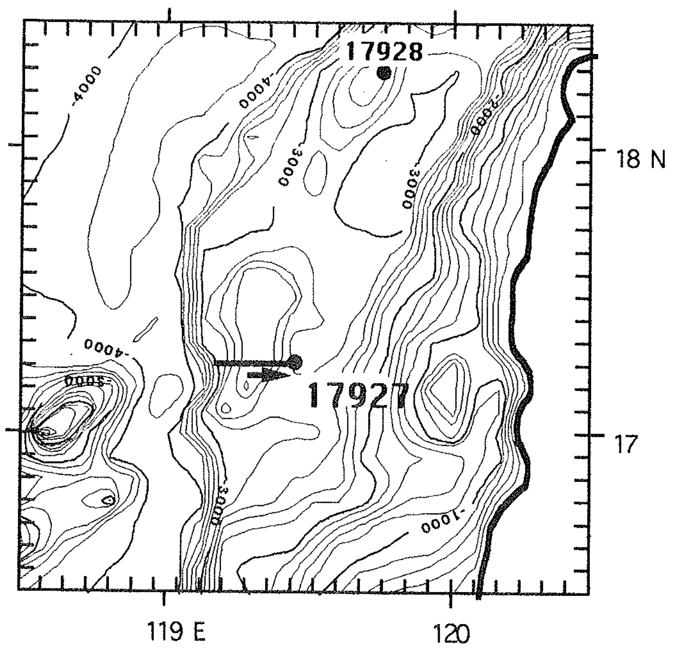

West of Luzon

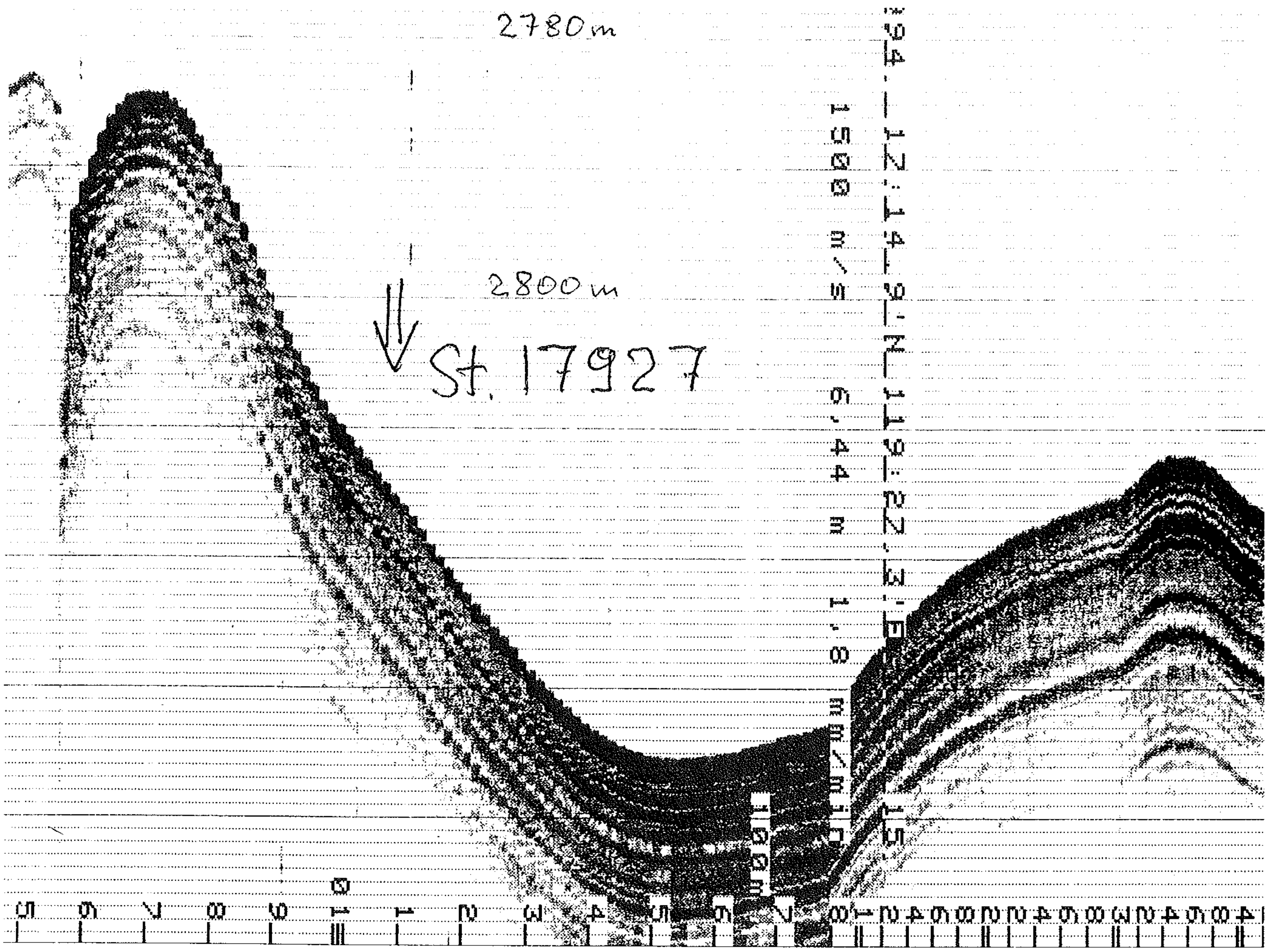

17927-2 17°15.1 N 119°27.2 E, 2804 m w.d., core length 5.58 m

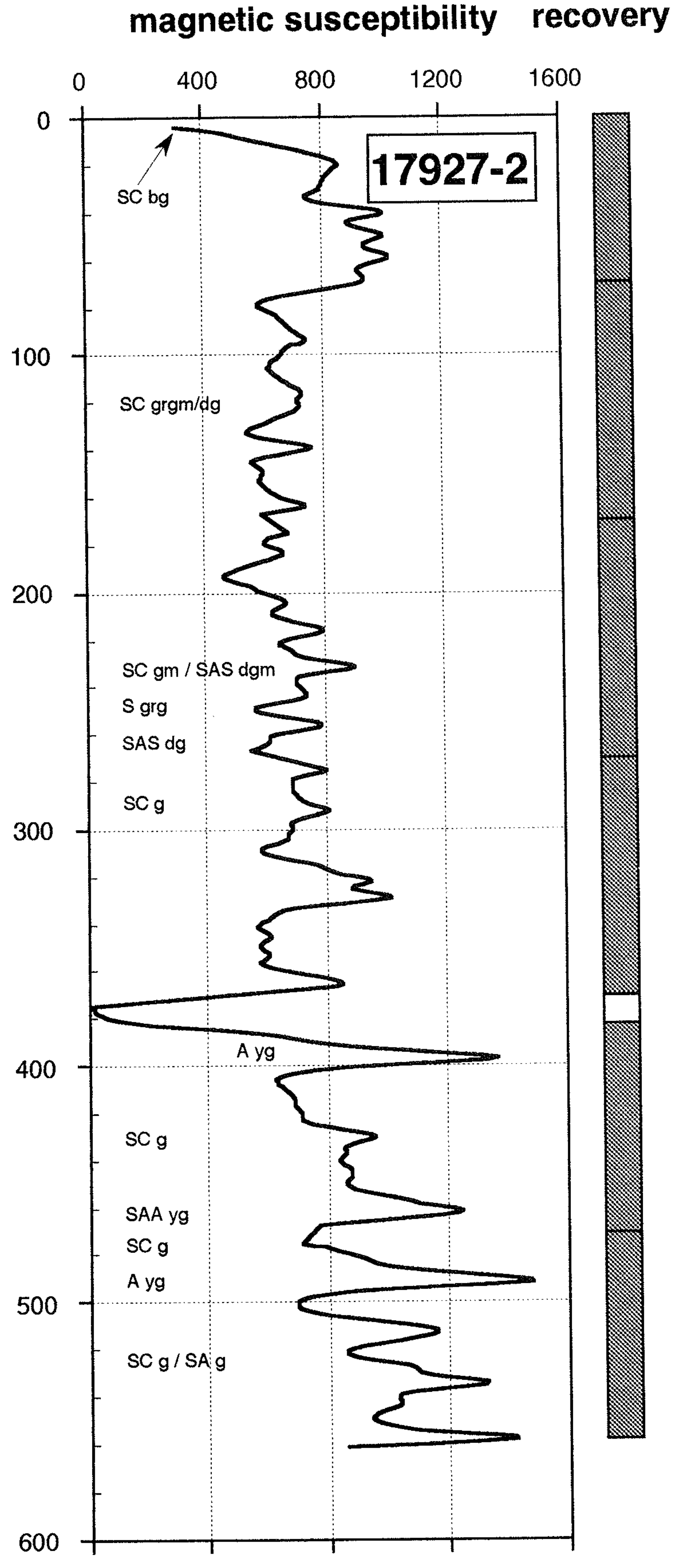

Core 17928-3

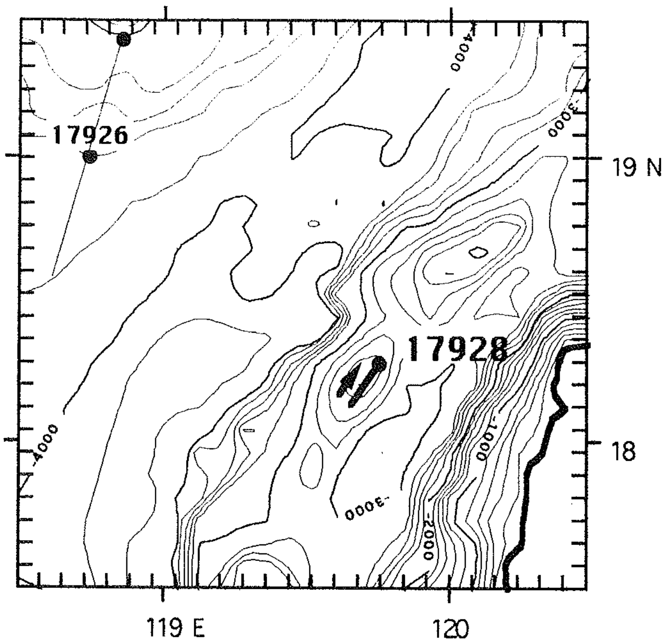

Ridge southwest of Bashi Strait

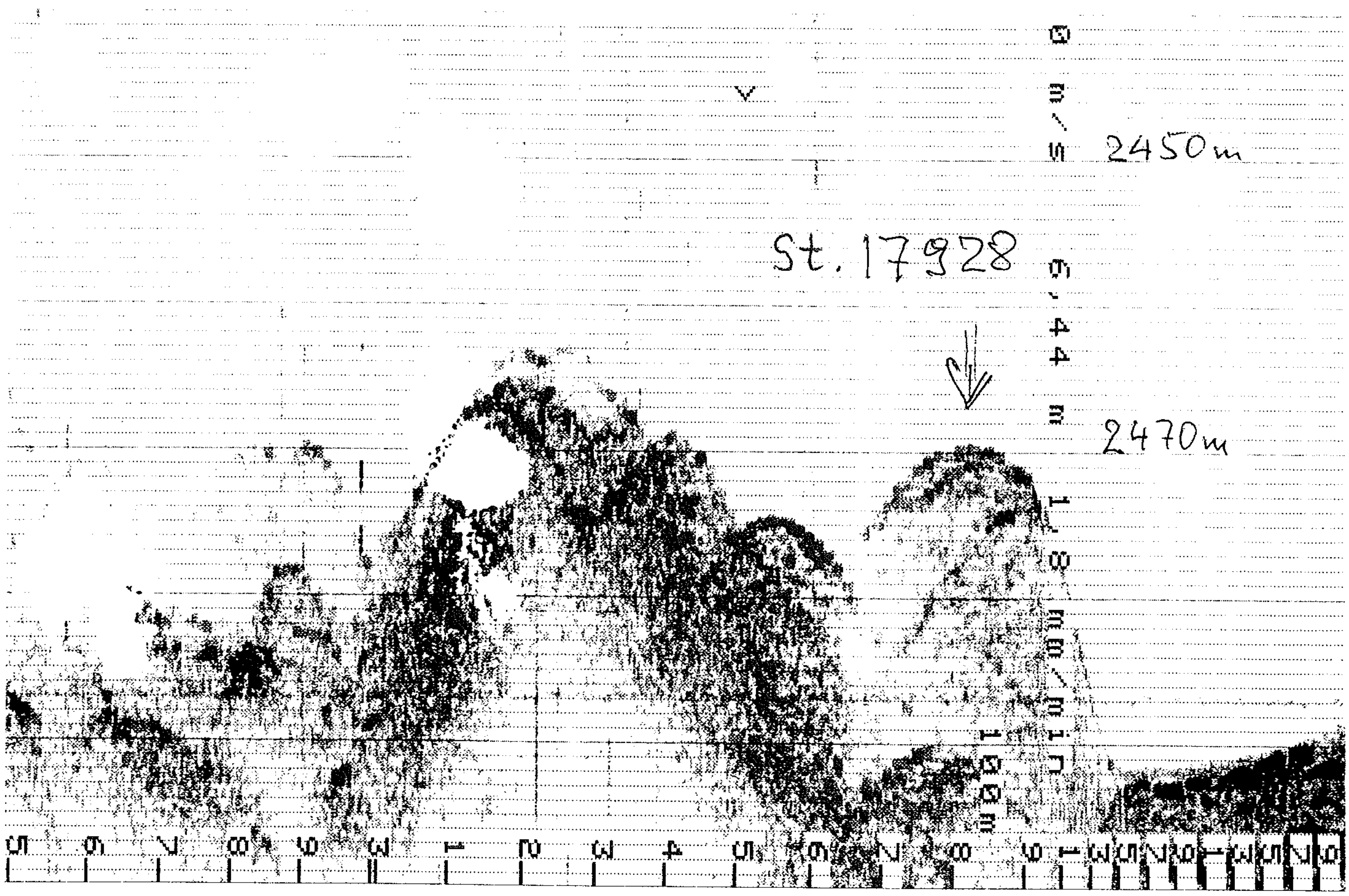

17928-3 18°16.3 N 119°44.7 E, 2484 m w.d., core length 3.41 m

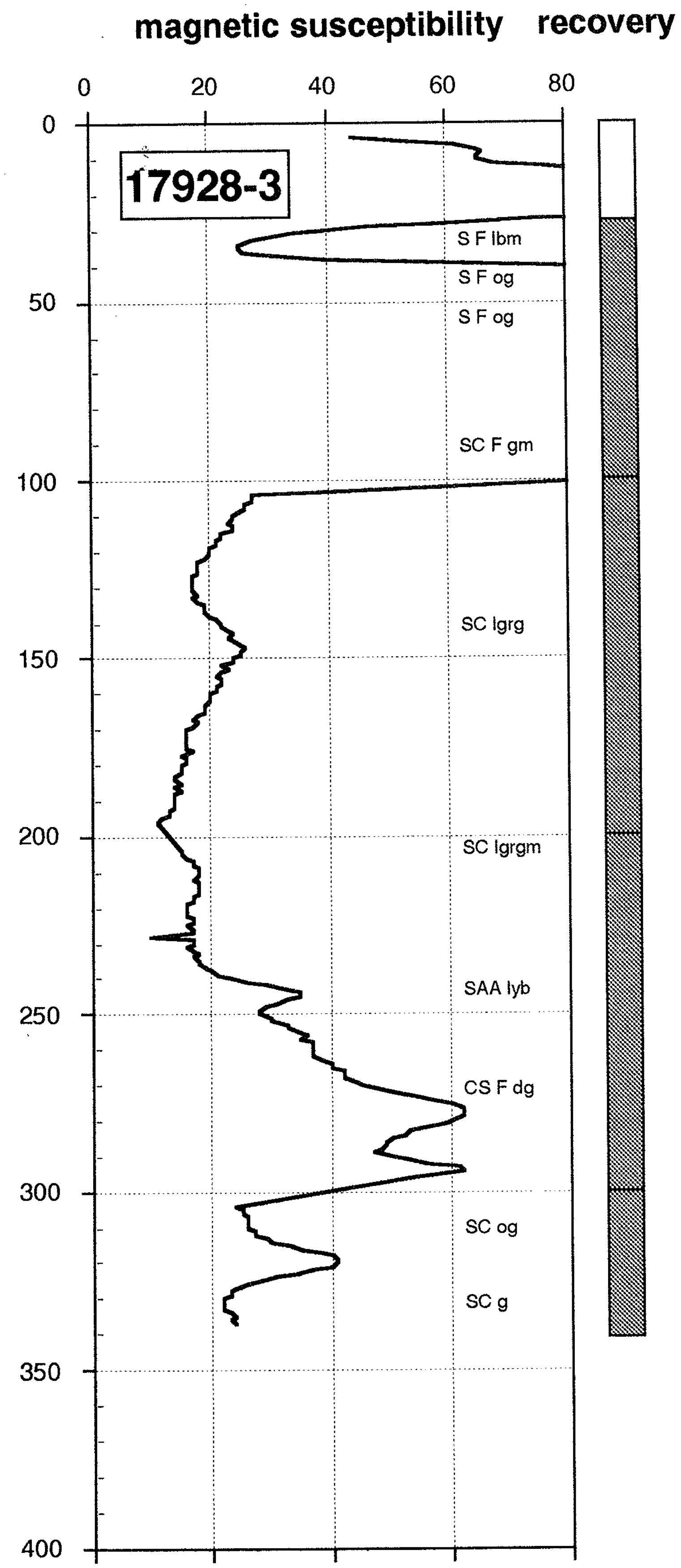

Core 17930-2

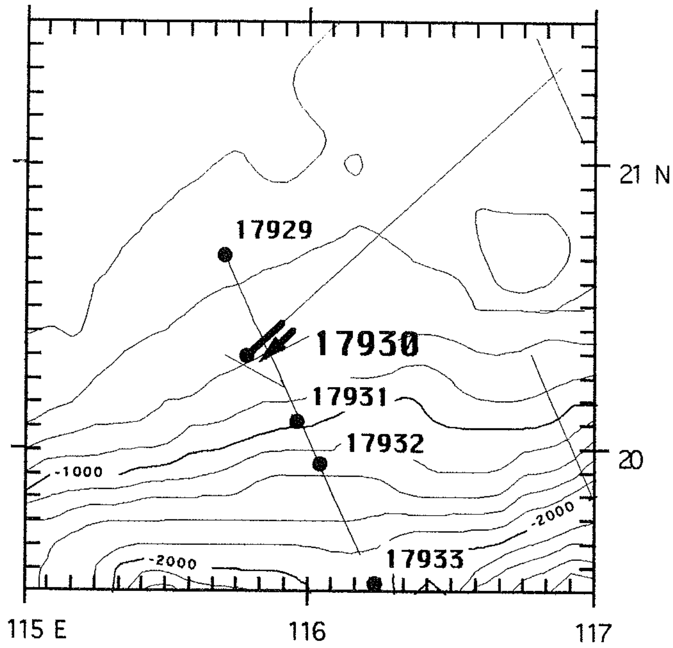

Continental slope southeast off Hong Kong

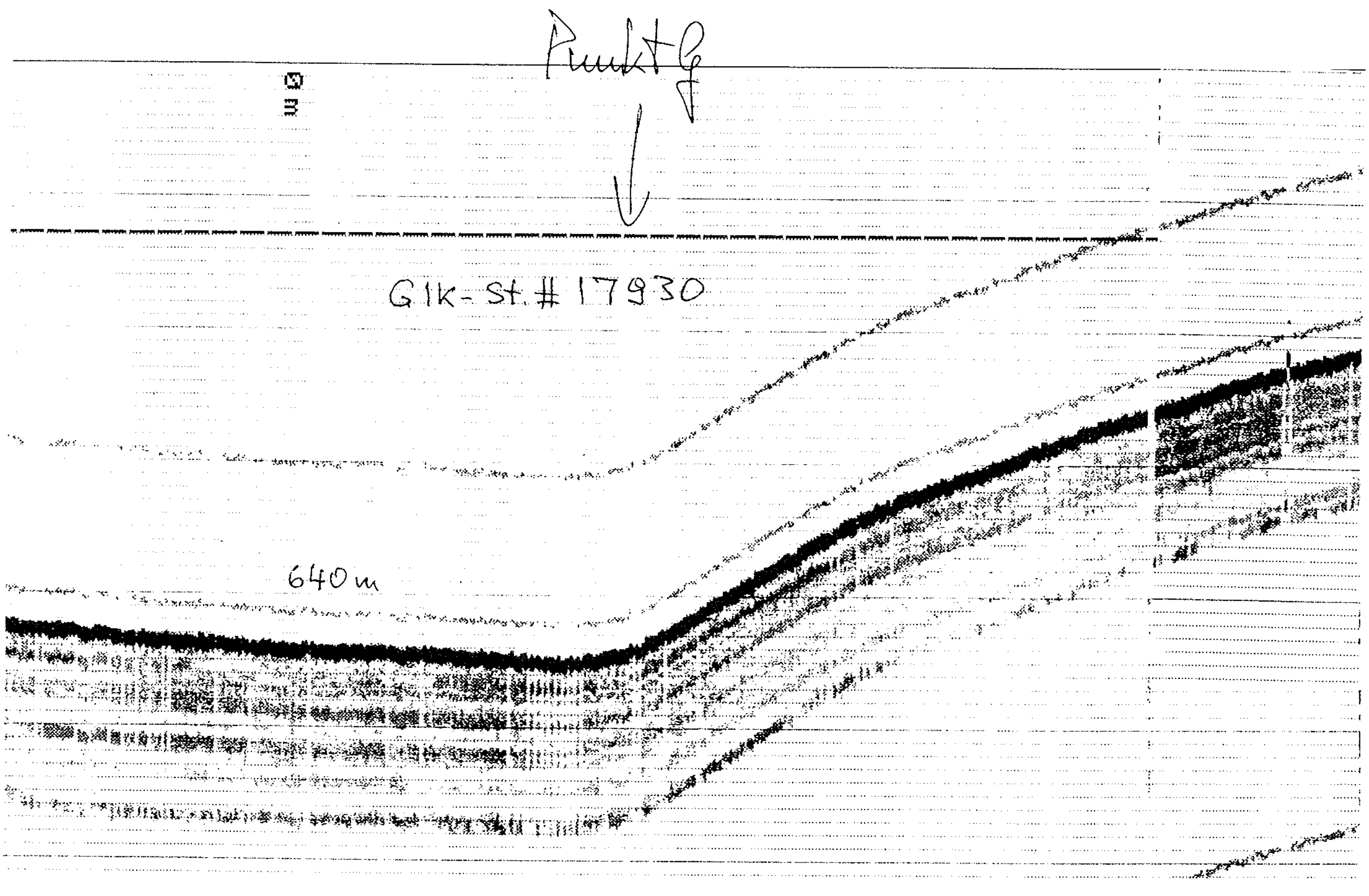

17930-2 20°20.0 N 115°46.9 E, 629 m w.d., core length 5.34 m

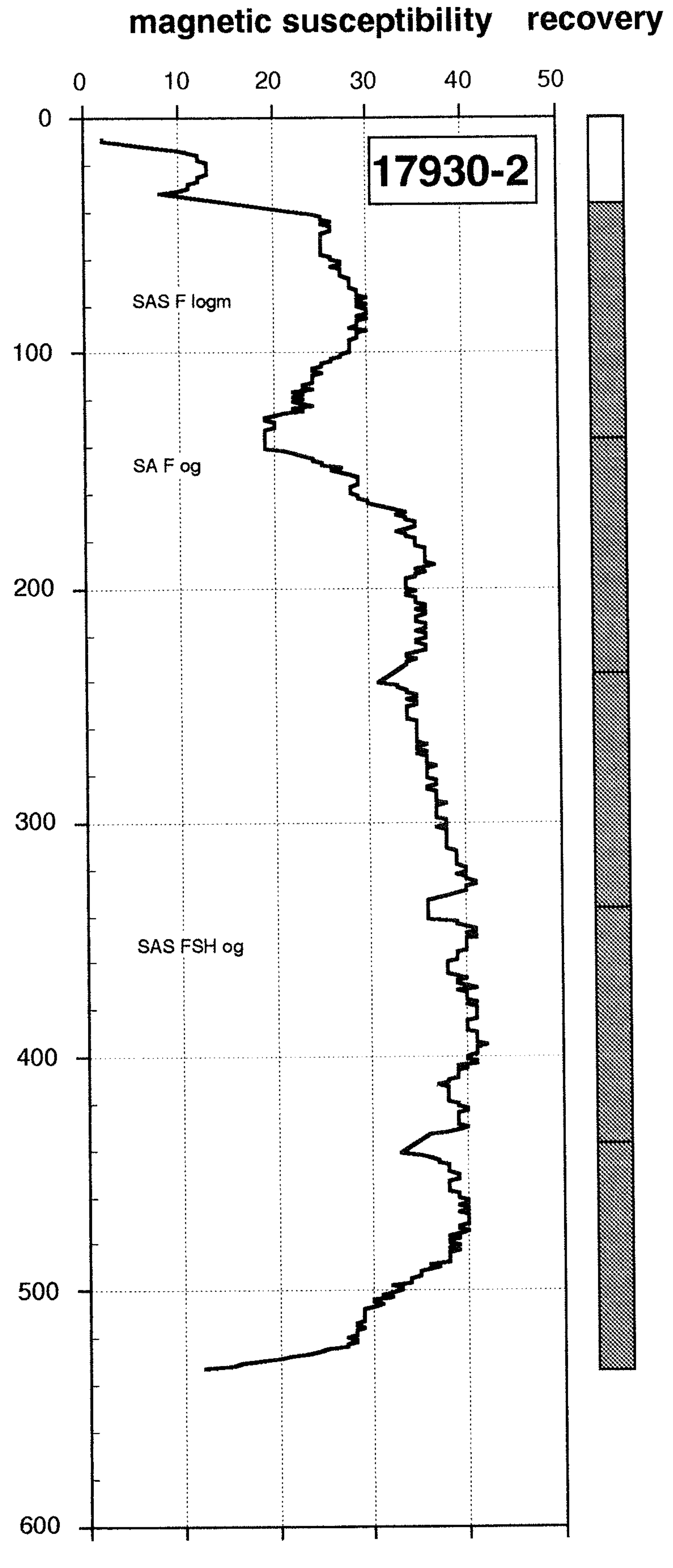

Core 17931-2
and
Core 17931-3

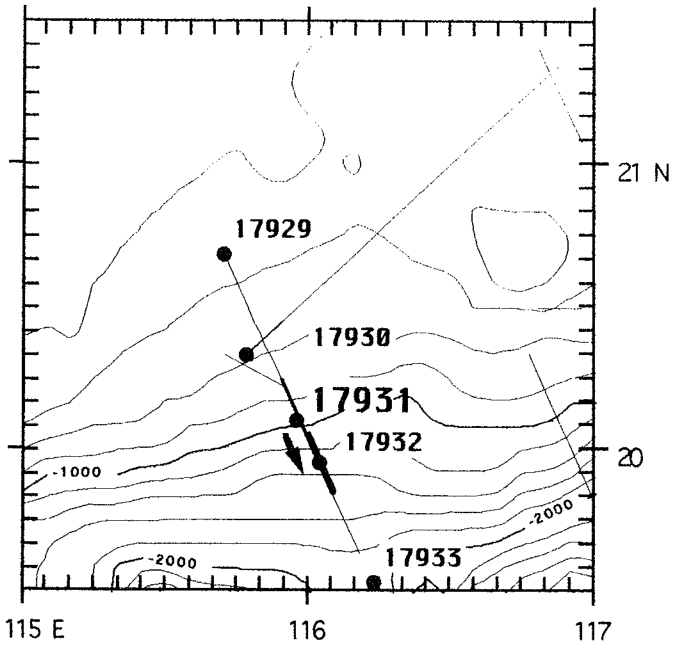

Continental slope southeast off Hong Kong

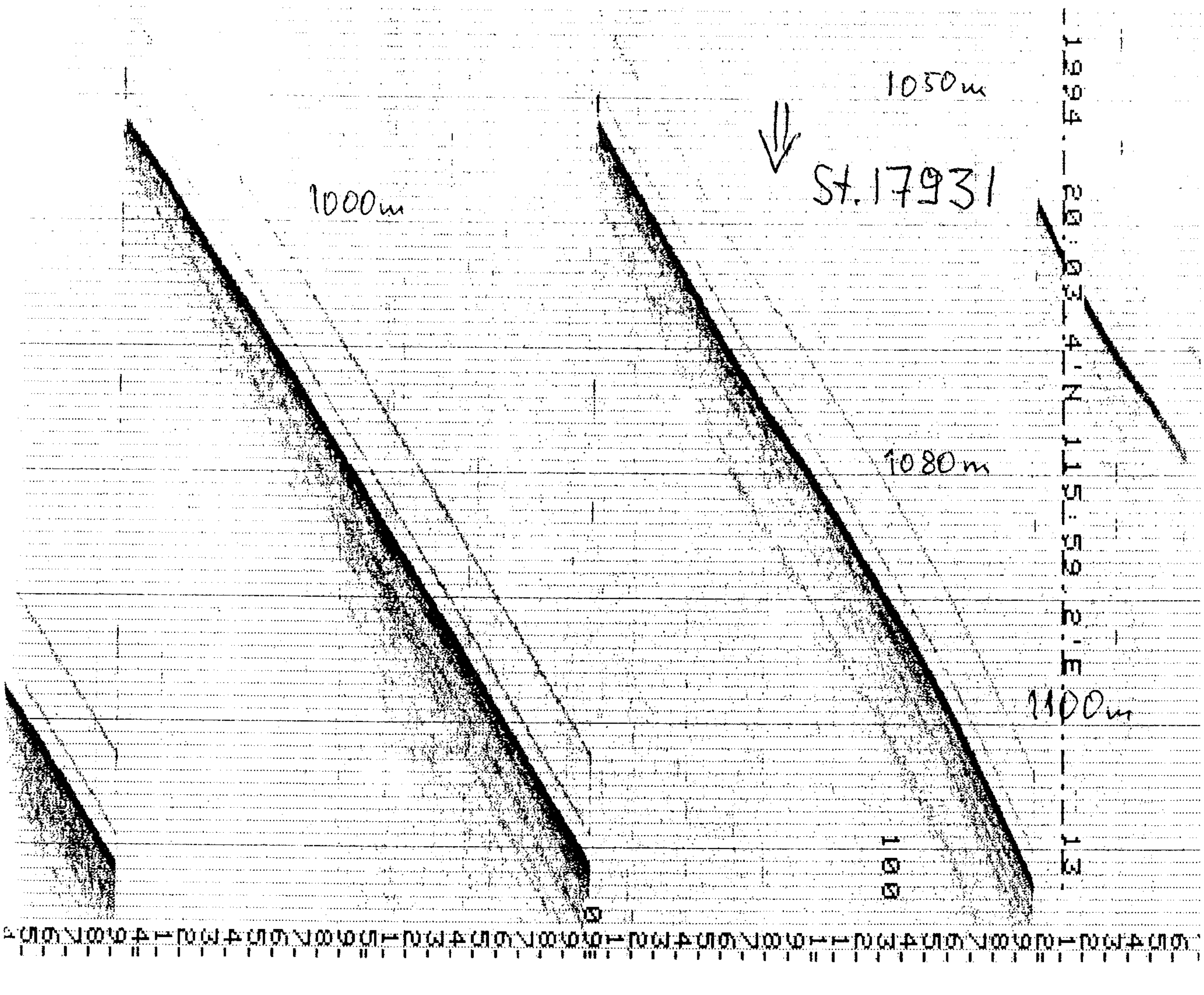

17931-2/3 20°06.0 N 115°57.8 E, 1003/1 m w.d., core length 3.00/4.31 m

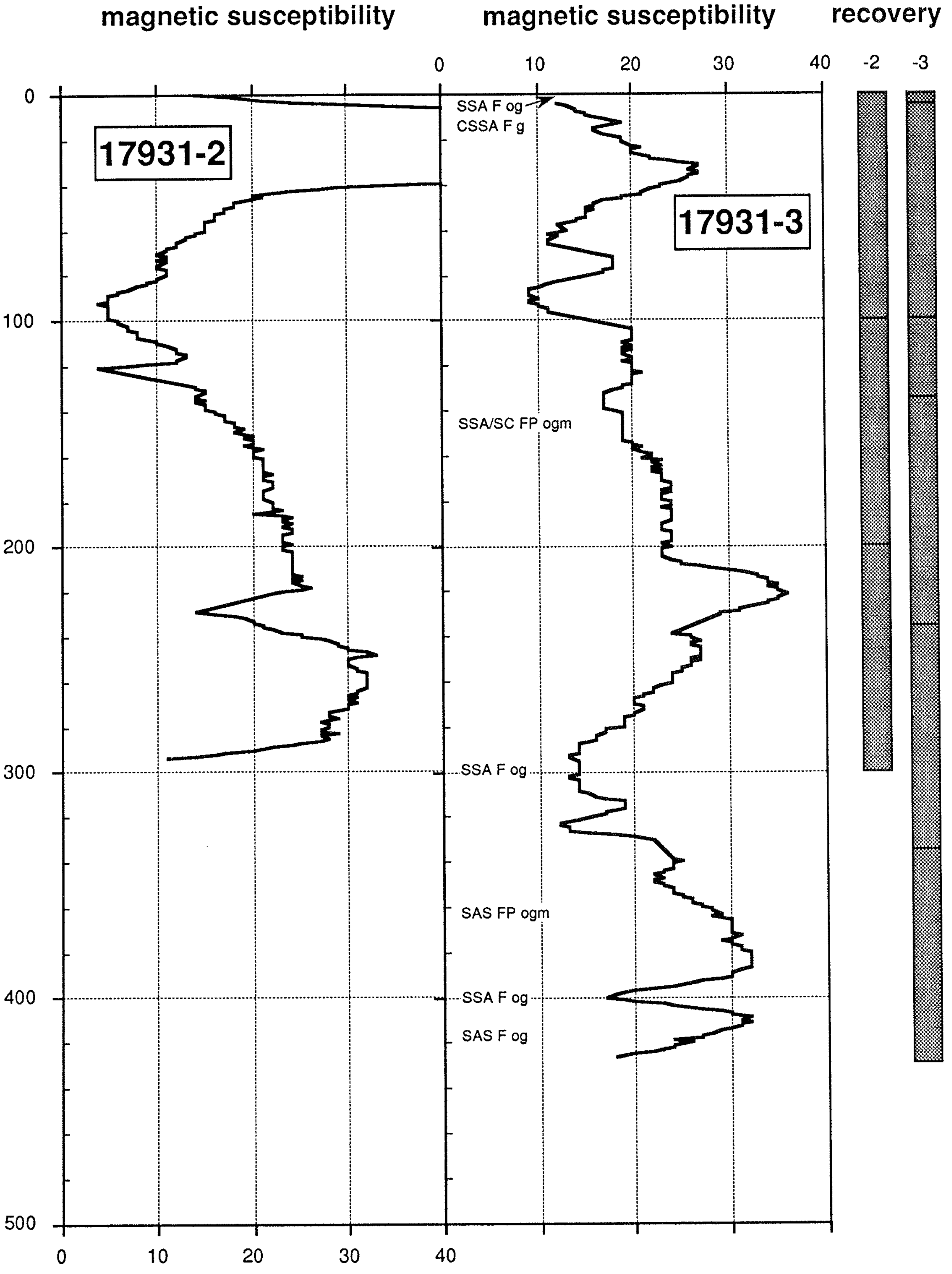

Core 17932-2

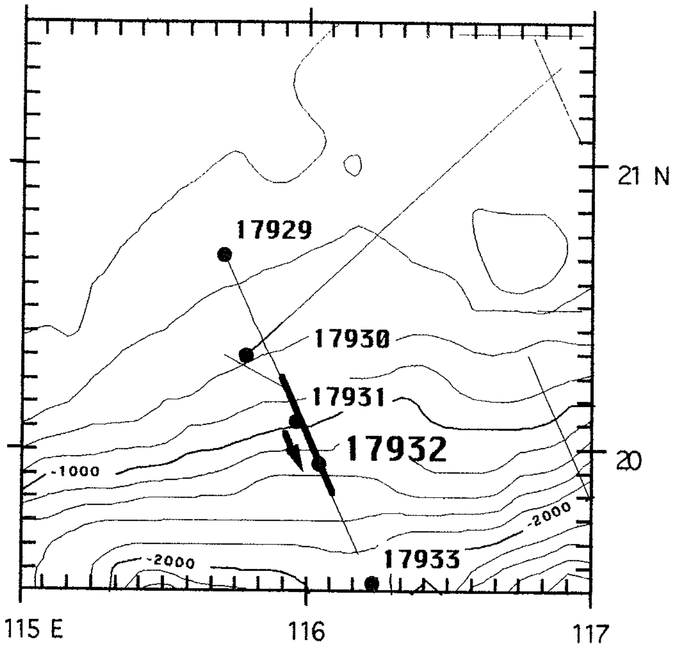

Continental slope southeast off Hong Kong

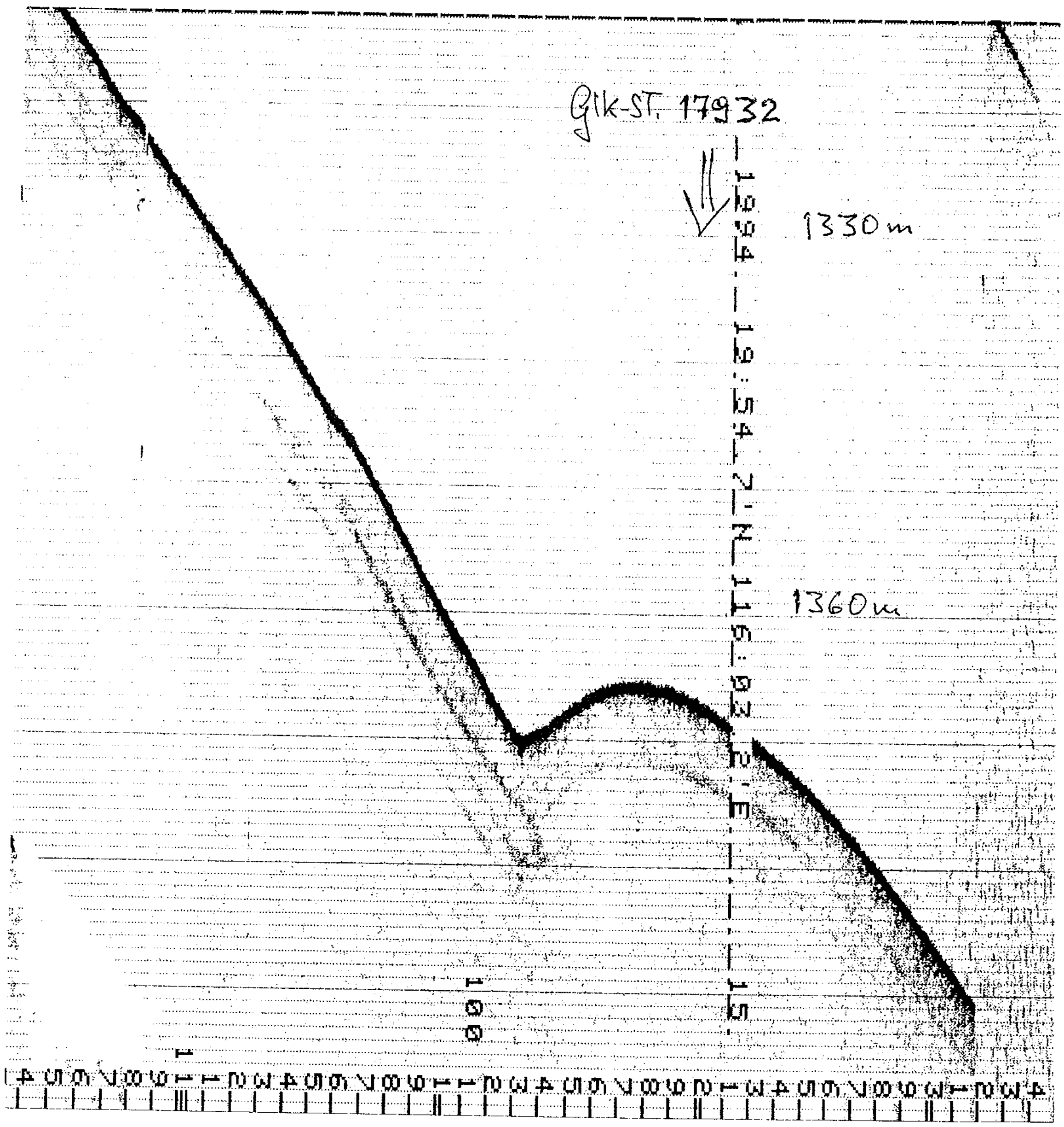

17932-2 19°57.1 N 116°02.2 E, 1360 m w.d., core length 7.56 m

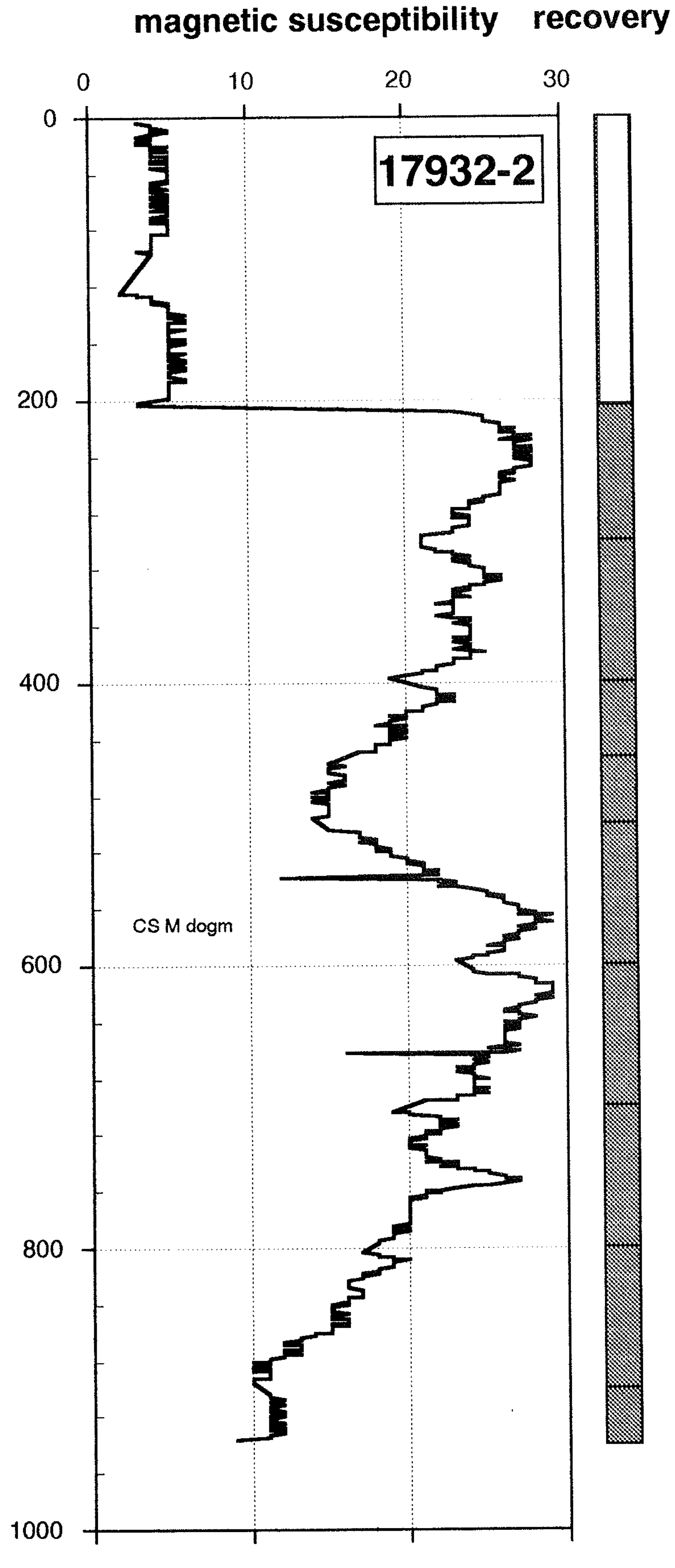

Core 17933-3
and
Core 17933-4

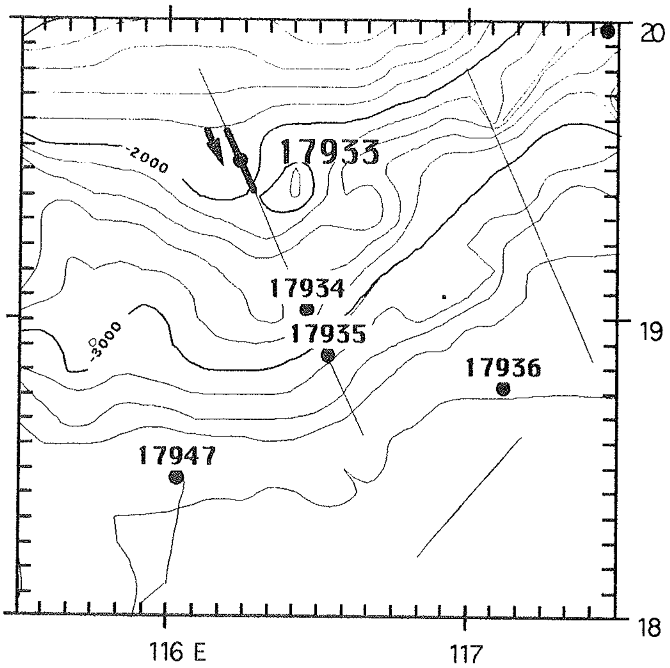

Continental slope southeast off Hong Kong

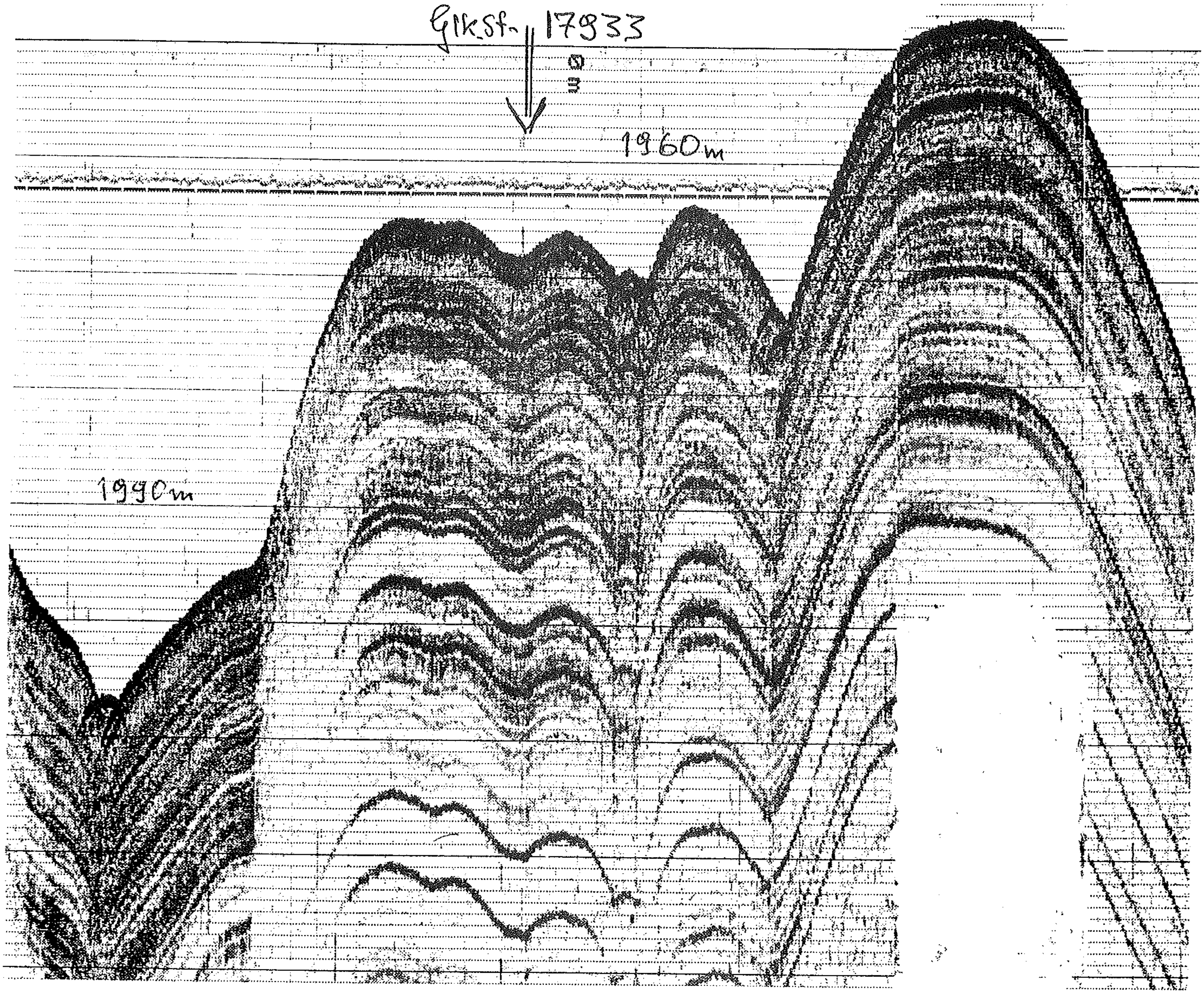

17933-3/4 19°32.0 N 116°13.6 E, 1970 m w.d., core length 12.48/19.75 m

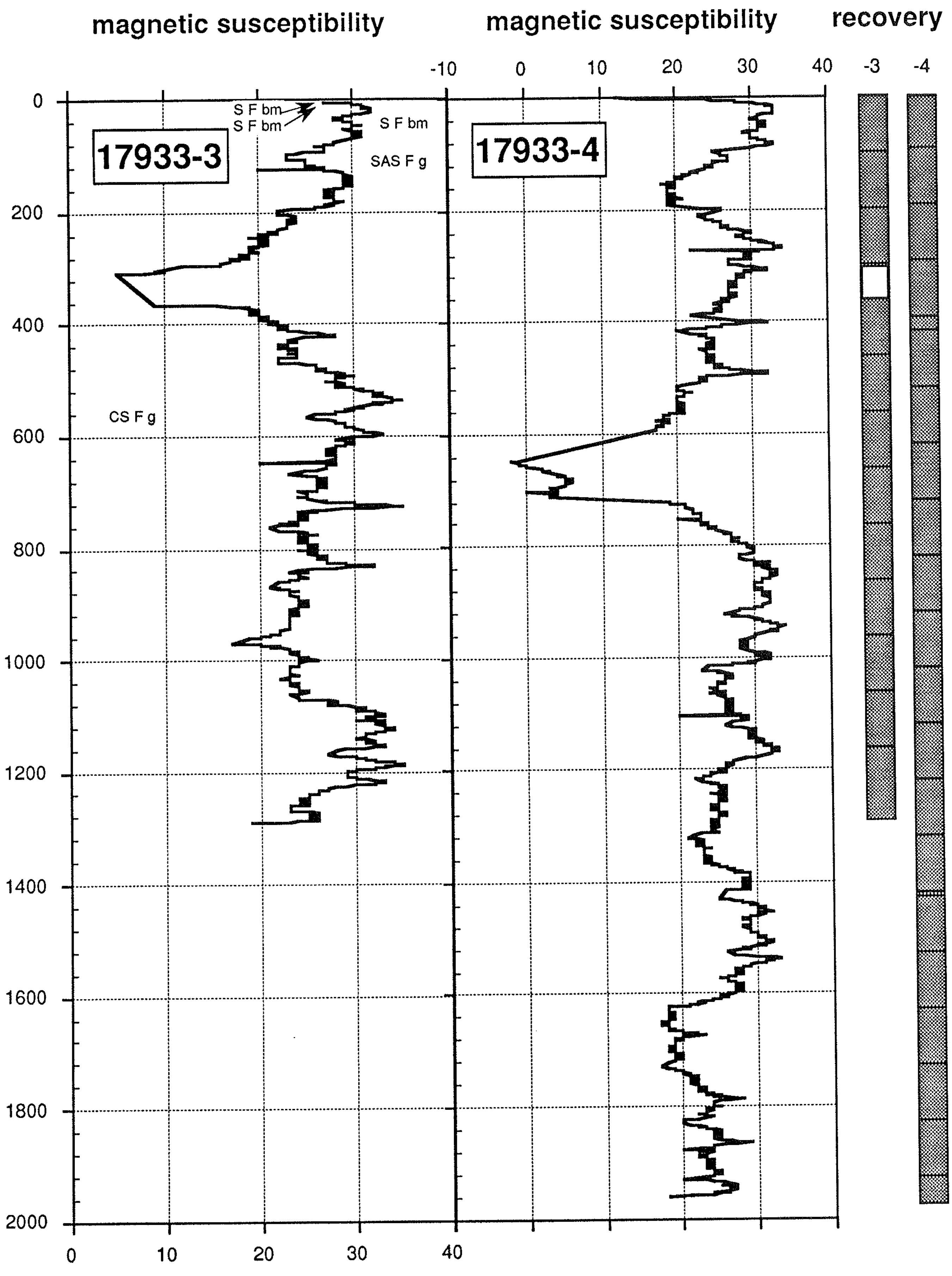

Core 17934-2

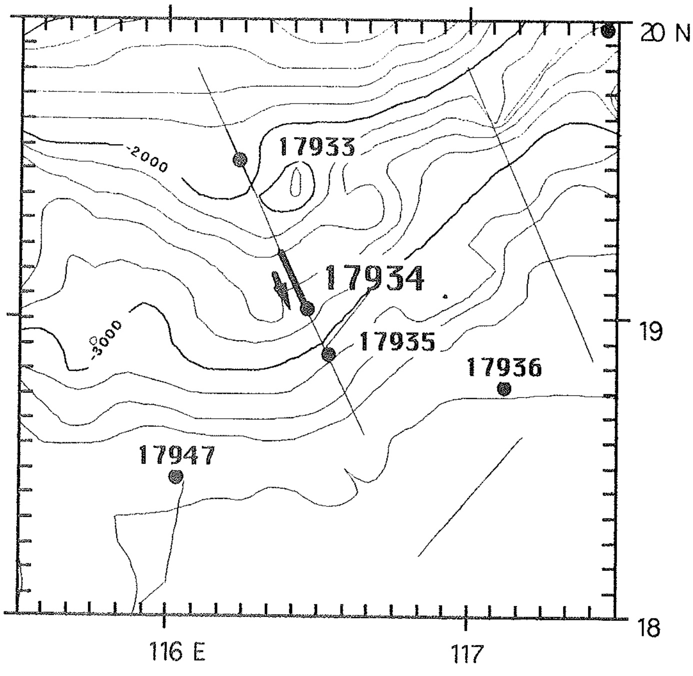

Continental slope southeast off Hong Kong

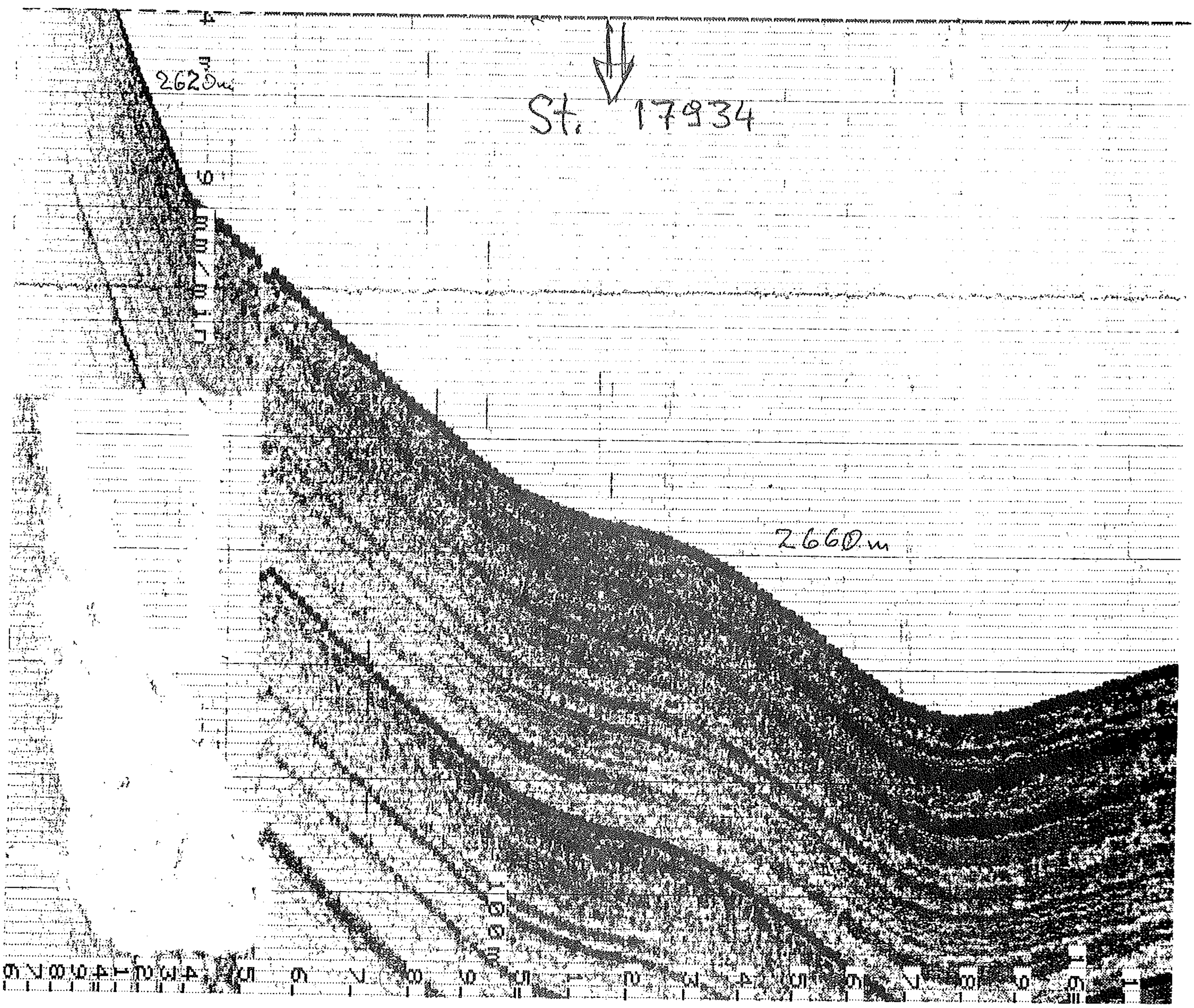

17934-2 19°01.9 N 116°27.7 E, 2665 m w.d., core length 11.87 m

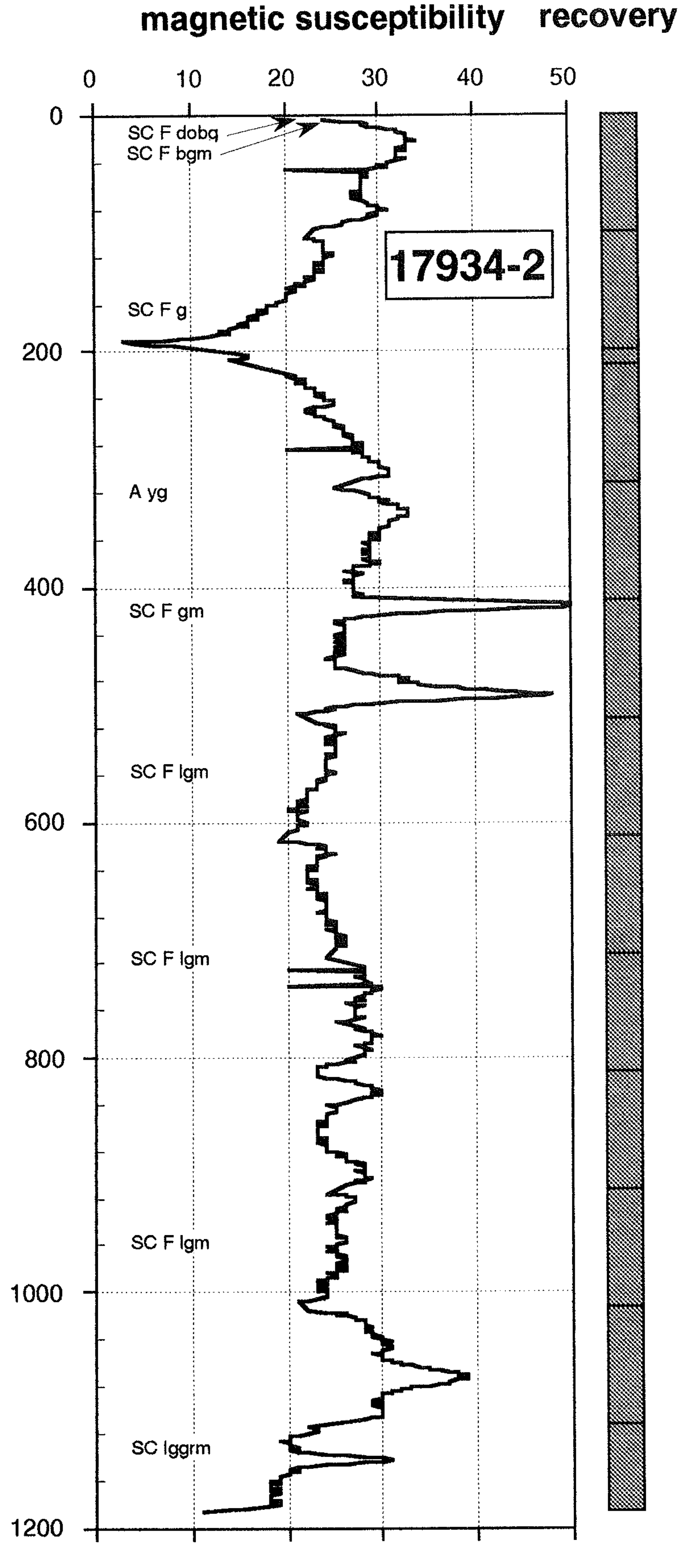

Core 17935-3

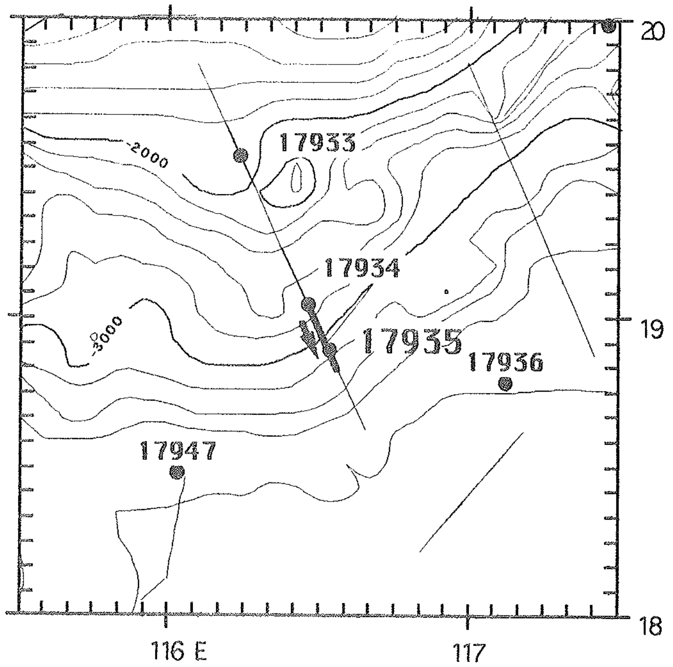

Continental slope southeast off Hong Kong

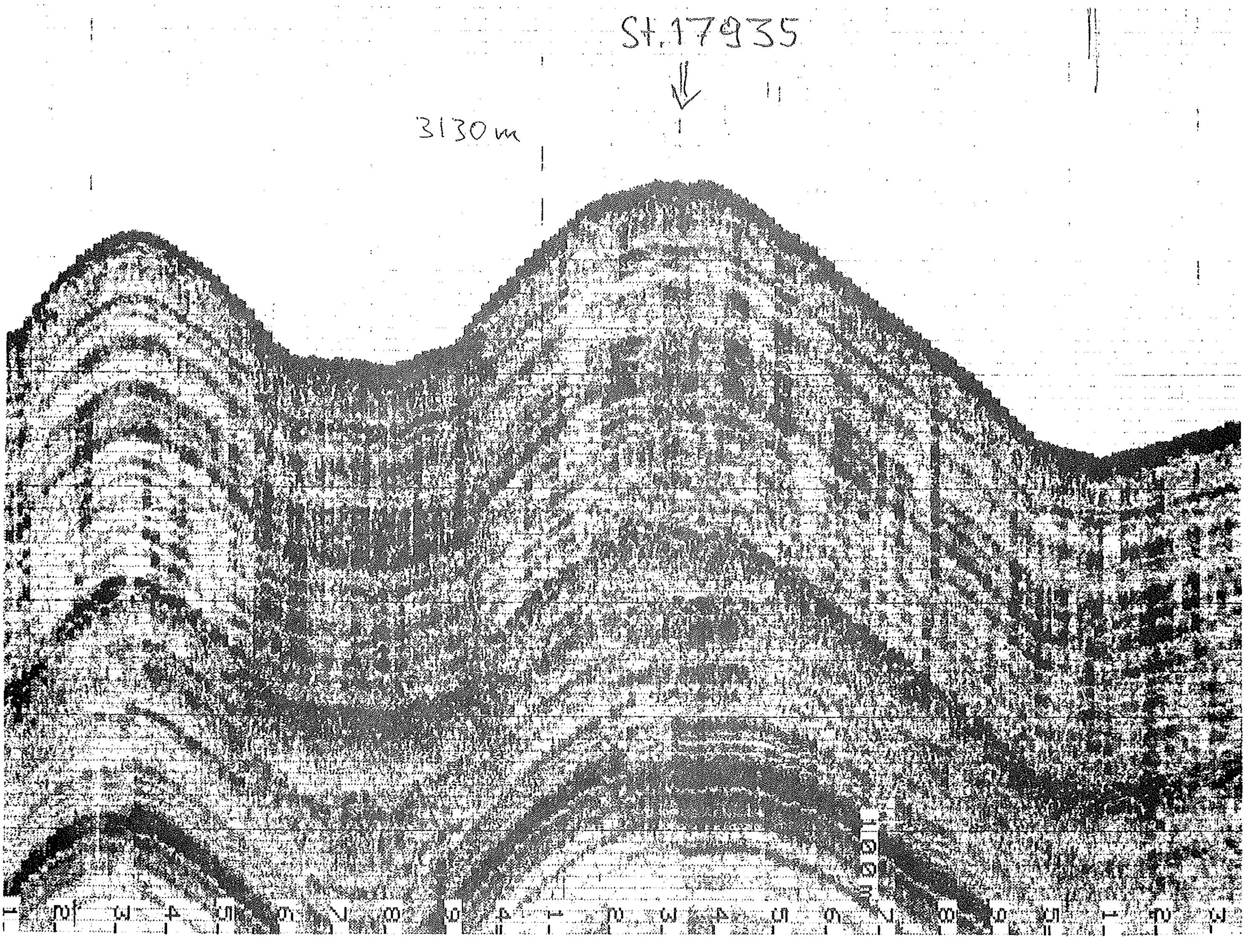

17935-3 18°52.7 N 116°31.6 E, 3148 m w.d., core length 12.27 m

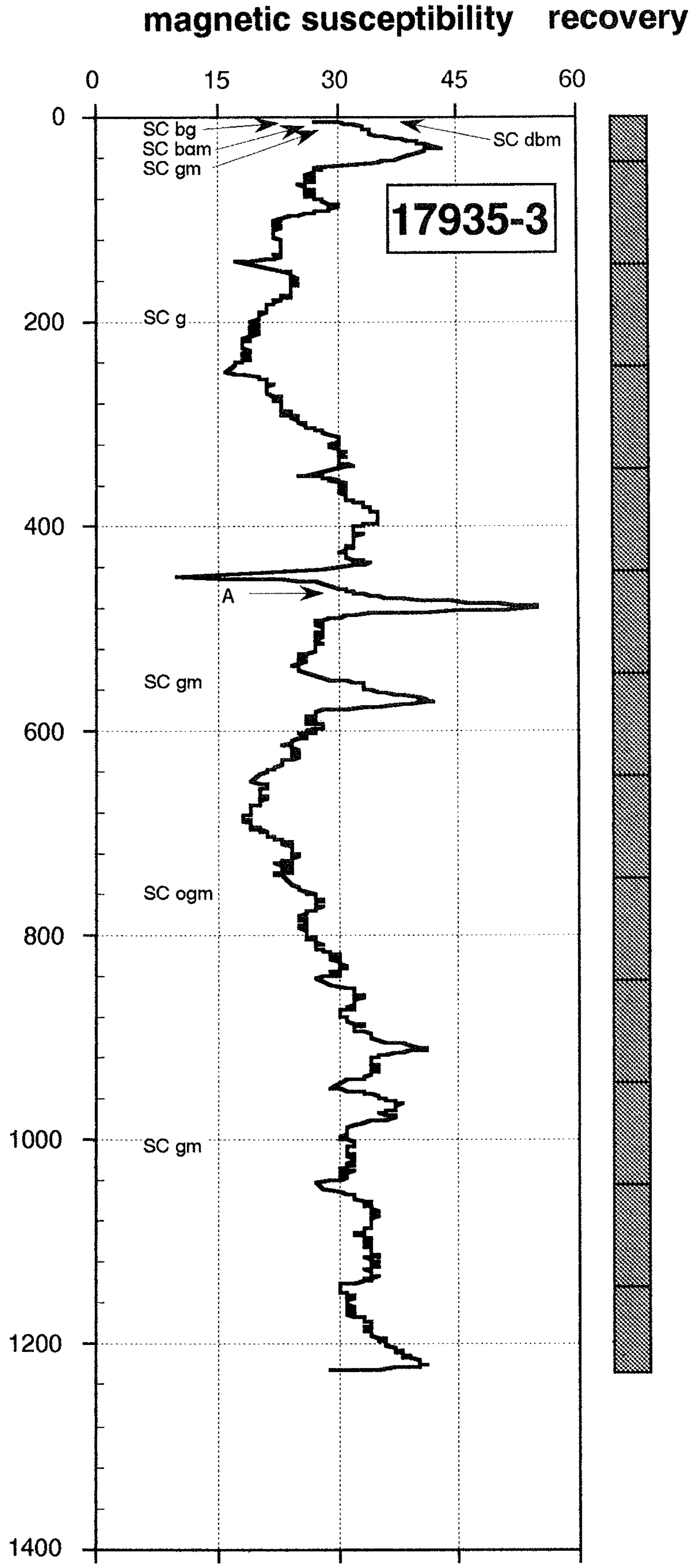

Core 17936-2

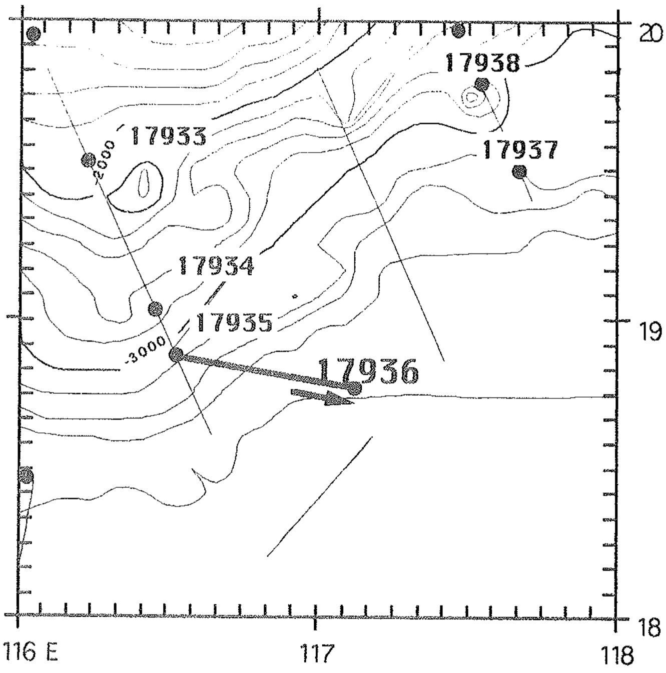

Continental slope southeast off Hong Kong

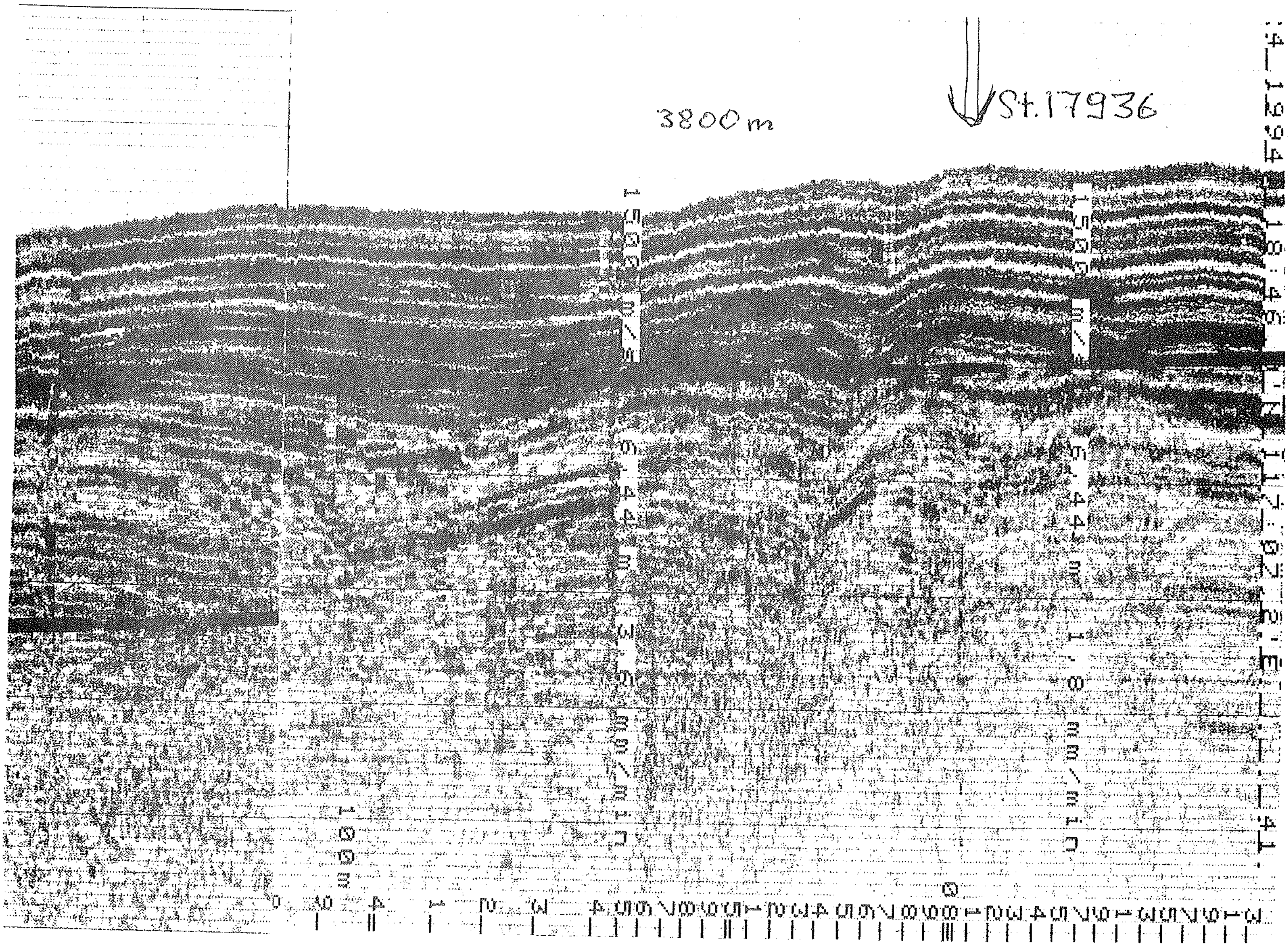

17936-2 18°46.0 N 117°07.2 E, 3809 m w.d., core length 13.33 m

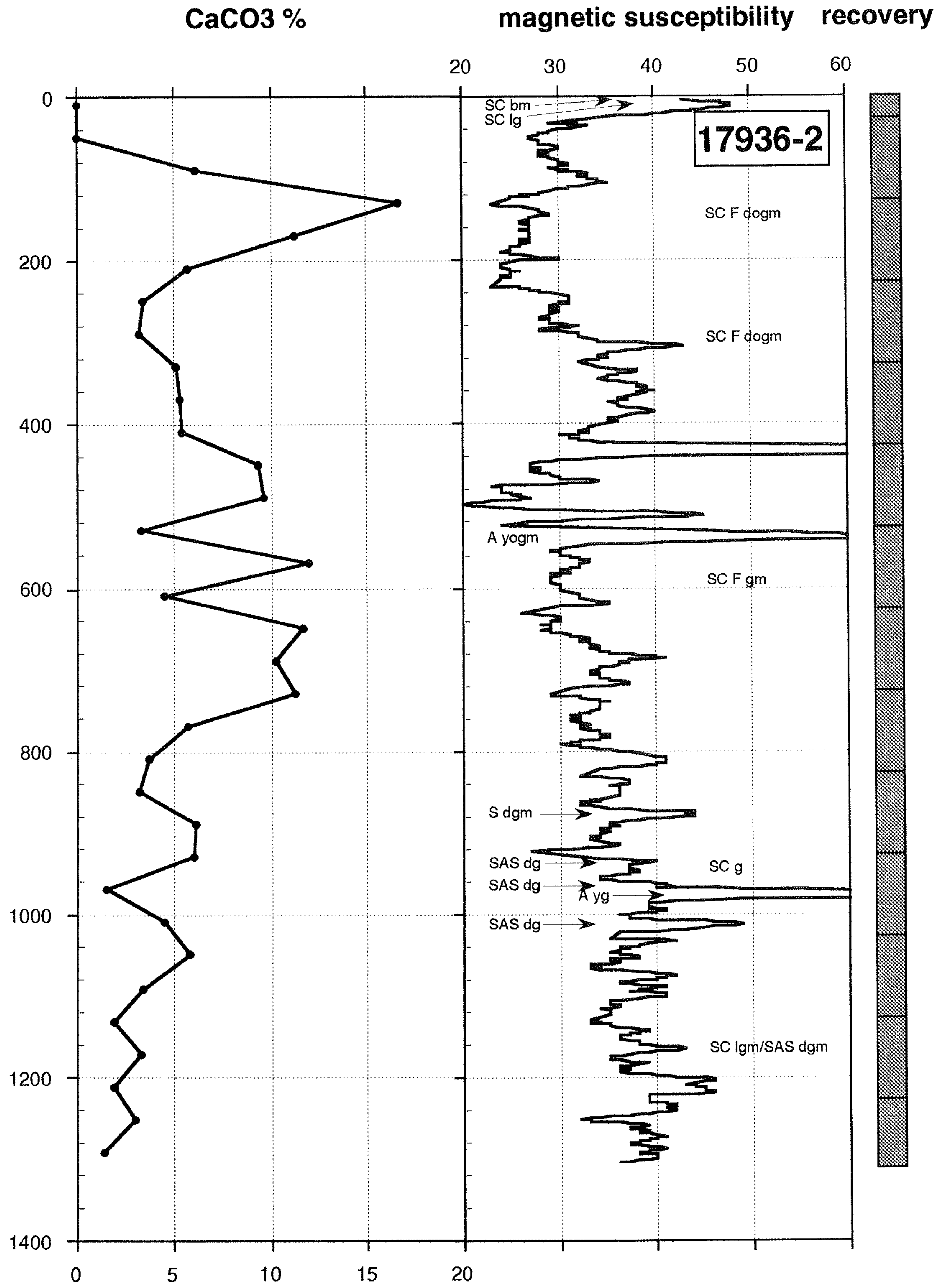

Core 17937-2

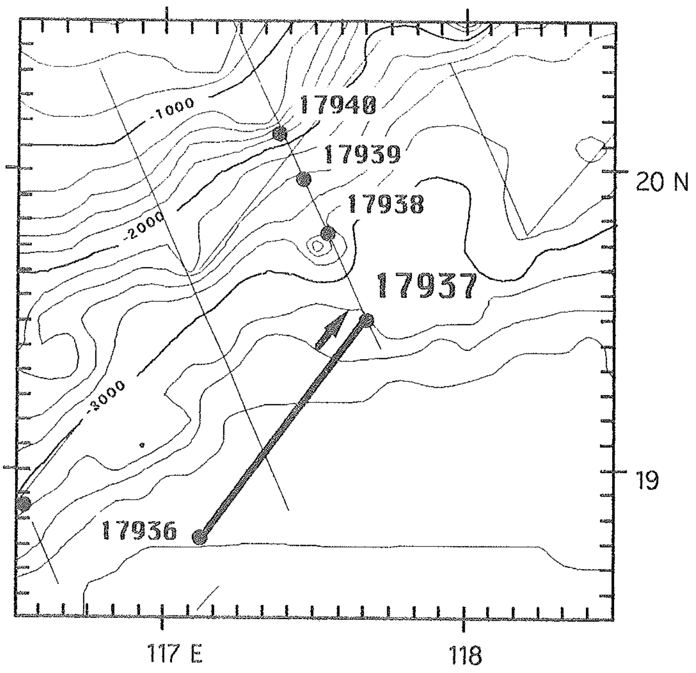

Continental slope southeast off Hong Kong

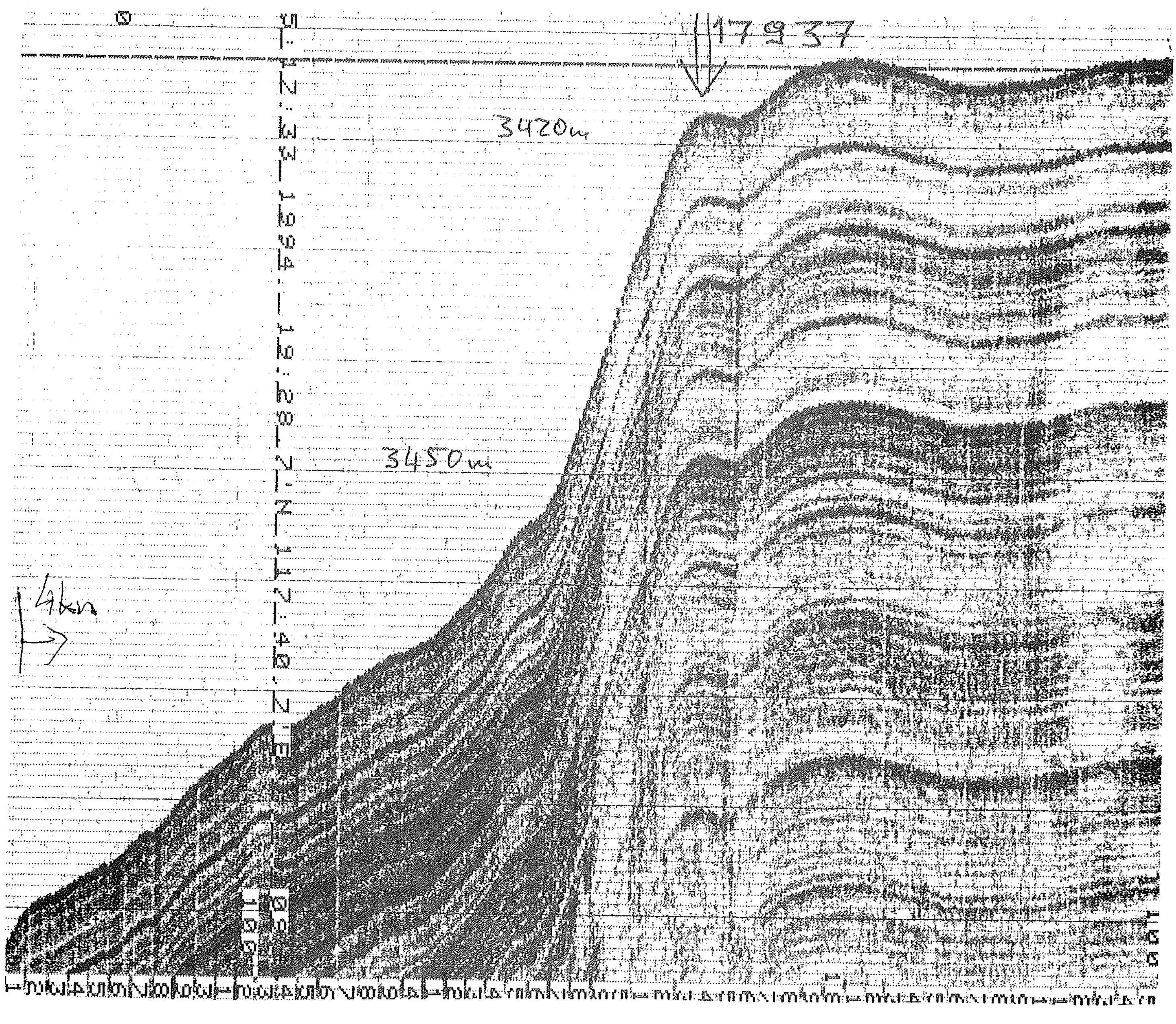

17937-2 19°30.0 N 117°39.9 E, 3428 m w.d., core length 12.92 m

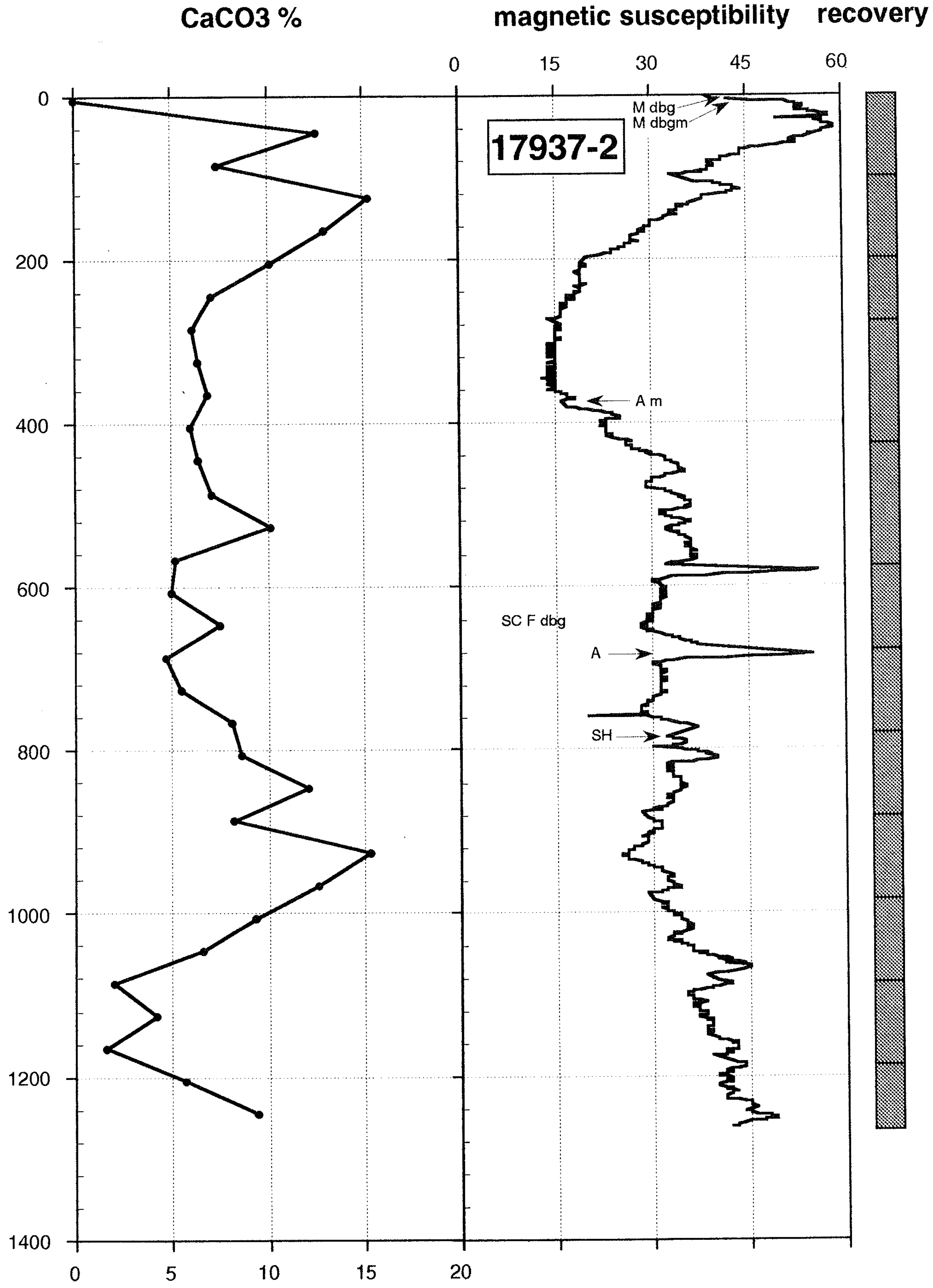

Core 17938-2

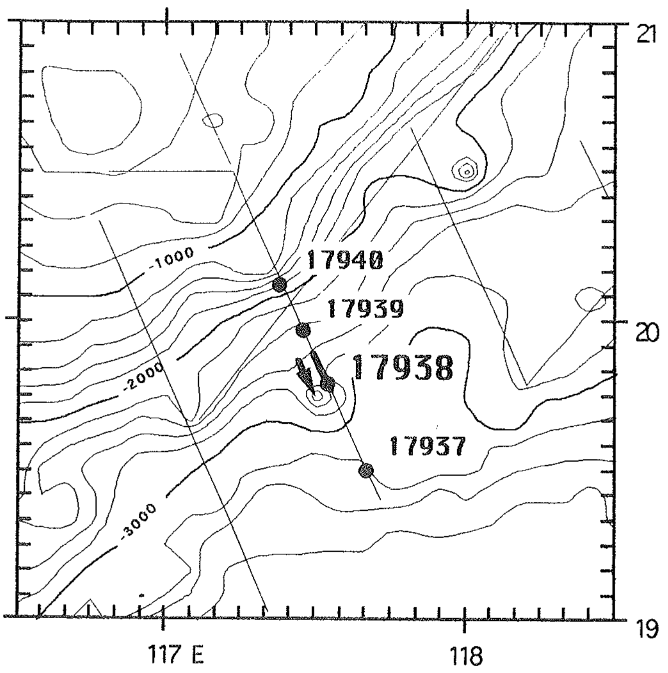

Continental slope southeast off Hong Kong

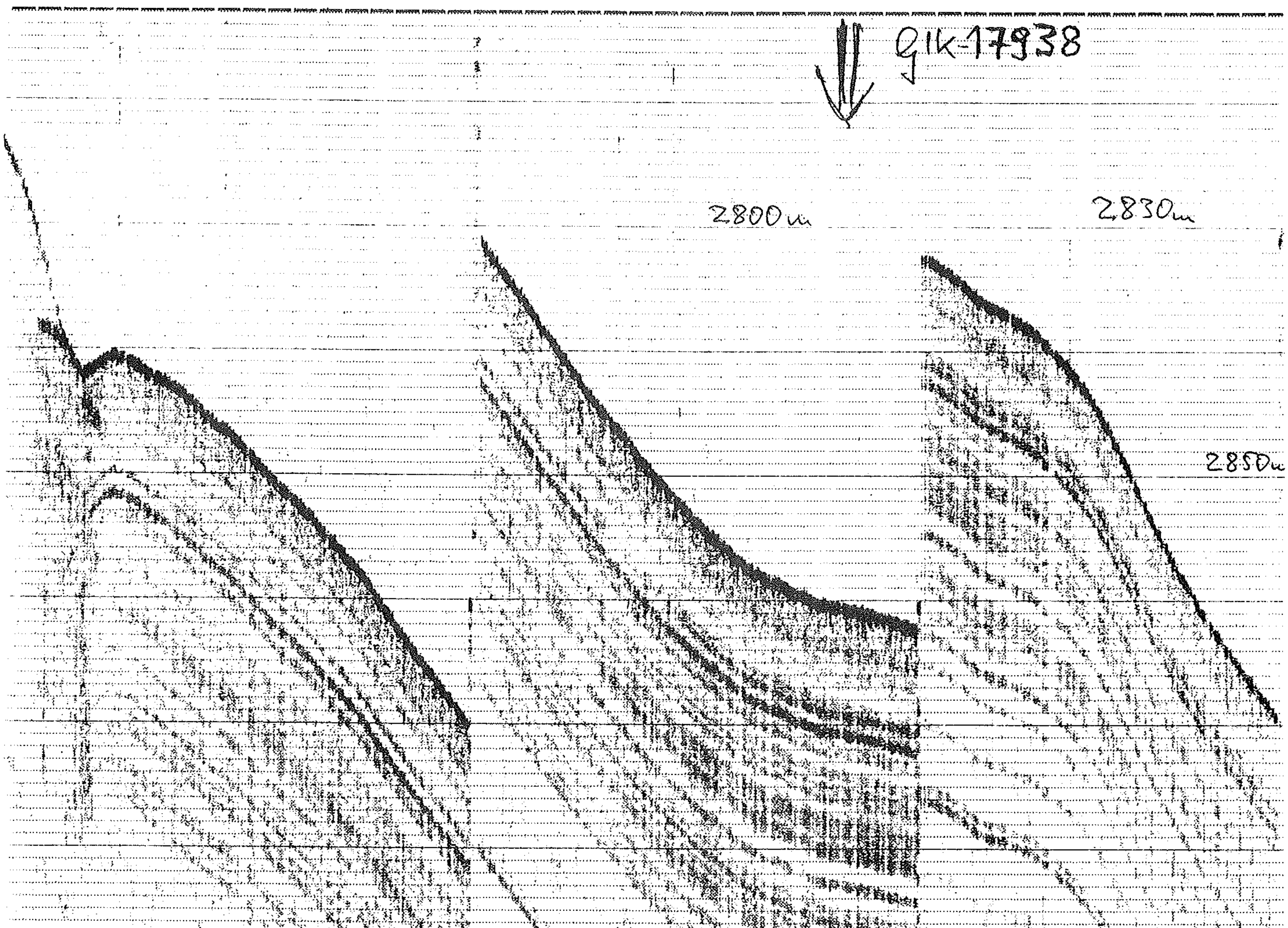

17938-2 19°47.2 N 117°32.3 E, 2840 m w.d., core length 11.78 m

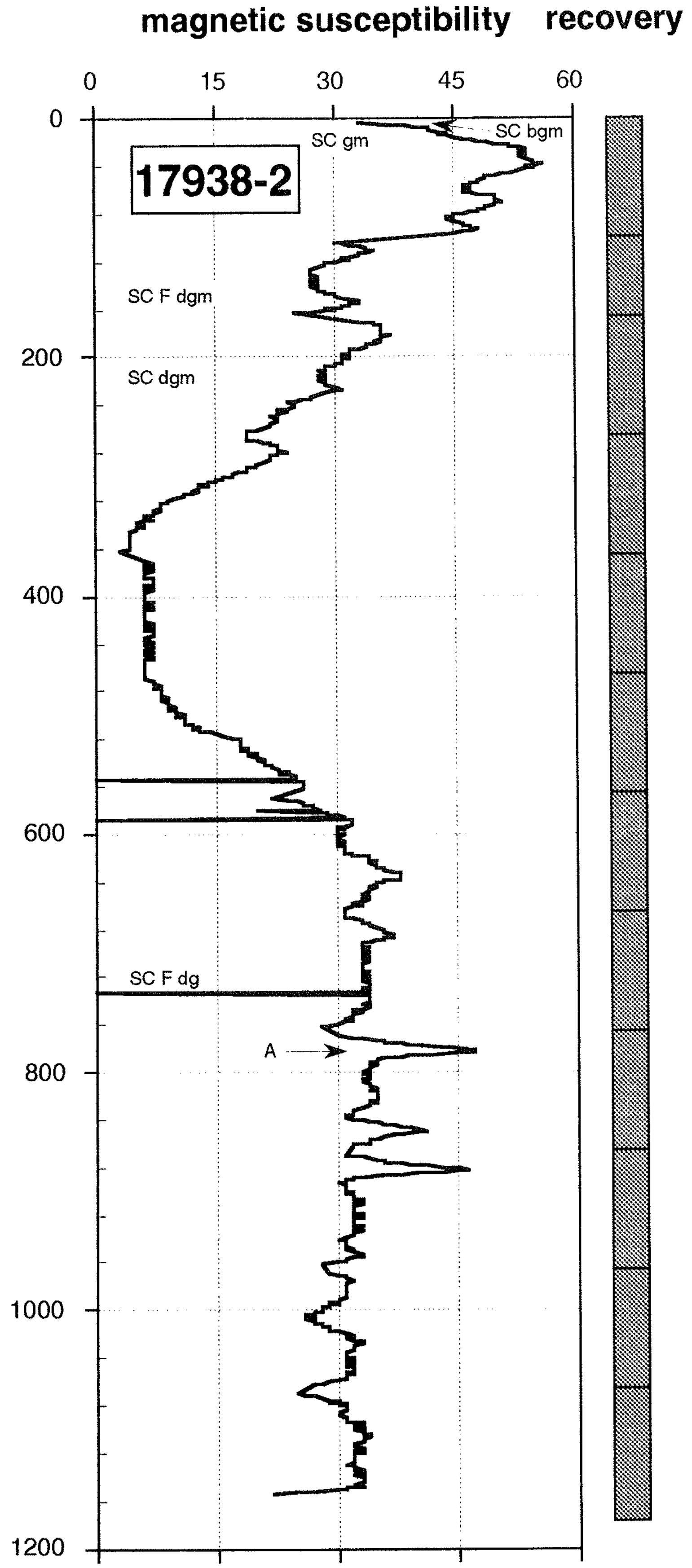

Core 17939-2

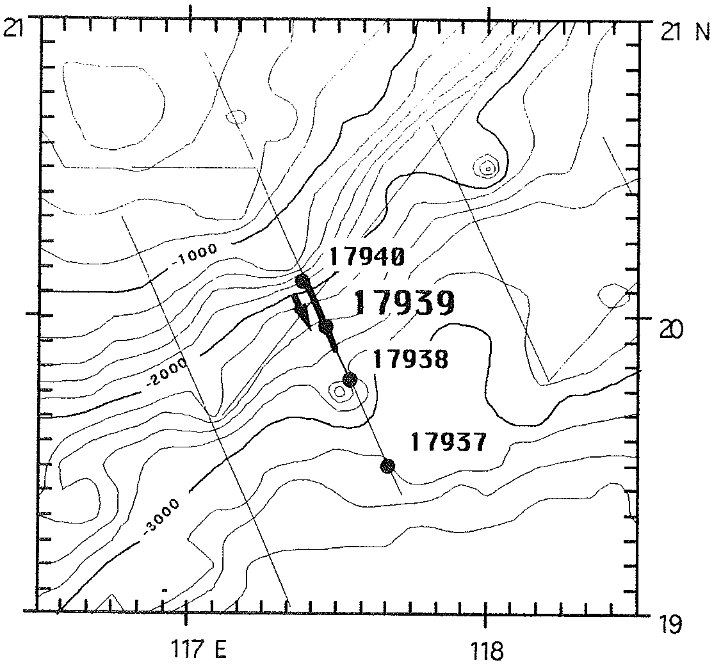

Continental slope southeast off Hong Kong

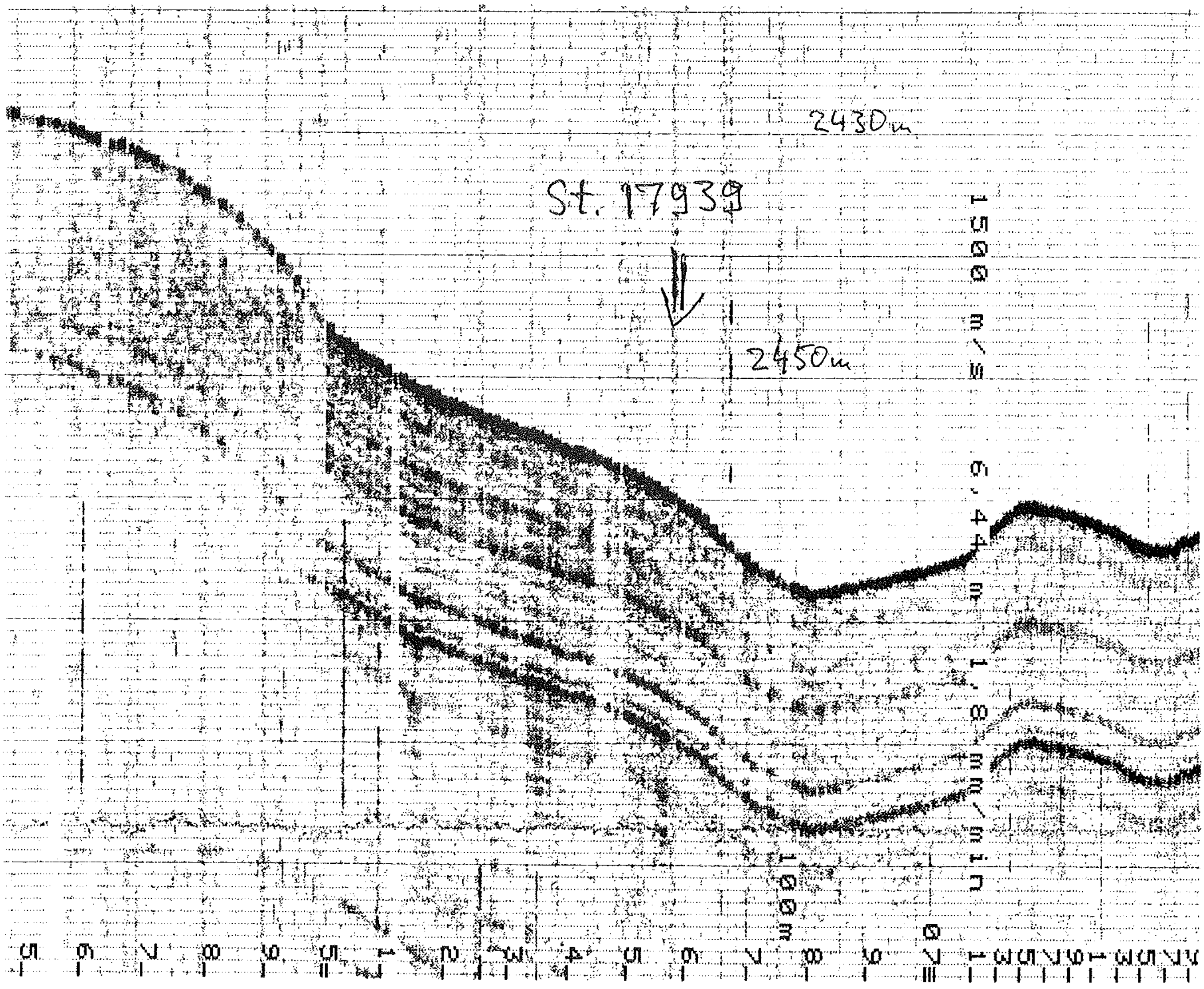

17939-2 19°58.2 N 117°27.3 E, 2474 m w.d., core length 12.74 m

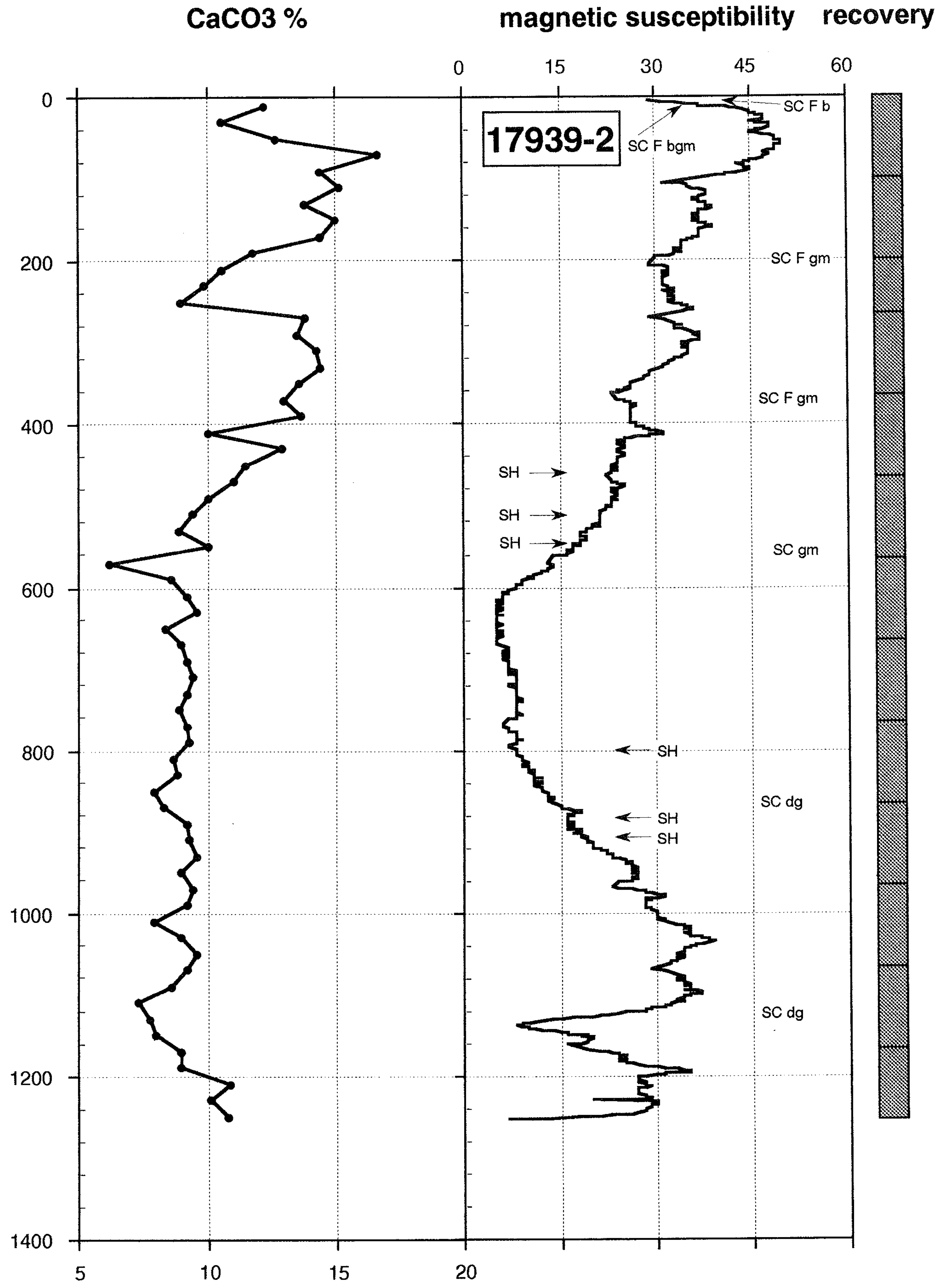

Core 17940-2

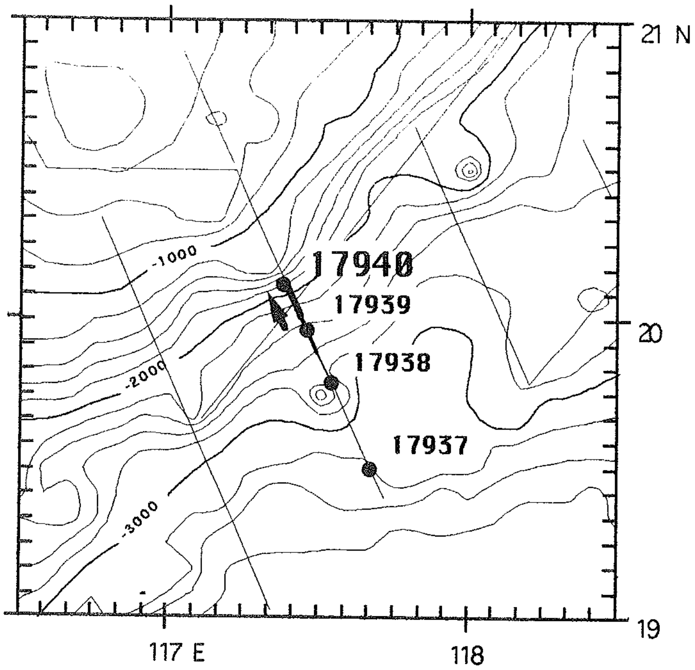

Continental slope southeast off Hong Kong

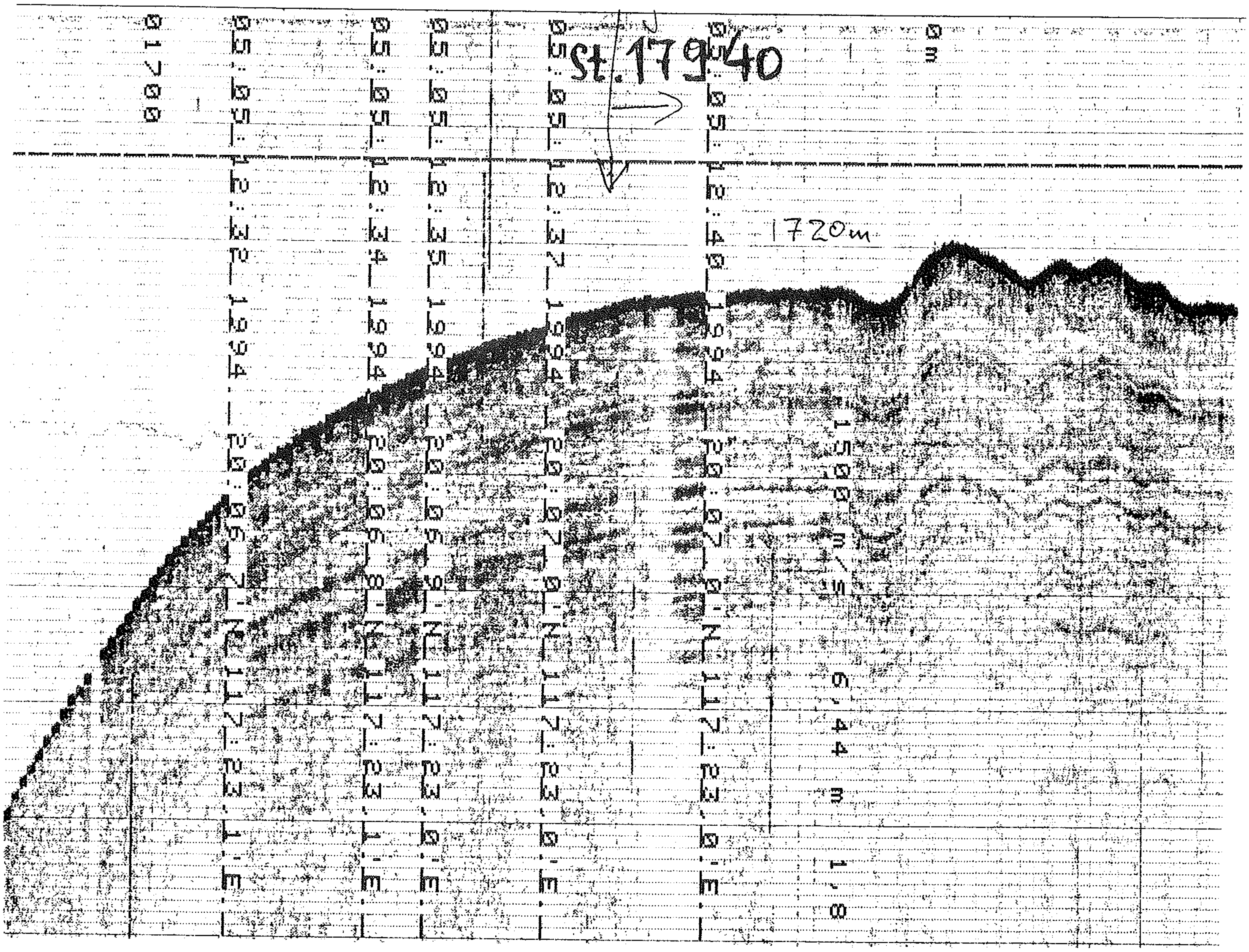

17940-2 20°07.0 N 117°23.0 E, 1727 m w.d., core length 13.30 m

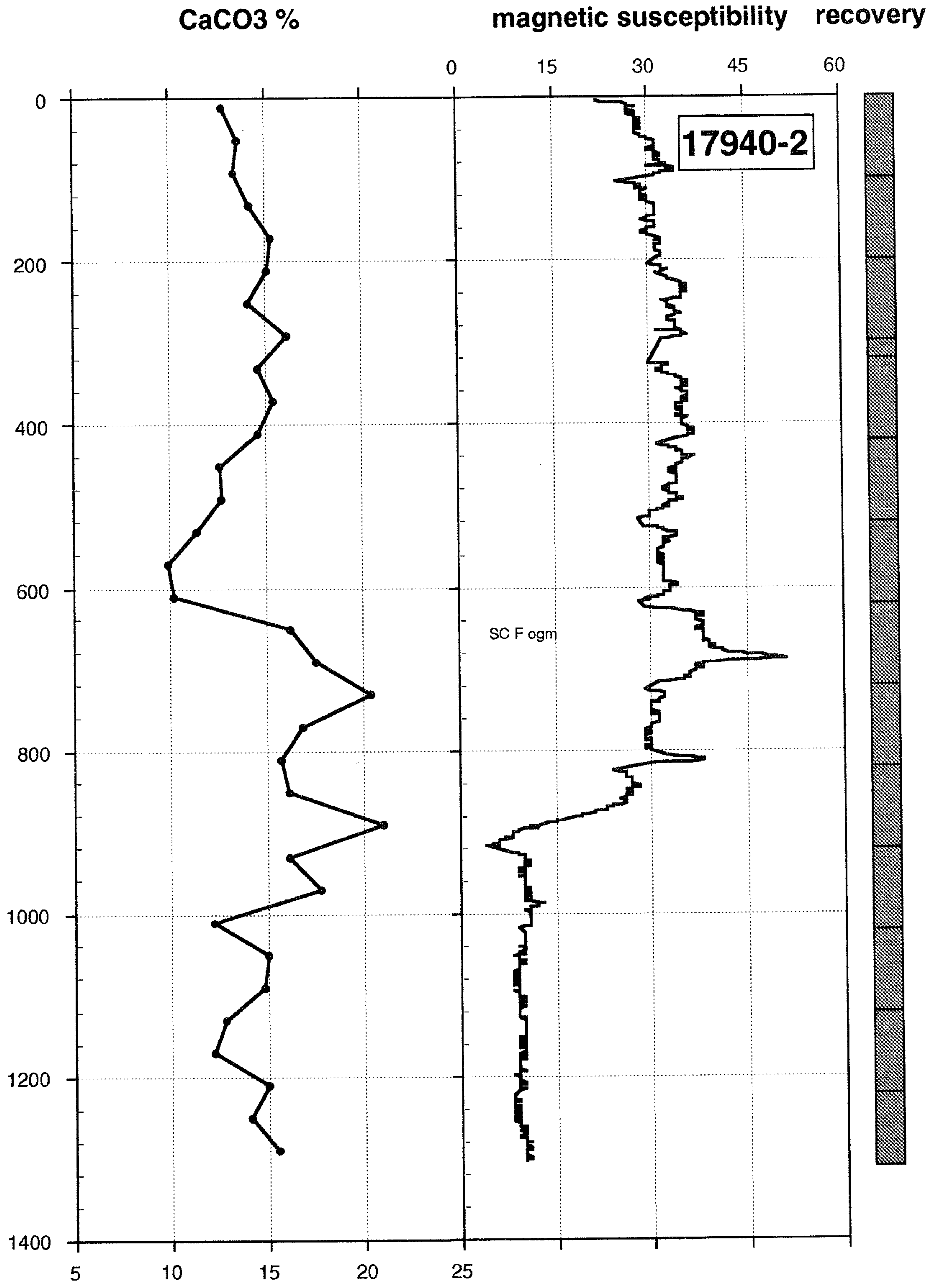

Core 17941-2

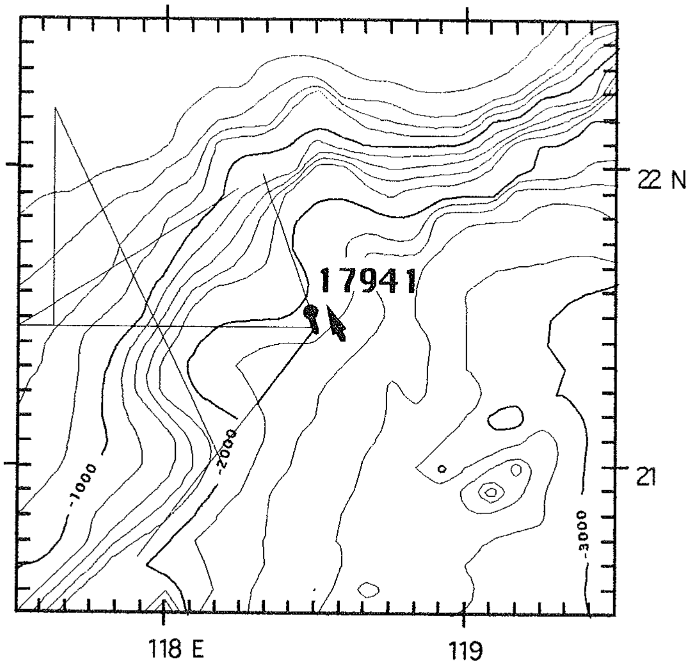

Continental slope southeast off Hong Kong

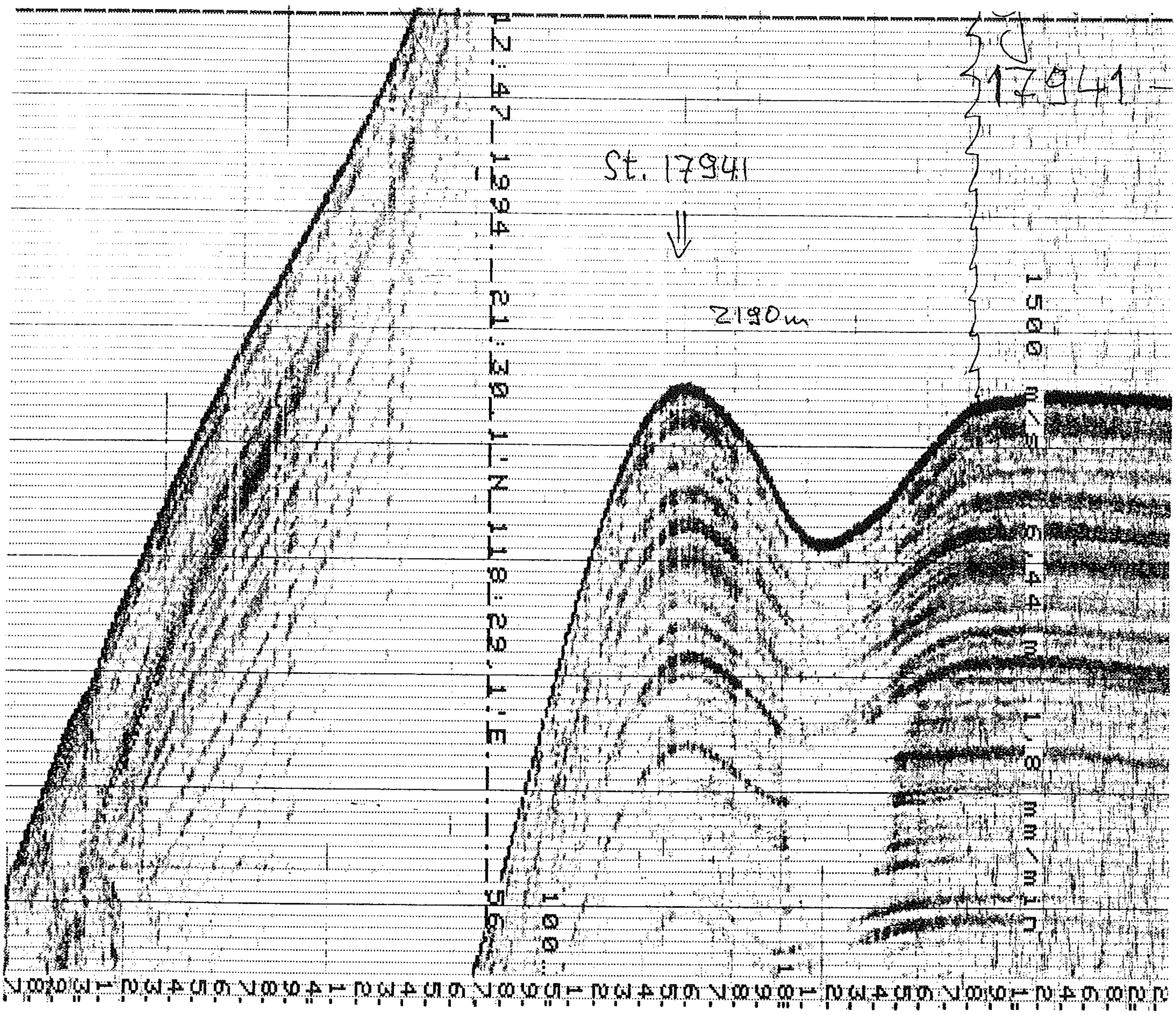

17941-2 21°31.0 N 118°29.0 E, 2200 m w.d., core length 9.90 m

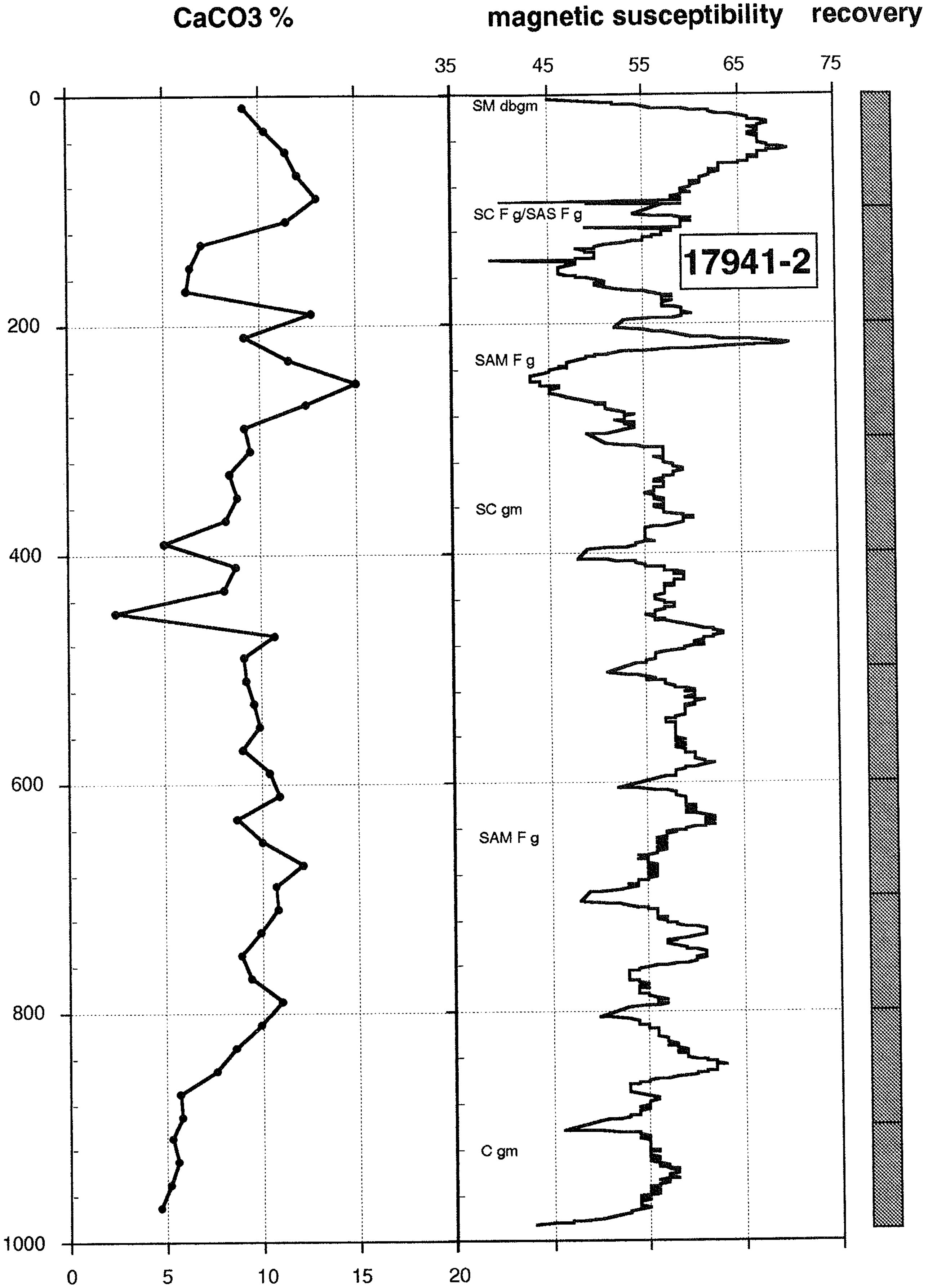

Core 17943-2

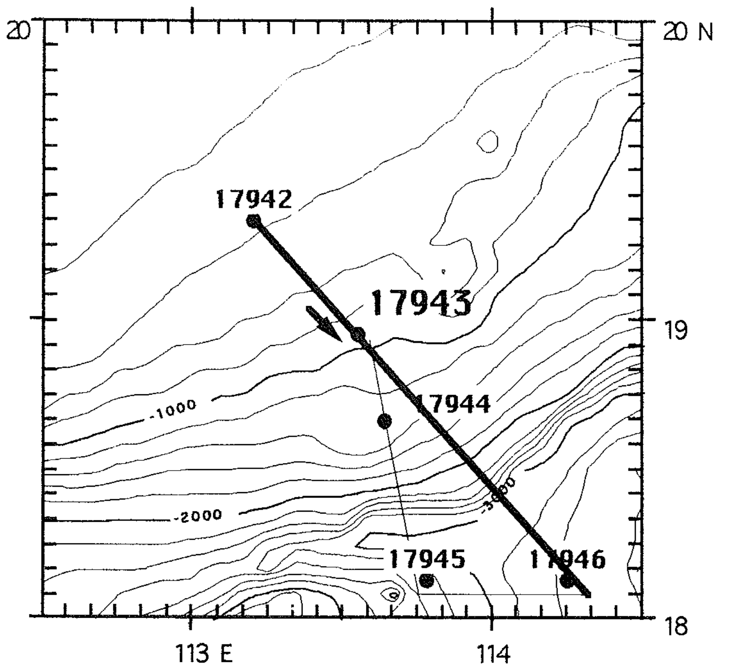

Continental slope southeast off Hong Kong

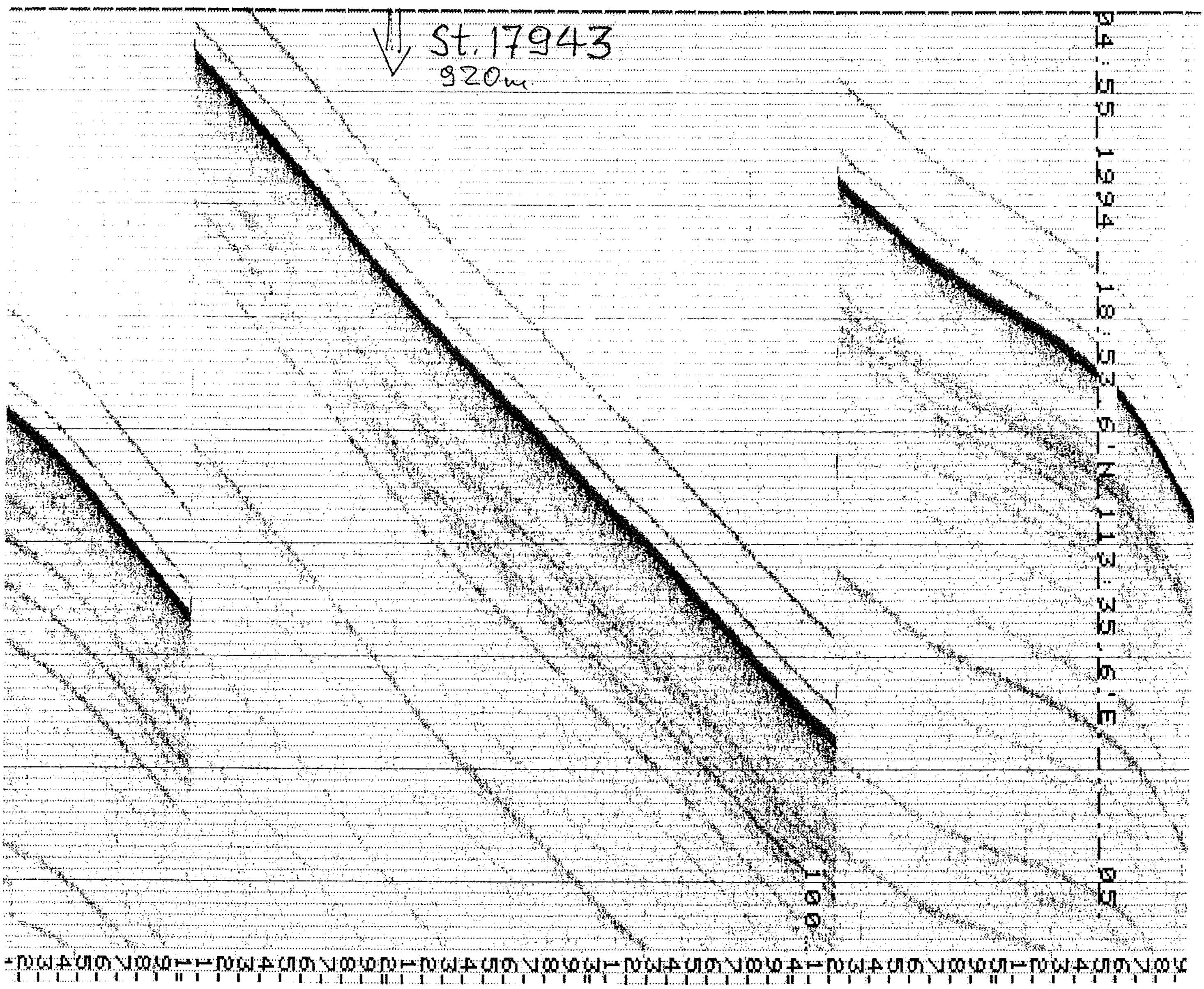

17943-2 18°57.0 N 117°33.2 E, 919 m w.d., core length 11.74 m

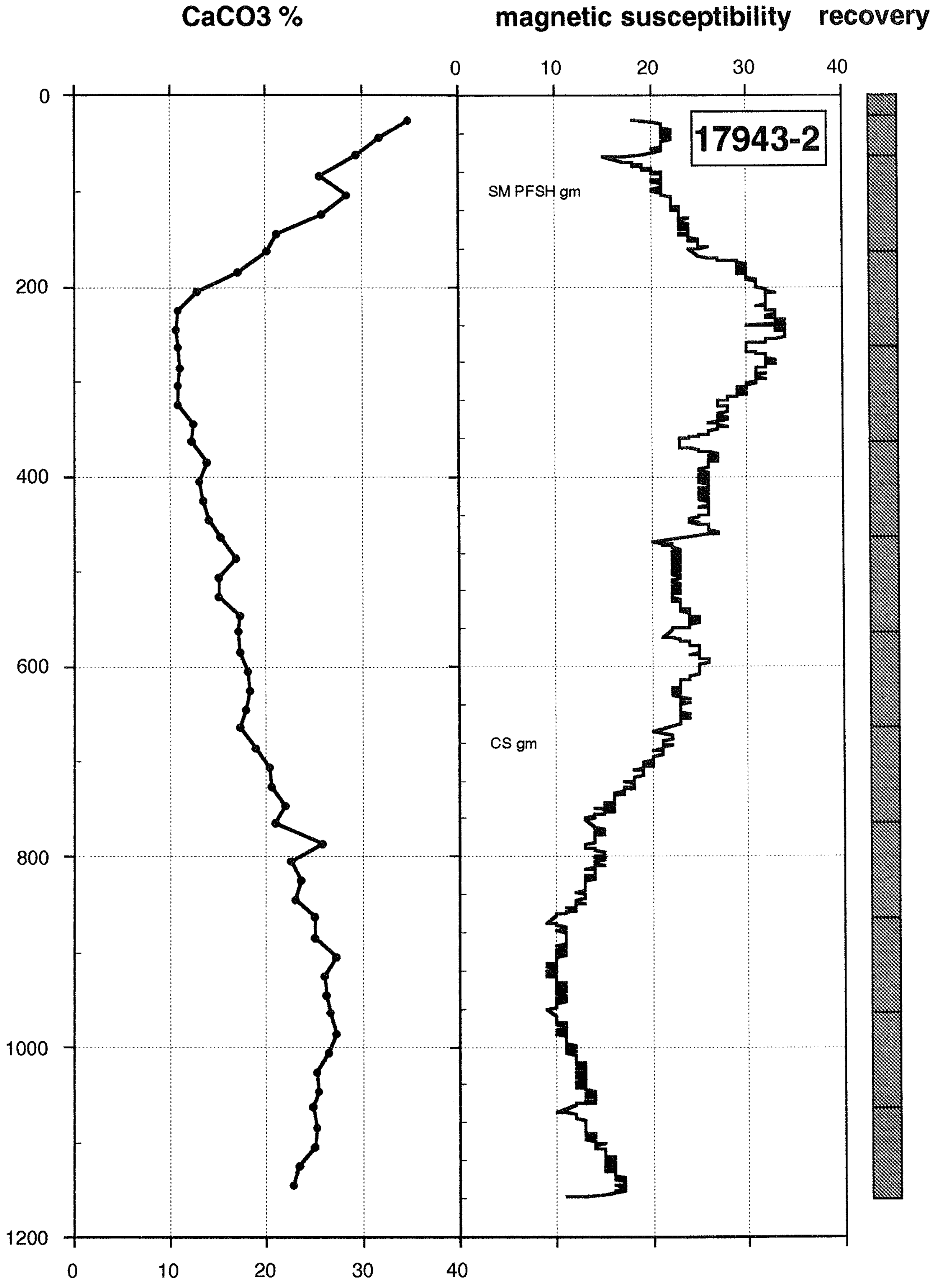

Core 17944-2

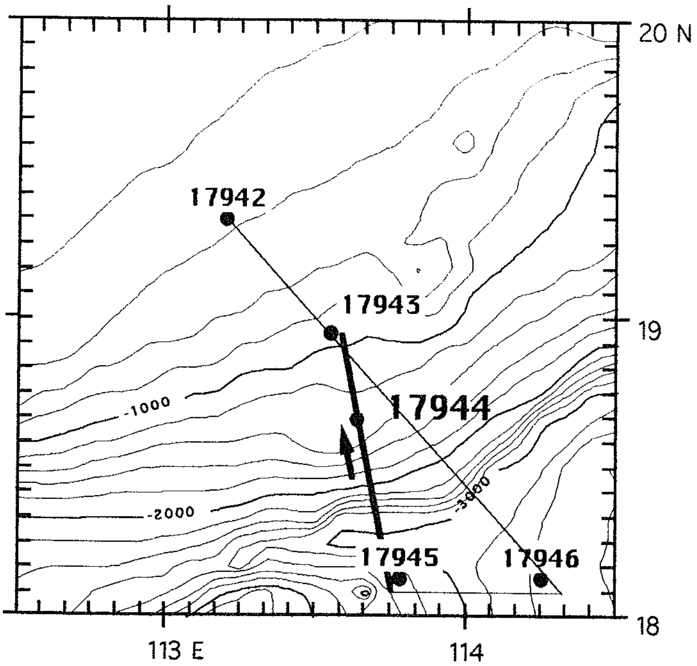

Continental slope southeast off Hong Kong

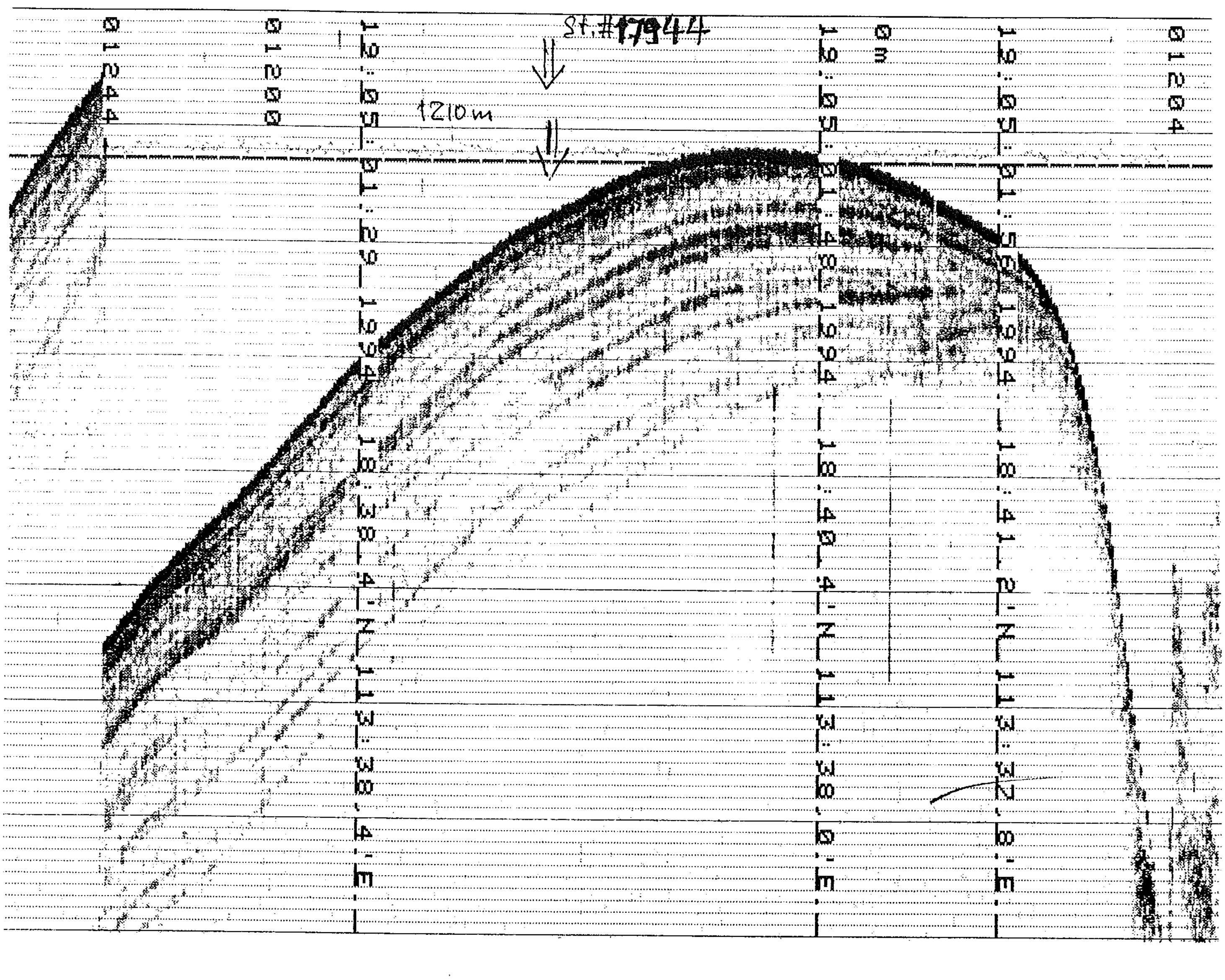

17944-2 18°39.5 N 113°38.2 E, 1217 m w.d., core length 8.92 m

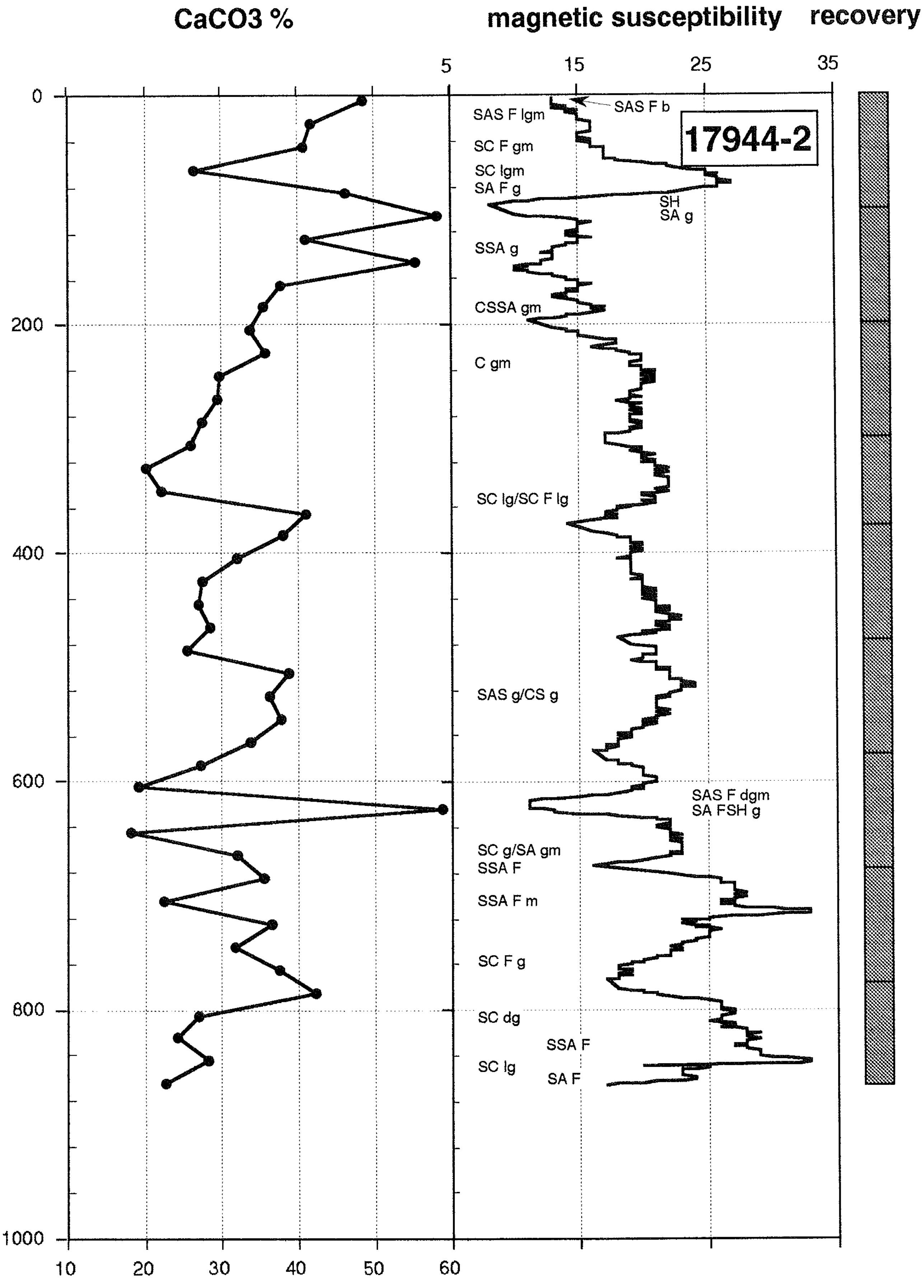

Core 17945-2 and Core 17945-3

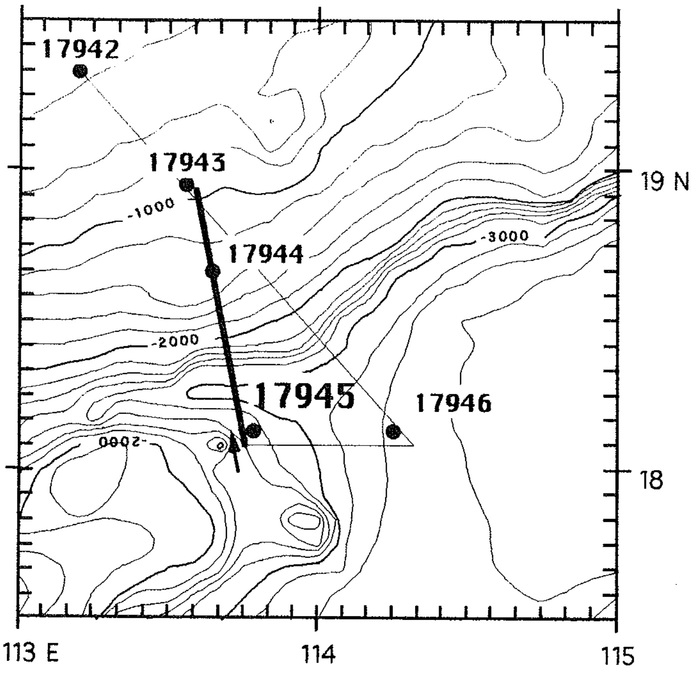

Continental slope southeast of Hong Kong

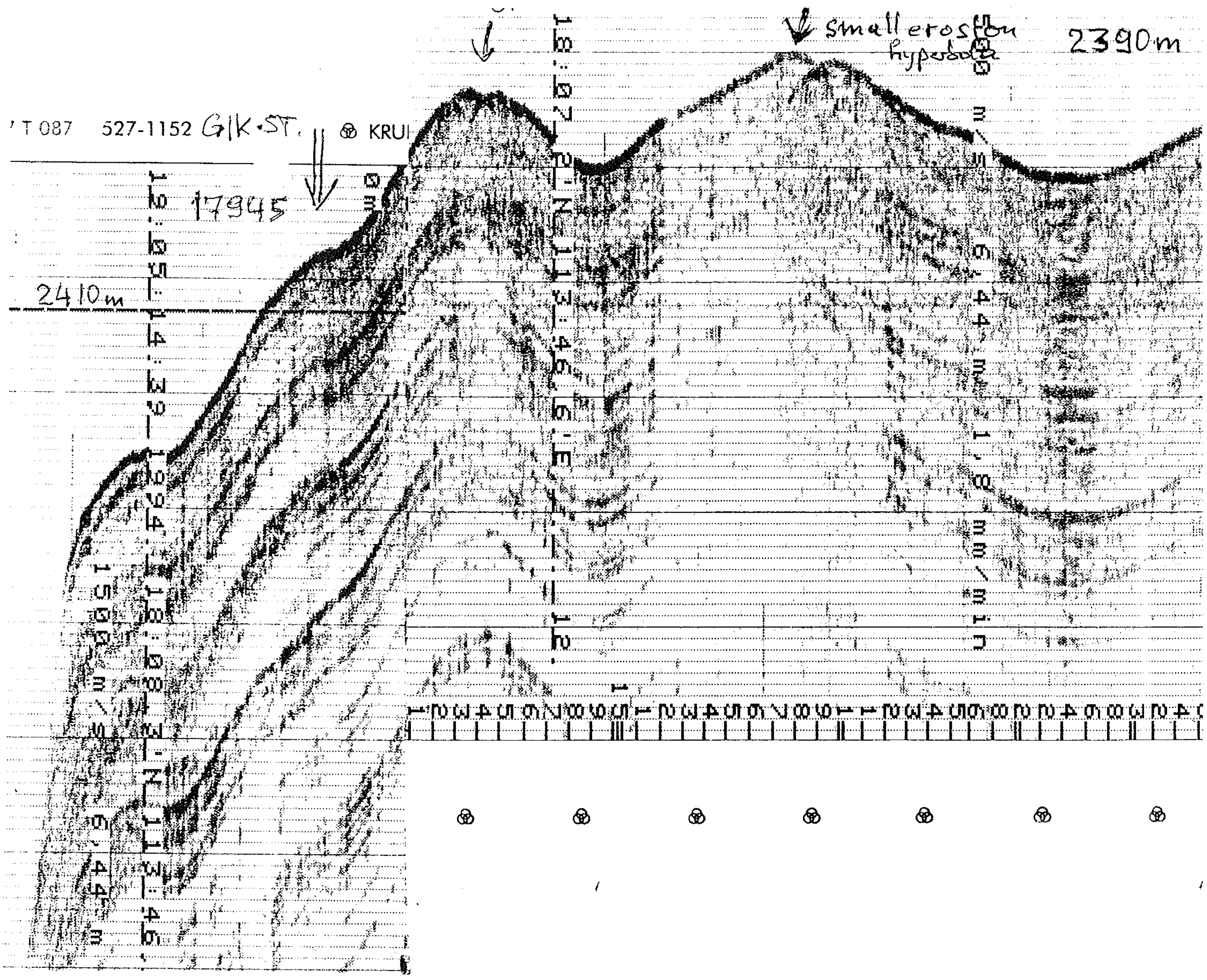

17945-2 18°07.6 N 113°46.6 E, 2403 m w.d., core length 10.21 m

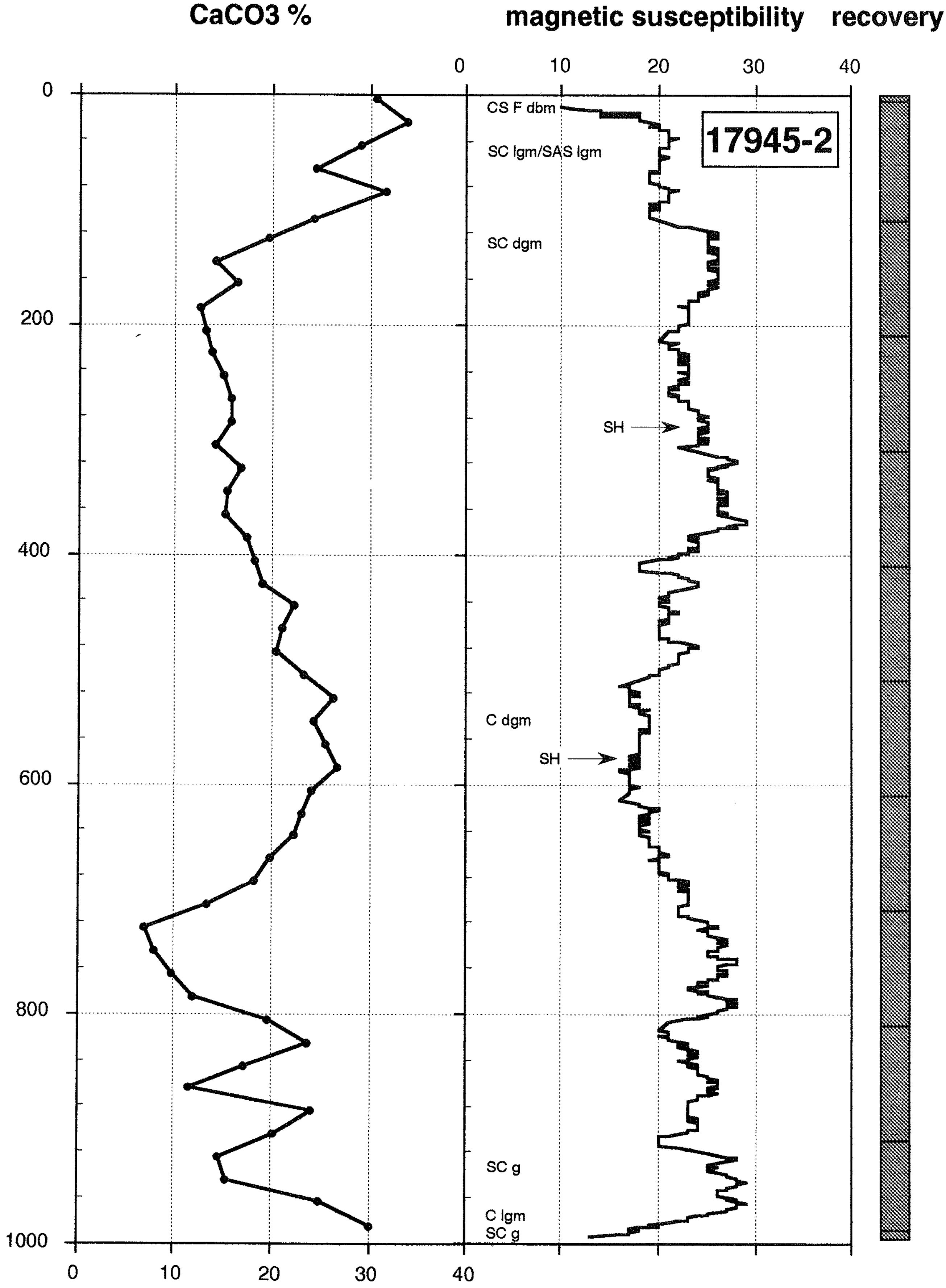

Core 17945-2
and
Core 17945-3

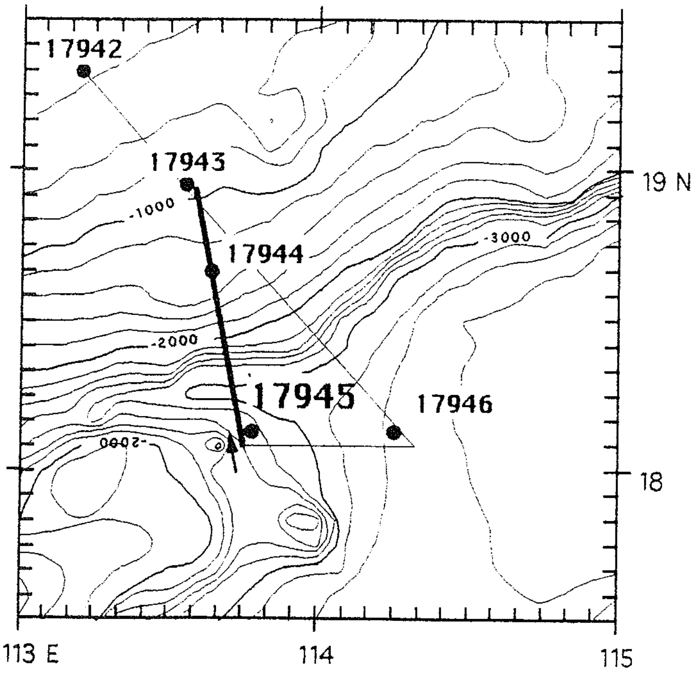

Continental slope southeast of Hong Kong

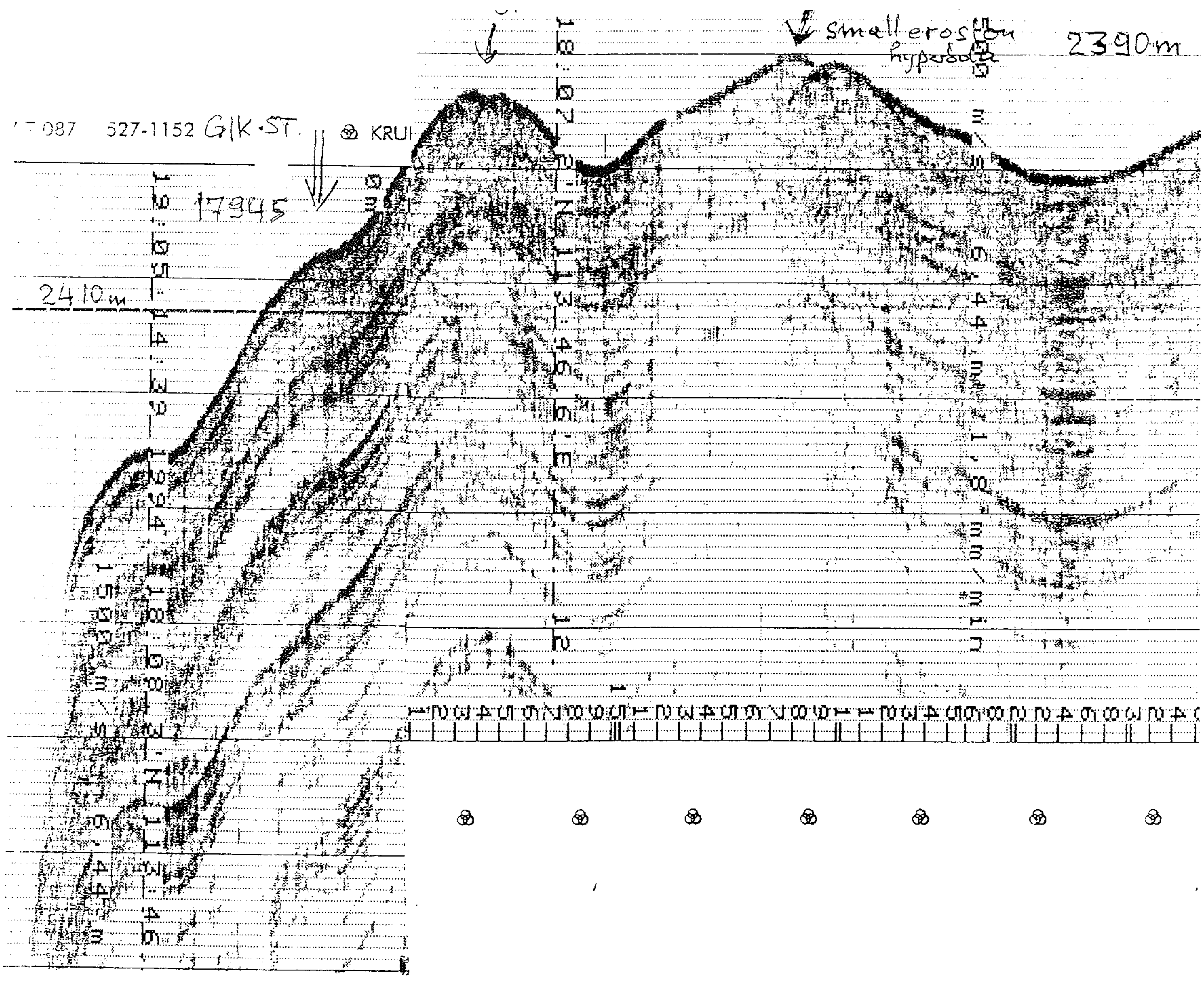

17945-3 18°07.6 N 113°46.6 E, 2404 m w.d. core length 14.44 m

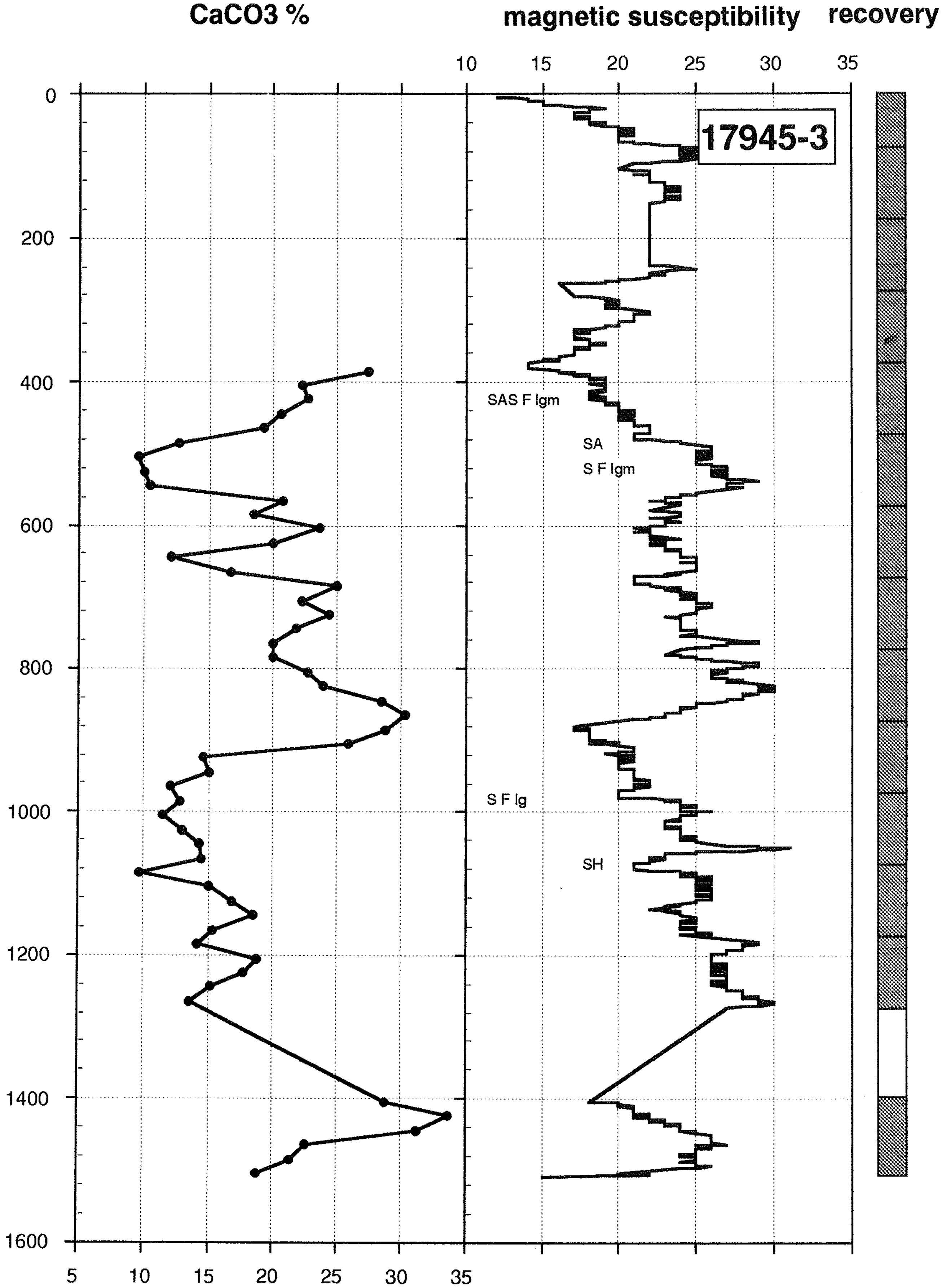

Core 17946-2

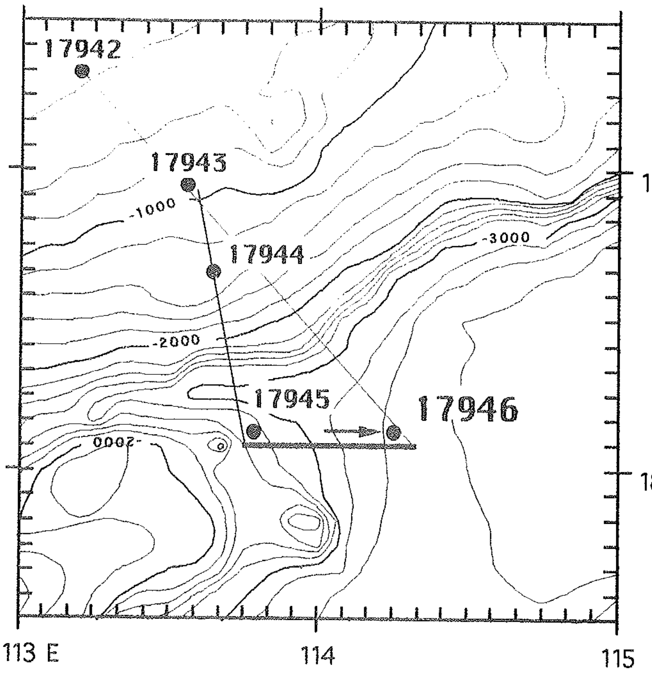

Continental slope southeast of Hong Kong

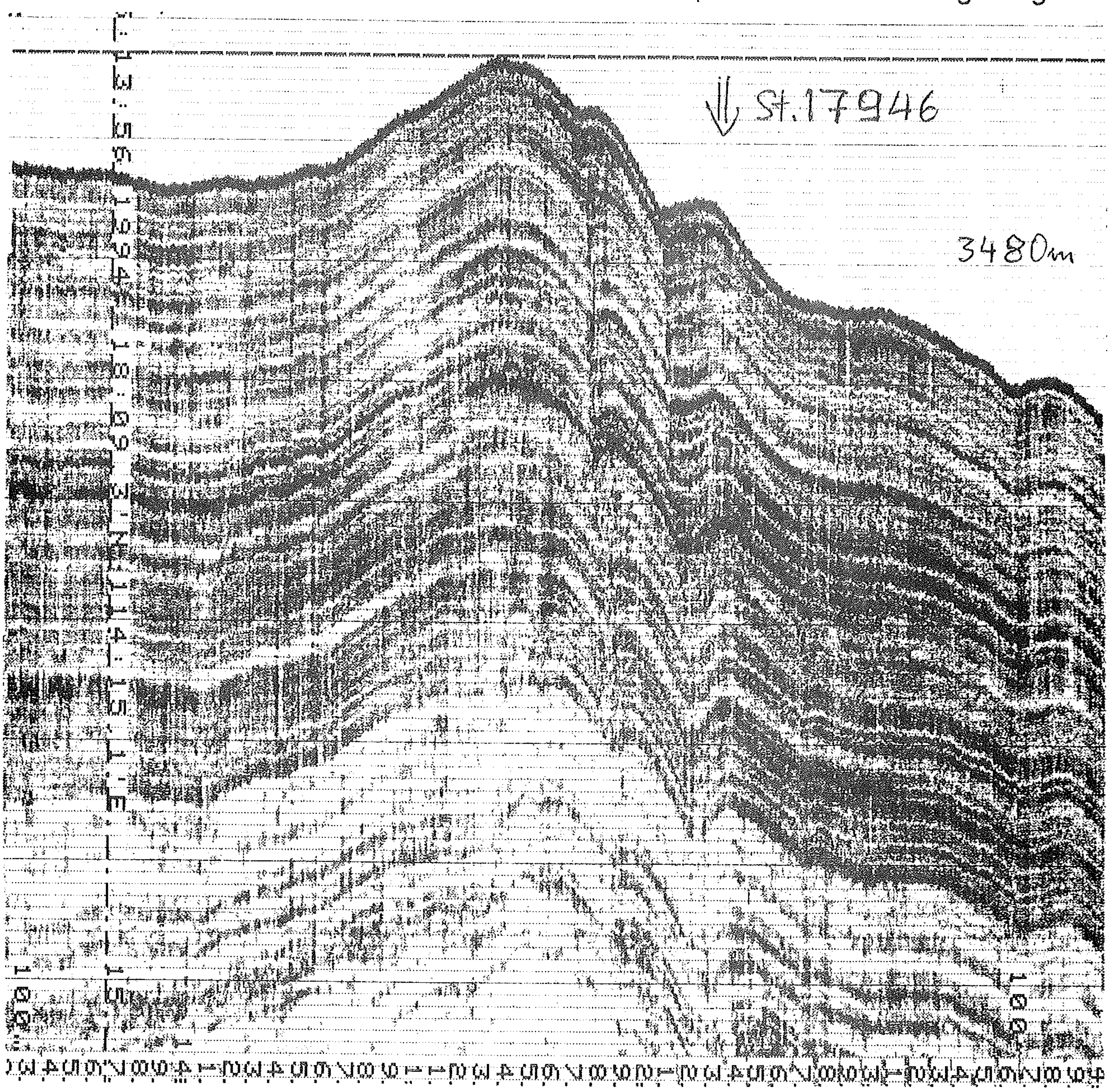

17946-2 18°07.5 N 114°15.0 E, 3464 m w.d., core length 11.34 m

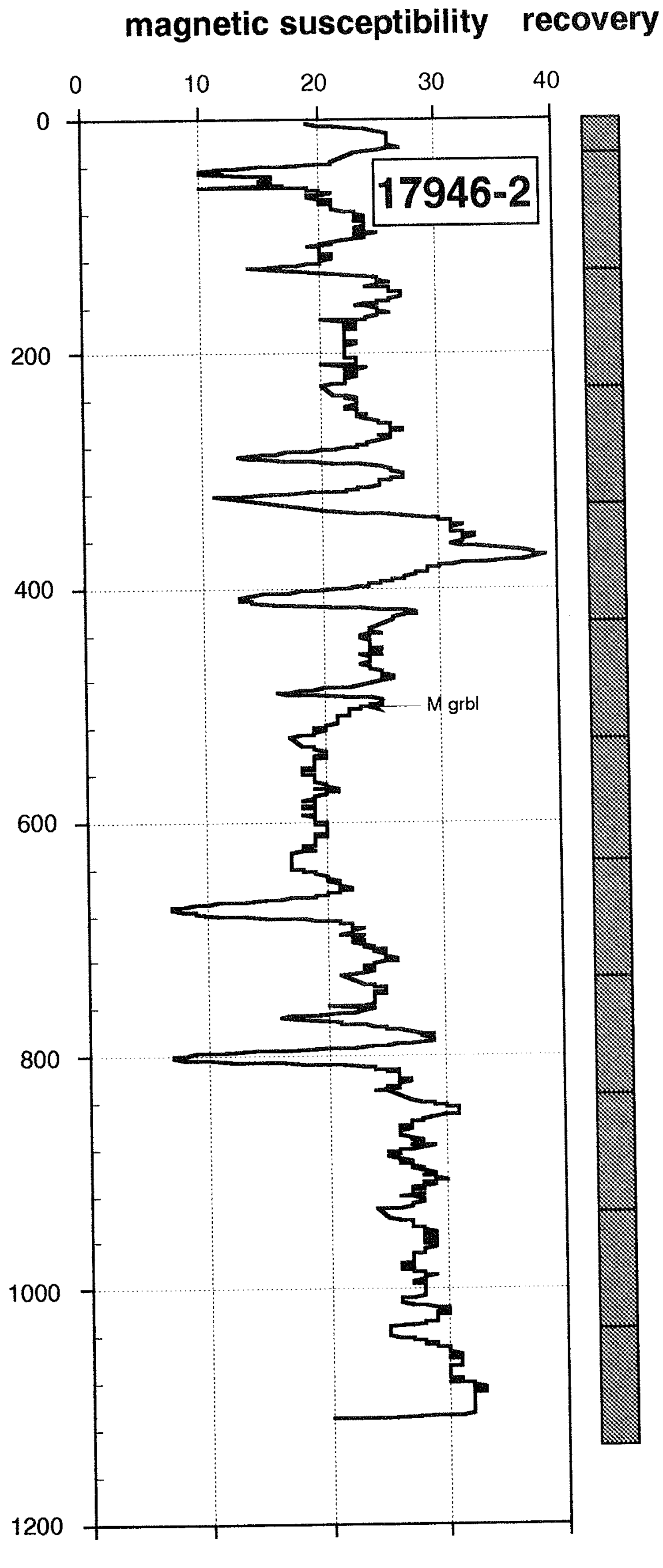

Core 17948-2

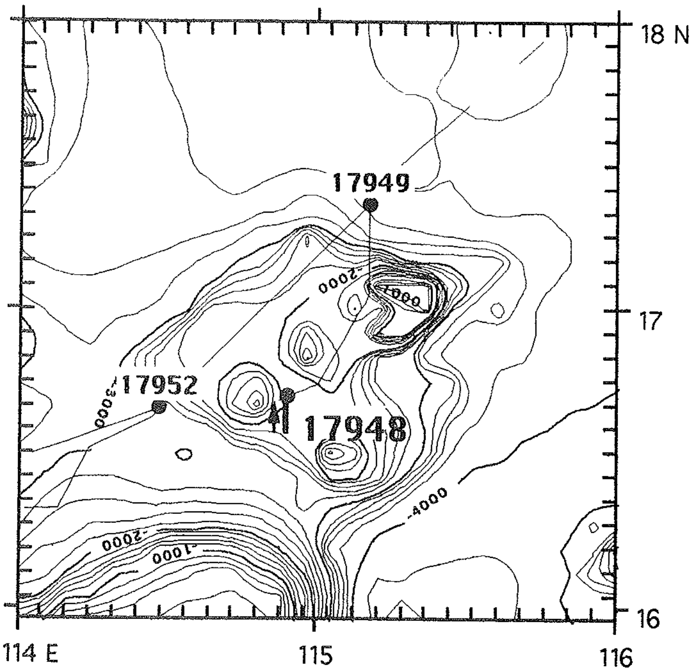

North of Macclesfield Bank

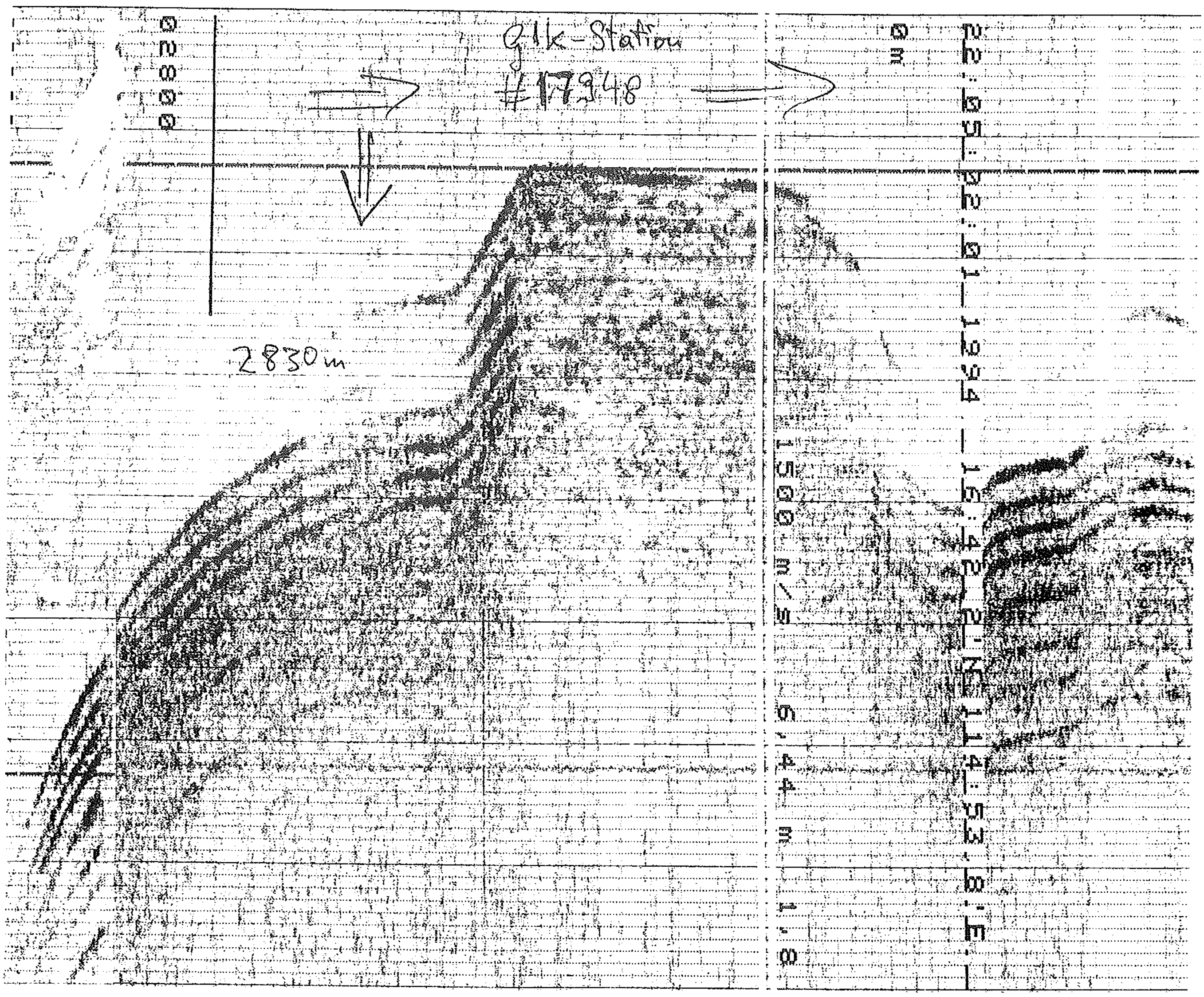

17948-2 16°42.3 N 114°53.8 E, 2855 m w.d. core length 12.70 m

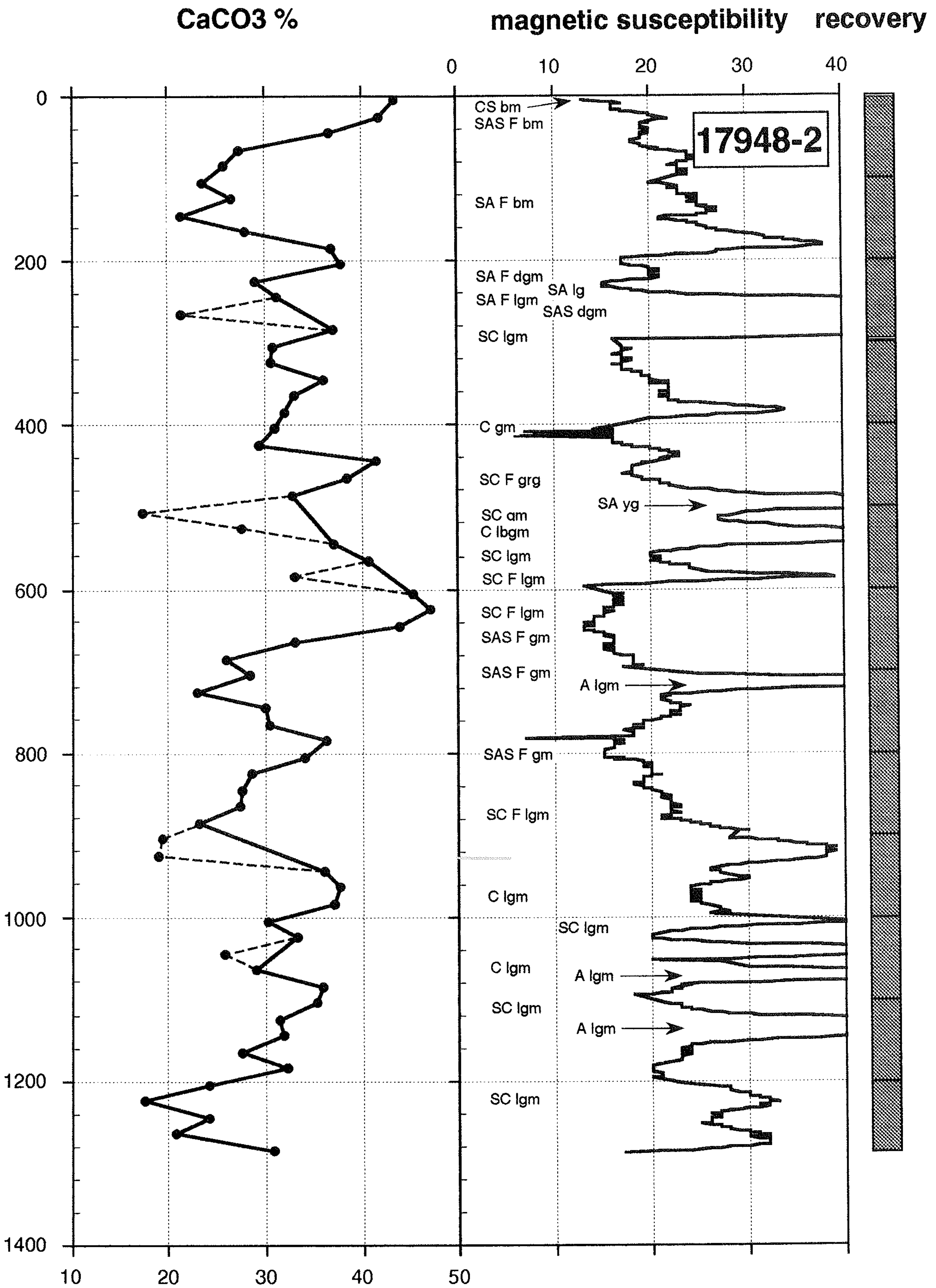

Core 17949-2

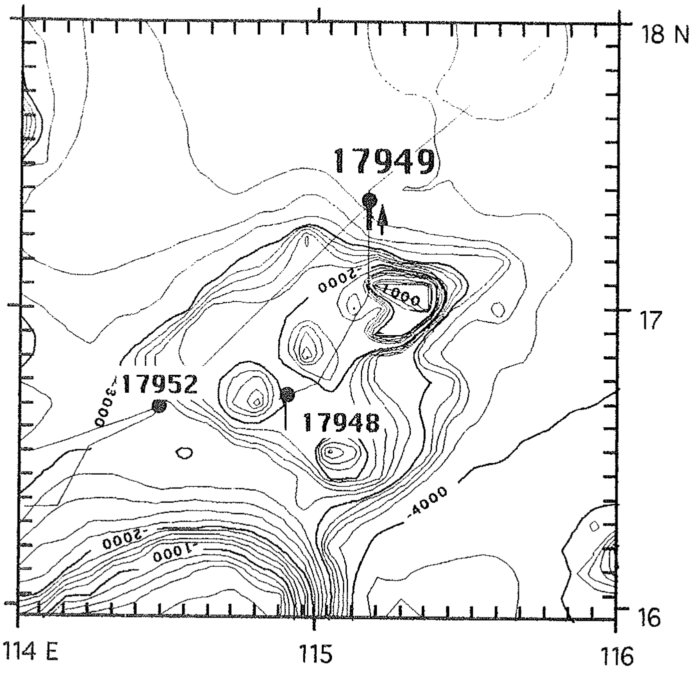

North of Macclesfield Bank

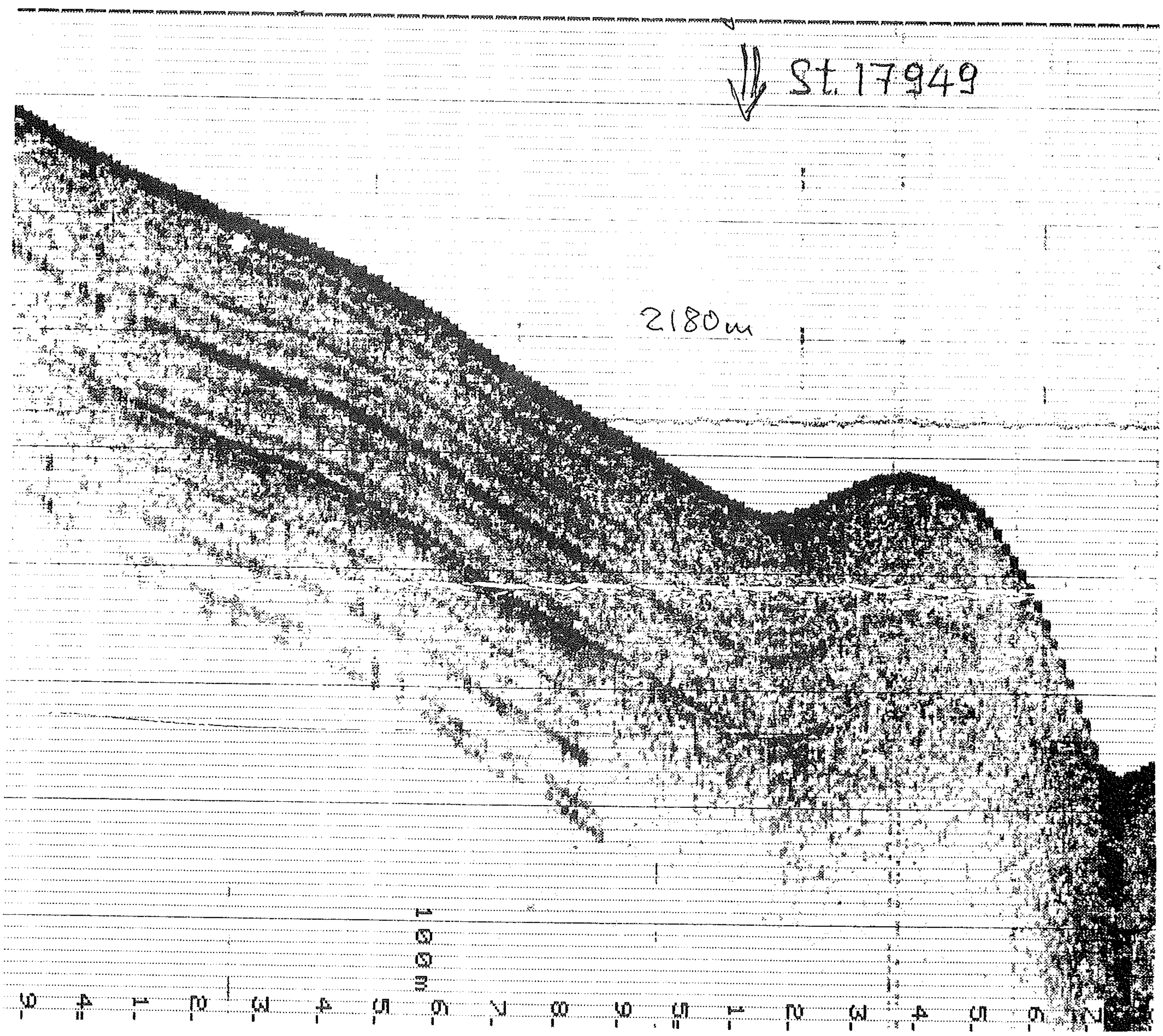

17949-2 17°20.9 N 115°10.0 E, 2197 m w.d. core length 13.34 m

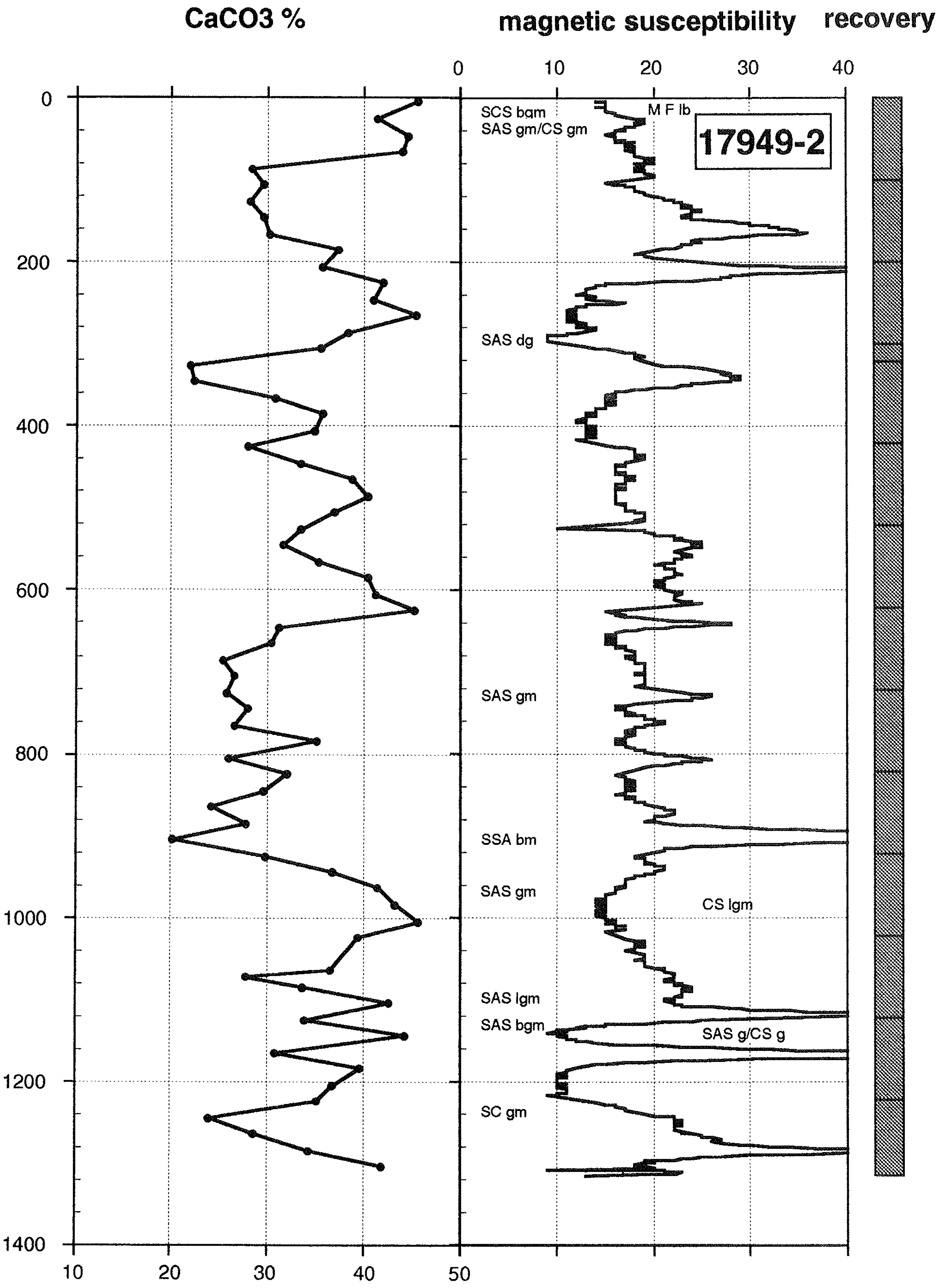

Core 17950-2

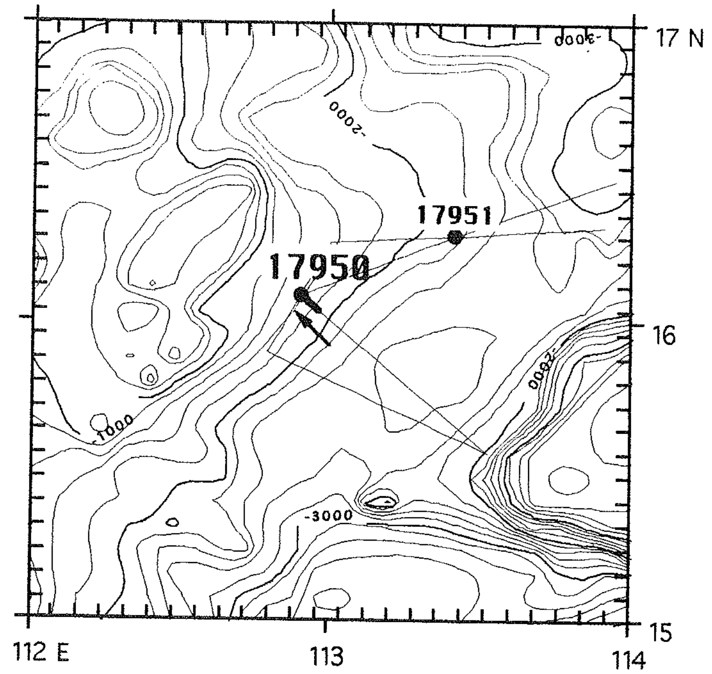

South of Paracel Islands

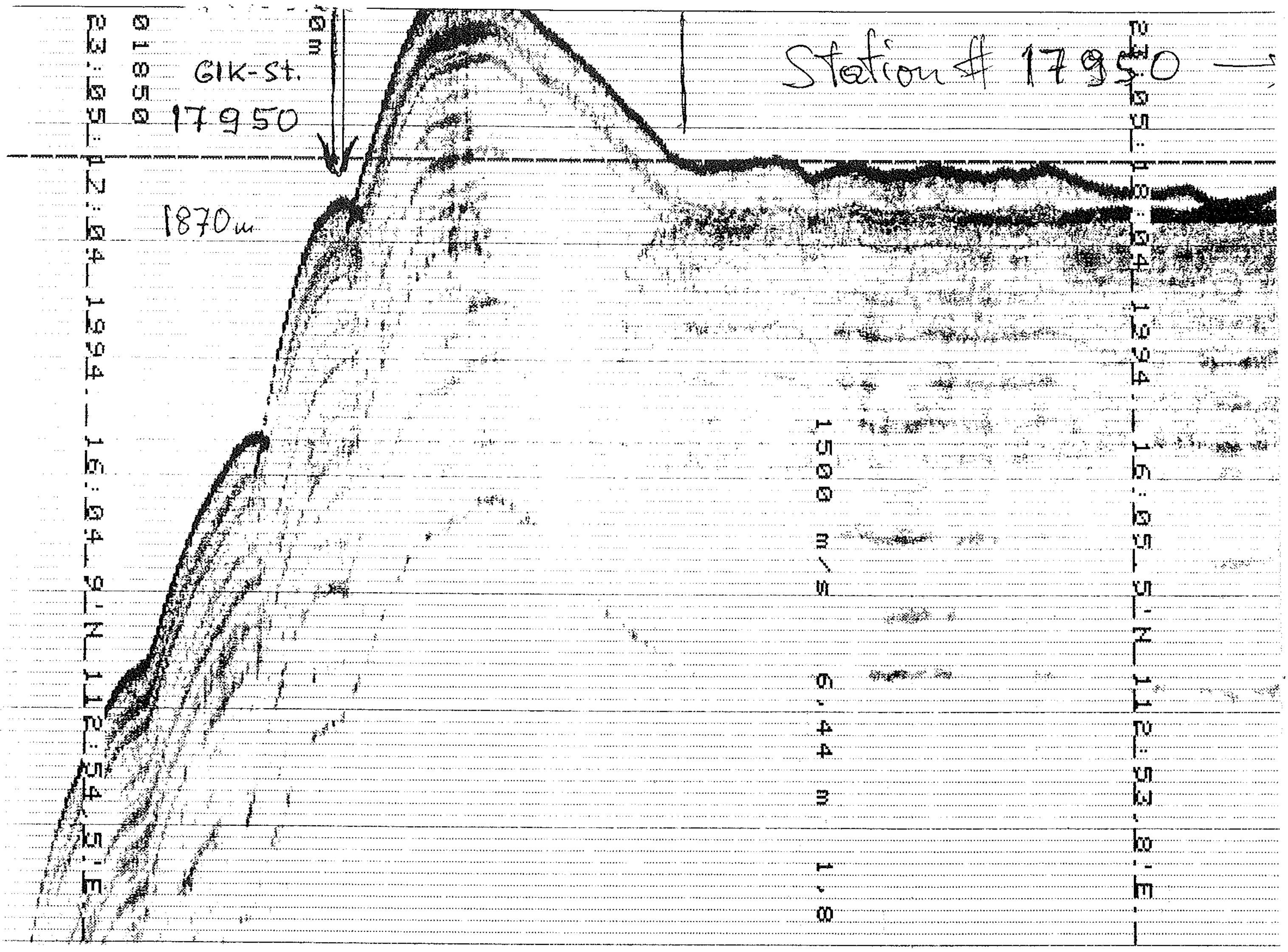

17950-2 16°05.6 N 112°53.8 E, 2403 m w.d., core length 9.91 m

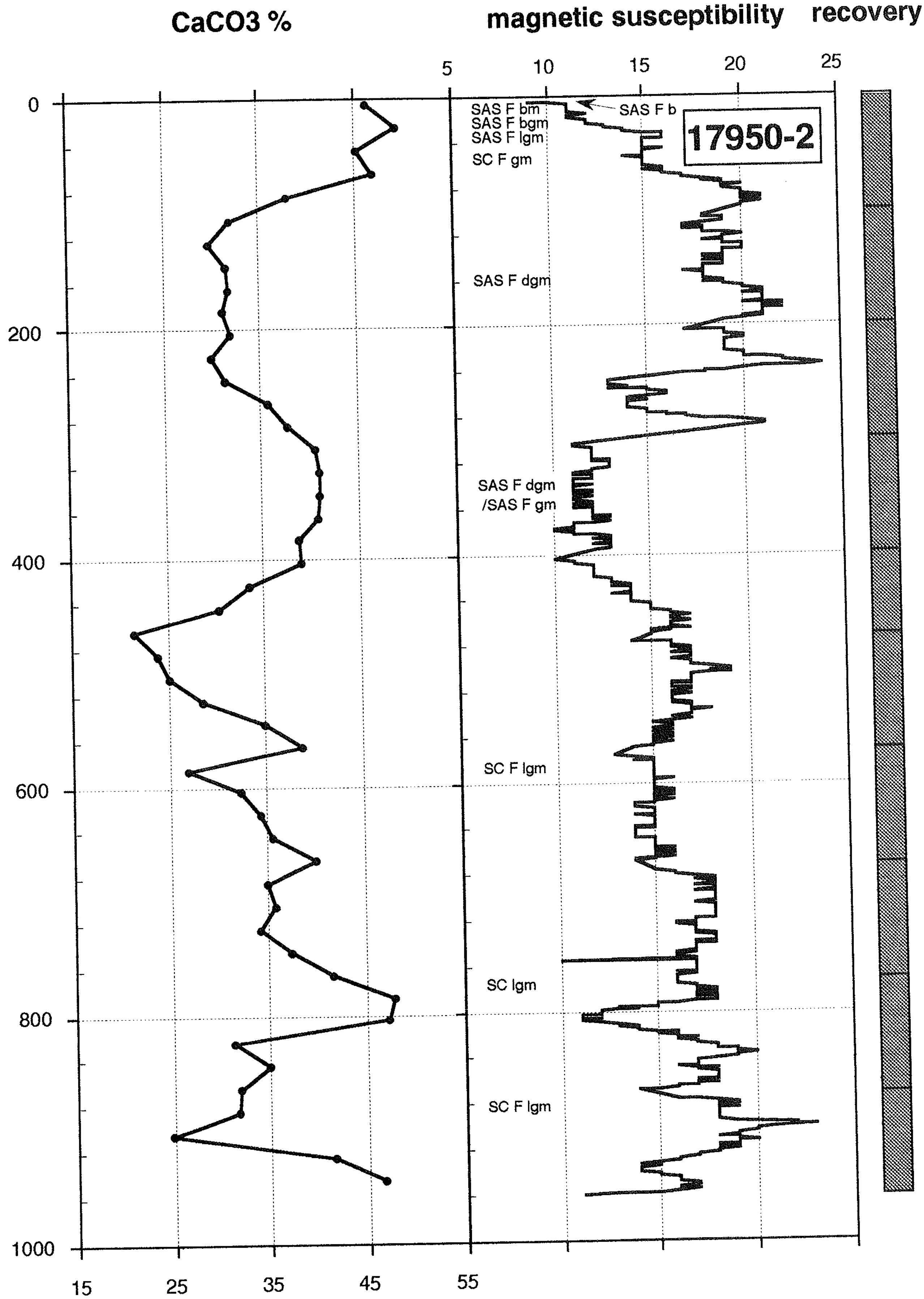

Core 17951-2

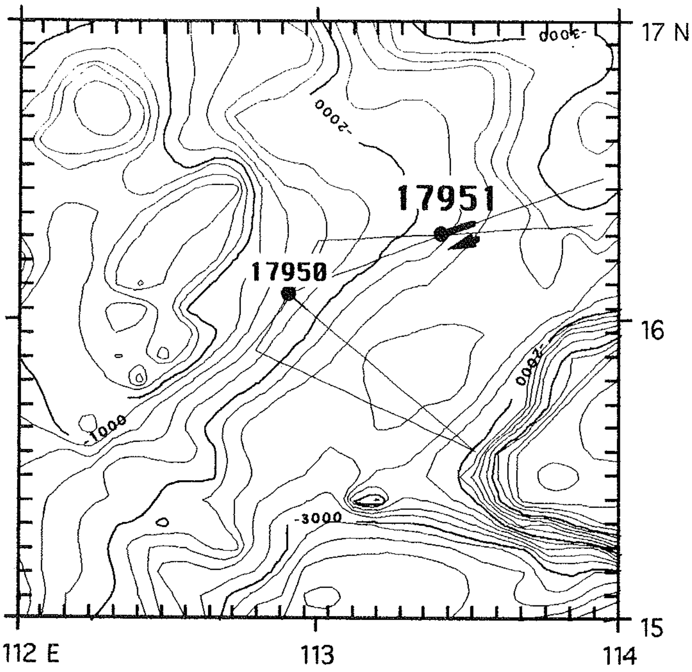

South of Paracel Islands

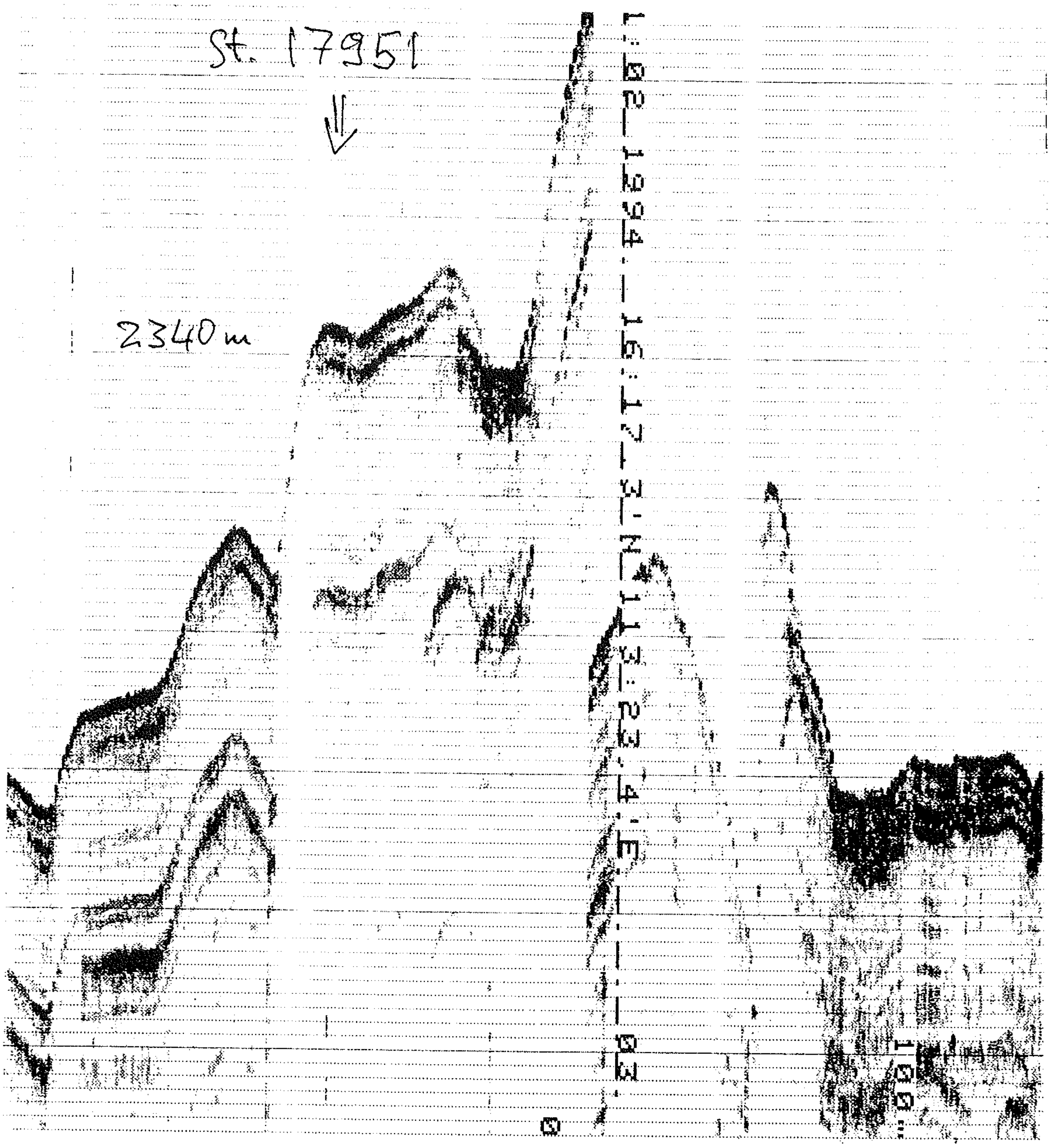

17951-2 16°17.3 N 113°24.6 E, 2341 m w.d., core length 12.04 m

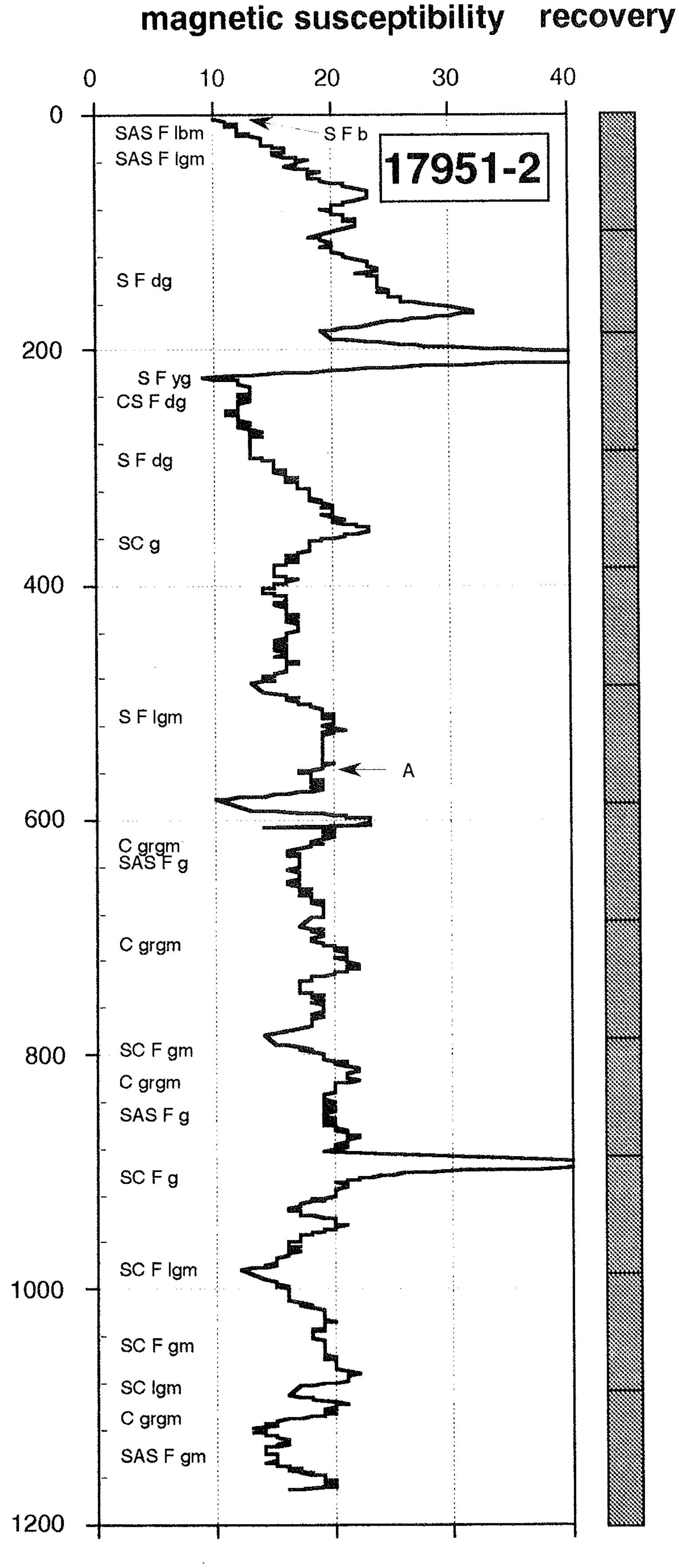

Core 17952-3

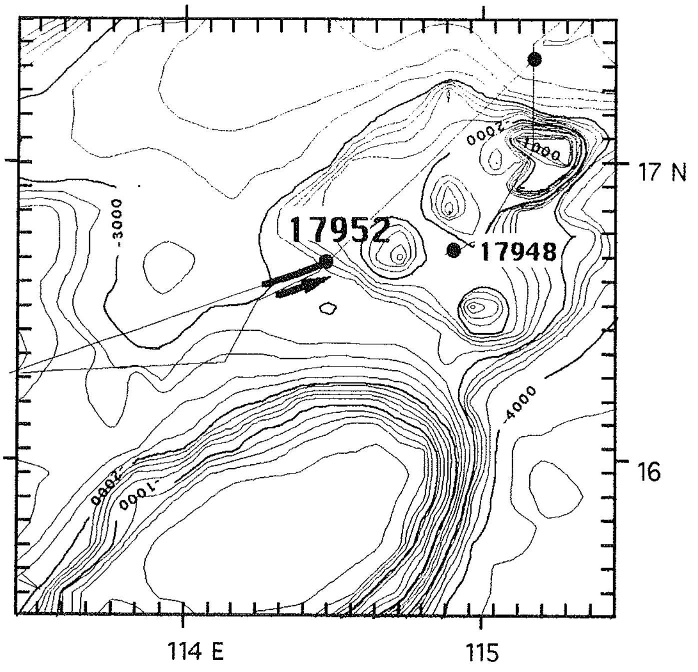

North of Macclesfield Bank

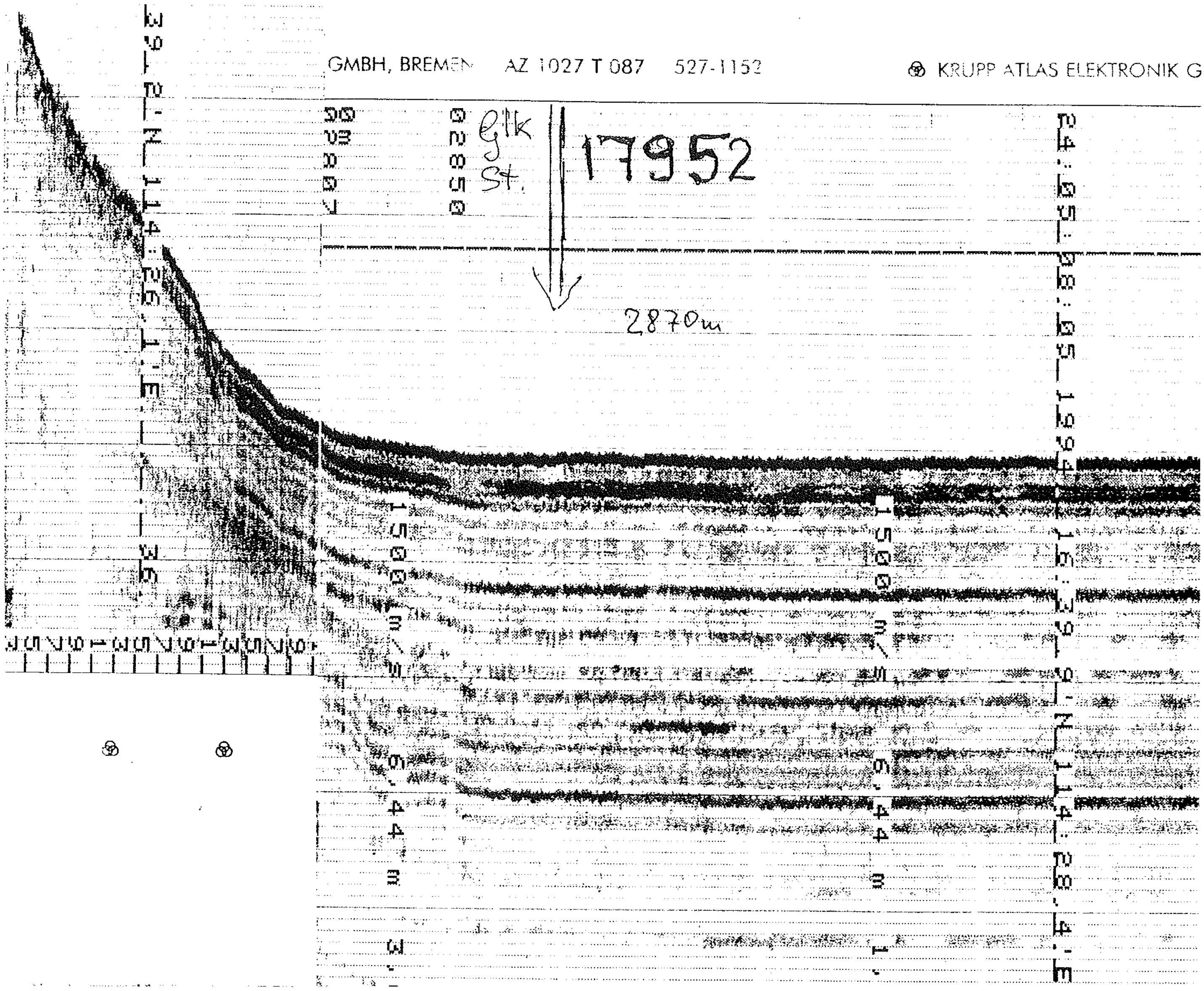

17952-3 16°40.0 N 114°28.4 E, 2883 m w.d. core length 12.04 m

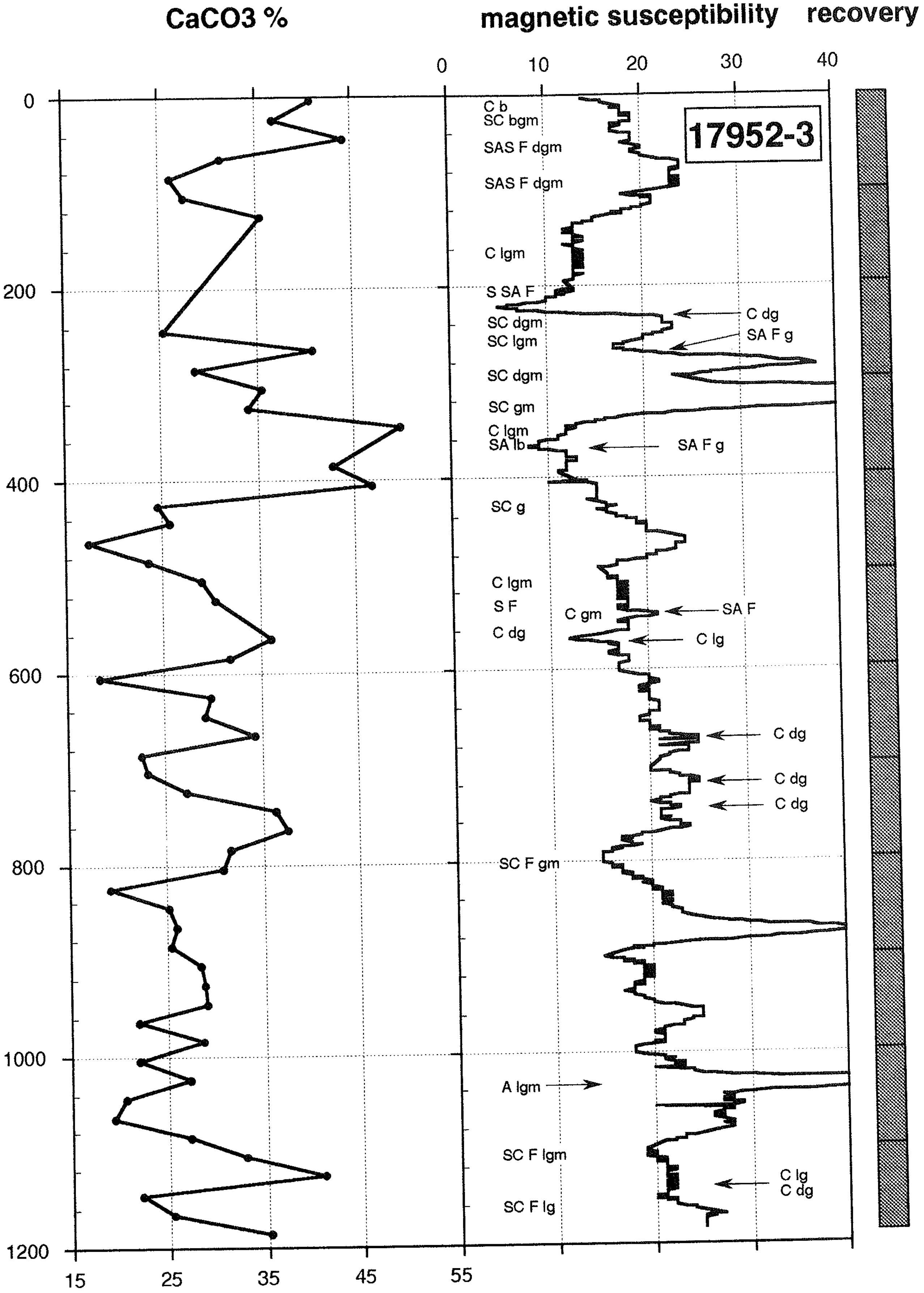

Core 17953-4

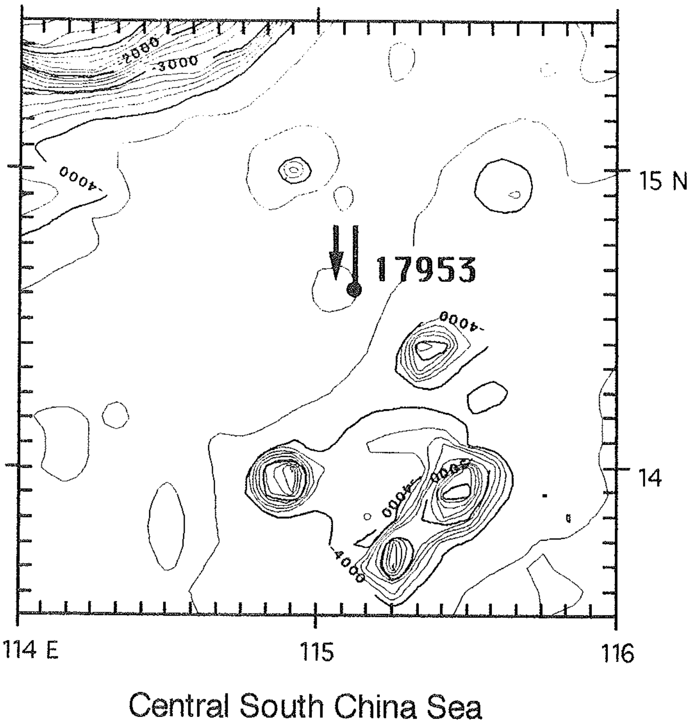

-2000
-3000
-4000
17953
15 N
14
114 E
115
116
Central South China Sea

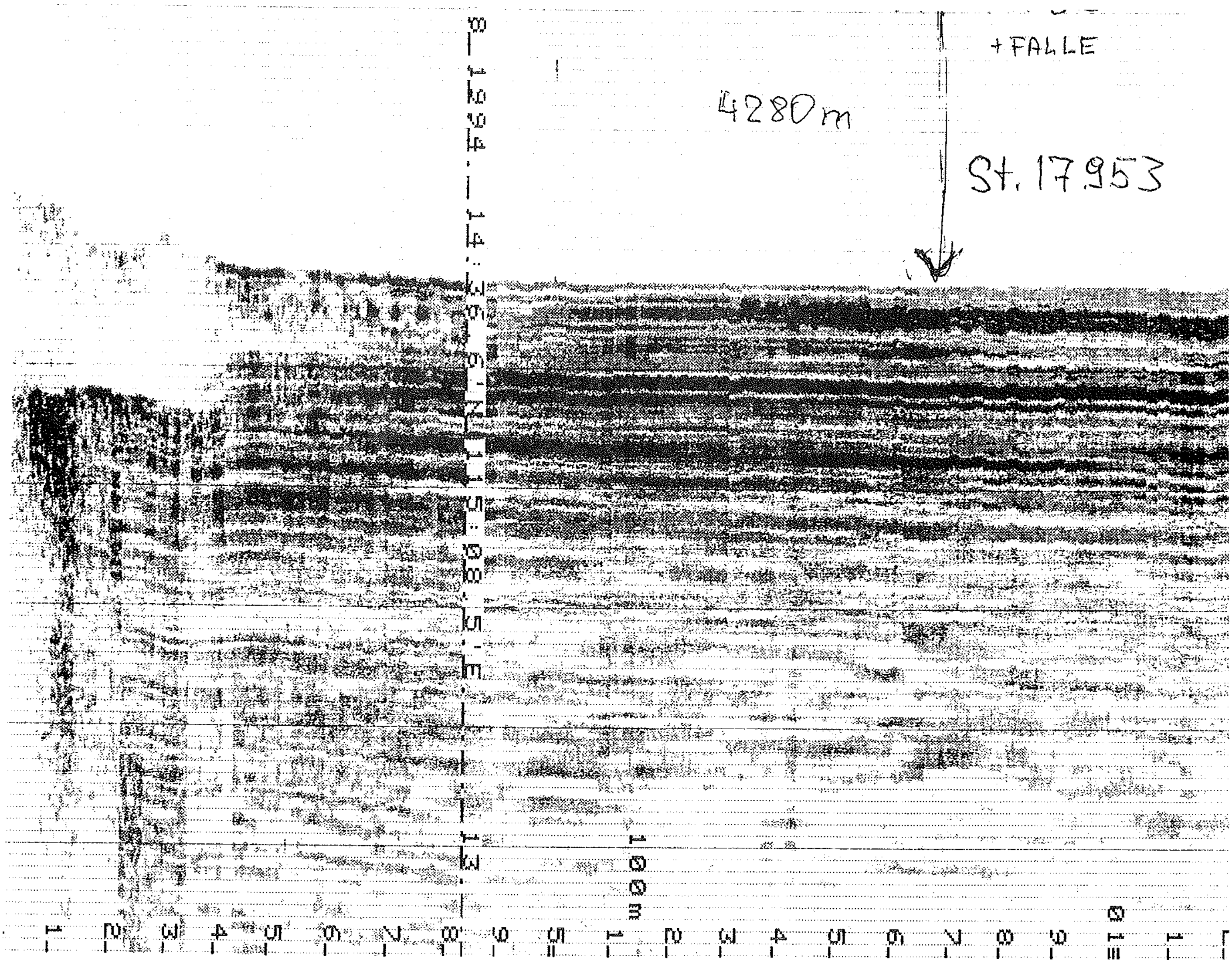

+FALLE
4280m
St. 17953
100m

17953-4 14°33.0 N 115°08.6 E, 4306 m w.d., core length 12.49 m

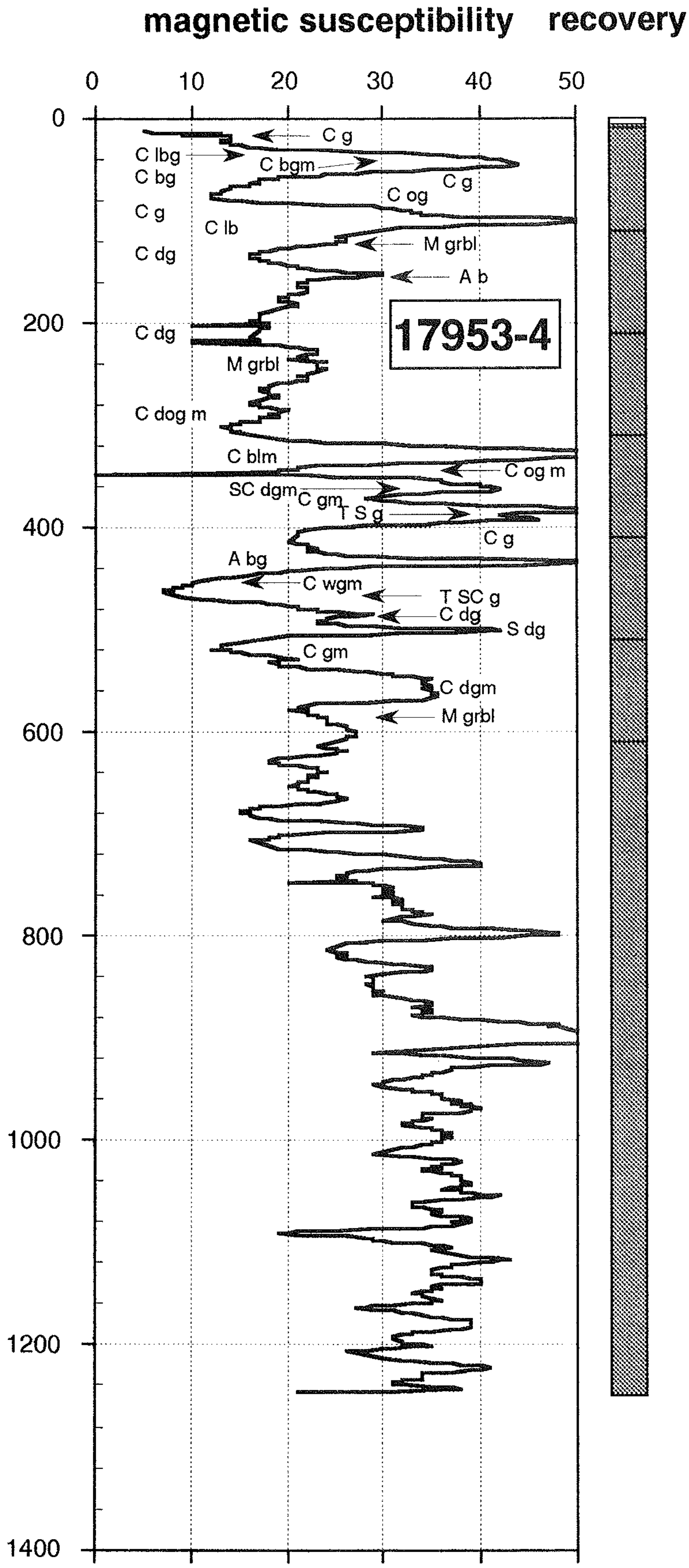

Core 17954-2
and
Core 17954-3

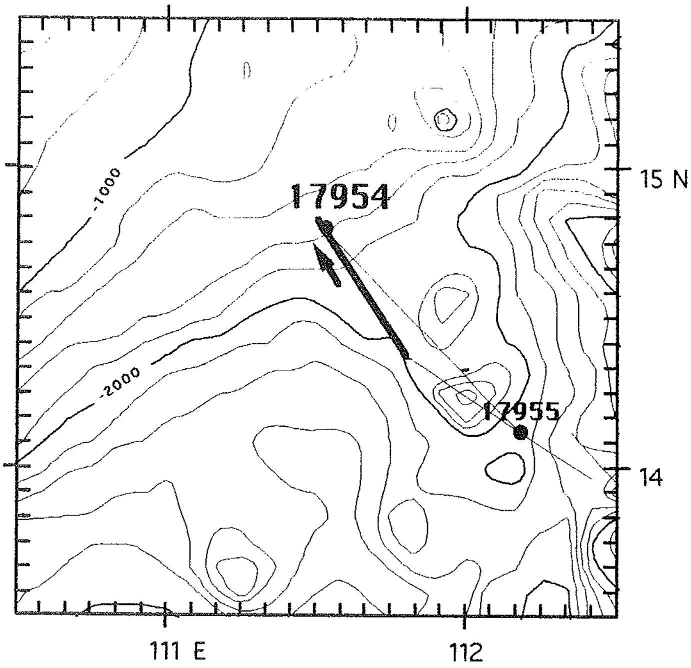

Continental Margin off Vietnam

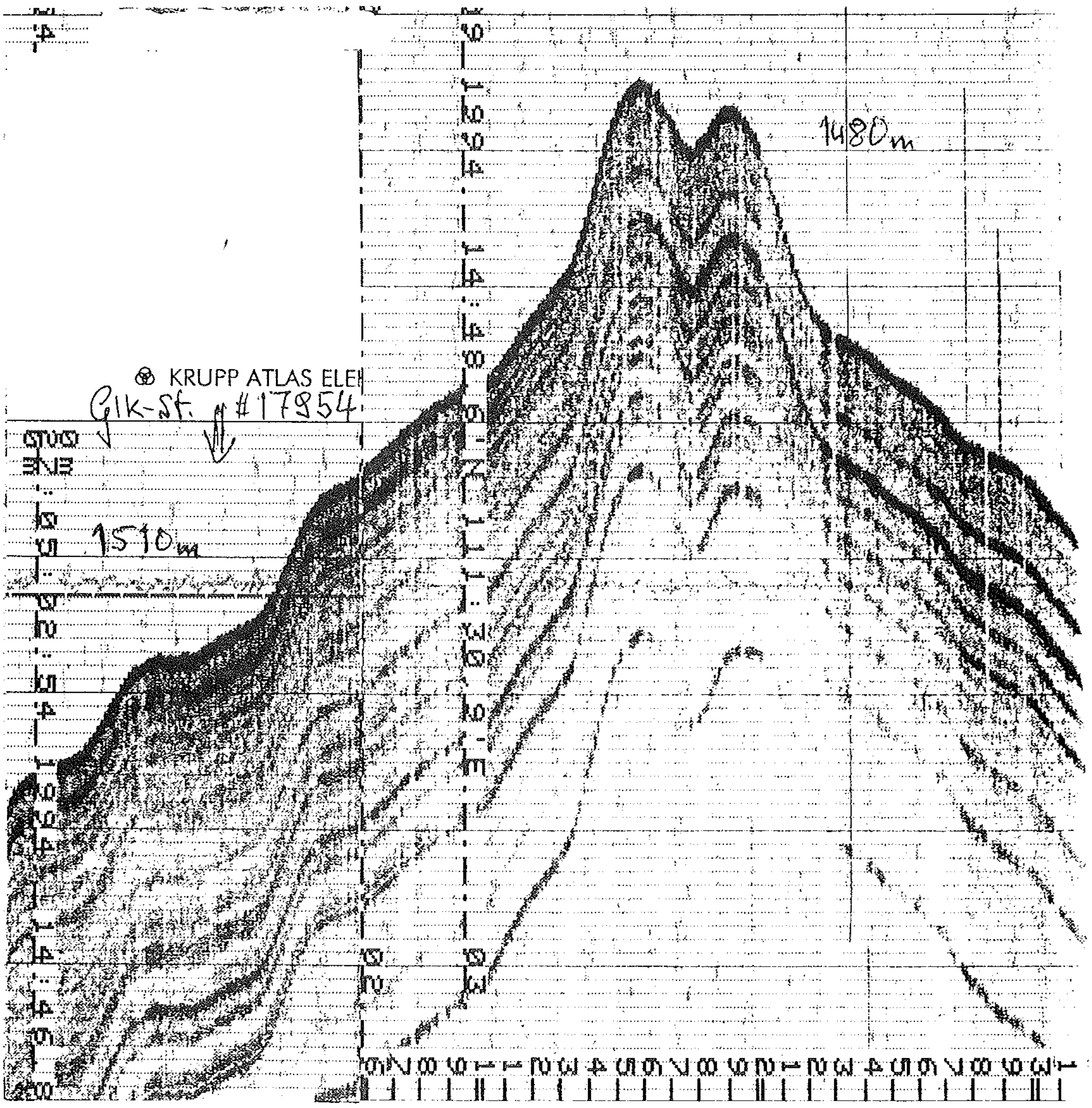

17954-2 14°47.7 N 111°31.5 E, 1515 m w.d., core length 11.49 m

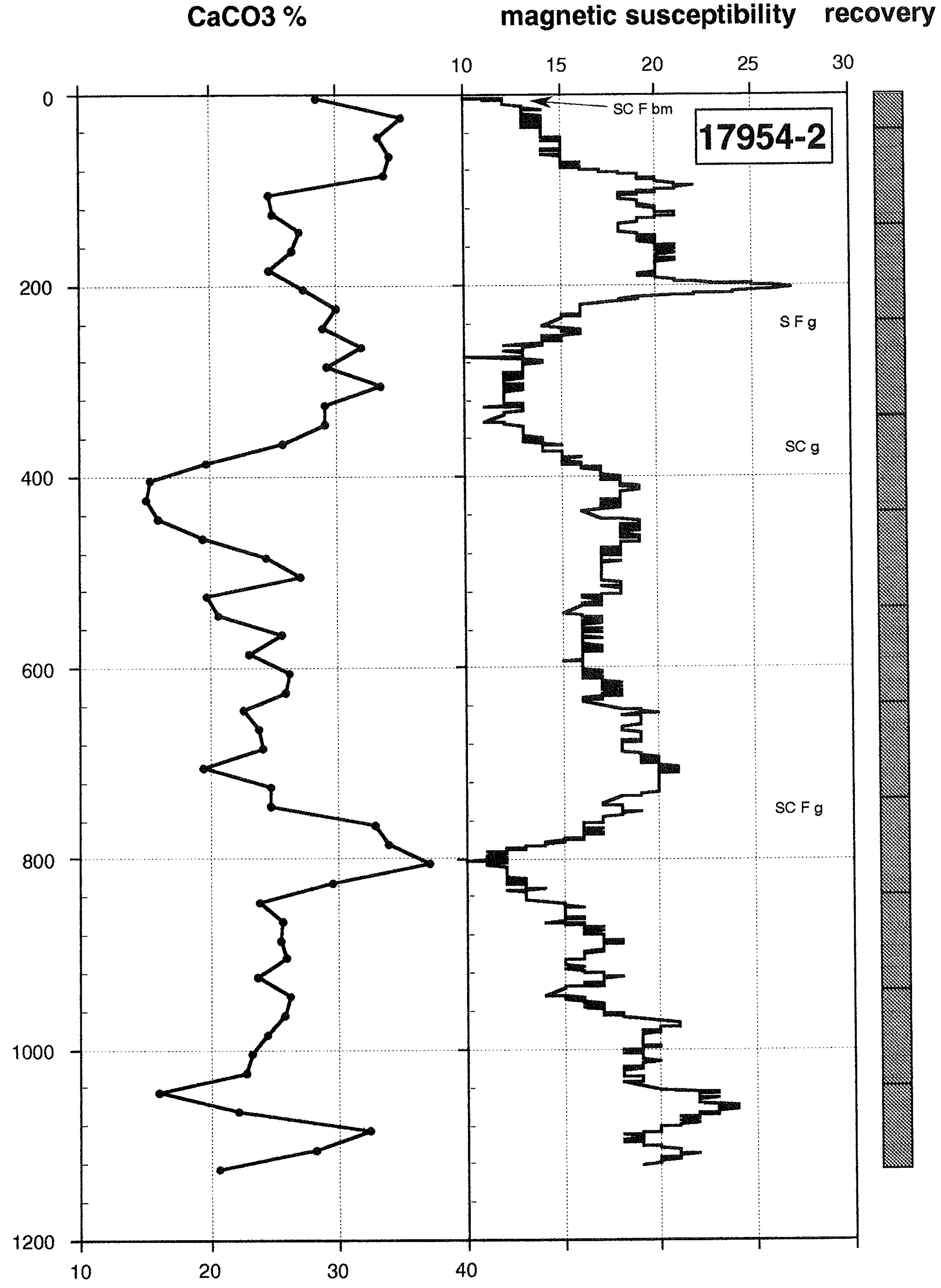

Core 17954-2
and
Core 17954-3

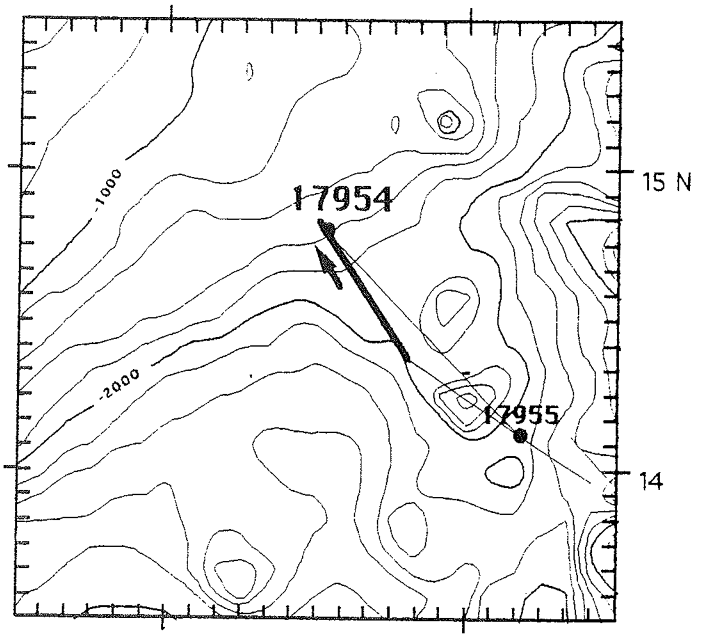

Continental Margin off Vietnam

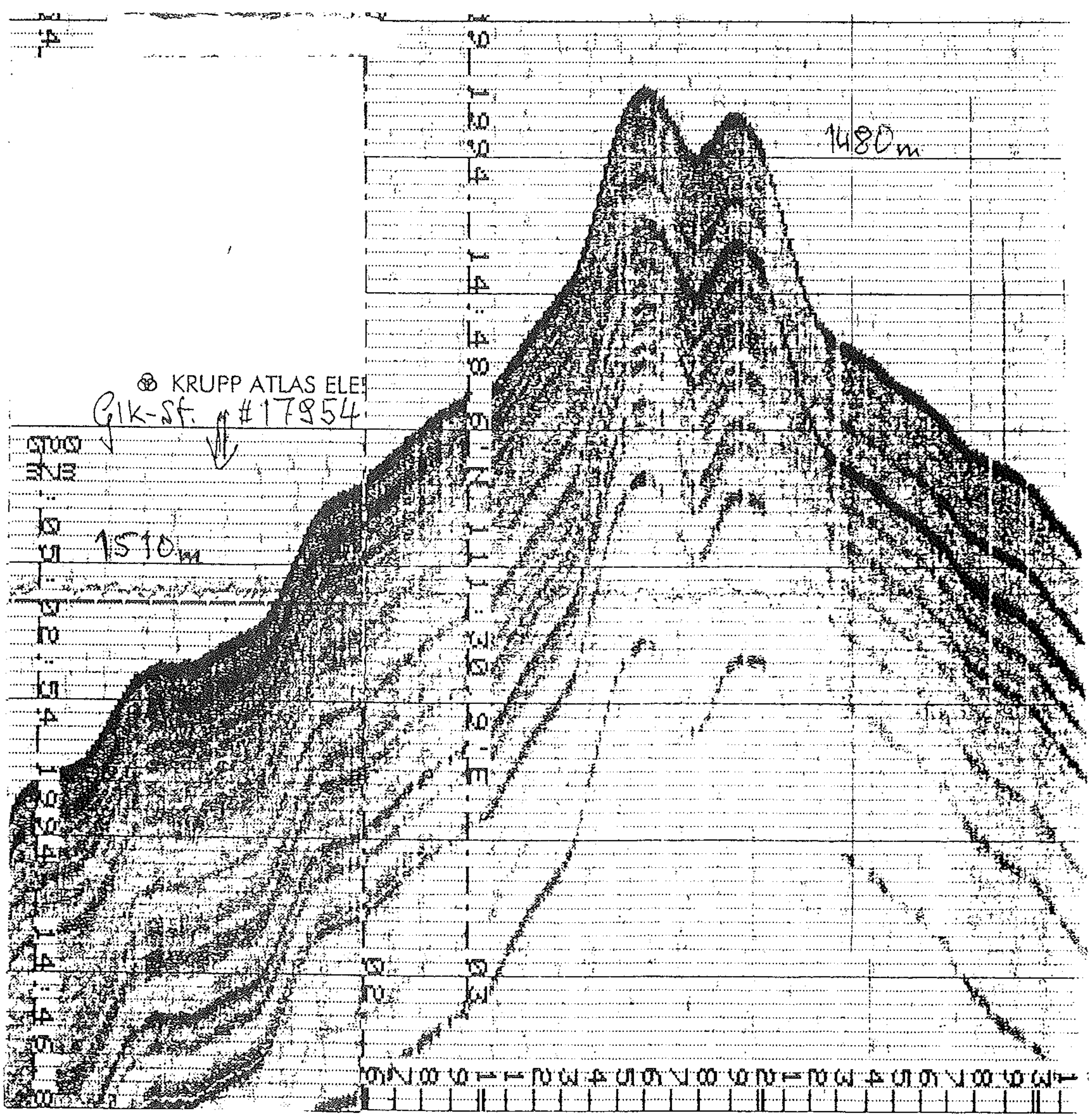

17954-3 14°47.0 N 111°31.5 E, 1515 m w.d., core length 11.49 m

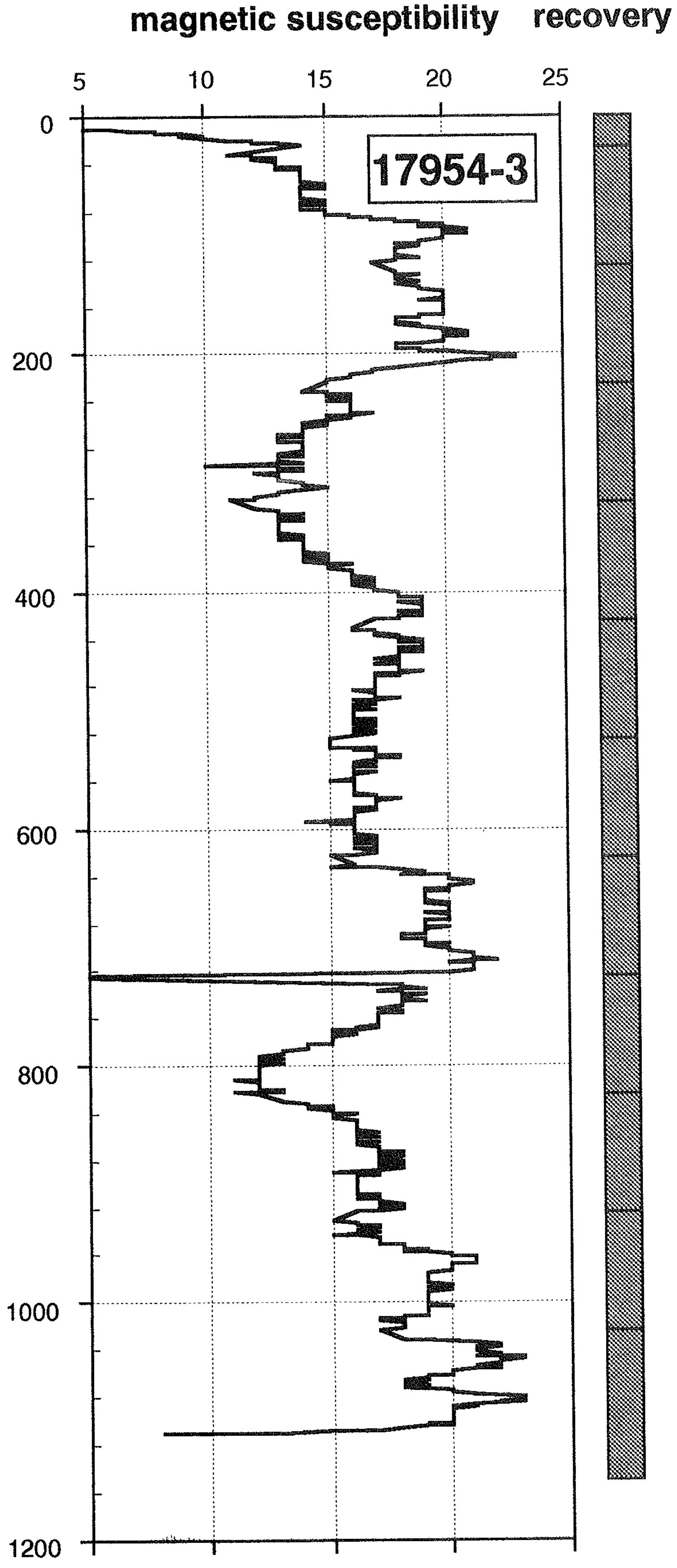

Core 17955-2

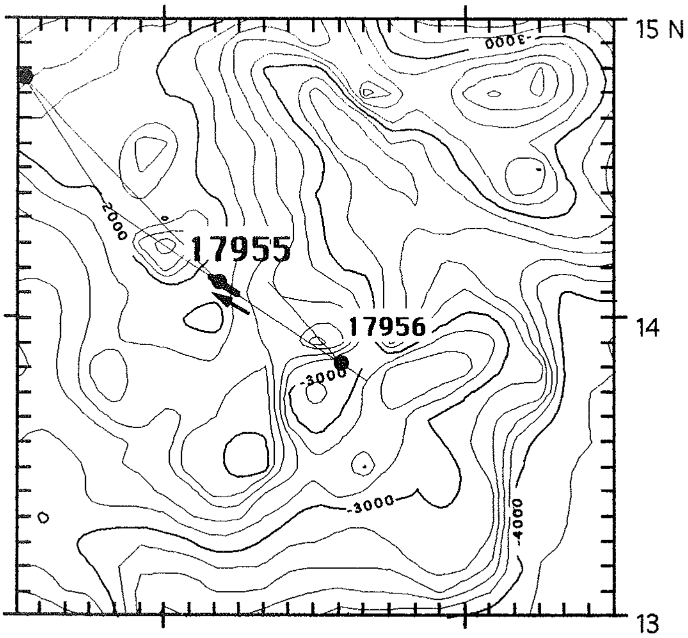

Continental Margin off Vietnam

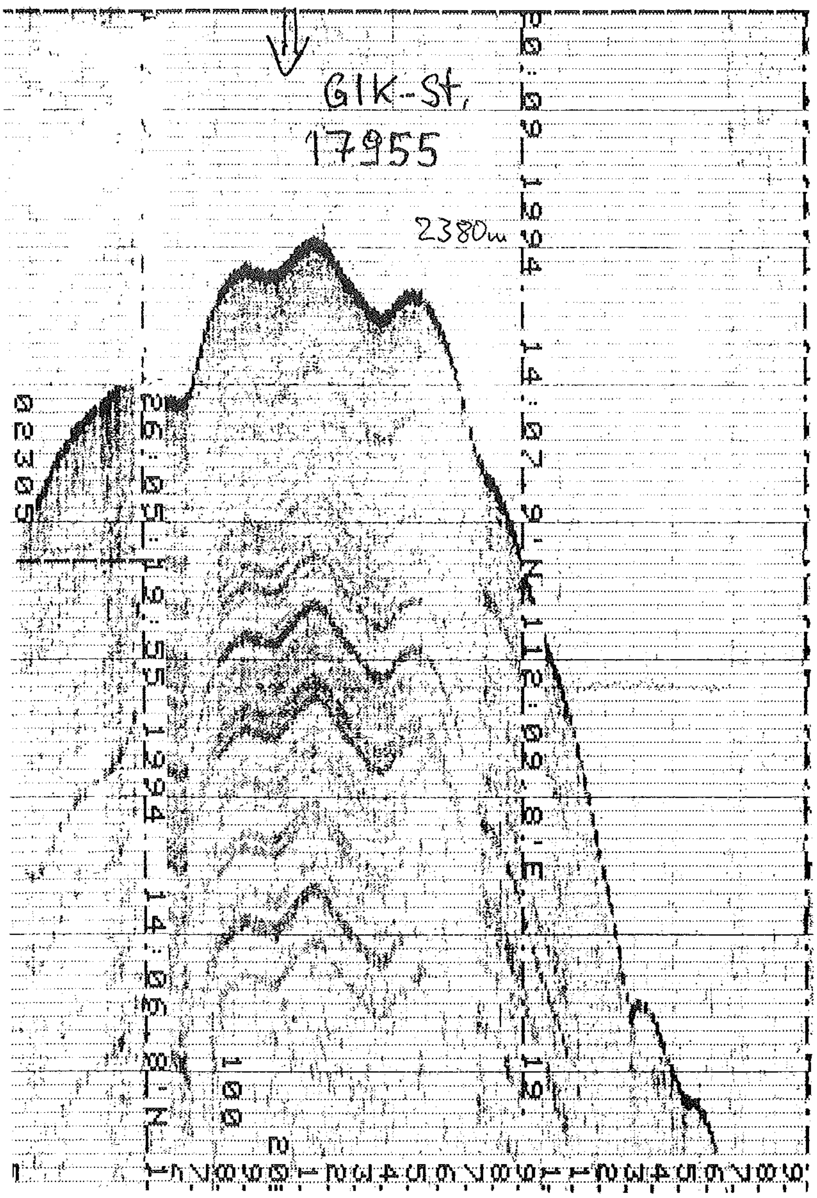

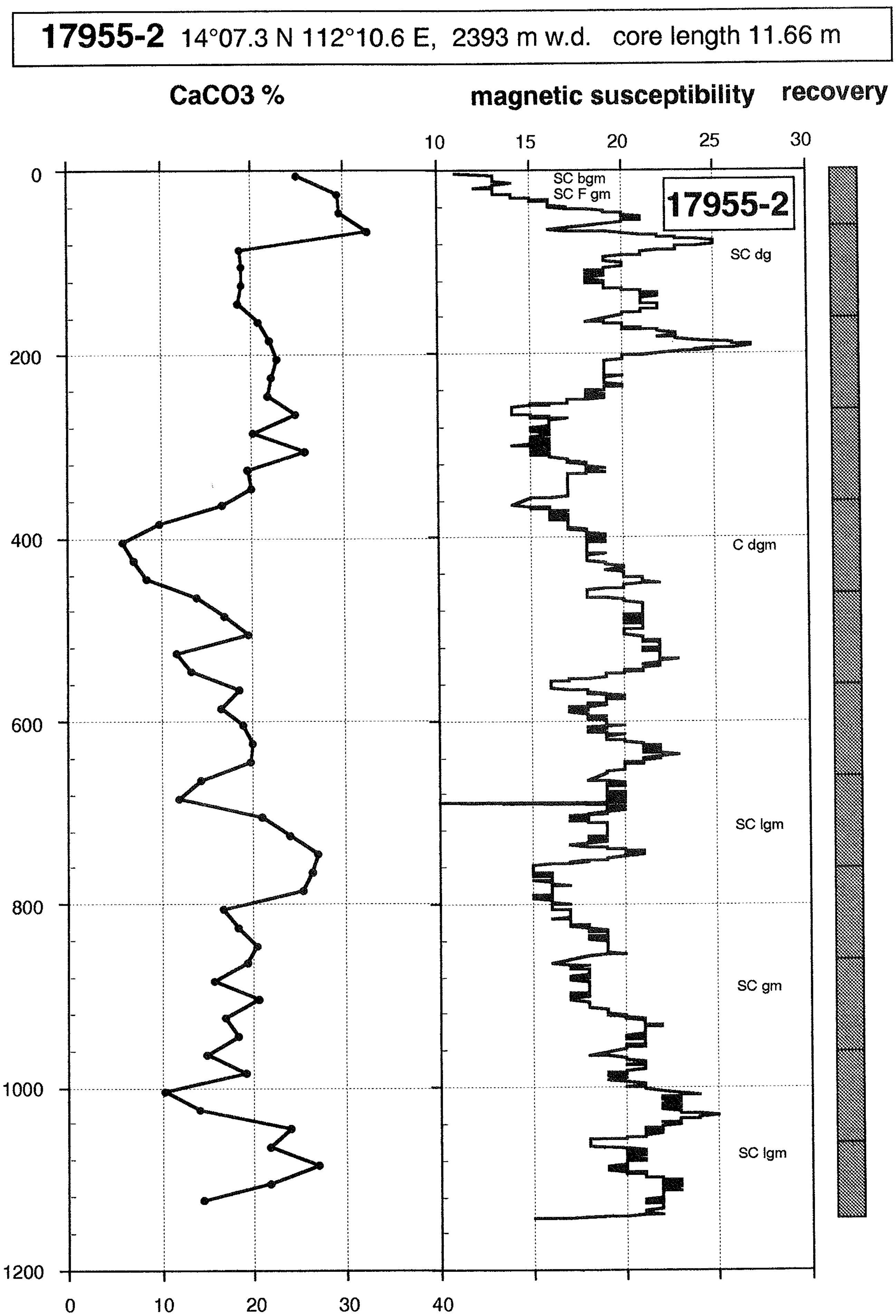

17955-2 14°07.3 N 112°10.6 E, 2393 m w.d. core length 11.66 m
CaCO3 %
magnetic susceptibility
recovery
10
15
20
25
30
SC bgm
SC F gm
17955-2
SC dg
C dgm
SC lgm
SC gm
SC lgm
0
200
400
600
800
1000
1200
0
10
20
30
40

Core 17956-2

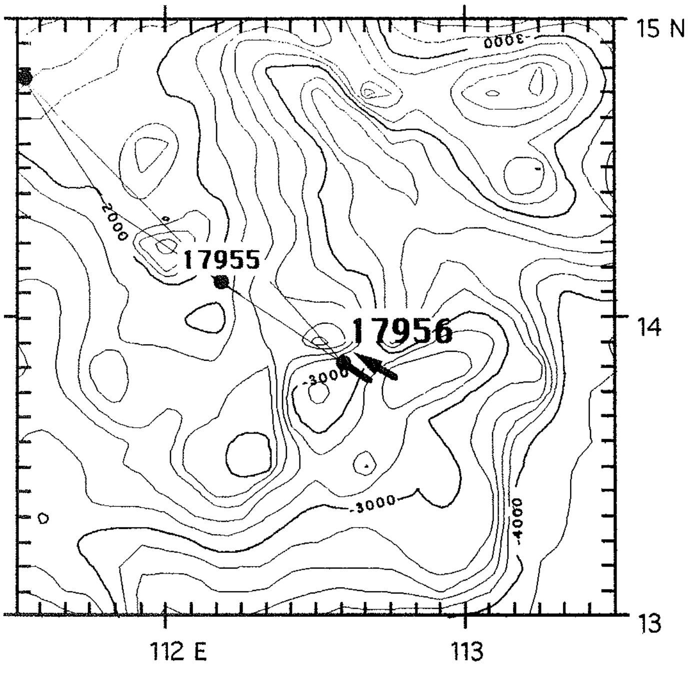

Continental Margin off Vietnam

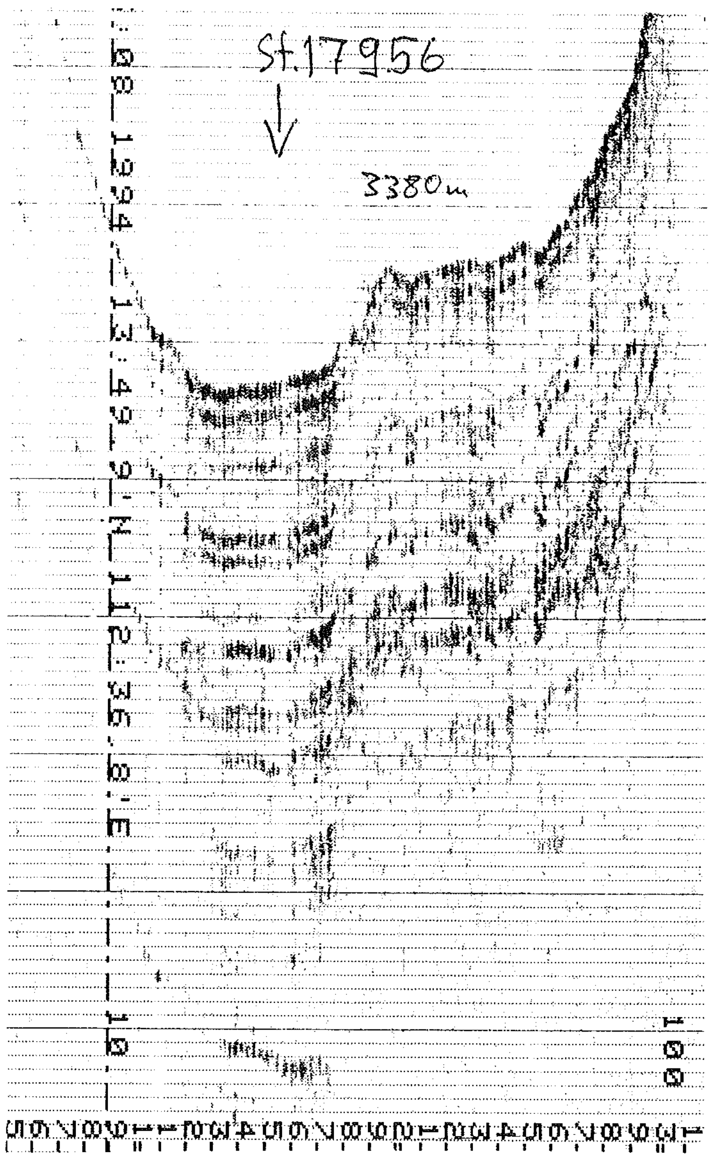

17956-2 13°50.9 N 112°35.3 E, 3388 m w.d., core length 13.56 m

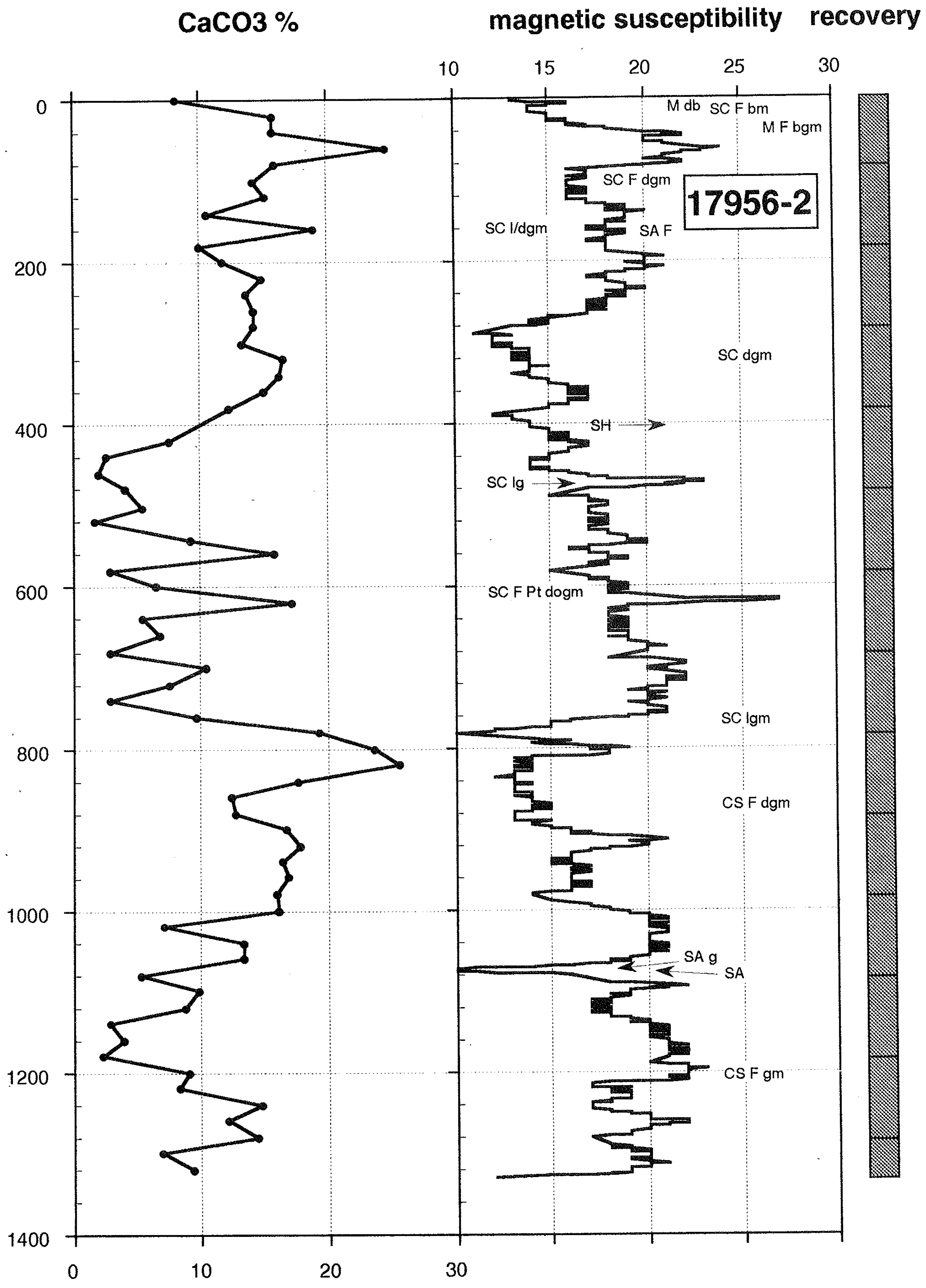

Core 17957-2

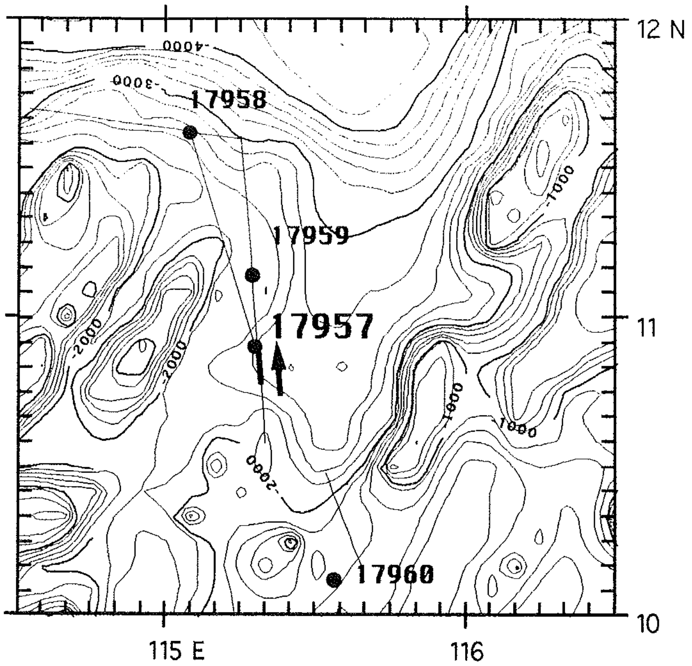

Northern slope of Dangerous Grounds

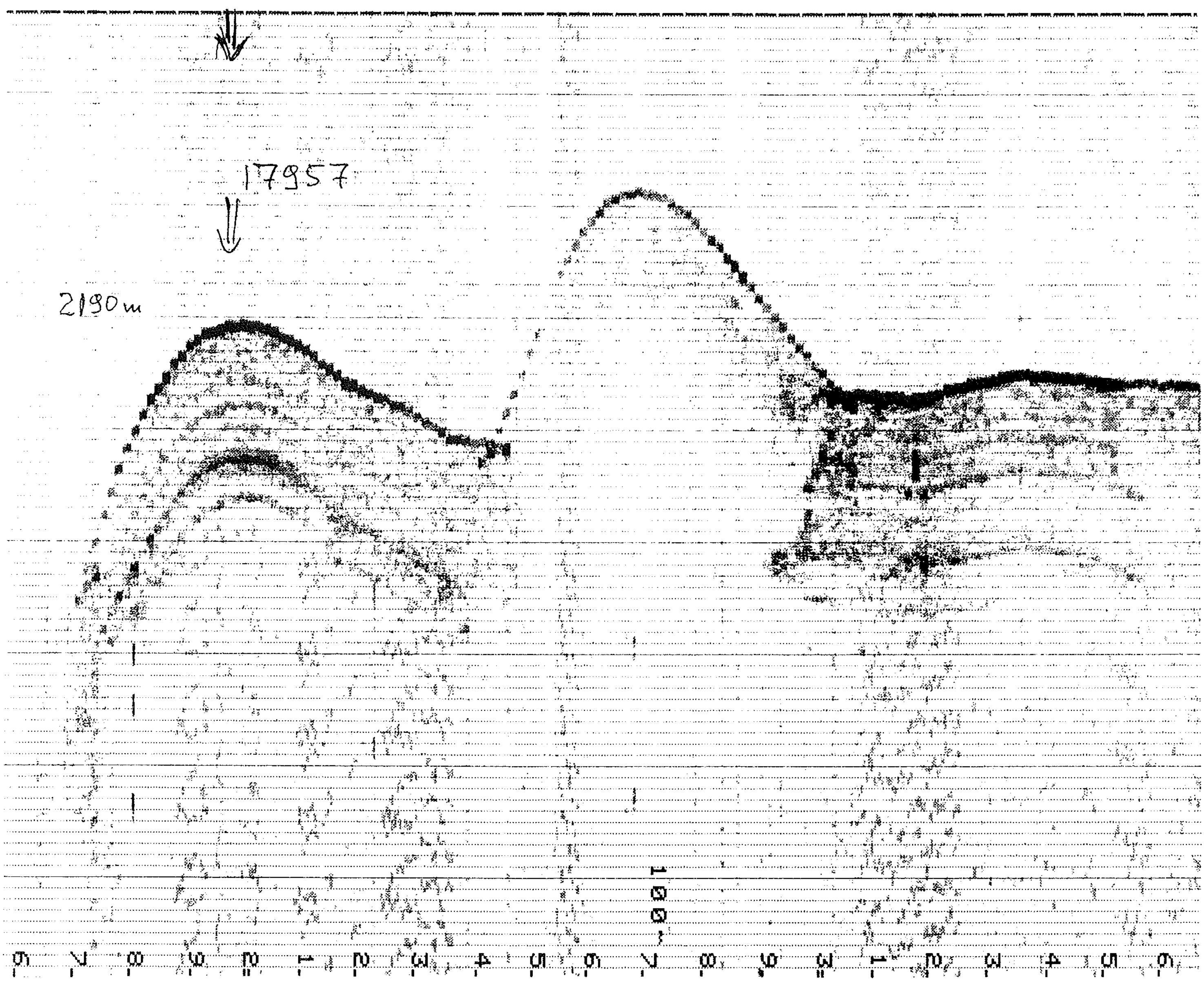

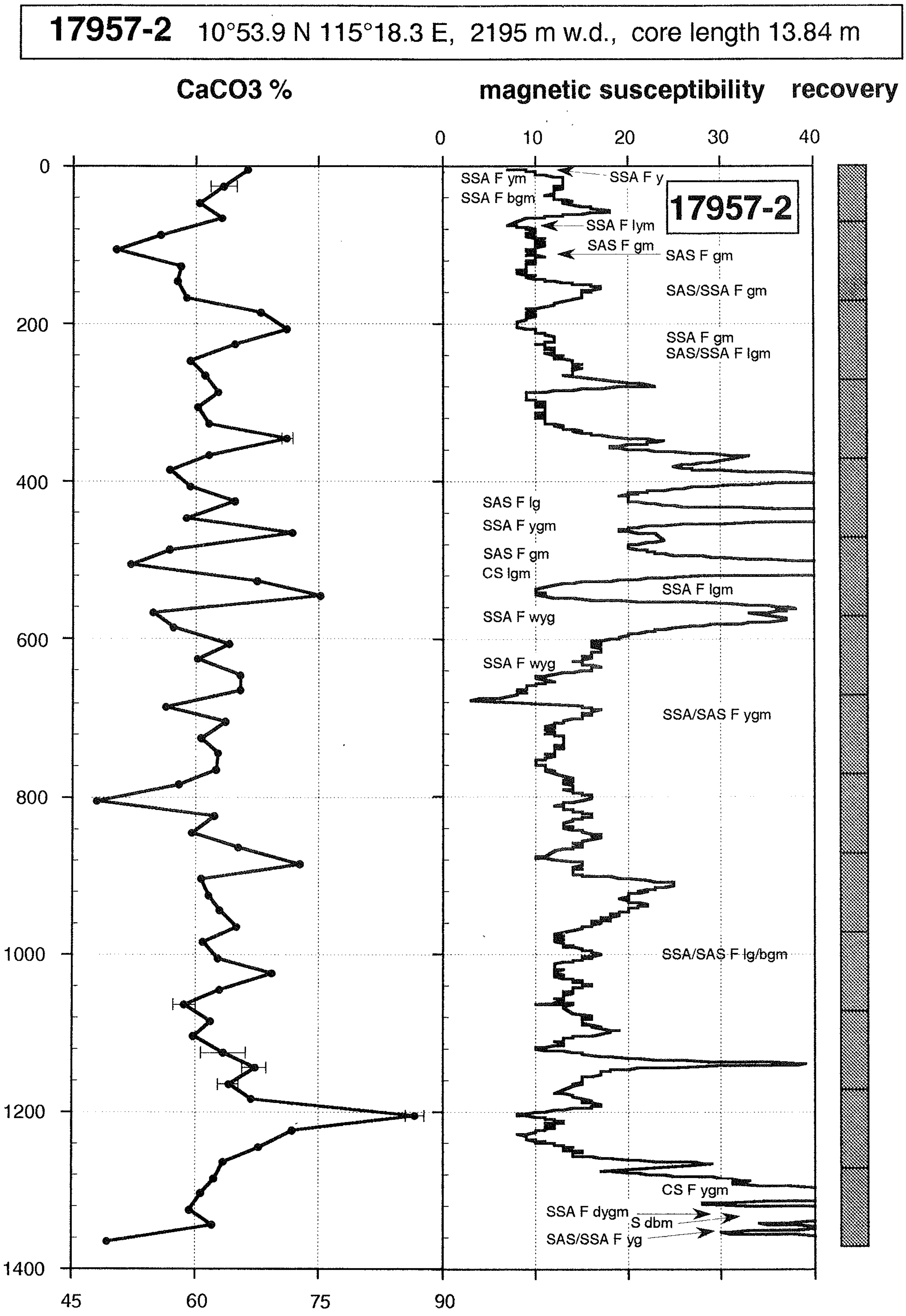

17957-2 10°53.9 N 115°18.3 E, 2195 m w.d., core length 13.84 m
CaCO3 %
magnetic susceptibility
recovery
17957-2
SSA F ym
SSA F bgm
SSA F y
SSA F lym
SAS F gm
SAS F gm
SAS/SSA F gm
SSA F gm
SAS/SSA F lgm
SAS F lg
SSA F ygm
SAS F gm
CS lgm
SSA F lgm
SSA F wyg
SSA F wyg
SSA/SAS F ygm
SSA/SAS F lg/bgm
CS F ygm
SSA F dygm
S dbm
SAS/SSA F yg
0
200
400
600
800
1000
1200
1400
45
60
75
90
0
10
20
30
40

Core 17958-2

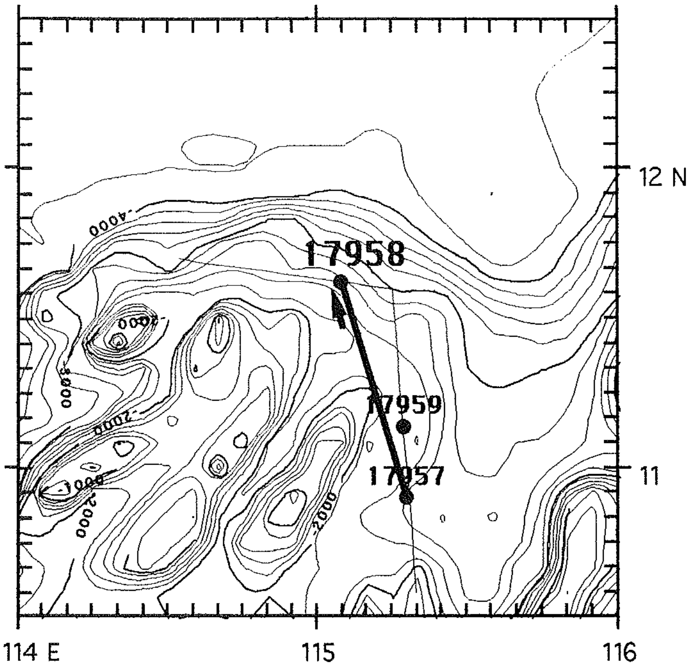

Northern slope of Dangerous Grounds

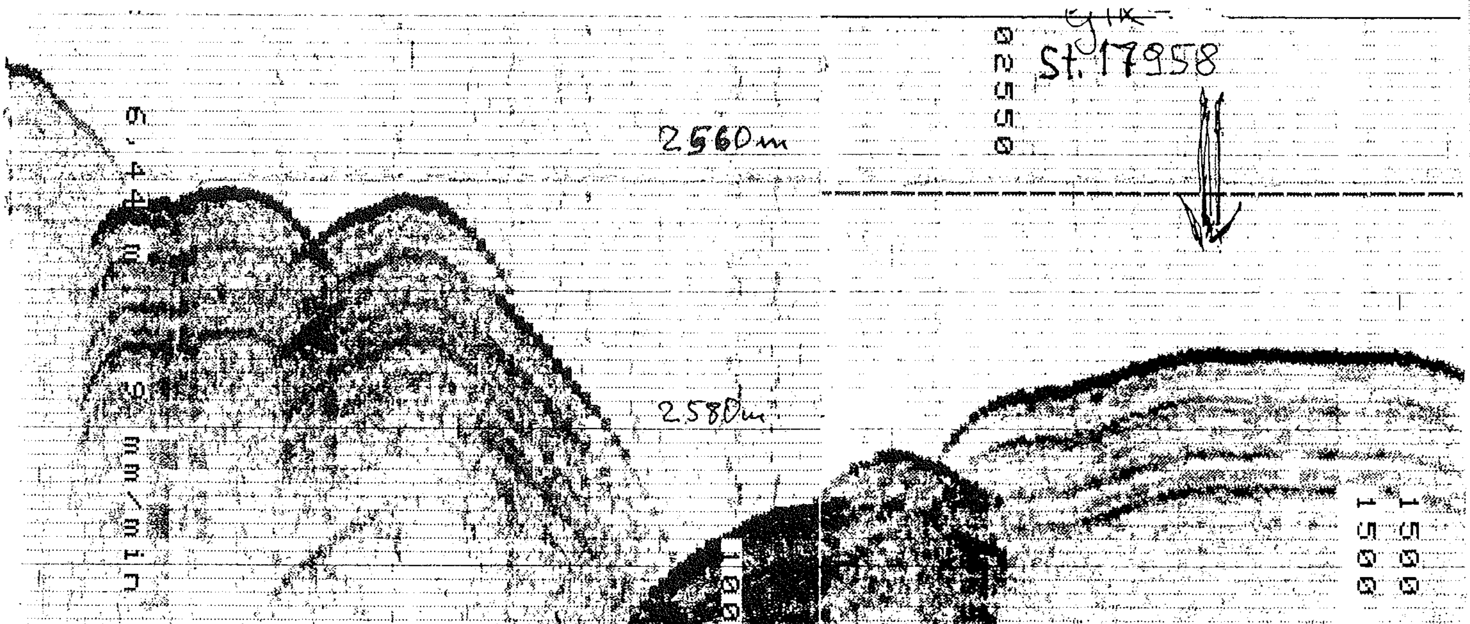

17958-2 11°37.3 N 115°04.9 E, 2581 m w.d., core length 10.73 m

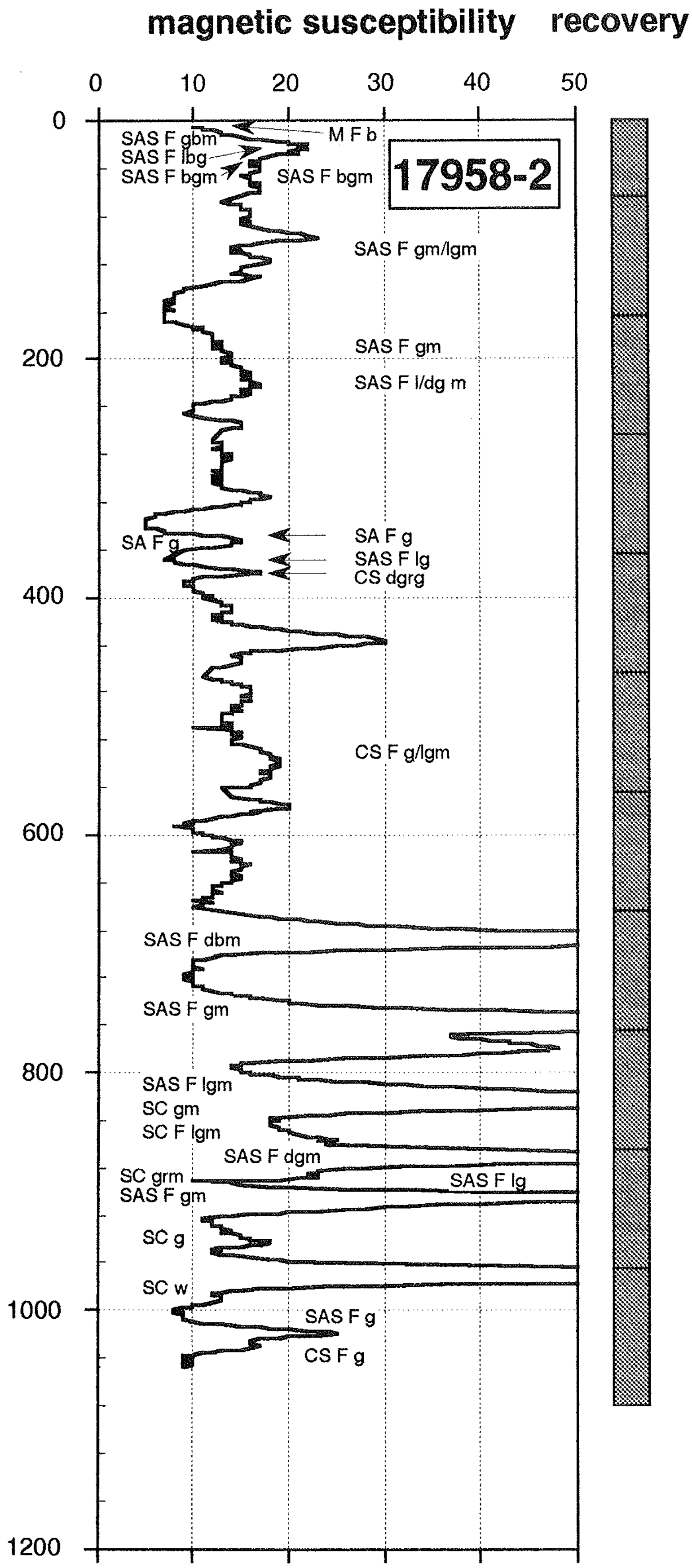

Core 17959-2

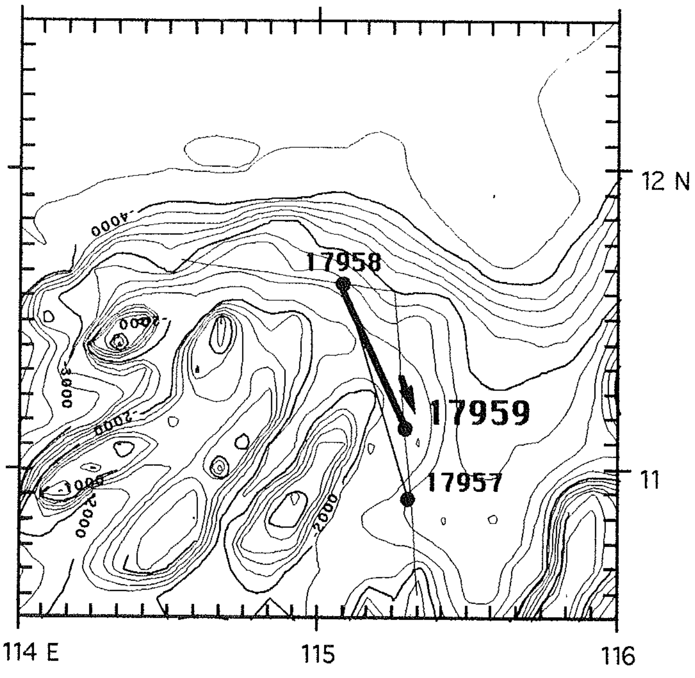

Northern slope of Dangerous Grounds

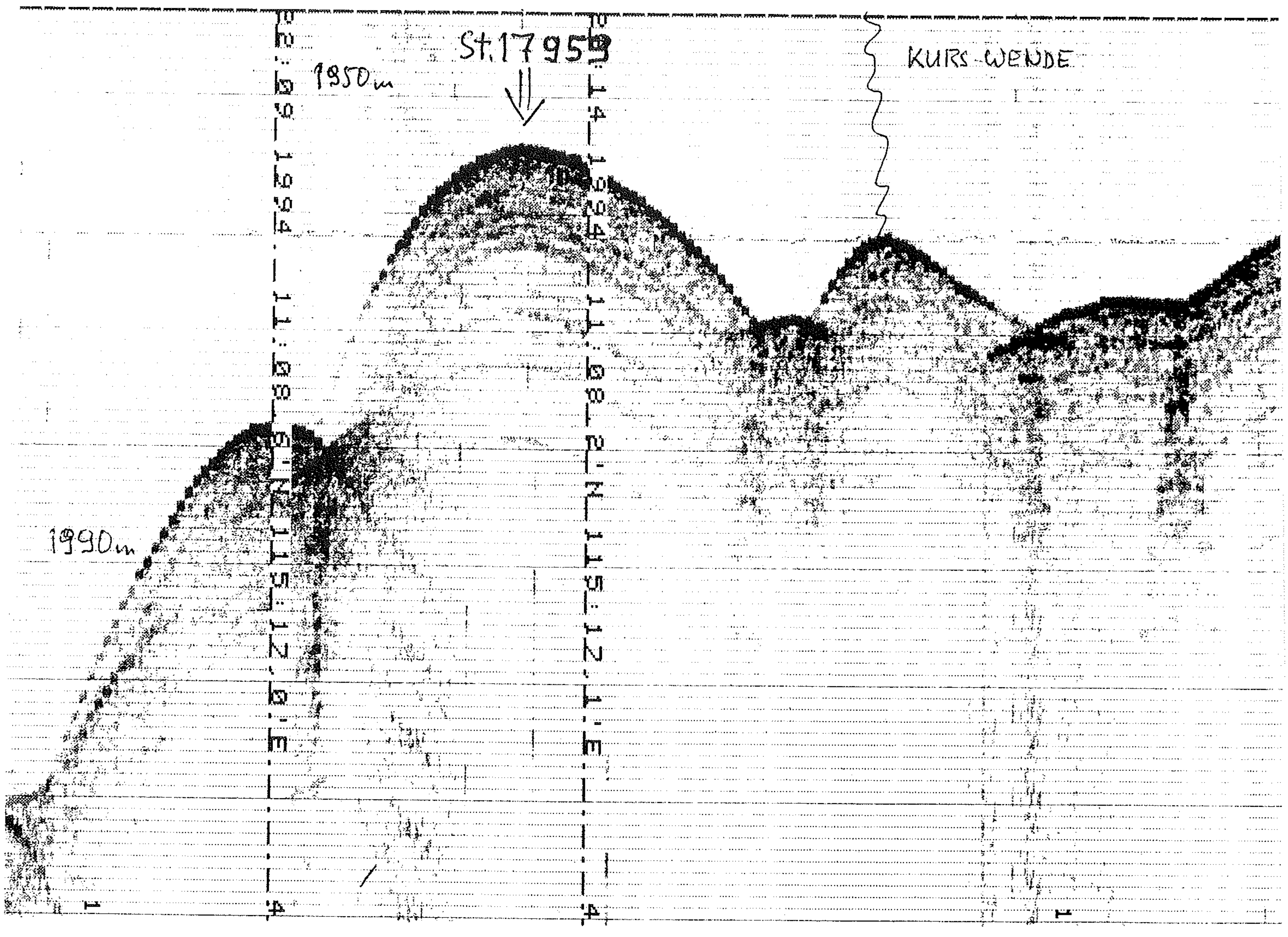

17959-2 11°08.3 N 115°17.2 E, 1959 m w.d., core length 13.93 m

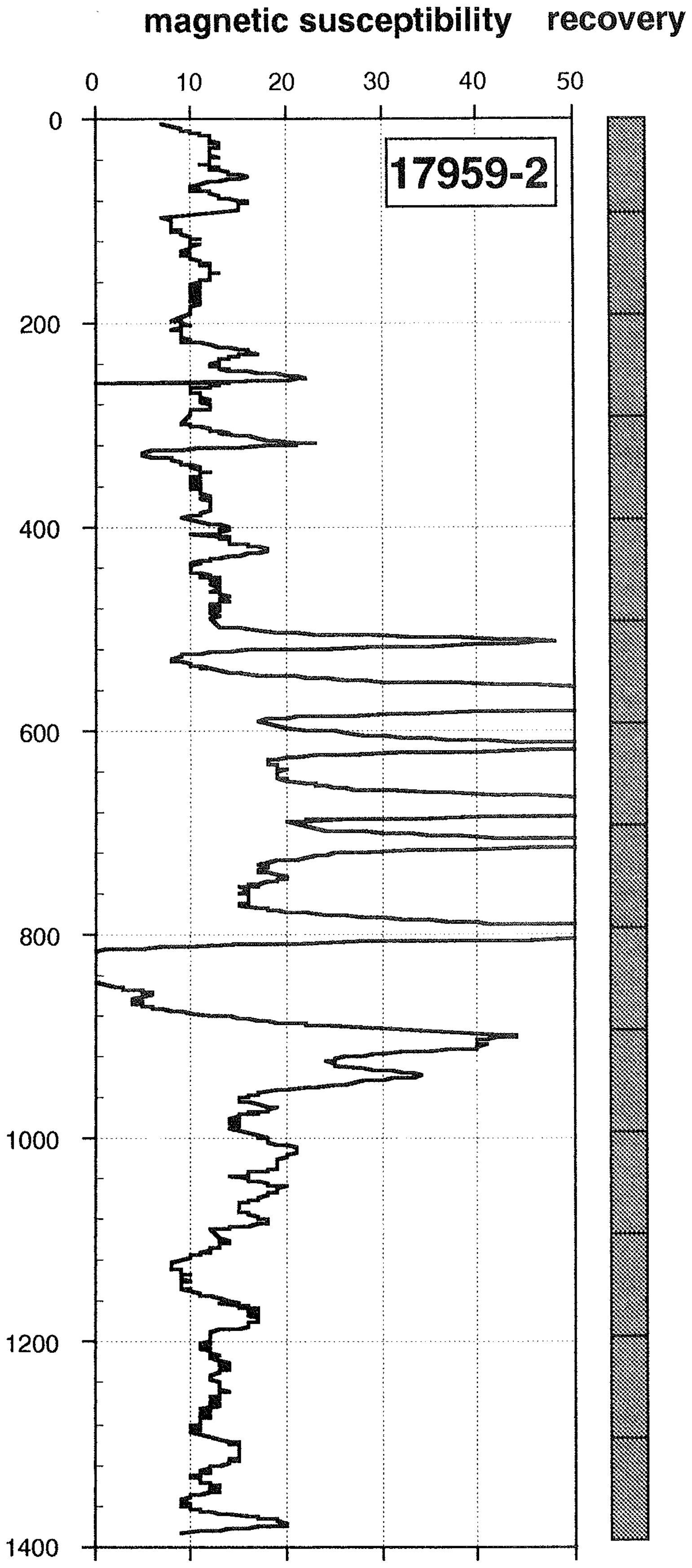

Core 17961-2

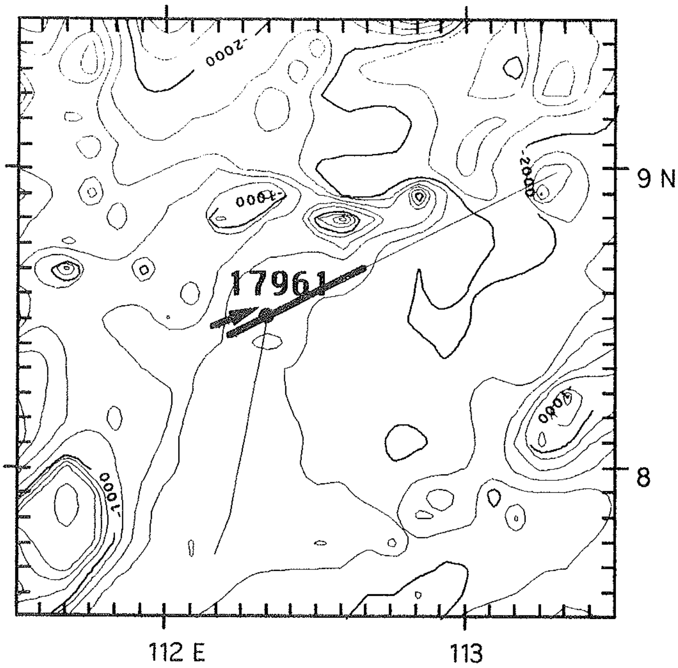

Southern part of Dangerous Grounds

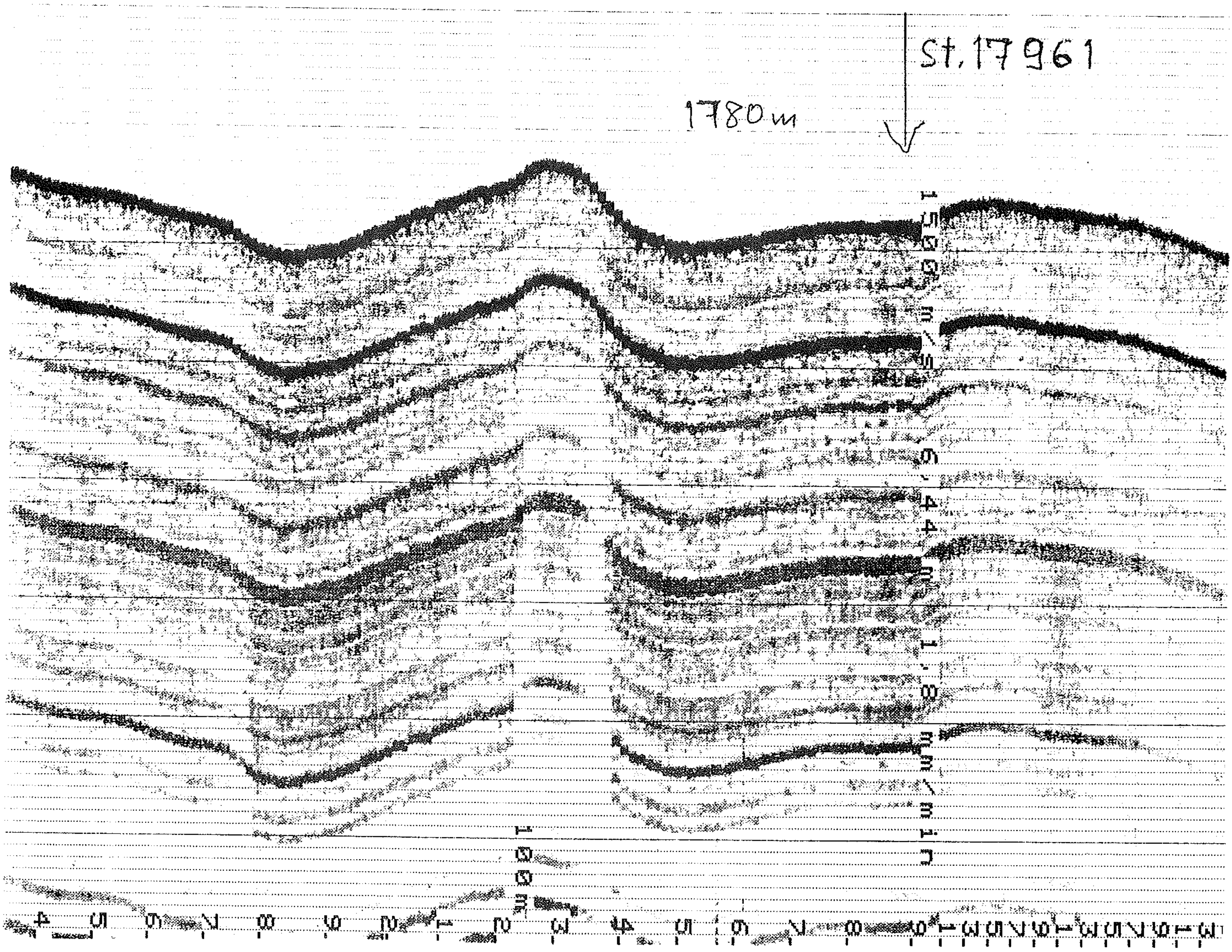

17961-2 08°30.4 N 112°19.9 E, 1968 m w.d., core length 10.30 m

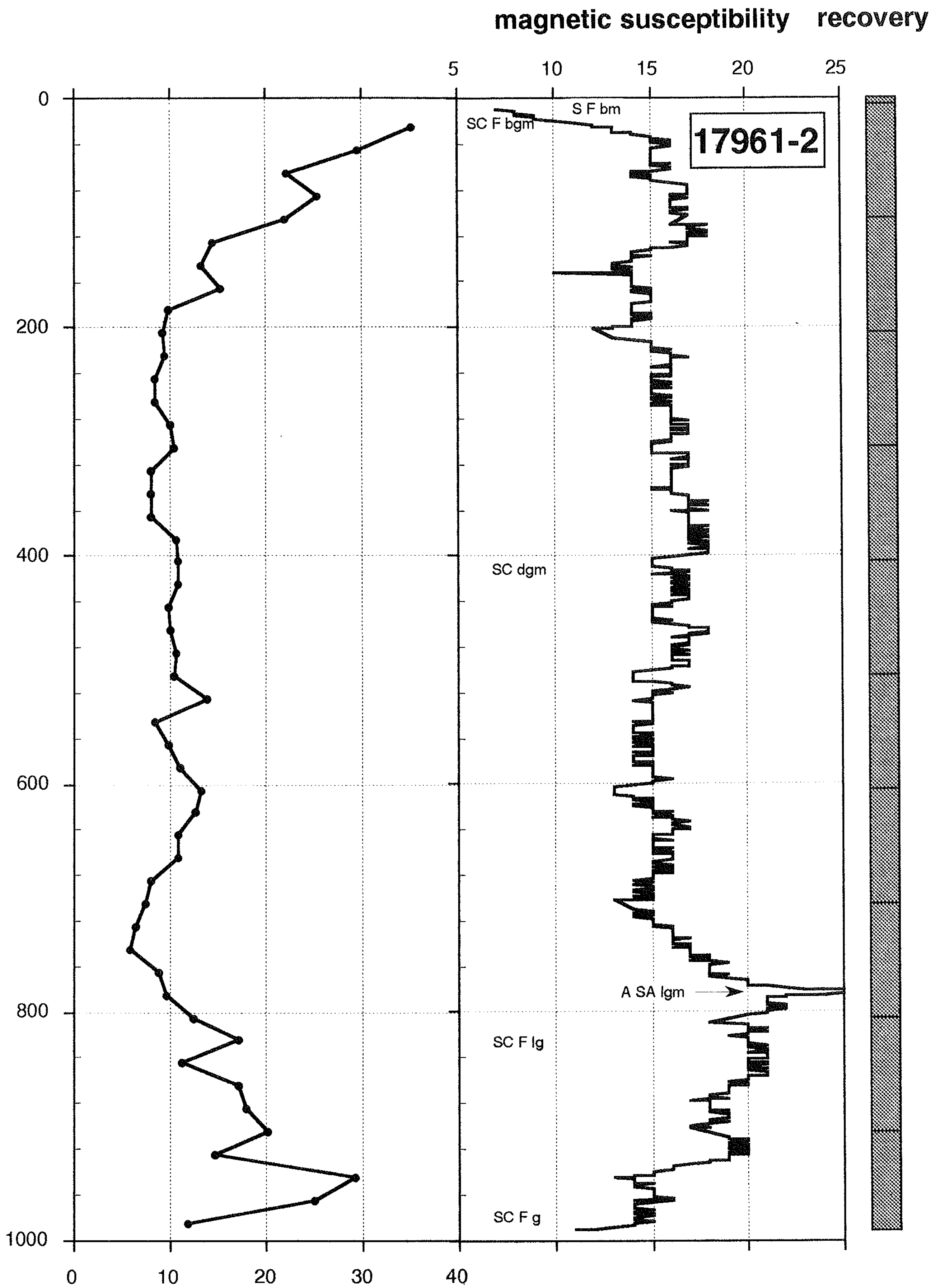

Core 17962-2
and
Core 17962-3
and
Core 17962-4

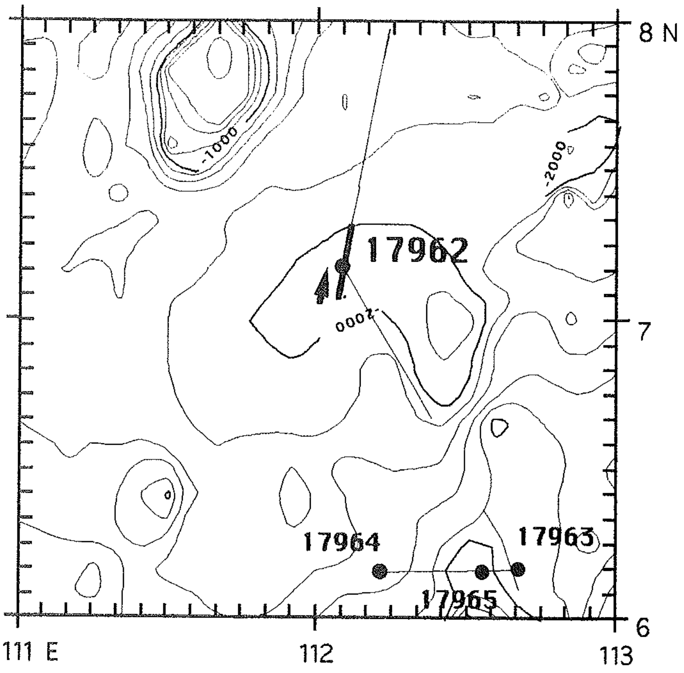

Southern part of Dangerous Grounds

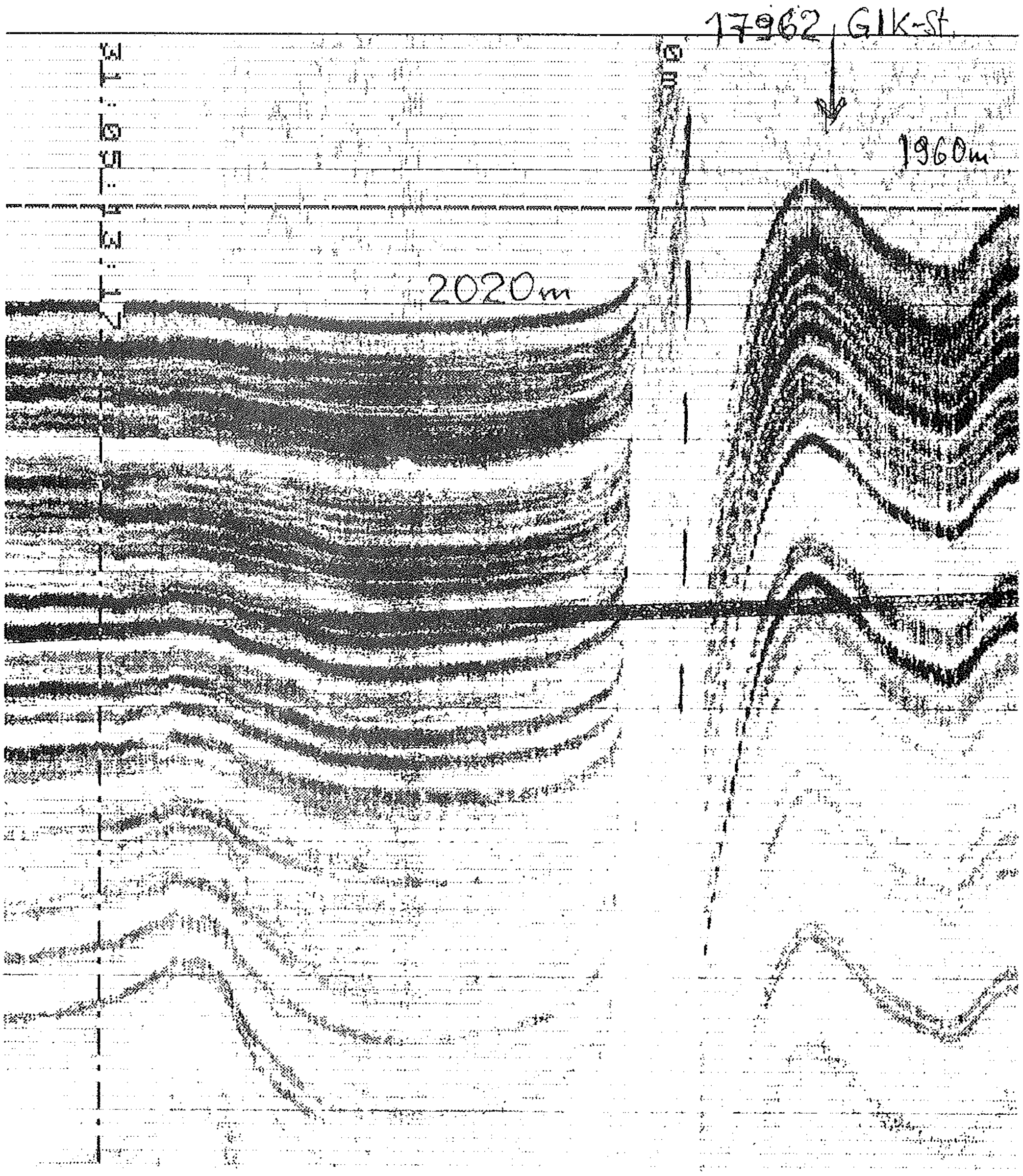

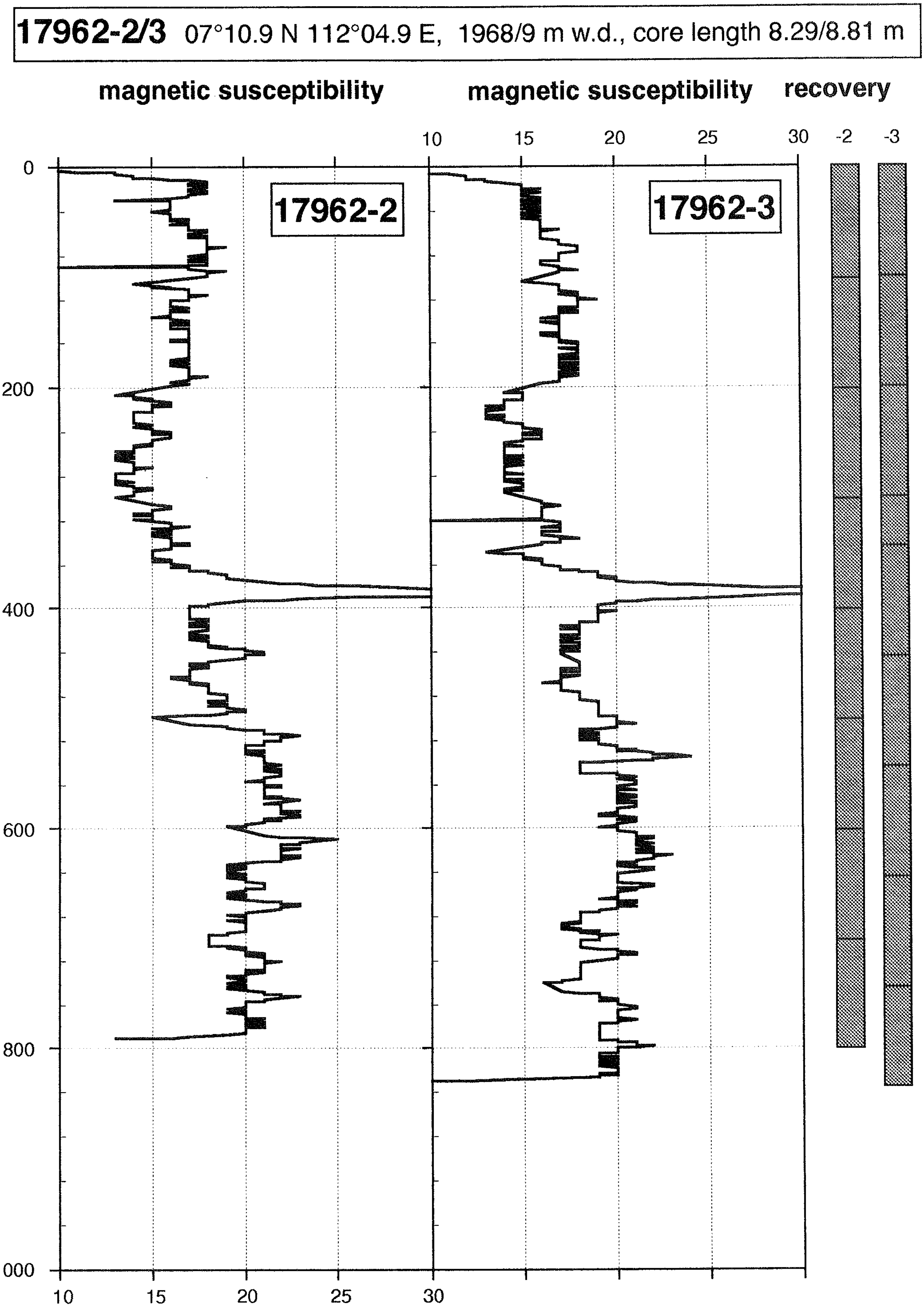

17962-2/3 07°10.9 N 112°04.9 E, 1968/9 m w.d., core length 8.29/8.81 m
magnetic susceptibility
magnetic susceptibility
recovery
10
15
20
25
30
-2
-3
0
200
400
600
800
1000
17962-2
17962-3
10
15
20
25
30

Core 17962-2
and
Core 17962-3
and
Core 17962-4

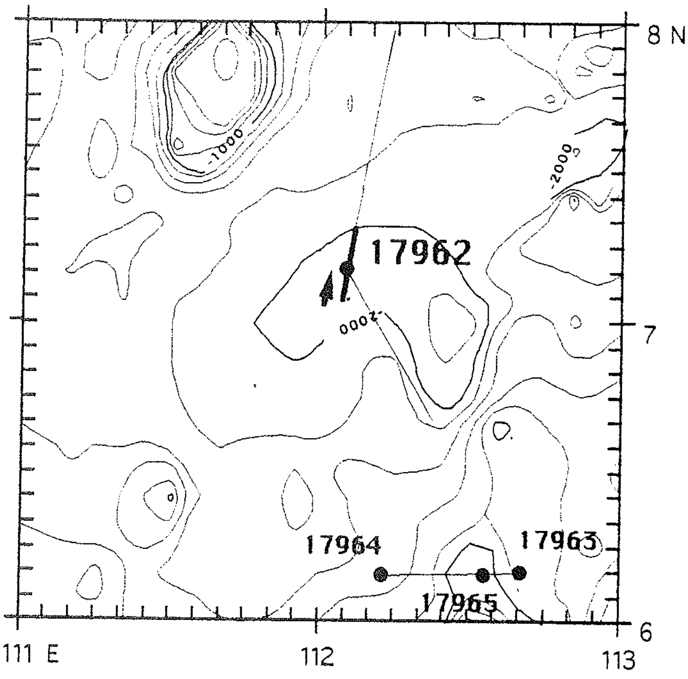

Southern part of Dangerous Grounds

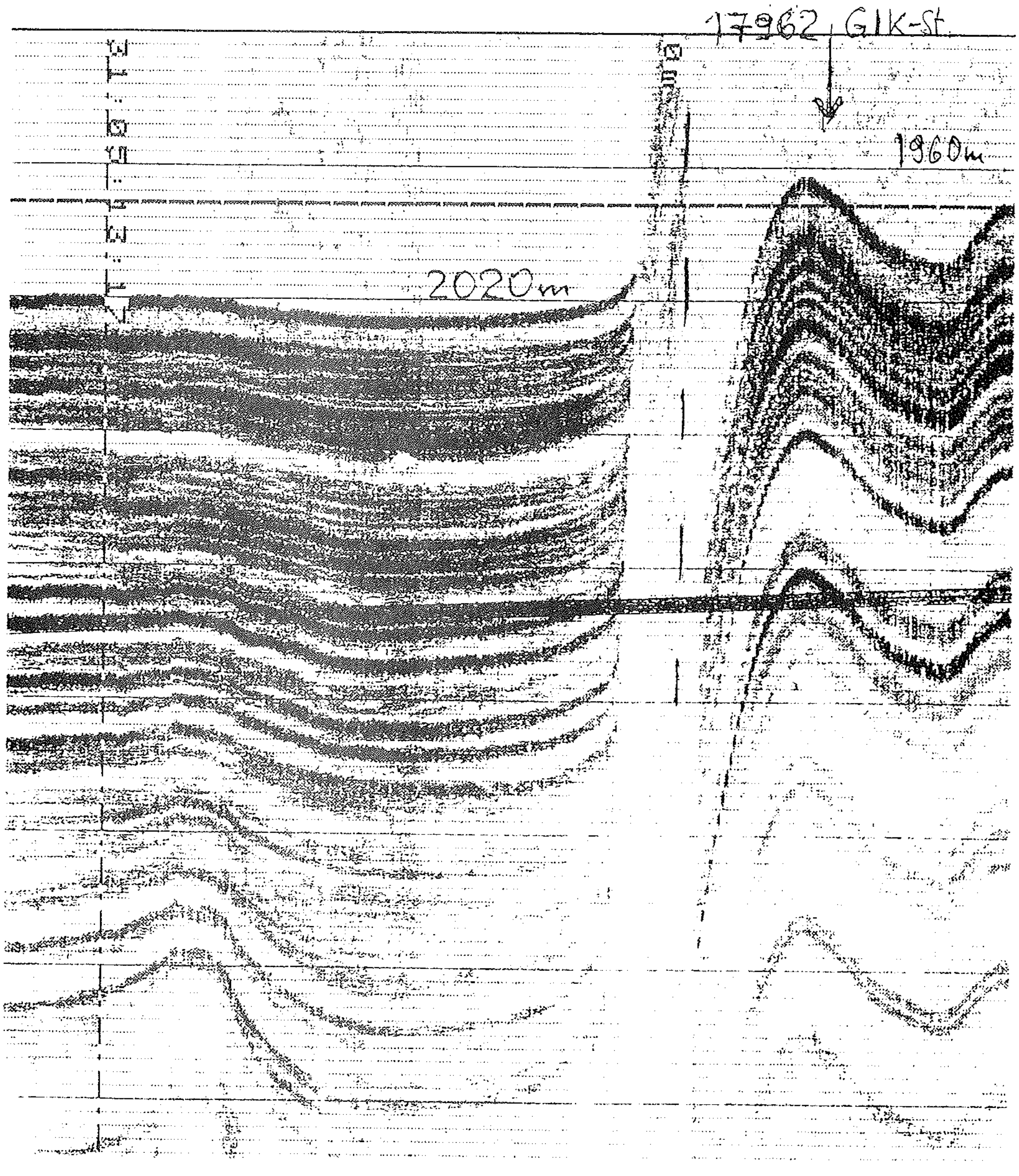

17962-4 07°10.9 N 112°04.9 E, 1969 m w.d., core length 14.80 m

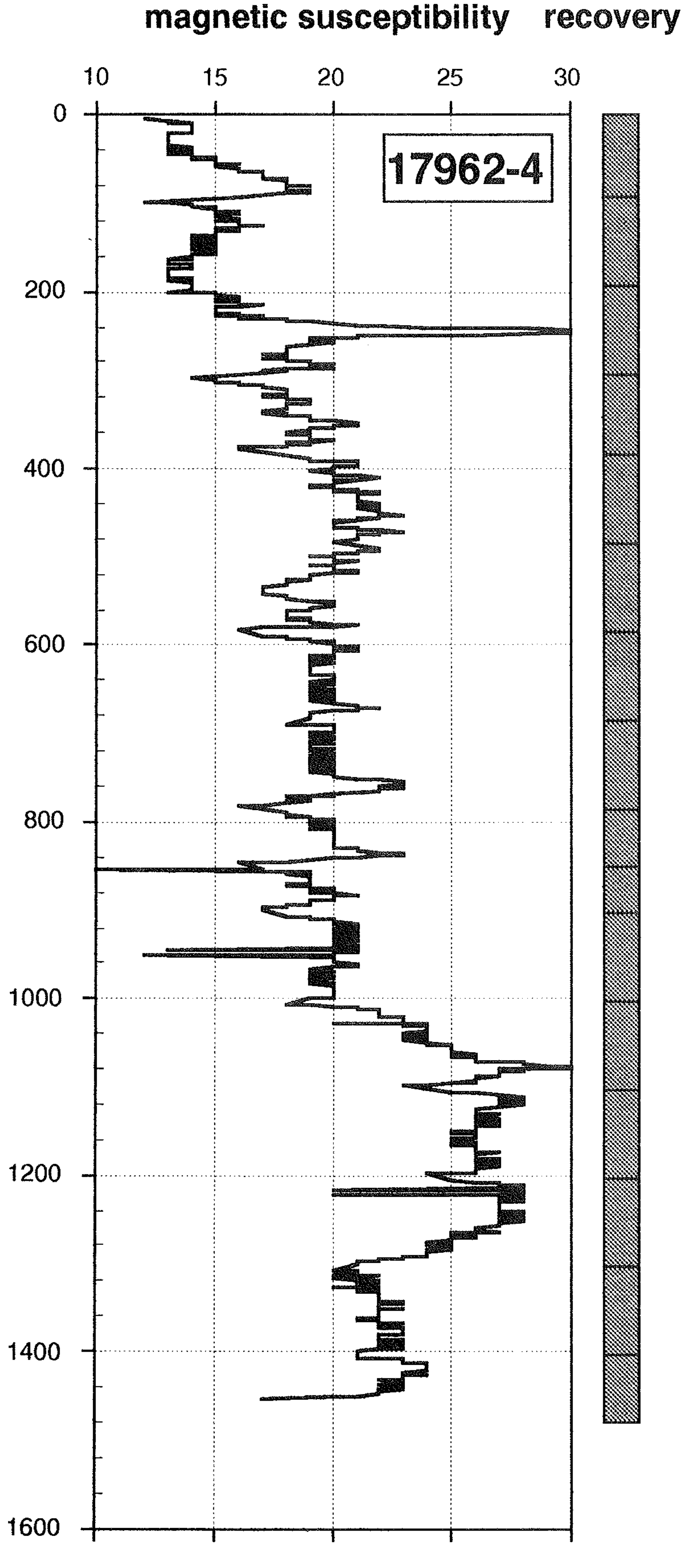

Core 17963-2

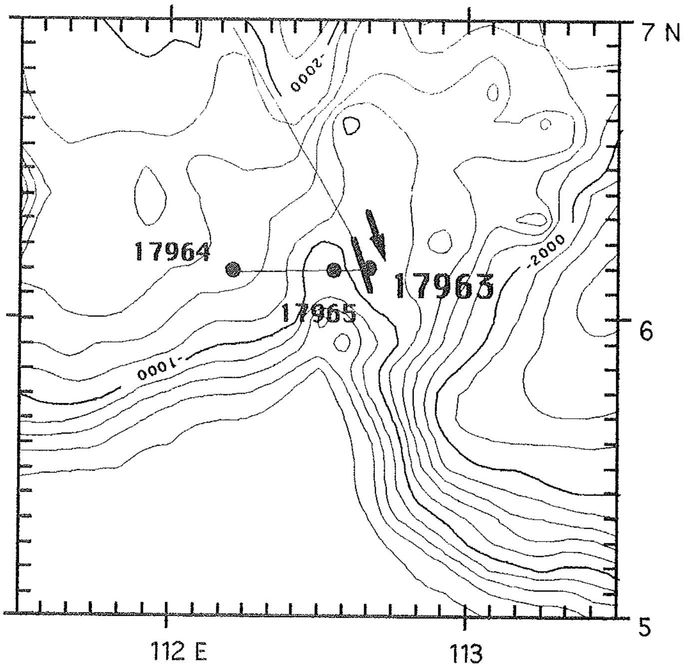

Northern slope of Luconia Shoals

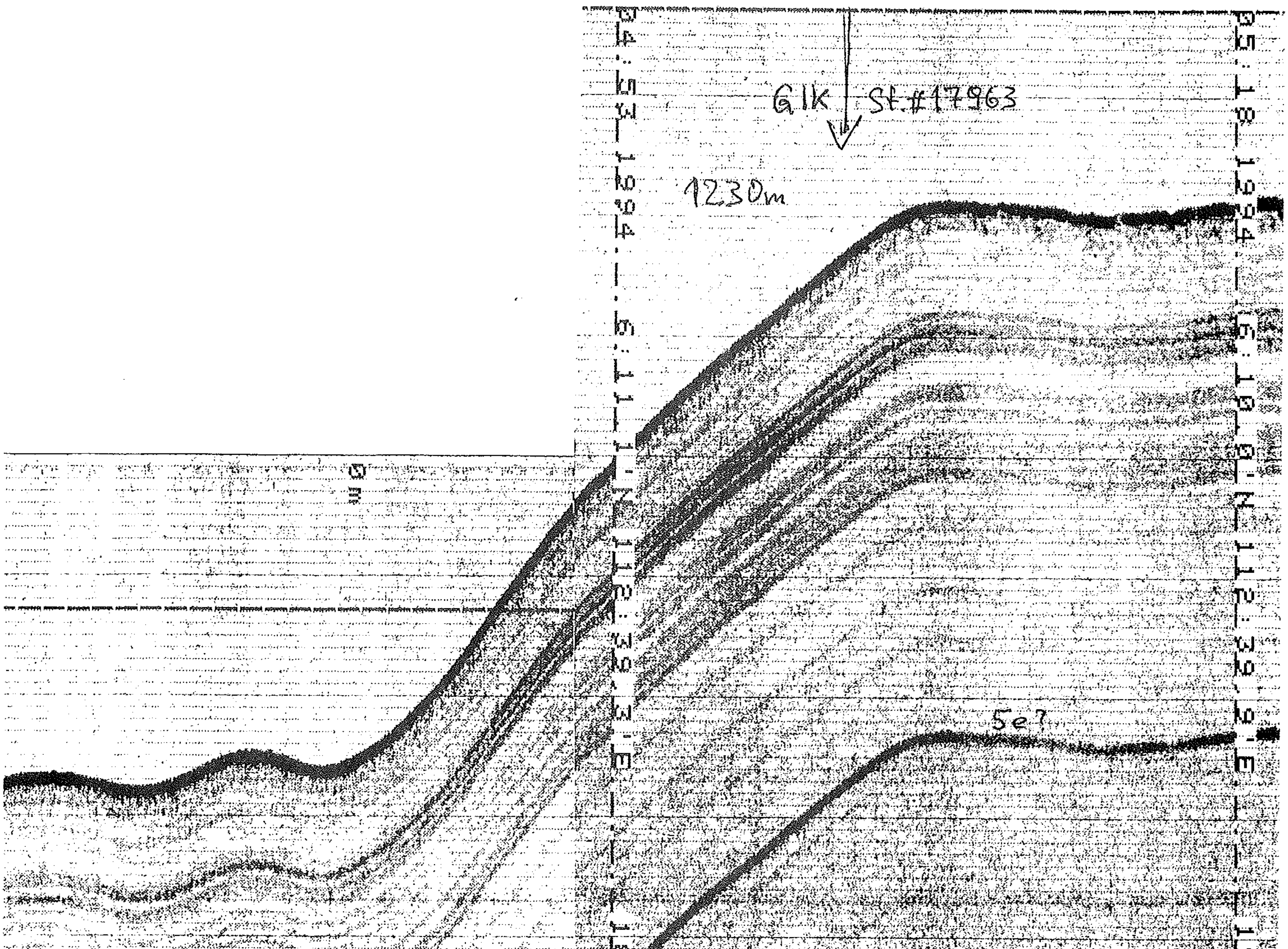

17963-3 06°10.0 N 112°40.0 E, 1232 m w.d., core length 8.57 m

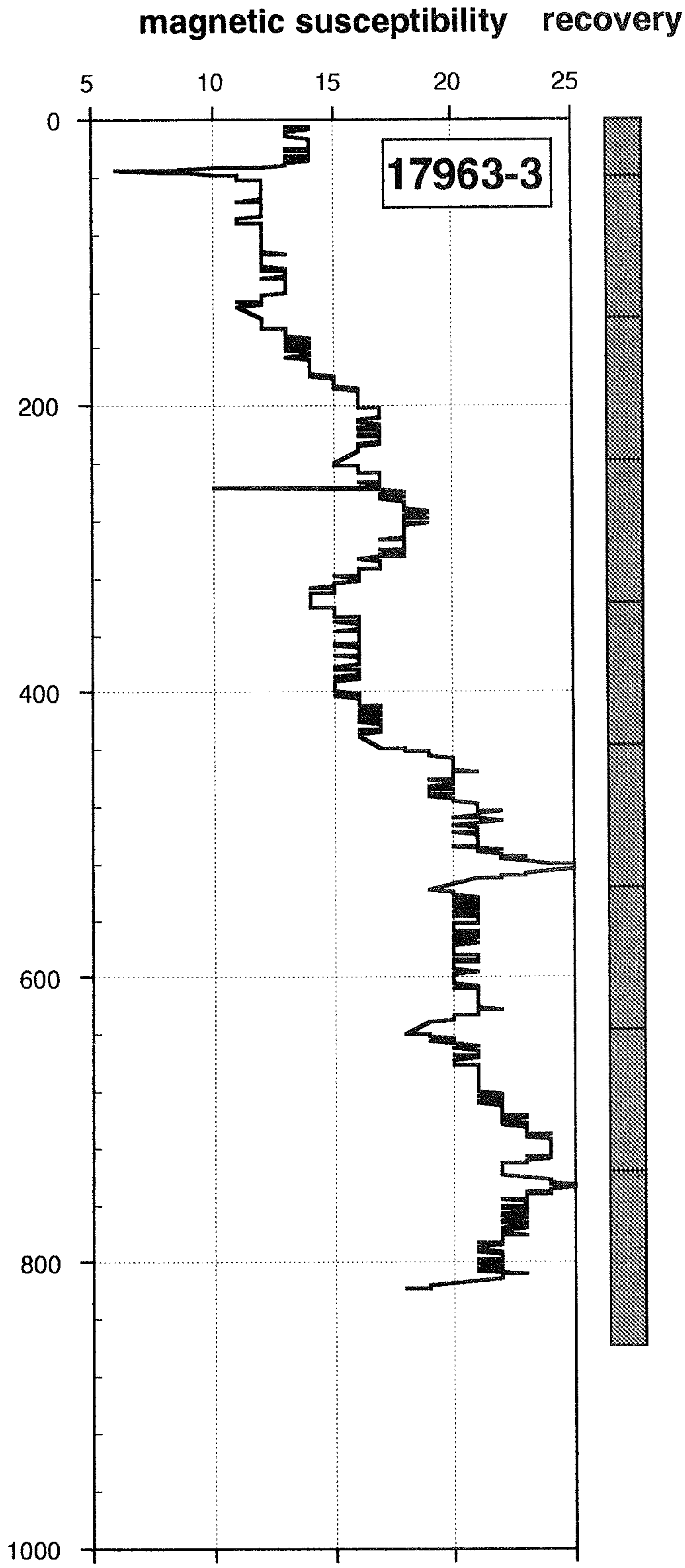

Core 17964-2
and
Core 17964-3

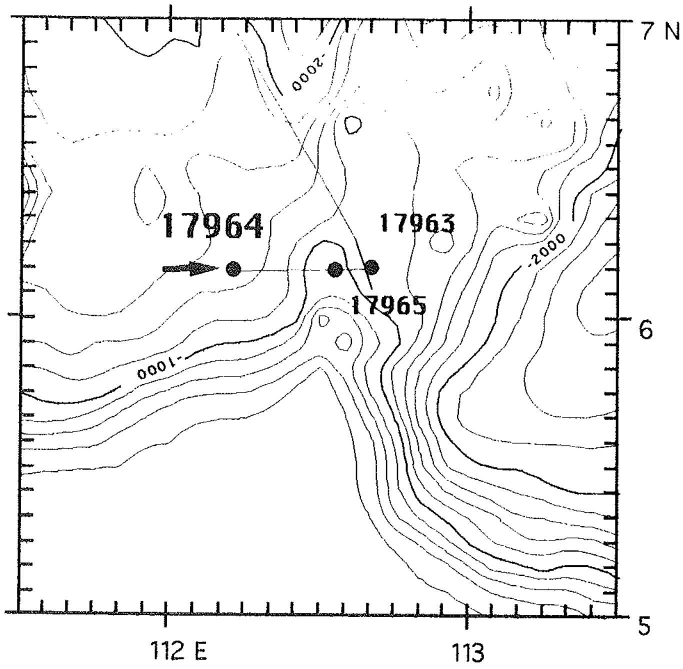

Northern slope of Luconia Shoals

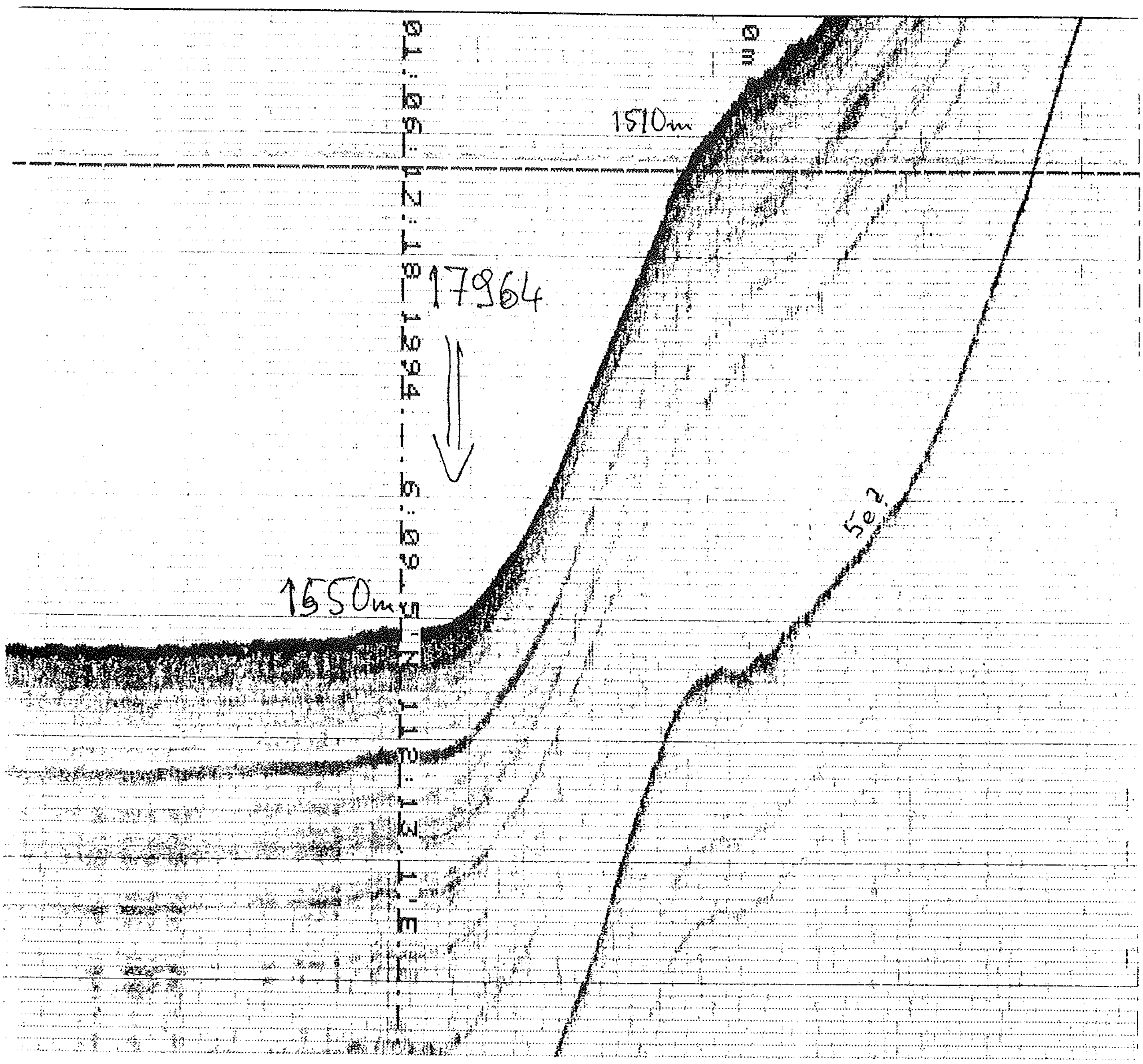

17964-2/3 06°9.5 N 112°12.8 E, 1556 m w.d., core length 13.04/9.12 m

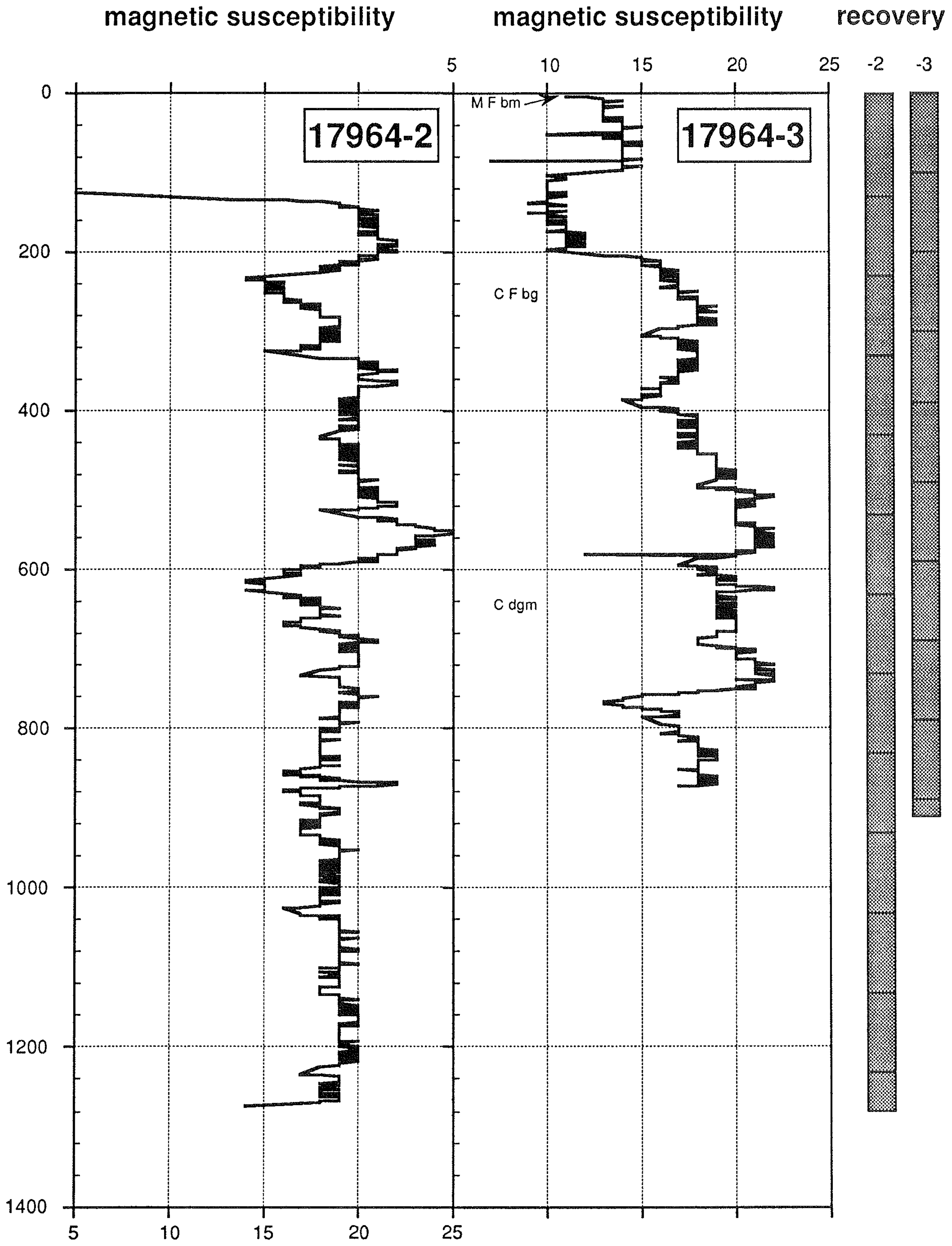

Core 17965-2

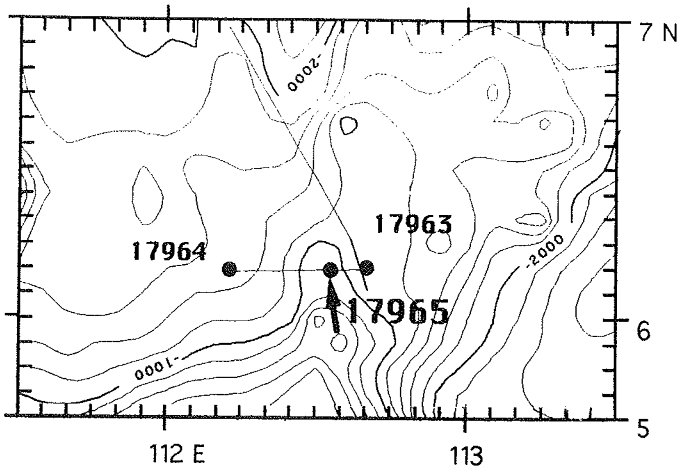

Northern slope of Luconia Shoals

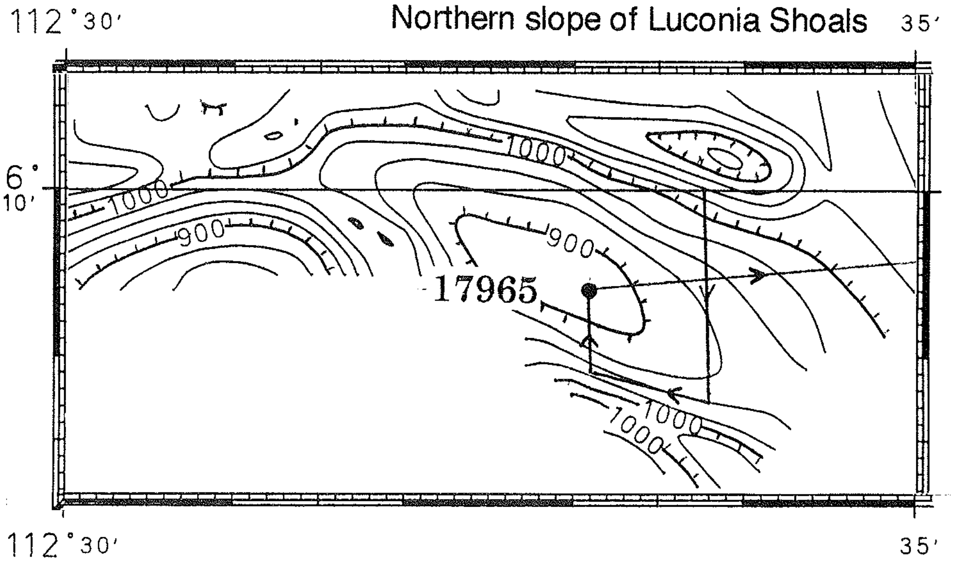

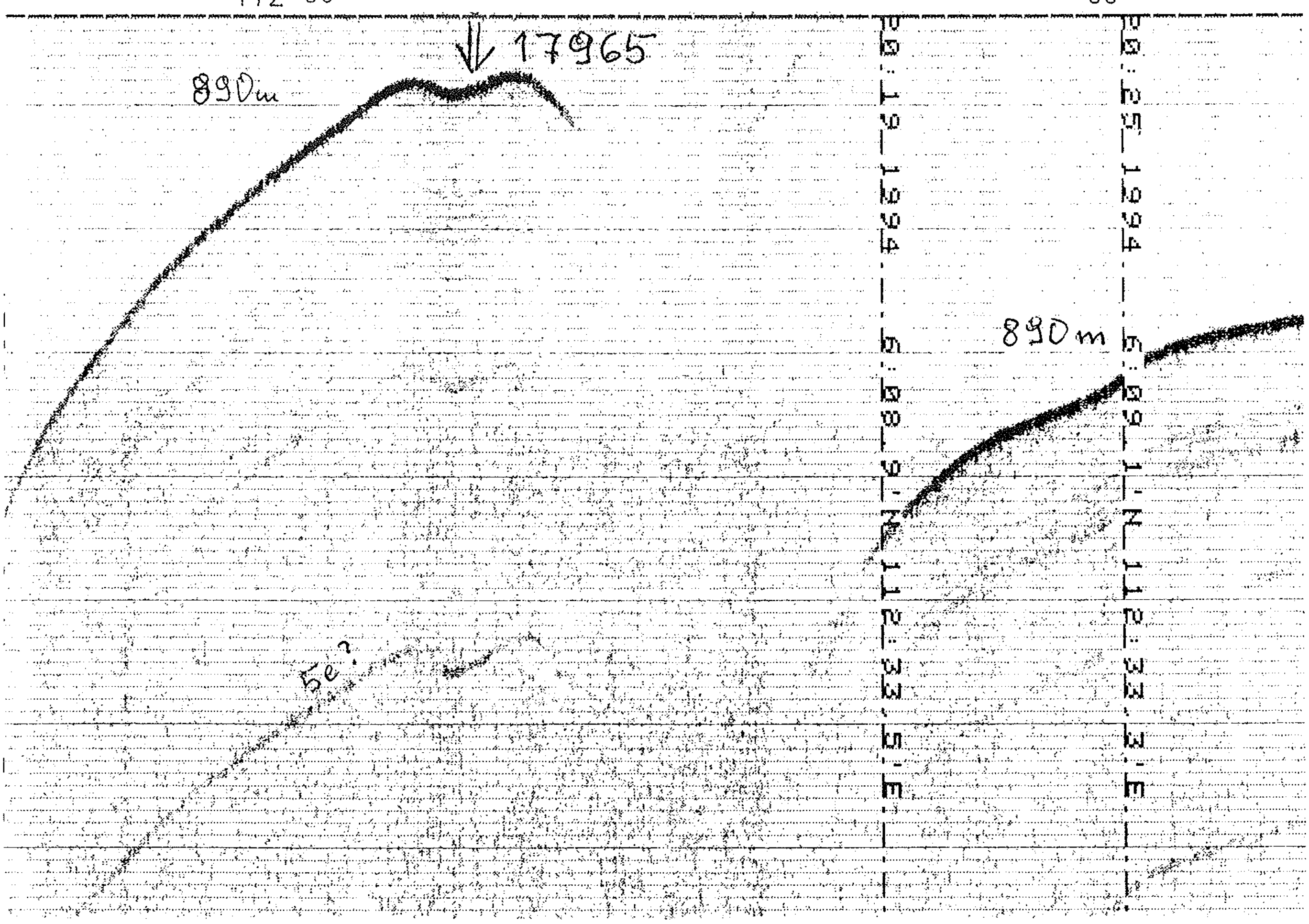

17965-2 06°09.4 N 112°33.1 E, 890 m w.d., core length 6.83 m

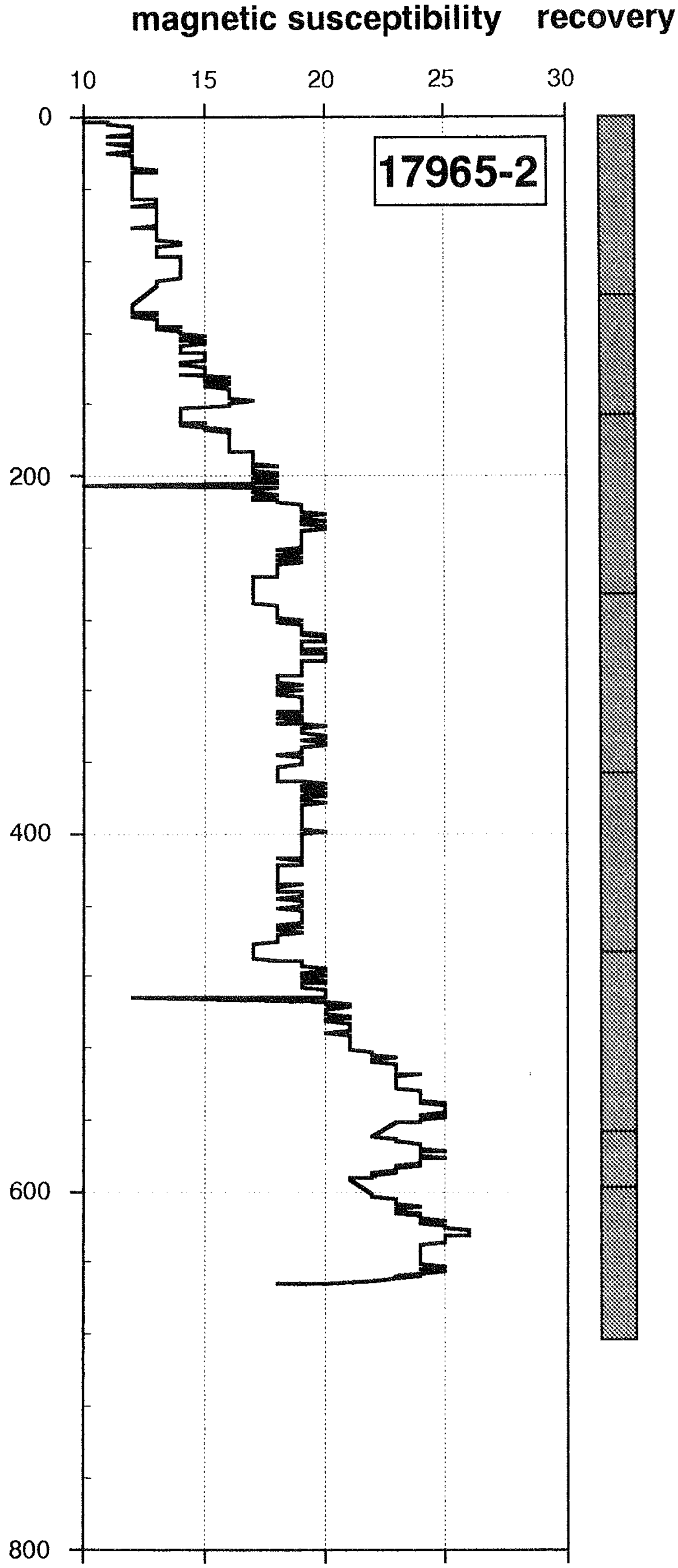

3.6 PRELIMINARY STRATIGRAPHY BASED ON MAGNETIC SUSCEPTIBILITY RECORDS AND $CaCO_3$ CURVES - AGE MODELS AND SEDIMENTATION RATES (SONNE-95 CRUISE)

M. Sarnthein[1], U. Pflaumann[1], Wang, L.J.[1], and Wang, P.X.[2]

[1] GPI Kiel, [2] TJU Shanghai

Introduction

In a number of recent studies, the $CaCO_3$ stratigraphy of the South China Sea was calibrated against oxygen isotope stratigraphy (Miao and Thunell, 1994; Schönfeld and Kudrass, 1993; Wang and Chen M.P.Ph, 1990; Wang, P.X. 199? and Wang P.X. et al., 1994). Accordingly, the key features of many $CaCO_3$ curves from water depths of less than 3500-4100 m are:
(1) $CaCO_3$ concentrations appear higher during warm than during cold stages, hence show an Atlantic-style fluctuation. (2) A number of short-term carbonate spikes are superimposed on this long-term variation, for example, during early termination IA and several times during $\delta^{18}O$ stage 3. (3) Most carbonate is dissolved today below the lysocline at more than 3800-4000 m depth. (4) Based on cores from the southeastern South China Sea Miao and Thunell (1993) concluded that the glacial-to-interglacial variations in $CaCO_3$ percentages largely result from dilution by terrigenous sediment during glacials and dissolution below 3000 m was more intense during interglacial time and reached a minimum during glacial termination I. (5) Schönfeld and Kudrass (1993) suggested that $CaCO_3$ accumulation rates were possibly higher during glacial stages than during the Holocene.

Chen W.B. and Zhou F.G. (1992) published a first rough age assignment of Late Quaternary ash layers based on a comparison with the $\delta^{18}O$ stratigraphy of Winn et al. (1992) (see Wiesner et al., this volume). The long time spans which the authors ascribe to the single ash layers (more than 17,000 years) appear unrealistic and may be a result of low-resolution core sampling. A detailed inspection of their figures, however, reveals that a major single spike of volcanic glass in cores Sonne 50-37 and Sonne 50-37 occurs near the stage 2-3 boundary, earlier spikes in the middle and earlier stage 3, early stage 4, and approximately in stage 5.3.

Based on the published isotope curves and the correlation of ash layers we tried to deduce a stratigraphic model from both the age calibrated high-resolution $CaCO_3$ logging (in some cores supported by grey-code records; Wang L.J., this volume) and the continuous magnetic susceptibility curves. The major excursions of the susceptibility curves we largely interpret as a product of volcanic ash layers. However, there are significant regional differences in volcanic ash supply and the dilution of carbonate records by terrigenous sediment discharge. Hence, we treated separately the para-stratigraphic records from the various core transects across the conti-

nental margins and along the carbonate platforms in the central South China Sea, gradually arriving at a joint correlation model.

Analytical Methods and Data Base

Magnetic susceptibility curves were measured at all cores retrieved at SONNE-95 cruise by methods described by Pflaumann and Chen (this volume). Carbonate values were determined via the carbonate bomb technique (Müller and Gastner, 1971), i.e., by measuring the CO_2 pressure created by HCl or PO_4 dissolution of $CaCO_3$ in a closed "bomb"- style flask. Because of time constraints on board, $CaCO_3$ records were only determined at about 1000 samples from 18 cores (out of a total of 47 cores) which were recovered during the last two thirds of the cruise at GIK stations 17936-17961.

The magnetic-susceptibility and $CaCO_3$ records are compiled in the section on Coring Sites, Core Logs, Initial Coring Descriptions at SONNE-95 Cruise (Pflaumann et al., this volume).

Stratigraphic Classification Scheme

Figure 1 gives an overview of all carbonate curves generated during the SONNE-95 cruise. Bold numbers indicate our tentative correlation of the $CaCO_3$ oscillations to the $\delta^{18}O$ event stratigraphy of Martinson et al. (1987). This correlation is based on published $CaCO_3$ stratigraphies in cores from the South China Sea that are correlated to $\delta^{18}O$ curves (referenced in the Introduction). Table 1 shows the preliminary stratigraphic range and the average sedimentation rates in most cores.

The correlation of the $CaCO_3$ records was facilitated by following features: (1) The values of the Holocene and antecedent warm stages are generally higher than during cold stages 2 and 4. An especially low $CaCO_3$ concentration marks the onset of stage 6. However, this rule of glacial-to interglacial carbonate fluctuations does not apply to some cores from the upper slope off South China, at the northern slope of the Dangerous Grounds carbonate platform, and to deepwater core 17936. (2) Most values of stage 3 are as high as during the Holocene. (3) The triple shaped spike of stage 5 can be recognized in most curves. (4) An outstanding $CaCO_3$ maximum occurs during early termination I, corresponding to about 13,500-14,000 ^{14}C years.

In general, magnetic susceptibility records reflect the ratio of the terrigenous sediment fraction that is enriched in magnetite and titanomagnetite versus the carbonate fraction which is largely free of magnetic minerals (except for some pyrite concretions). Superimposed on this general and long-term trend the susceptibility curves of the South China Sea show a number of narrow, in part extremely large excursions that mostly result from volcanic ash layers. As expected, the frequency and extent of these excursions clearly increases in cores recovered close to the Philippine volcanoes (cores 17922-17928) and in cores with reduced pelagic sedimentation rates near the carbonate platforms of the central South China Sea. Thus no preliminary tephrostratigraphy has been established in these regions.

At the South China continental margin, a simple pattern characterizes the susceptibility curves of cores recovered below about 1300 m water depth (e.g., cores 17933-3 and -4 and 17934-2; Pflaumann et al., this volume). High susceptibility values characterize the top 2-3 m sediment; downsection an about 1 m thick interval with lower values is observed; in a third section further below, magnetic susceptibility rises to a level similar to that of the top section. This third section is marked by a pair of narrow, but prominent spikes, which represent ash layers in the sediment section (Wiesner et al., this volume, and core descriptions in Pflaumann et al., this volume). Based on comparison with the age-calibrated $CaCO_3$ curves, the upper susceptibility spike correlates with the ash layer depicted by Chen and Zhou (1992) near the stage 2-3 boundary. The lower spike fits to the second spike described for the middle-to-early stage 3. A further significant pair of magnetic susceptibility spikes (and ash layers) is resolved in some cores with extremely high sedimentation rates during the early termination I (cores 17932, 17933, 17939, and 17940).

The prominent magnetic susceptibility spike and ash layer near the stage 2-3 boundary was also found at the southern end of the Dangerous Grounds carbonate platform in cores 17961-17963 (Pflaumann et al., this volume). At core site 17962 it was possible to directly correlate the ash layer to the ^{14}C dated stratigraphy of neighbour core V35-5.

Preliminary Distribution Pattern of Bulk Sedimentation Rates

The areal distribution of average sedimentation rates is shown in the transect plot of Fig. 2. The new preliminary estimates enable us to distinguish some major sedimentary provinces in the South China Sea, supplementing previous estimates of Schönfeld and Kudrass (1993). Moreover, the preliminary estimates may help us selecting high priority cores for future studies.

Extremely high hemipelagic sedimentation rates that reach more than 50 cm per 1000 y at 1000-2600 m water depth characterize wide parts of the *central continental slope of South China*. Possibly, these high rates result from a continuous slope parallel sediment supply which may partly originate from an ongoing erosion of hemipelagic sediment immediately east of our core transects. Contour current driven erosion is evidenced in this area by widespread erosional furrows in the PARASOUND records (Sarnthein et al., this volume). - The sedimentation rates are high also south of Hongkong, but less extreme (up to 26 cm/1000 y).

Similarly high sedimentation rates (average rates of 15-32 cm/1000 y; glacial rates of up to 60 cm/1000 y) occur *in front of the Sunda Shelf* ("Sunda tongue"), at the southwestern end of the South China Sea. These high rates of hemipelagic deposition lead to a fast burial of the various reefs near the southern margin of the Dangerous Ground carbonate platform (i.e. the Luconia Shoals), especially during times of glacial sea-level lowstands. Based on our preliminary data, we suggest a strong glacial discharge of clayey sediments from the Sunda peninsula, which may imply strong chemical weathering and humide climate.

In the vicinity of the *carbonate platforms in the central South China Sea,* the pelagic sedimentation rates are medium high, varying from 5.0-8.5 cm/1000 y at 2000-3000 m water depth and mainly originating from carbonate deposition (up to 70 %).

In the *abyssal plains below 4000 m* the sedimentation rates can be hardly assessed because of low $CaCO_3$ concentrations. The rates are probably low and partly result from distal fine-grained turbidites (e.g., core 17953).

REFERENCES

Chen, W.B. and F.G. Zhou (1992): A study of volcanic glass in northern South China Sea during the last 100 ka. - In: Xianglong, J., H.-R. Kudrass, and G. Pautot (eds), Marine Geology and Geophysics of the South China Sea. Proceedings of the Symposium on the Recent Contributions to the Geological History of the South China Sea, 174-178.

Miao, Q., R. Thunell and D.M. Anderson (1994): Glacial-Holocene carbonate dissolution and sea surface temperatures in the South China and Sulu seas. - Paleoceanogr., 9, 269-290.

Müller, G. and M. Gastner (1971): The "Karbonat-Bombe", a simple device for the determination of the carbonate content insediments, soils, and other materials. - N. Jahrb. Miner. Monatsh. 10, 466-469.

Martinson, D.G., N.G. Pisias, J.D. Hays, J. Imbrie, T.C. Moore, N.J., Shackleton (1987): Age dating and the orbital theory of the ice ages: development of a high resolution 0 to 300,000-years chronostratigraphy, Quat. Res., 27, 1-29.

Schönfeld, J. and H.-R. Kudrass (1993): Hemipelagic sediment accumulation rates in the South China Sea related to late Quaternary sea level changes. - Quat. Res., 40, 368-379.

Wang, P.X. (1991): West Pacific marginal seas in last glaciation: Paleocean ography and its environmental impact. - In: Proc. Sci. Seminar WESTPAC/IOC, Panang Malaysia, Dec. 1991.

Wang, P.-X., L.-J. Wang and Z.-M. Jian (1994): Late Quaternary Paleoceanography of the South China Sea: Surface circulation and carbonate cycles. - Mar. Geol., in press.

Winn, K., L. Zheng, H. Erlenkeuser, and P. Stoffers (1992): Oxygen/carbon isotopes and paleoproductivity in the South China Sea during the past 110,000 Years. - In: Xianglong, J., Kudrass, H. R. and Pautot, G. (eds), Marine Geology and Geophysics of the South China Sea. Proceedings of the Symposium on the Recent Contributions to the Geological History of the South China Sea, 154-166.

Table 1. Preliminary stratigraphic ranges and average sedimentation rates estimated for sediment cores of SONNE-95 cruise.

Core no.	Stratigr. Range $\delta^{18}O$ Event	Average Sedim. Rate (cm/kyr)	Evidence (analogies based on magnetic susc. curves)
17922-2	(?)	4.5 ?	ash layers
17924-2/-3	(?)	(?)	
17925-3	(?)	(?)	
17926-3	(?)	(?)	
17927-2	(?)	(?)	
17928-3	(?)	(?)	
17930-2	(?)	(?)	
17931-2	(?)	(?)	
17932-2	2.2 (20 ky)	50.0	ash layers, per analogy
17933-3/-4	5.3	22.7	grey code, per analogy with $CaCO_3$ curves
17934-2	5.1	18.0	ash layers, per analogy
17935-3	4.2	18.5	ash layers, per analogy
17936-2	4.4	18.5	grey code, $CaCO_3$ curve
17937-2	5.1	24.0	grey code, $CaCO_3$ curve, and ash layers
17938-2	4.4 ?	13.5 ?	ash layers, per analogy
17939-2	3.1	41.1	$CaCO_3$ curve, ash layers planktonic foraminifera
17940-2	2.2	55.5	$CaCO_3$ curve, ash layers planktonic foraminifera
17941-2	6.2/6.4 ?	6.0 ?	$CaCO_3$ curve, ash layers
17943-2	3.2	26.5 (to st. 3.1)	$CaCO_3$ curve
17944-2	??	??	
17945-2/-3	7.4	8.8	$CaCO_3$ curve, triple peak of $\delta^{18}O$ stage 5
17946-2	5.5 ?	8.8	ash layers, per analogy
17948-2	8.4	5.0	$CaCO_3$ curve, per analogy
17949-2	8.5	5.0	$CaCO_3$ curve, per analogy
17950-2	6.6/7.1 ?	6.4	$CaCO_3$ curve, per analogy
17951-2	7.3/7.4 ?	4.75	per analogy
17952-2	7.4	6.0 4.75 (without turbidites)	$CaCO_3$ curve, per analogy
17953-4	15 ?/16 ?	2.0 ?	per analogy extrapolations
17954-2/-3	7.4	6.4	$CaCO_3$ curve, per analogy
17955-2	7.3/7.4	6.25	$CaCO_3$ curve, per analogy
17956-2	7.3/7.4	6.5	$CaCO_3$ curve, ash layers
17957-2	10.4	4.5	$CaCO_3$ curve, ash layers
17958-2	5.5 ?	8.5 ?	per analogy, ash layers
17959-2	7.1/7.3 ?	6.5 ?	per analogy, ash layers
17961-2	3.2 (about 33 ky)	32.0, up to 60.0	$CaCO_3$ curve, ash layer
17962-2/-3/-4	5.3	15.0	per analogy with ^{14}C dated c. V 35-5, ash layer near st. 3.1
17963-3	3.2 (about 40 ky)	20.0	ash layer near st. 3.1, per analogy
17964-2/-3	4.4	20.5	per analogy
17965-2	3.2 (>40 ky)	15.0	per analogy

Figure 1. $CaCO_3$ values measured at SONNE-95 cruise. Numbers show tentative correlations to the $\delta^{18}O$ event stratigraphy of Martinson et al. (1987) and termination IA. Solid arrows show pair of ash layers near stage 2/3 boundary and further below in stage 3. Asterisks mark pair of ash layers at Termination IA.

Figure 2. Preliminary estimates of average sedimention rates of cores recovered at SONNE-95 cruise (see Table 1). Prominent sedimentary provinces are enveloped.

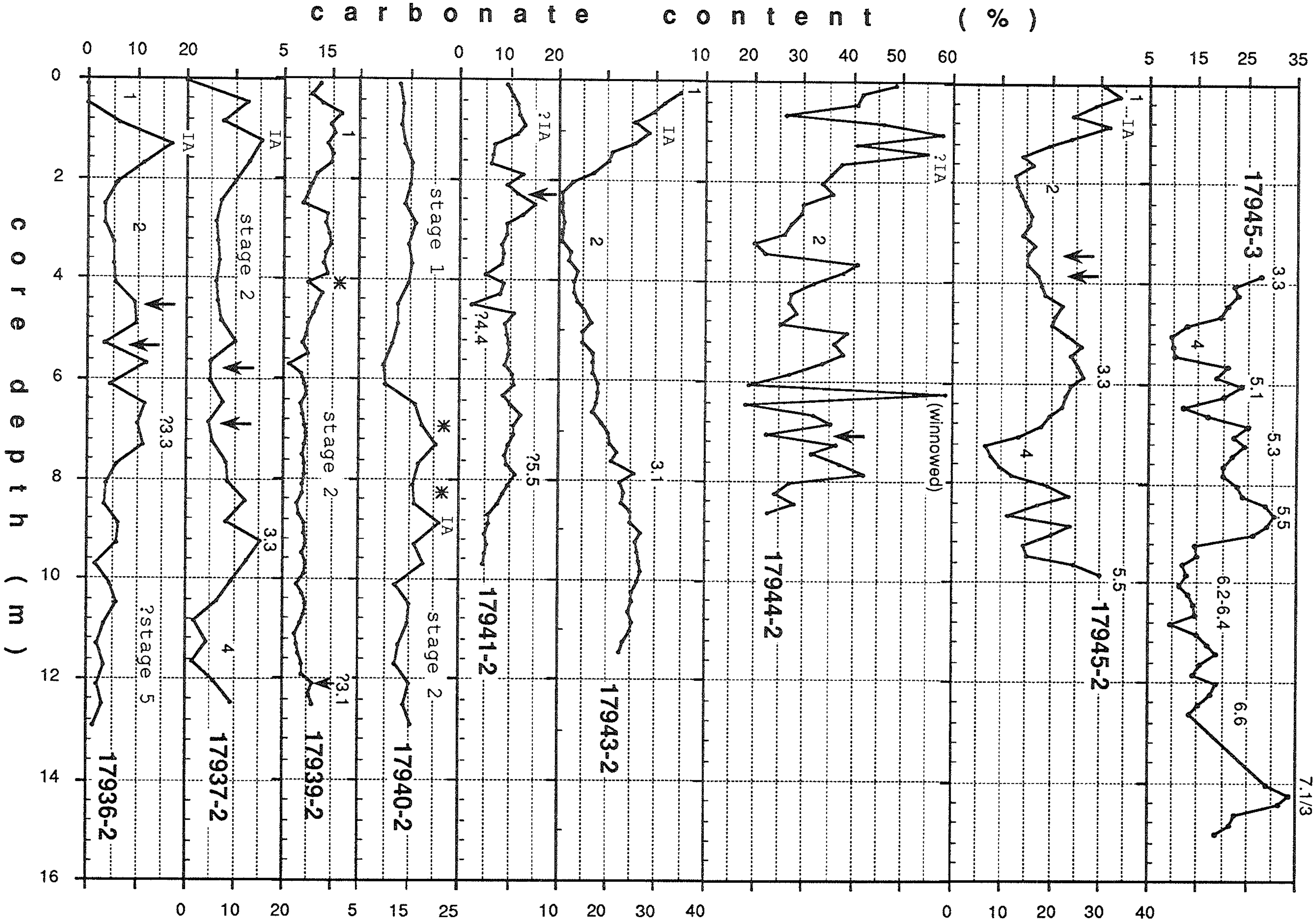

Figure 1. $CaCO_3$ values measured at SONNE-95 cruise. Numbers show tentative correlations to the $\delta^{18}O$ event stratigraphy of Martinson et al. (1987) and termination IA. Solid arrows show pair of ash layers near stage 2/3 boundary and further below in stage 3. Asterisks mark pair of ash layers at Termination IA.

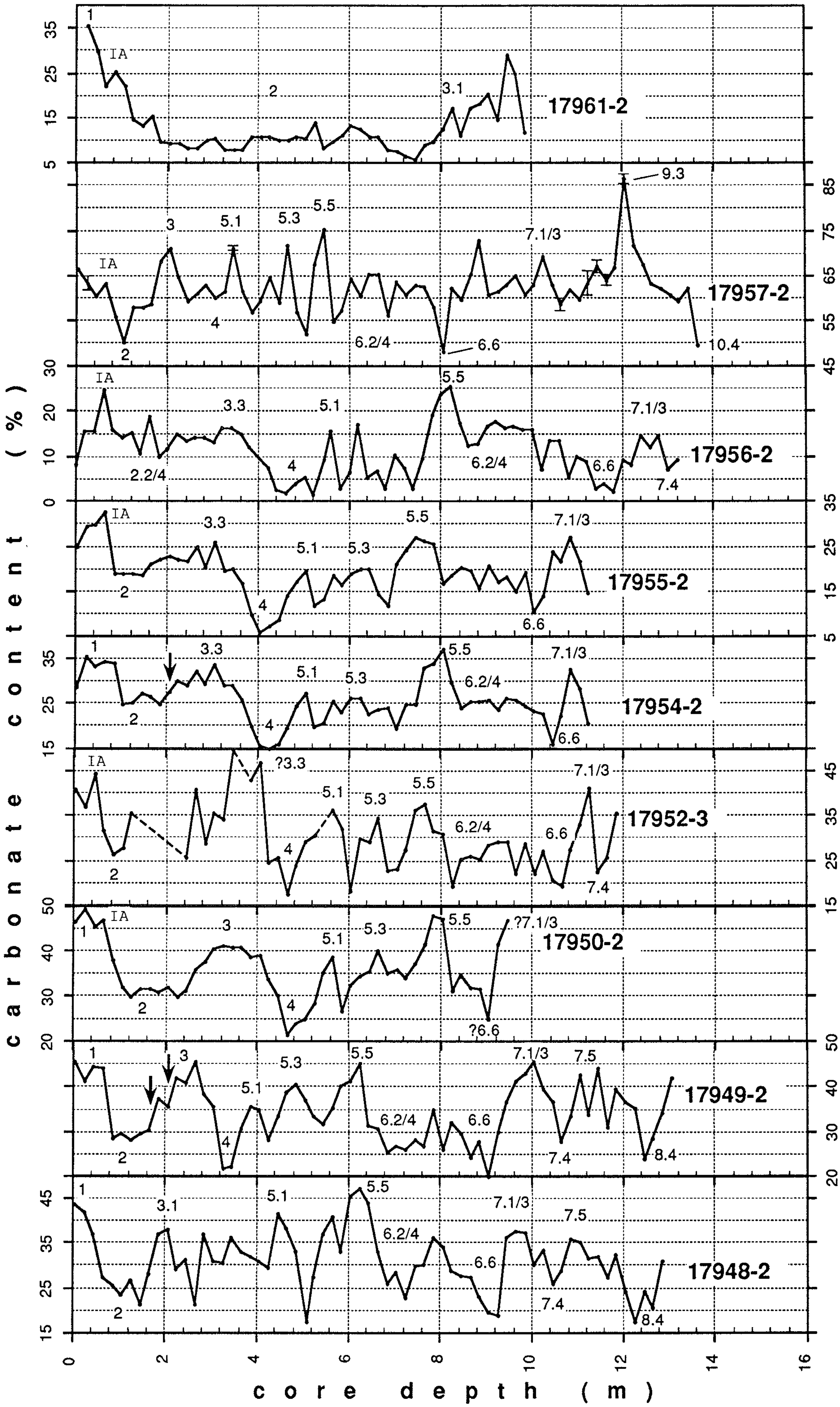

Figure 1. Continued

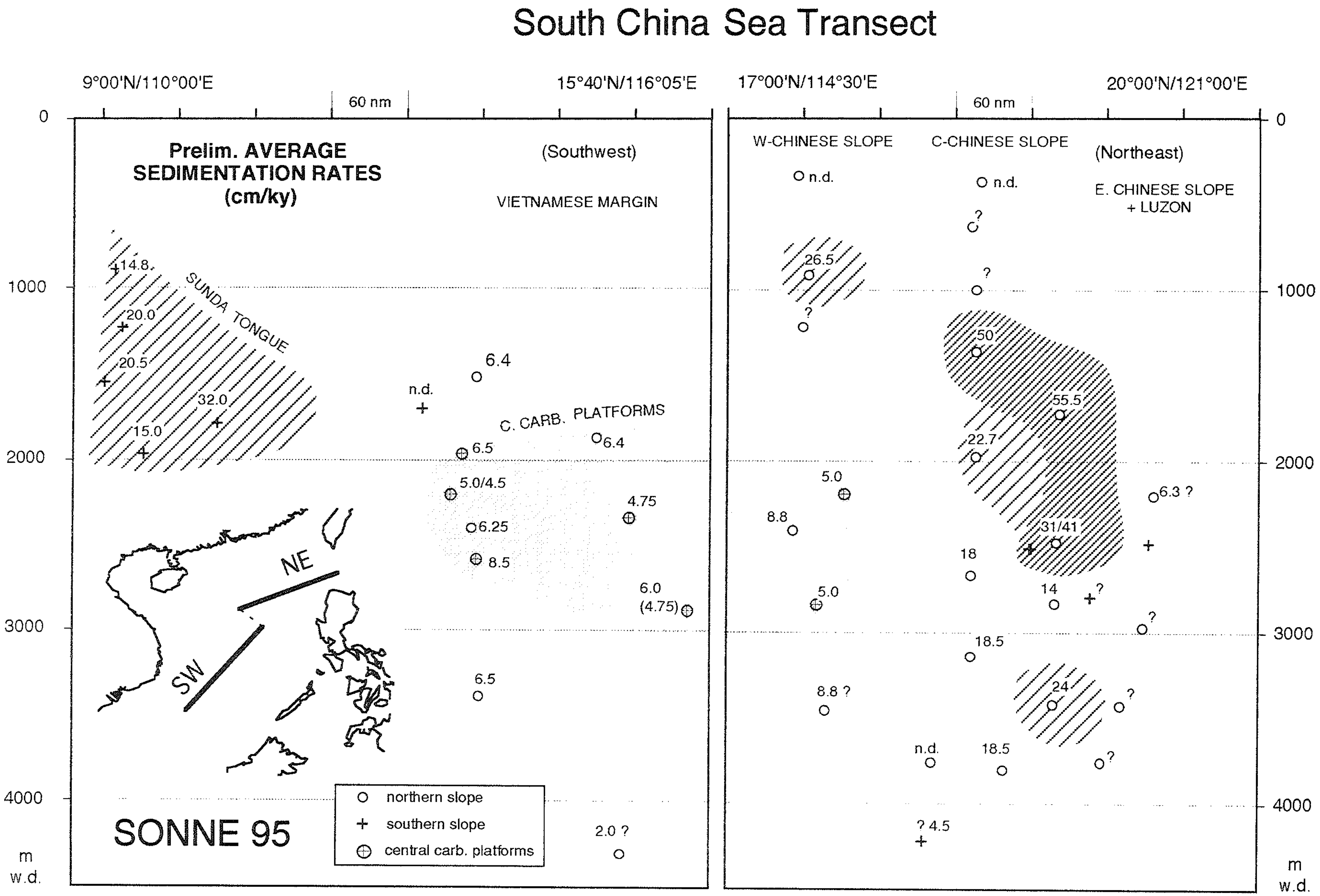

Figure 2. Preliminary estimates of average sedimention rates of cores recovered at SONNE-95 cruise (see Table 1). Prominent sedimentary provinces are enveloped.

3.7 COMPOSITE - DEPTH SECTIONS OF CORES RECOVERED ON SONNE-95 CRUISE

M. Sarnthein and L.J. Wang (University of Kiel)

At a number of stations (GIK no. 17924, 17931, 17933, 17945, 17954, 17962, 17964) both gravity and piston cores were recovered. Gravity cores were retrieved because they generally contain a fairly undisturbed record of the top 3-6 m sediment profile, whereas piston cores show distortions and losses within the top 4-6 m sediment, but recover a significantly longer sediment section, with the deeper parts of the profile better preserved than in gravity cores (see Mühlhan et al., this volume). Thus *composite sections of gravity and piston cores* are most promising for the reconstruction of long sedimentary records, once the core depths of the different profiles are properly adjusted. Gravity cores also have a (minor) sediment loss near the core top, which can be precisely estimated by composite-depth sections including the records from the undisturbed sediment surface in box-cores. The correlation to box core depths, however, was not finished during SONNE-95 cruise.

Figs. 1-7 show the adjustment of core depths in different gravity and piston core profiles by comparison of prominent oscillation features in both continuous magnetic-susceptibility logs and high-resolution $CaCO_3$ curves. The stratigraphic switch points between nominal and composite-depth sections and the total lengths of the composite-depth sections are compiled in Table 1. The greatest core length recovered as composite-depth section amounts to 23.14 m (cores 17933-3/4).

Table 1. Composite-depth sections based on a correlation of features in magnetic susceptibility logs and $CaCO_3$ curves of SONNE-95 cores.

CORE NO.	Nominal Depth at Switchpoint Gravity Core (cm bsf)	Piston Core (cm bsf)	Difference (cm bsf)	Comp. Depth (cm bsf)	Total Length of Comp.-Depth Section (cm bsf)
17924-2	981.0	--		981.0	
17924-3	--	773.5	(Δ207.5)	981.0	2196.5
17931-2	(no precise switchpoints identified)				
17931-3					
17933-3	831.0	--		831.0	
17933-4	--	491.5	(Δ339.5)	831.0	2314.5
17945-2	792.5	--		792.5	
17945-3	--	547.5	(Δ245.0)	792.5	1813.0
17954-2	1058.0	--		1058.0	1152.0
17954-3	1048.0	--	(Δ 10.0)	1058.0	
17962-2	386.5	--		386.5	
17962-3	386.5	--		386.5	
17962-4	--	245.0	(Δ141.5)	386.5	1621.5
17964-2	--	613.0	(Δ153.5)	766.5	1457.5
17964-3	766.5	--		766.5	

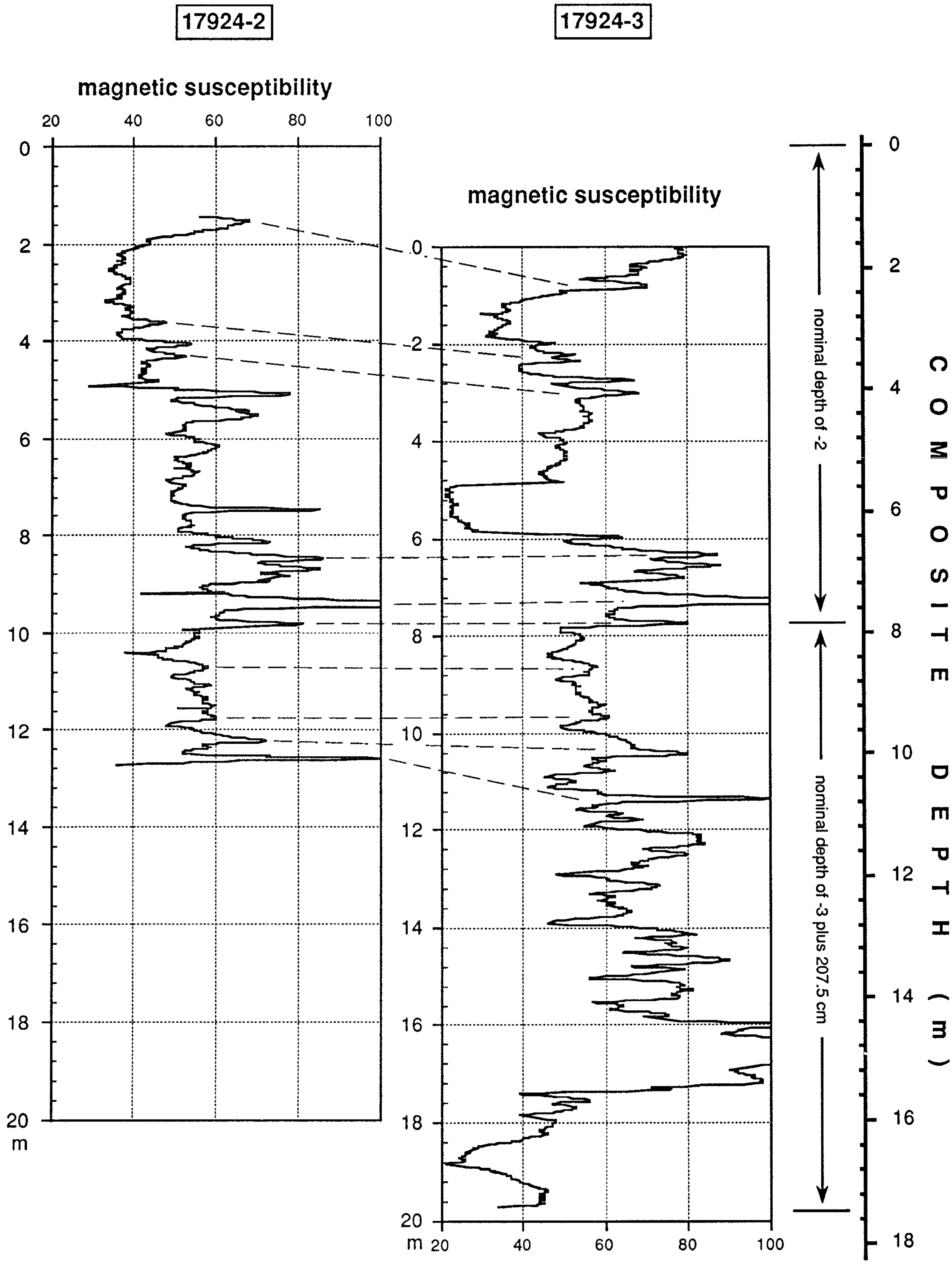

Figure 1. Comparison of prominent oscillation features in continuous magnetic-susceptibility logs of cores 17924-2 (gravity core) and -3 (piston core). Depth of switchpoint (981.0 cm) between nominal and composite depth scales (cm below sea floor) is given in Table 1.

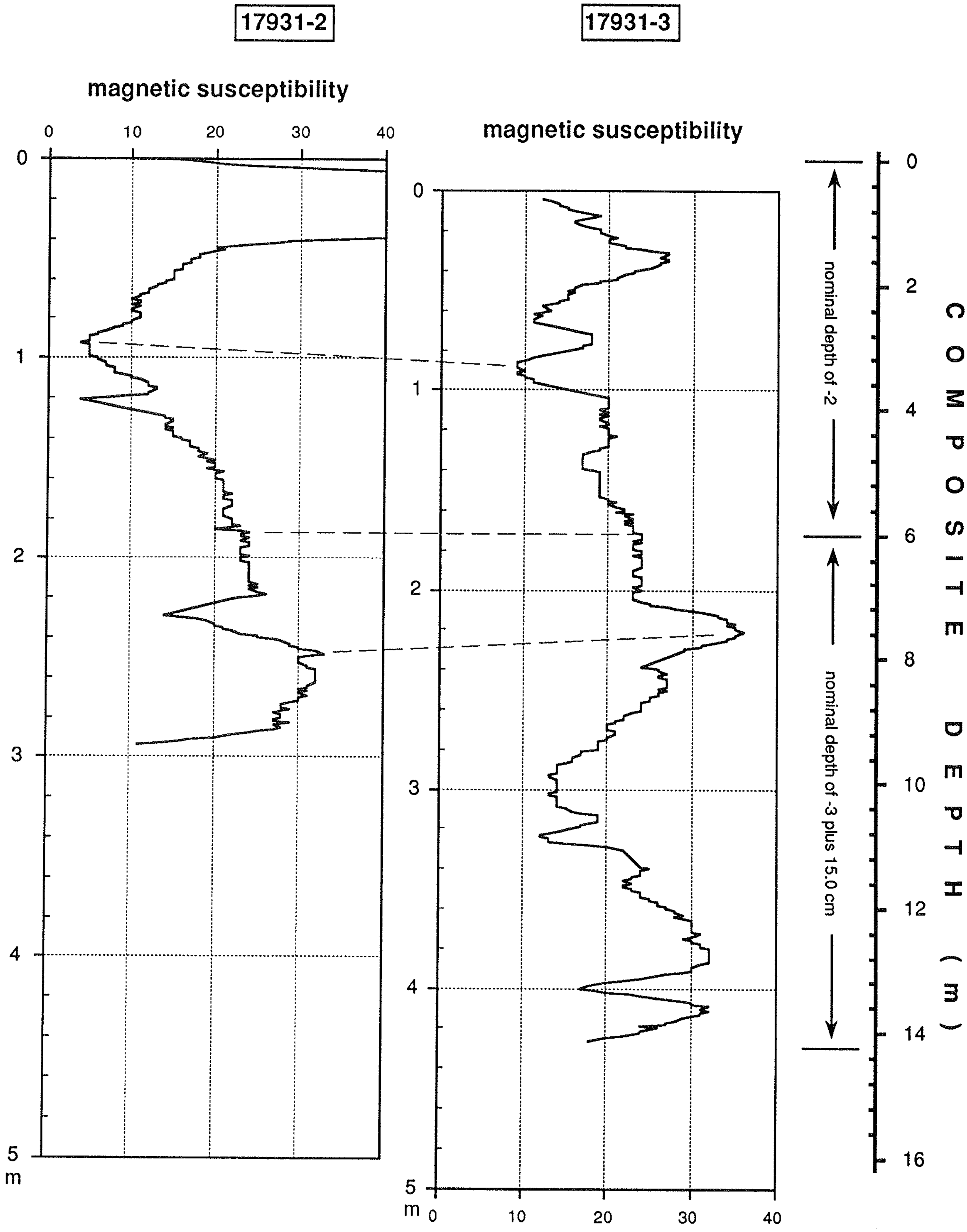

Figure 2. Comparison of prominent oscillation features in continuous magnetic-susceptibility logs of gravity cores 17931-2 and -3. Depth of switchpoint between nominal and composite depth scales (cm below sea floor) is given in Table 1.

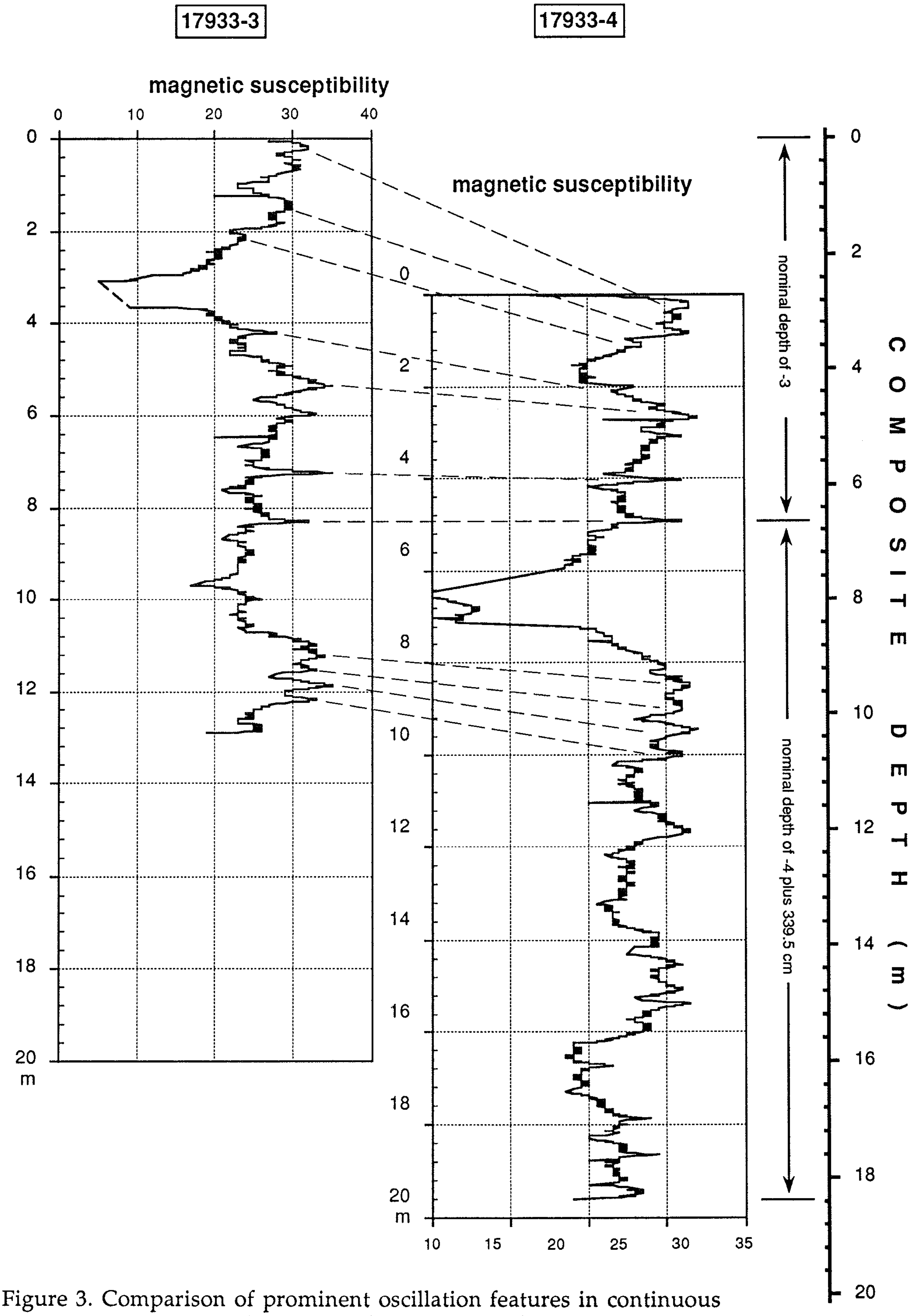

Figure 3. Comparison of prominent oscillation features in continuous magnetic-susceptibility logs of cores 17933-3 (gravity core) and -4 (piston core). Depth of switchpoint (831.0 cm) between nominal and composite depth scales (cm below sea floor) is given in Table 1.

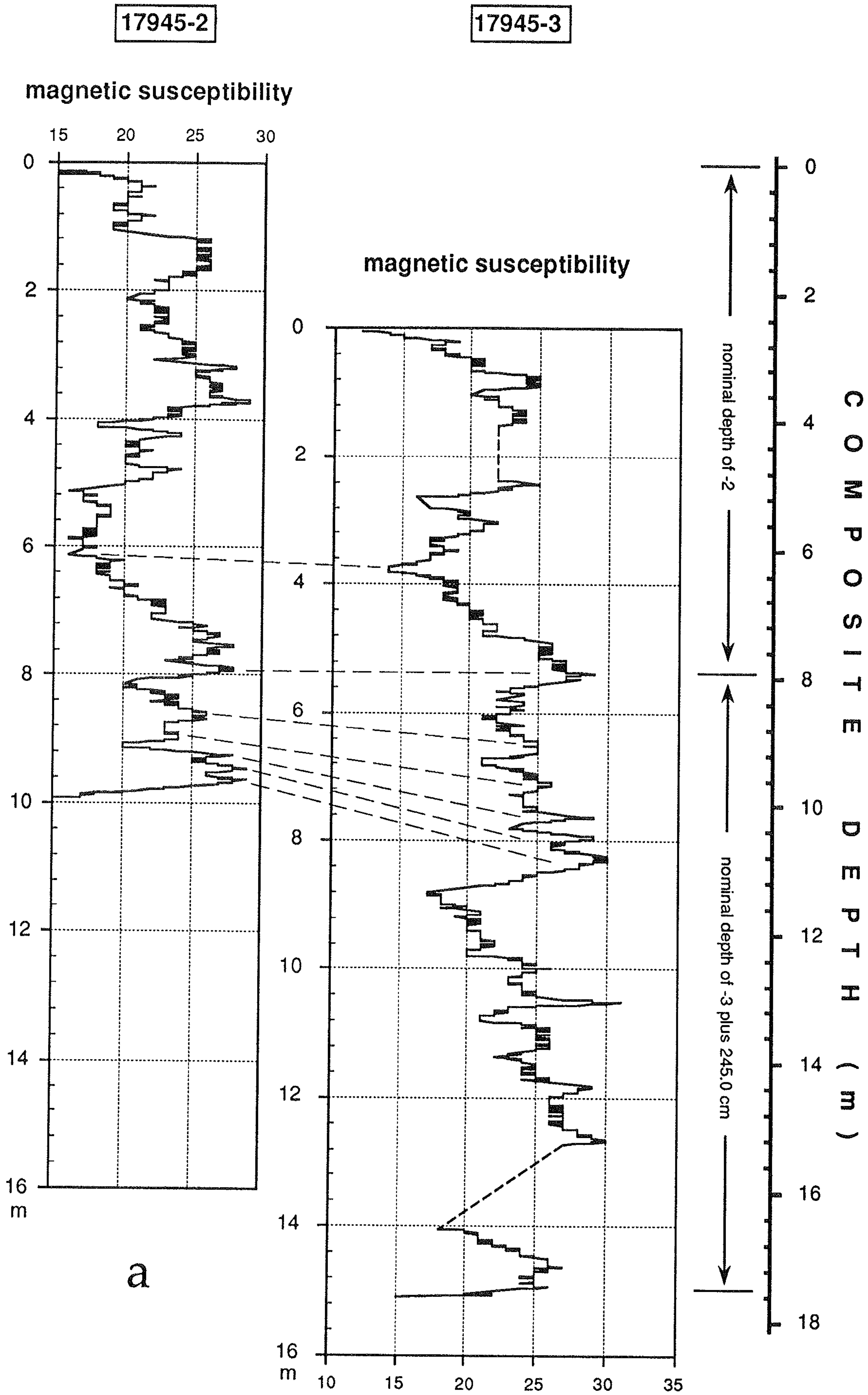

Figure 4. Comparison of prominent oscillation features in both continuous magnetic-susceptibility logs (a) and high-resolution $CaCO_3$ curves (b) of cores 17945-2 (gravity core) and -3 (piston core). Depth of switch-point (792.5 cm) between nominal and composite depth scales (cm below sea floor) is given in Table 1.

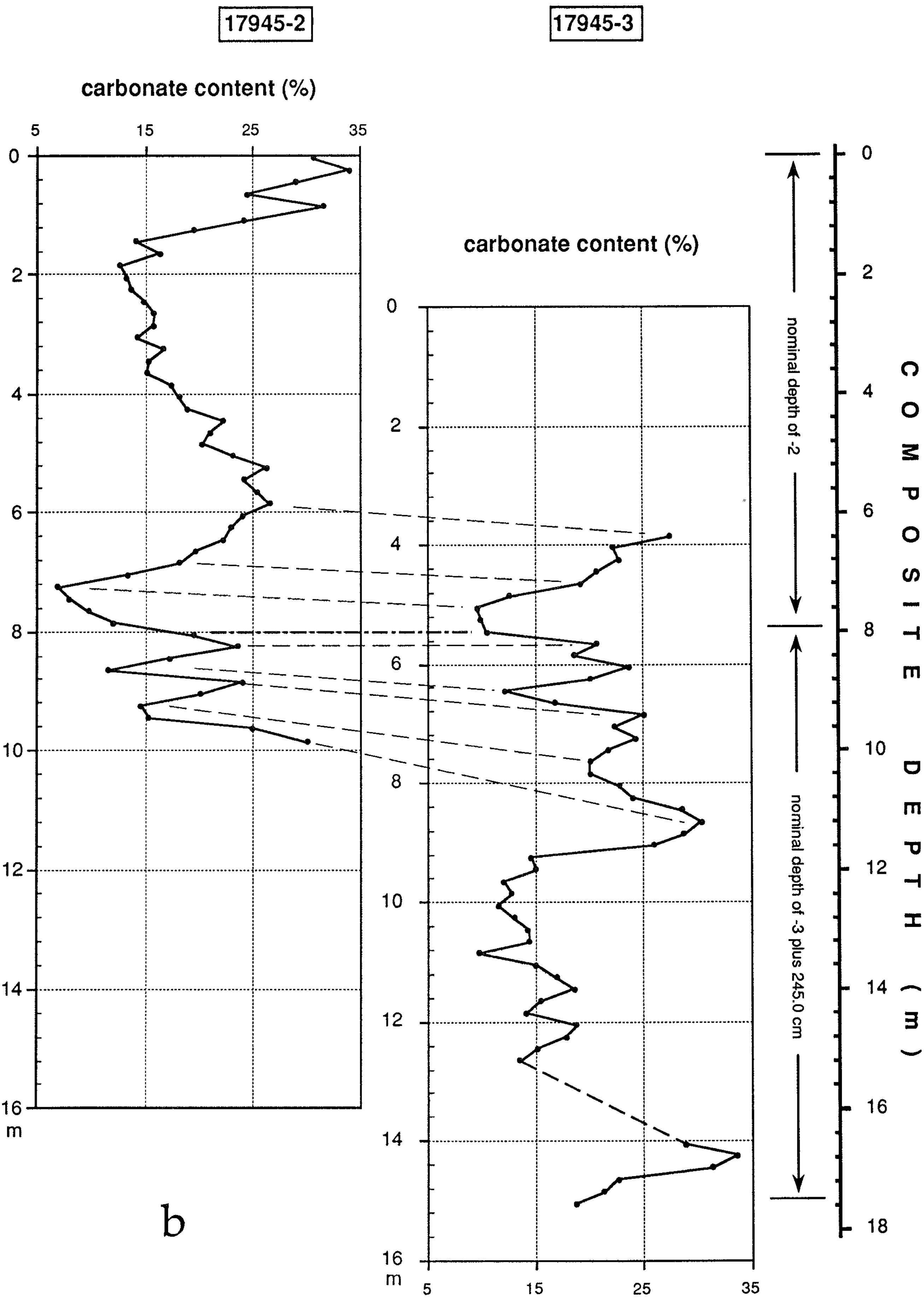

17945-2
17945-3
carbonate content (%)
5
15
25
35
0
2
4
6
8
10
12
14
16
m
nominal depth of -2
nominal depth of -3 plus 245.0 cm
COMPOSITE DEPTH (m)
18

b

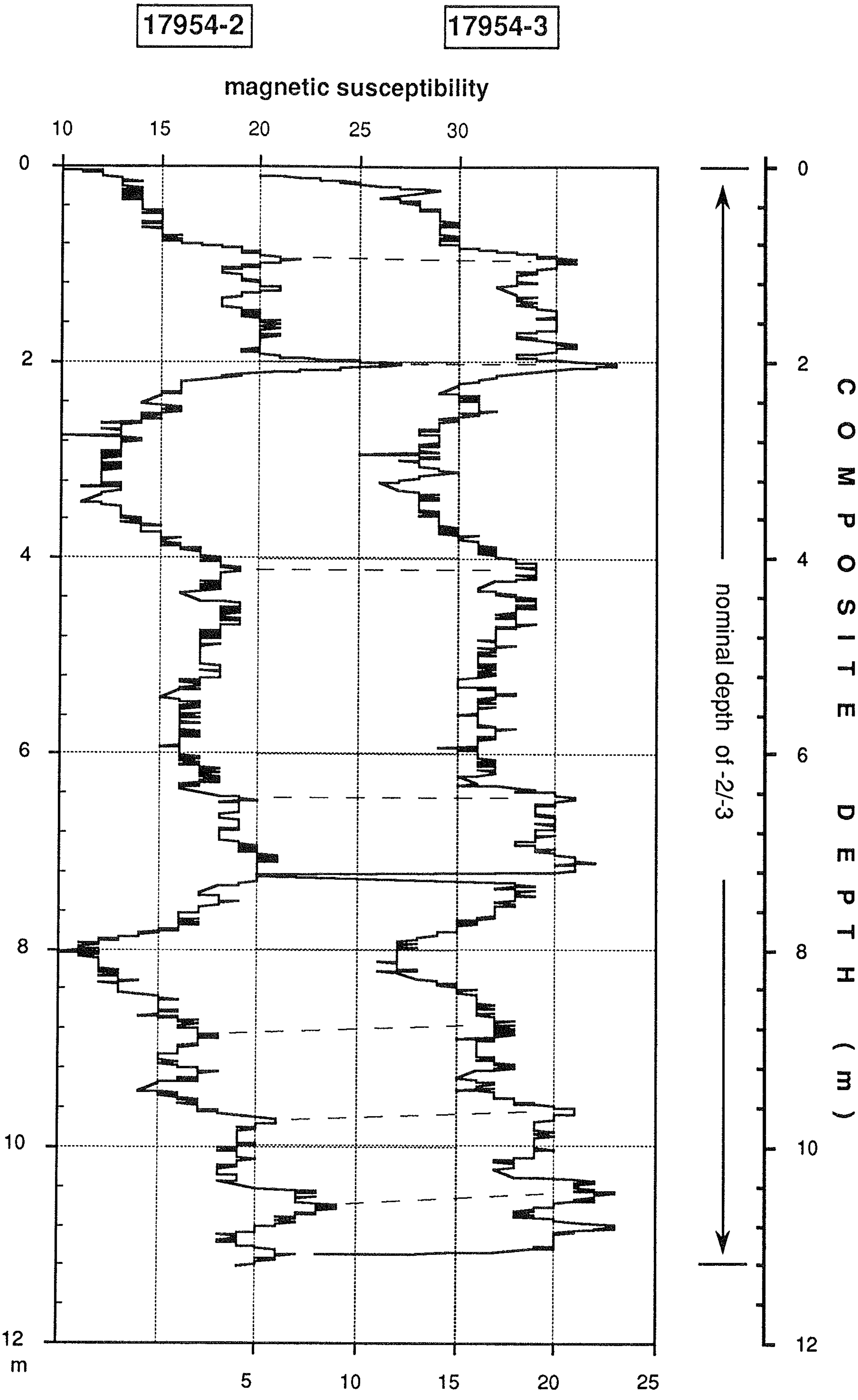

Figure 5. Comparison of prominent oscillation features in continuous magnetic-susceptibility logs of gravity cores 17954-2 and -3. Depth of switchpoint (1058.0 cm) between nominal and composite depth scales (cm below sea floor) is given in Table 1.

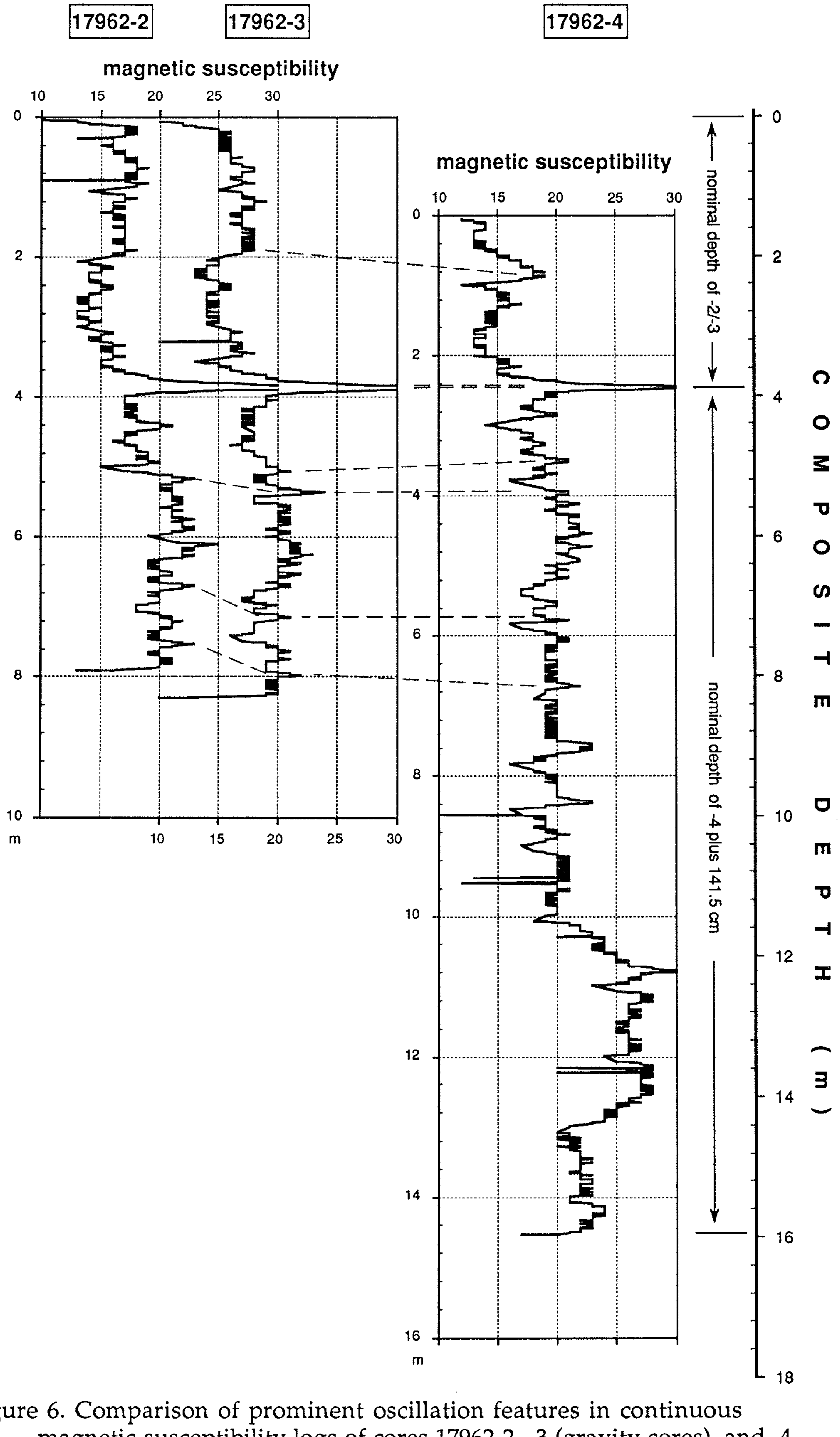

Figure 6. Comparison of prominent oscillation features in continuous magnetic-susceptibility logs of cores 17962-2, -3 (gravity cores), and -4 (piston core). Depth of switchpoint (386.5 cm) between nominal and composite depth scales (cm below sea floor) is given in Table 1.

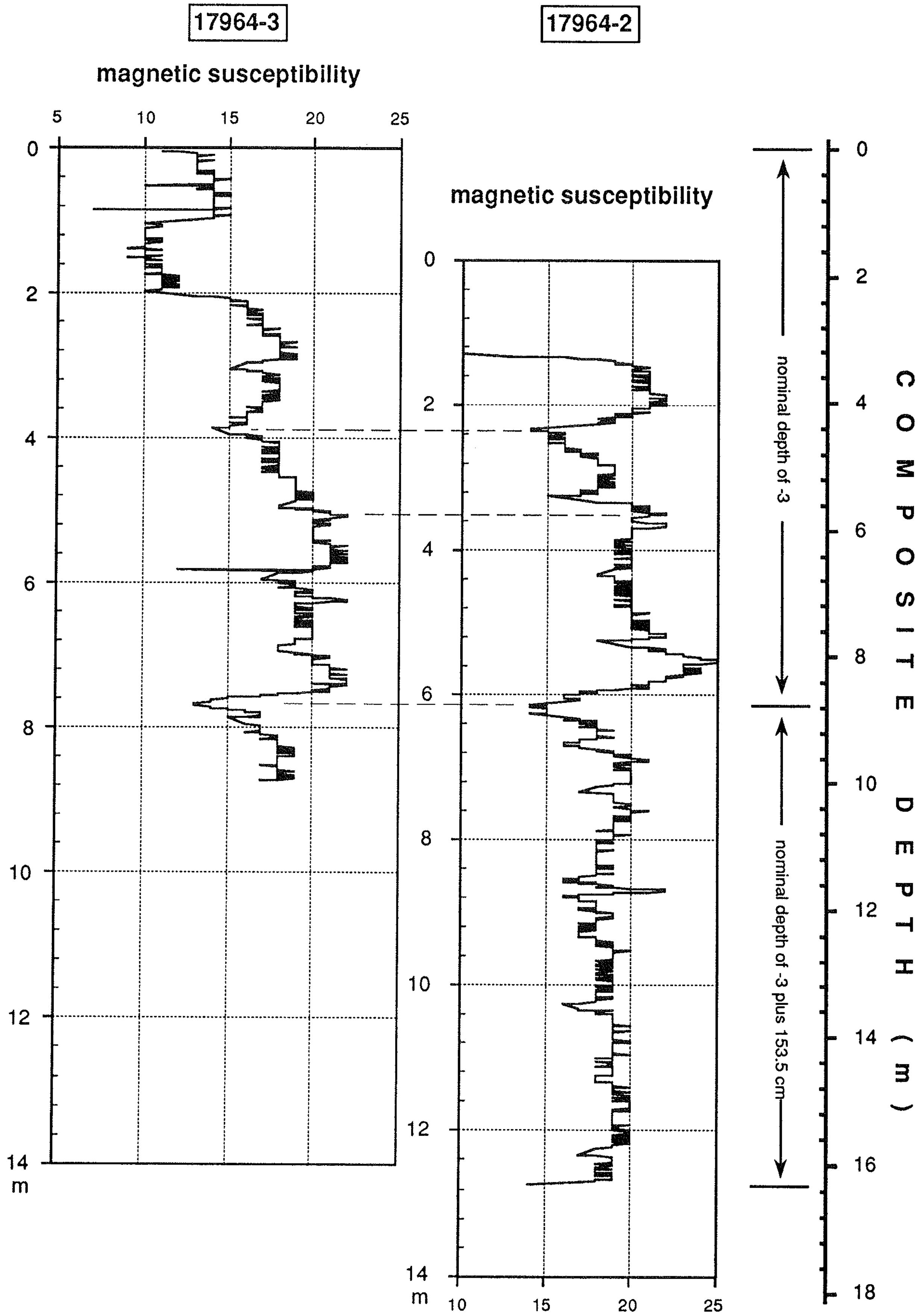

Figure 7. Comparison of prominent oscillation features in continuous magnetic-susceptibility logs of cores 17964-2 (piston core) and -3 (gravity core). Depth of switchpoint (766.5 cm) between nominal and composite depth scales (cm below sea floor) is given in Table 1.

3.8 CTD PROFILES AND BOTTOM WATER TEMPERATURES IN THE SOUTH CHINA SEA (SONNE-95 CRUISE)

B. Haupt[1], M.G. Wiesner[2] and M. Sarnthein[1]

[1]Geological-Paleontological Institute, University of Kiel; [2]Institute of Biogeochemistry and Marine Chemistry, University of Hamburg.

INTRODUCTION

The values and variations of temperature, salinity and density of the water in the South China Sea are affected primarily at the surface by the monsoons and at depth by bottom topography. In general, the surface temperature decreases northward. It is coldest in January and February, when the circulation induced by the winter monsoon drives the cold waters of the north southward, and warmest in August, when the current pattern is reversed and solar heating is at a maximum (LaViolette and Frontenac 1967).

The surface salinity increases from south to north. It is less than 34 ppt over much of the sea, owing to the heavy monsoonal precipitation and river outflow. Seasonally, surface salinity varies between a maximum during the NE monsoon and a minimum during the SW monsoon. During the NE monsoon, a branch of the Pacific North Equatorial Current is forced into the South China Sea and raises the values of surface salinity in the north. This saline surface water spills over the sill of Luzon Strait and, being constantly modified, spreads over the central South China Sea as far west as Vietnam (LaFond 1966). With the reversal in the circulation associated with the SW monsoon, rain-diluted local waters replace the more saline Pacific water over most of the sea. The subsurface layer of Pacific water that hurdles the peripheral sill is well defined as a tongue of higher salinity between 100 and 200 m water depth; in the deep portions of the sea, the water below the sill is generally isothermal and isohaline in space and time (LaViolette and Frontenac 1967).

MATERIALS AND METHODS

The Kiel conductivity-temperature-depth (CTD) rosette system used (KMS II) is a multiparameter probe for fast hydrographic measurements in water depths up to 6000 m. The system is equipped with C, T and D- sensors plus two sensors to measure oxygen, light attenuation and sound velocity. The raw data are transmitted from the *in-situ* unit to the board unit. The latter consists of an ME-Interface powering the probe and translating the data into a IBM PC-readable format. The physical values and derived parameters such as salinity, density and oxygen are calculated via generally used standard formulas (UNESCO formulas, DIN tables for oxygen).The accuracies of the various sensors are ±0.005 mS cm^{-1} for conductivity, ±0.005

°C for temperature, ±0.1 %fs for pressure, ±1 % for oxygen, ±0.5 % for light attenuation and ±0.2 m s^{-1} for sound velocity.

The CTD-system is fitted with 12 water samplers. The water samples were analysed on board for Ph, conductivity and oxygen (Winkler method). Nutrient analyses (nitrate, nitrite phosphate and silicate) will be carried out in Hamburg, carbon isotope analyses in Kiel. Moreover subsurface sediment temperatures were measured in box cores by an AMA-digit AD 30 TH thermometer with a 0.1° precision (Kuhnt et al., this vol.). These temperature values correspond to the potential bottom water temperature and are generally consistent with the CTD-values.

PRELIMINARY RESULTS

During leg 1, 2 and 3 of cruise SO-95, CTD-measurements were carried out at five stations (Figs. 1, 2, 3, 4 and 5). The temperature and salinity profiles of all stations were very similar. Temperature decreases continuously from the surface waters down to about 1500 m from around 30 °C to values between 2 and 3 °C. Below 1500 m water depth, temperatures remain constant. The great uniformity of bottom water temperature is underlined by the temperature values of the box core sediments plotted in Figure 1 as transect from the Sunda Shelf up to Taiwan. Slight deviations towards higher temperatures are recognized west of Luzon Island, possibly a result of insufficient measuring precision.

Salinity increases down to 175 m water depth from about 34.0 to 34.7 ppt. reflecting the wedge of Pacific water. Between 175 and 1500 m values are lower with a pronounced minimum at about 400 m (34.5 ppt). Below 1500 m the water masses are isohaline (34.7 ppt).

Contradictory results were obtained for oxygen and light attenuation as down-column and up-column profiles were completely different (cf. Fig 1, 17953-5 and 17953-5up). Because of the slow sensor adjustment the upward profiles may come closer to reality. Problems with the oxygen sensor are also indicated by the mismatch of the oxygen data obtained from chemical (duplicate) analyses and the CTD-oxygen curves which was particularly evident in the upper water column (< 1000 m). According to the former data set the oxygen minimum lies between 400 and 1300 m with values ranging from 1.7 to 1.9 mg O_2 / l H_2O.

AREAL DISTRIBUTION OF BOTTOM WATER TEMPERATURES

Further information on regional oceanography was obtained from measuring the temperature 5 cm below the sediment surface of box cores (see sections of Kuhnt et al., this volume). The sediment temperatures from all stations (equating to potential deepwater temperatures) are compiled in an oceanographic transect running southwest-northeast across the South

China Sea (Fig. 6) and form a reference base for interpreting benthic oxygen isotope values. Below 2000 m water depth, bottom water temperatures are 2.3-2.5°C and show a striking uniformity. Further above, the temperatures rise to about 5°C near 1000 m depth and 12°C near 350 m depth. Slight areal differences occur between data from the northern and southeastern slopes, with little higher bottom-water temperatures in the southeast, near Luzon.

REFERENCES

LaFond, E.C. (1966): South China Sea. In: The Encyclopedia of Oceanography. (Reinhold Publ., New York), 829-836. .

LaViolette P.E. and Frontenac T.R. (1967): Temperature, Salinity and Density of the World's Seas: South China Sea and adjacent Gulfs. - Informal Manuscript No. 67-5 (U.S. Naval Oceanographic Office, Washington D.C.), 134 pp.

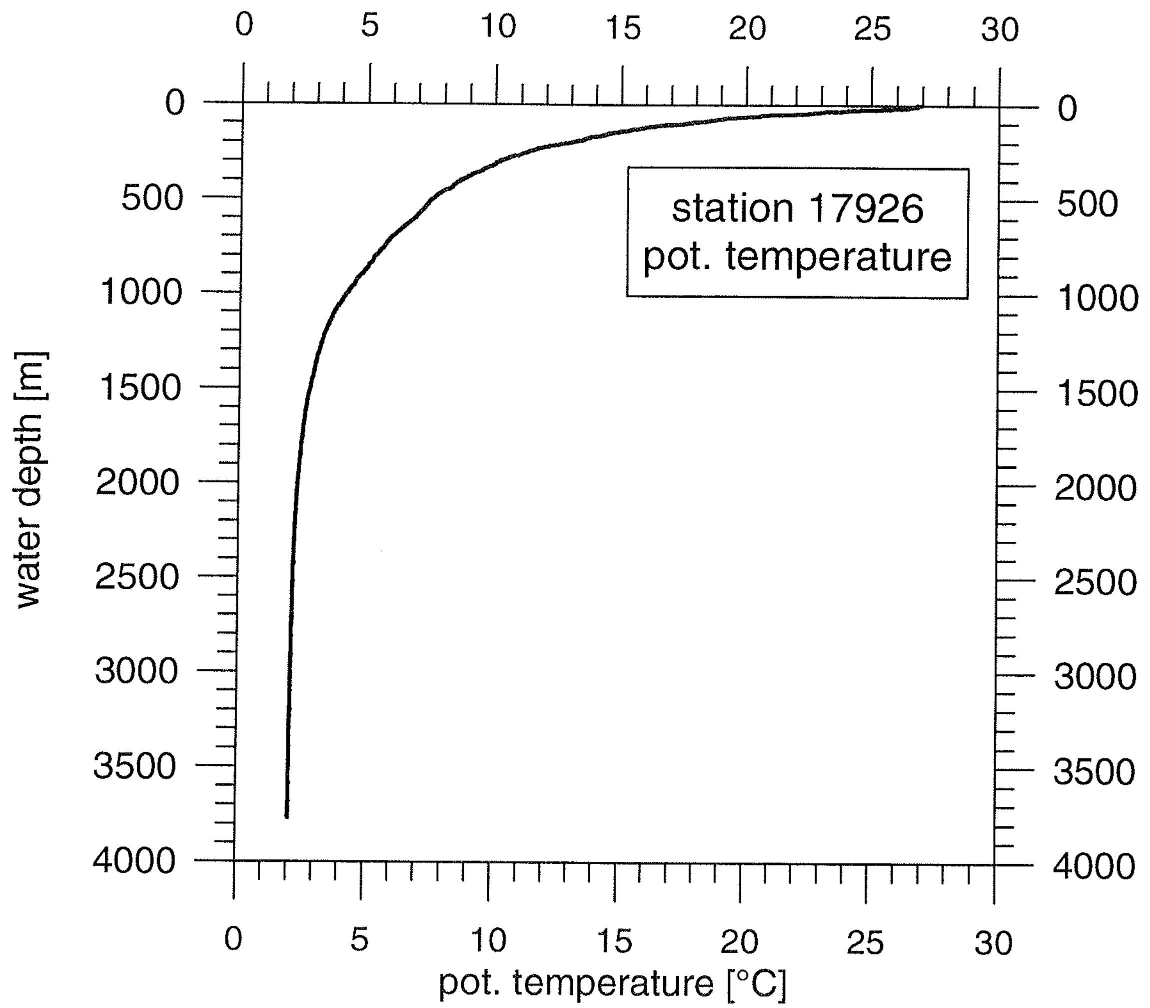

station 17926
pot. temperature
water depth [m]
pot. temperature [°C]

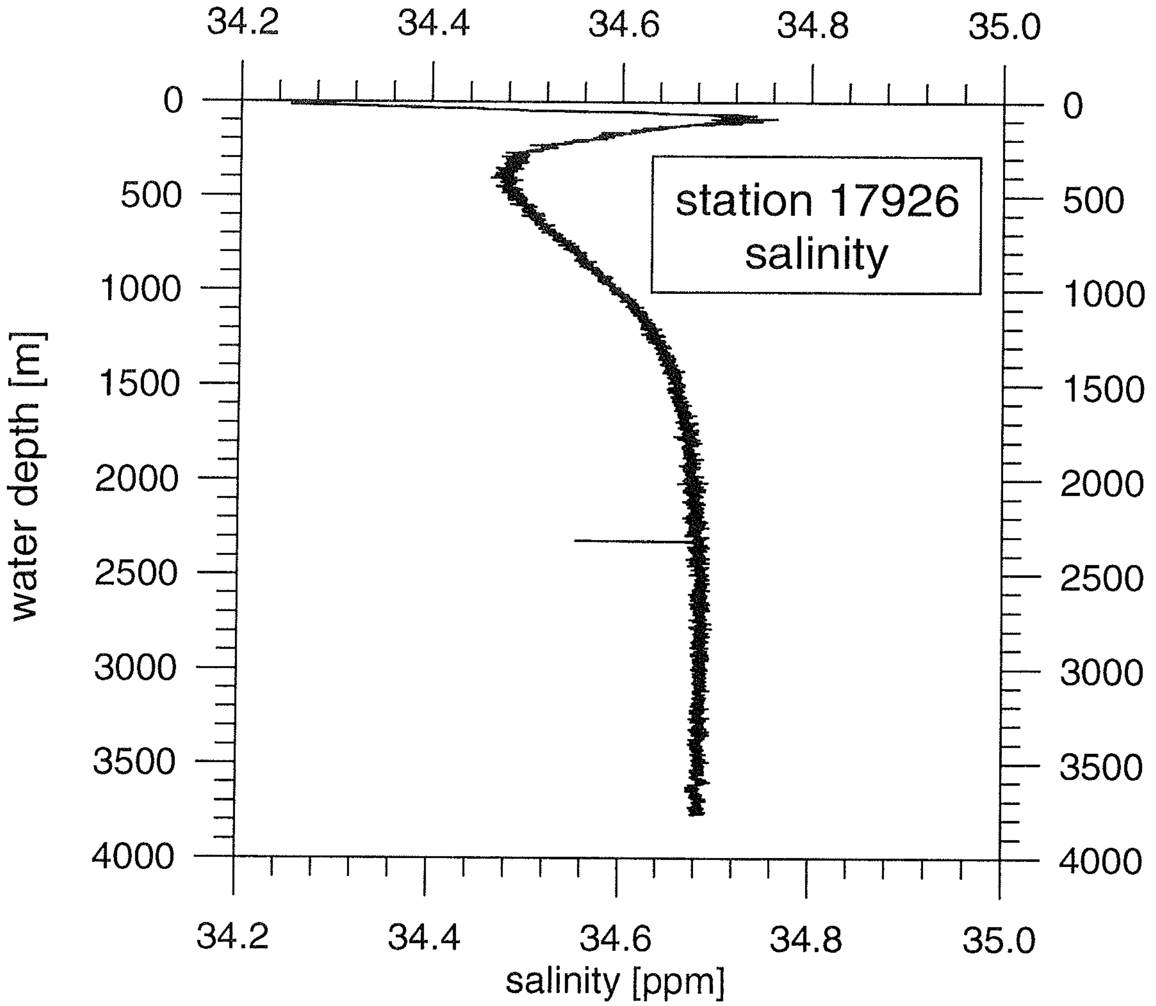

station 17926
salinity
water depth [m]
salinity [ppm]

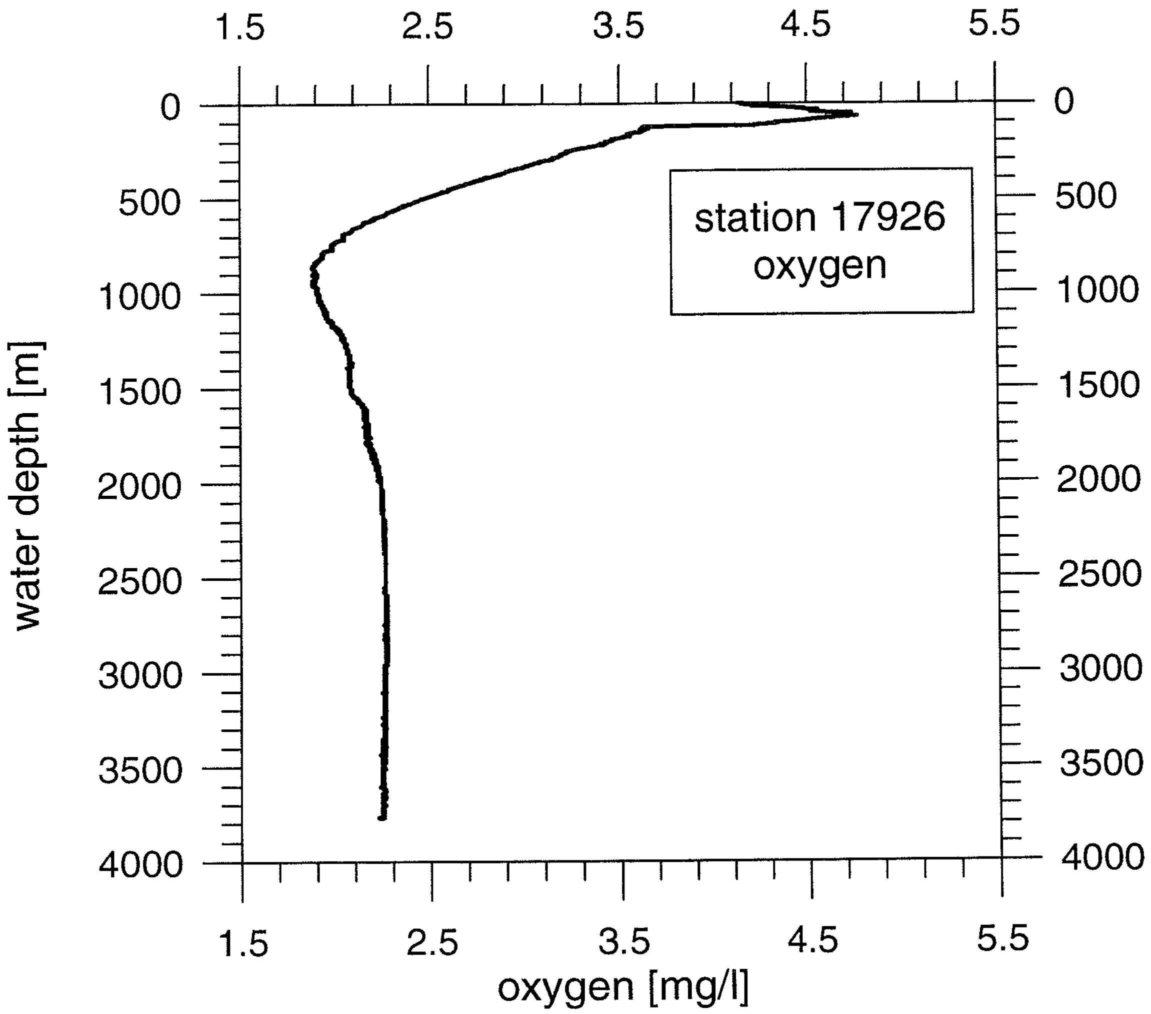
1.5
2.5
3.5
4.5
5.5
0
500
1000
1500
2000
2500
3000
3500
4000
station 17926
oxygen
water depth [m]
oxygen [mg/l]

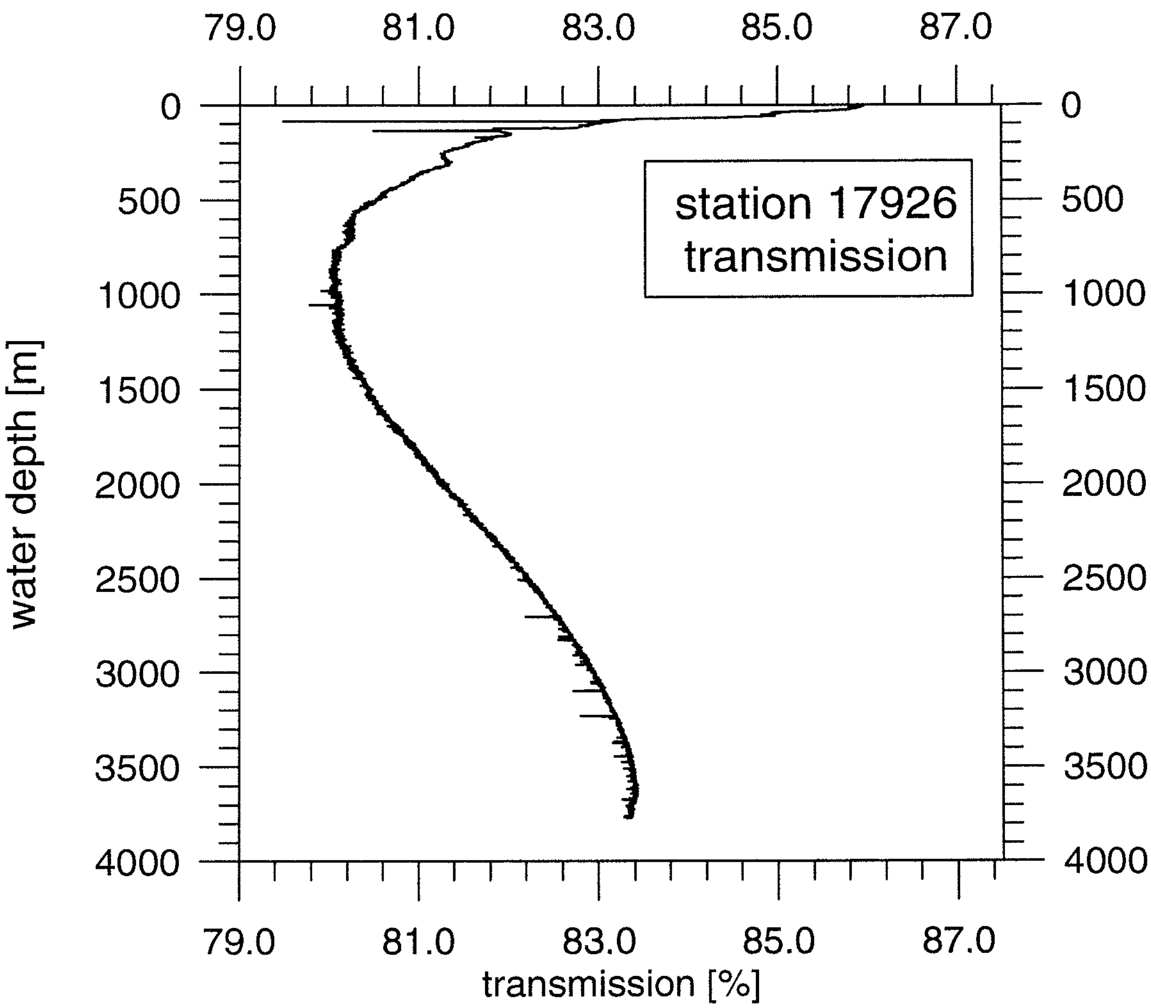
79.0
81.0
83.0
85.0
87.0
0
500
1000
1500
2000
2500
3000
3500
4000
station 17926
transmission
water depth [m]
transmission [%]

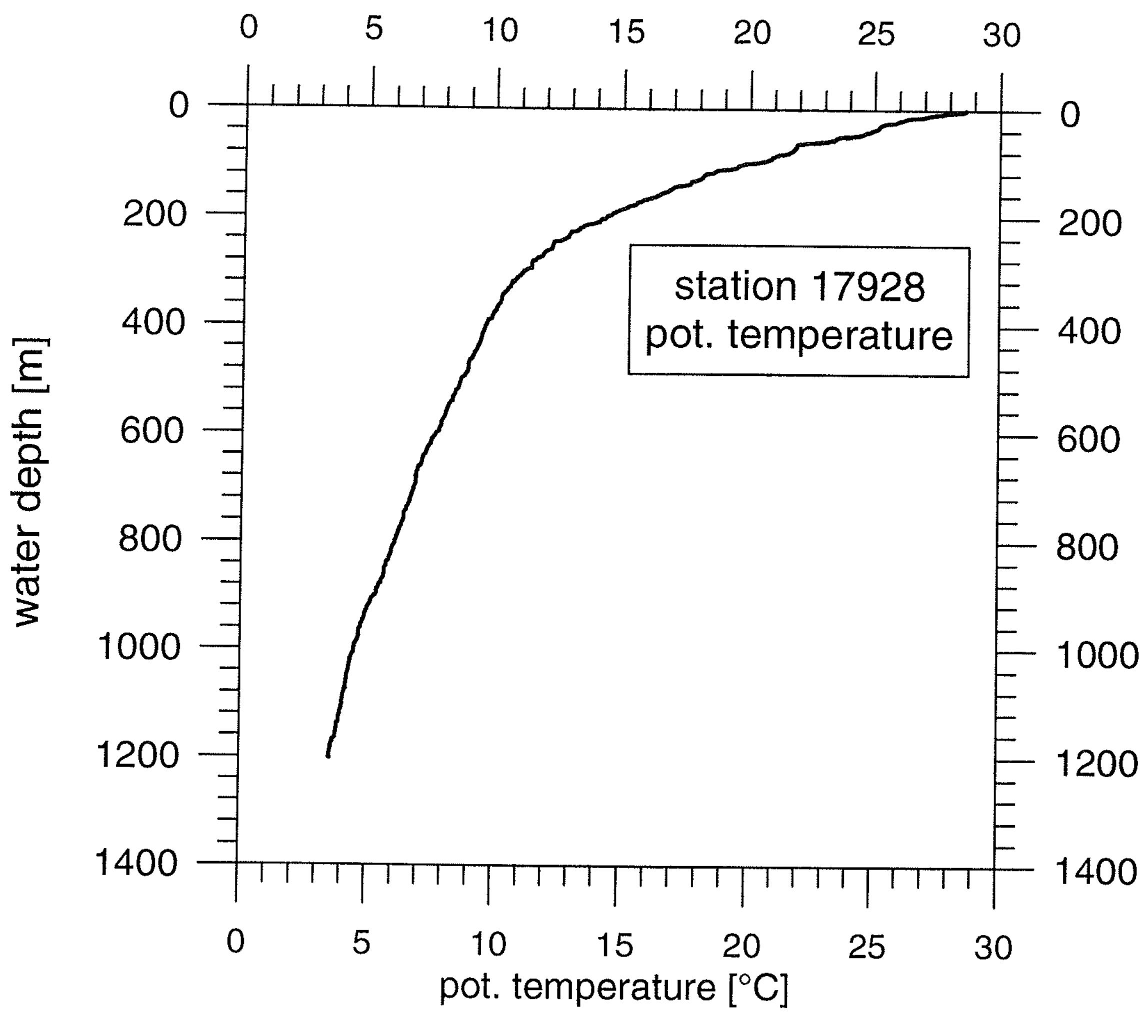
station 17928
pot. temperature
water depth [m]
pot. temperature [°C]

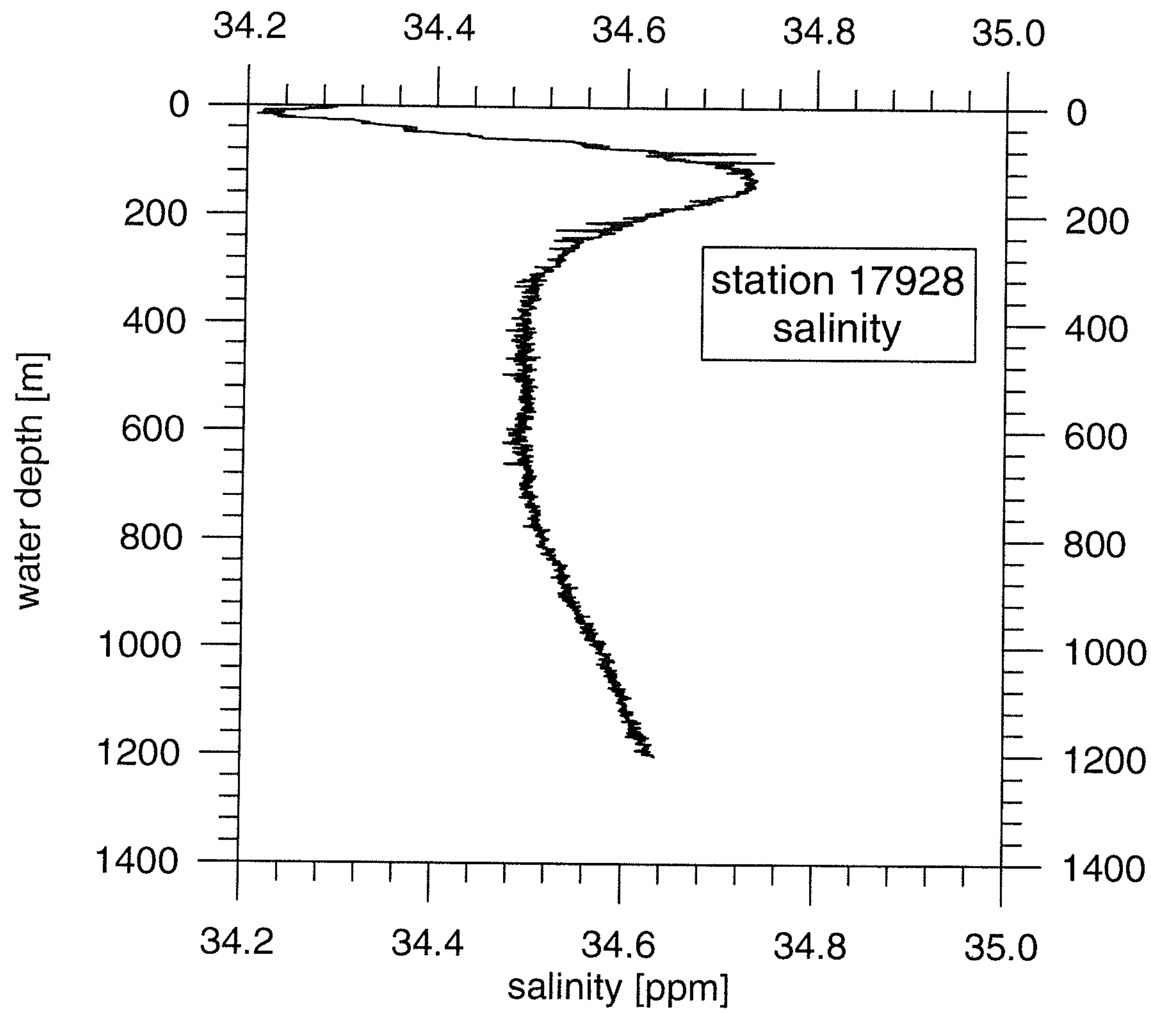
station 17928
salinity
water depth [m]
salinity [ppm]

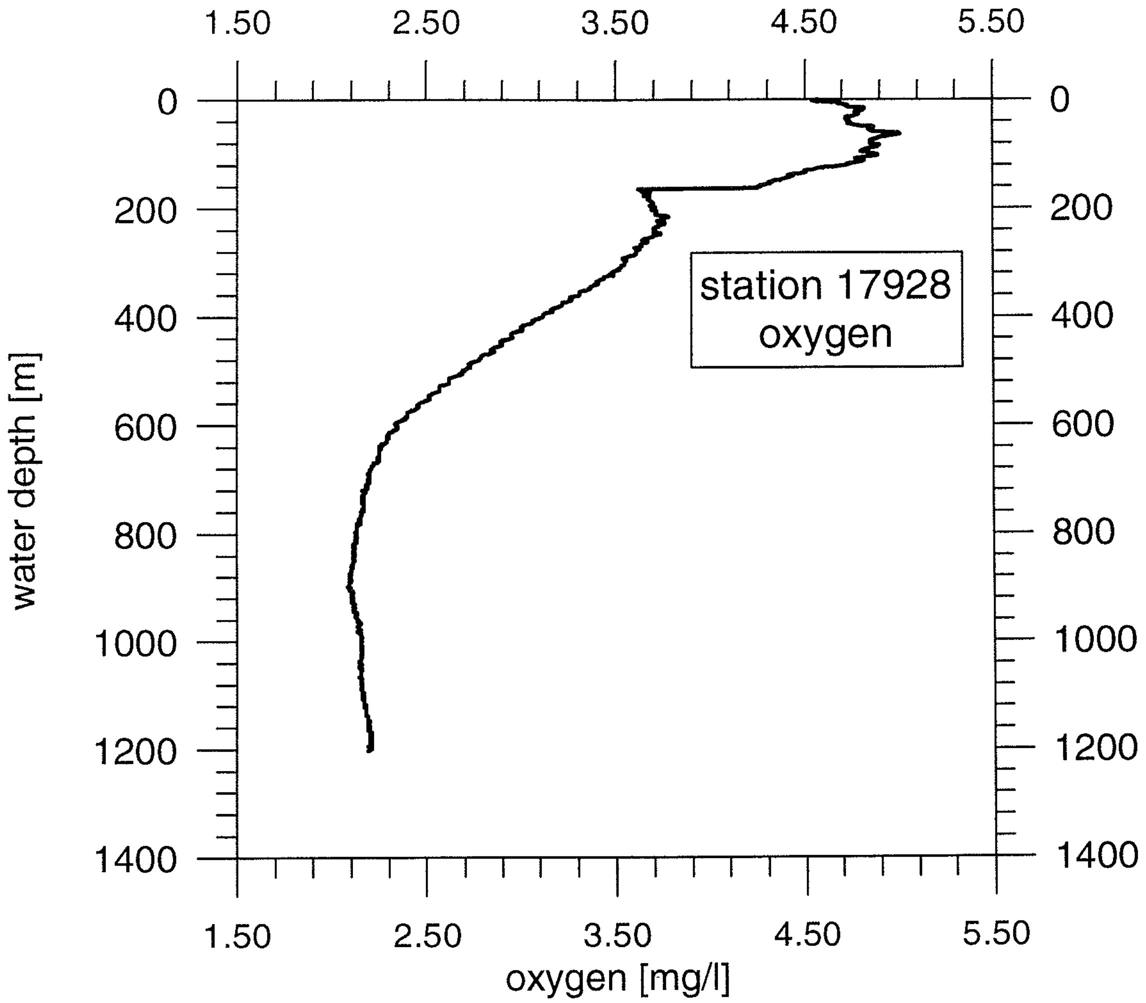

1.50
2.50
3.50
4.50
5.50
0
200
400
600
800
1000
1200
1400
water depth [m]
station 17928
oxygen
oxygen [mg/l]

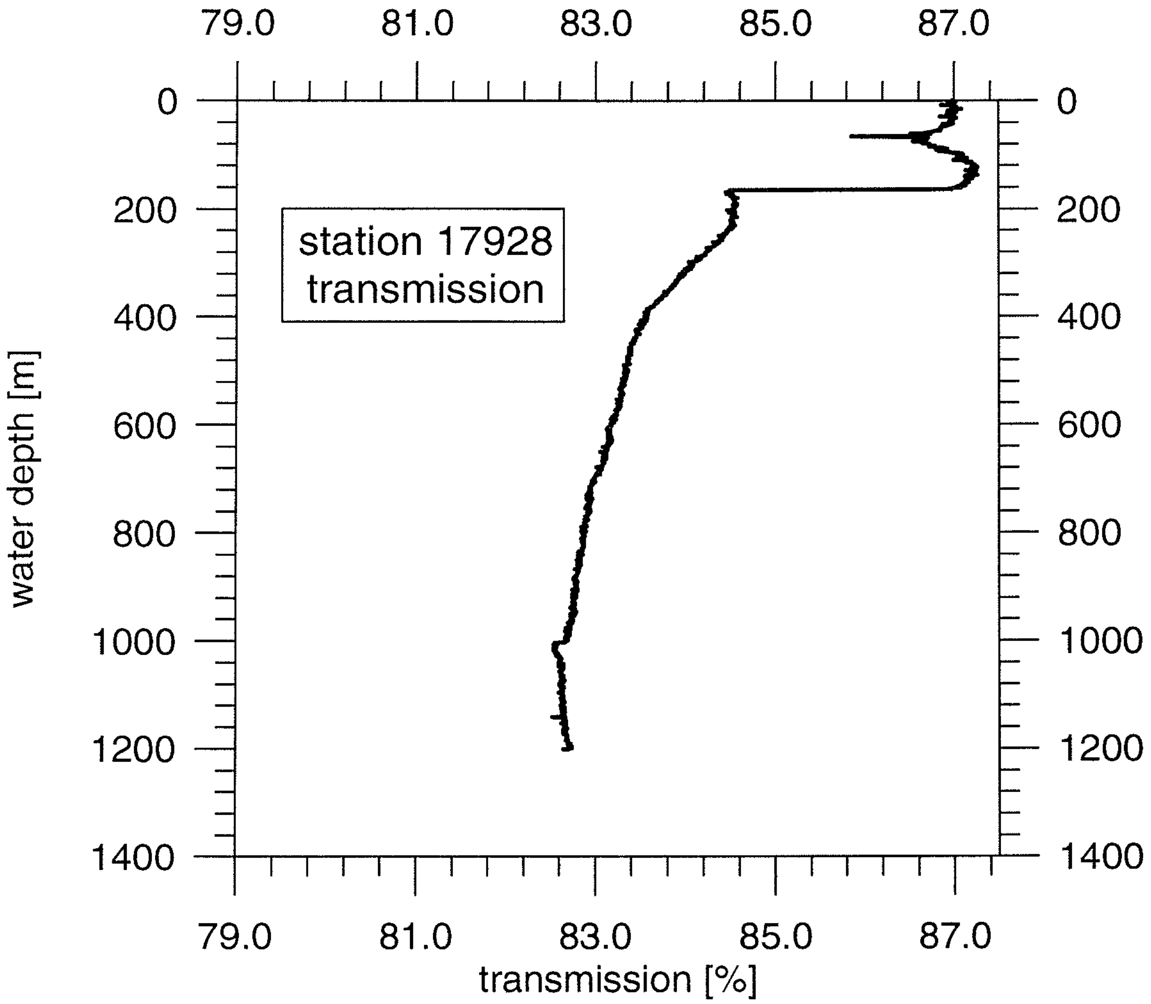

79.0
81.0
83.0
85.0
87.0
0
200
400
600
800
1000
1200
1400
water depth [m]
station 17928
transmission
transmission [%]

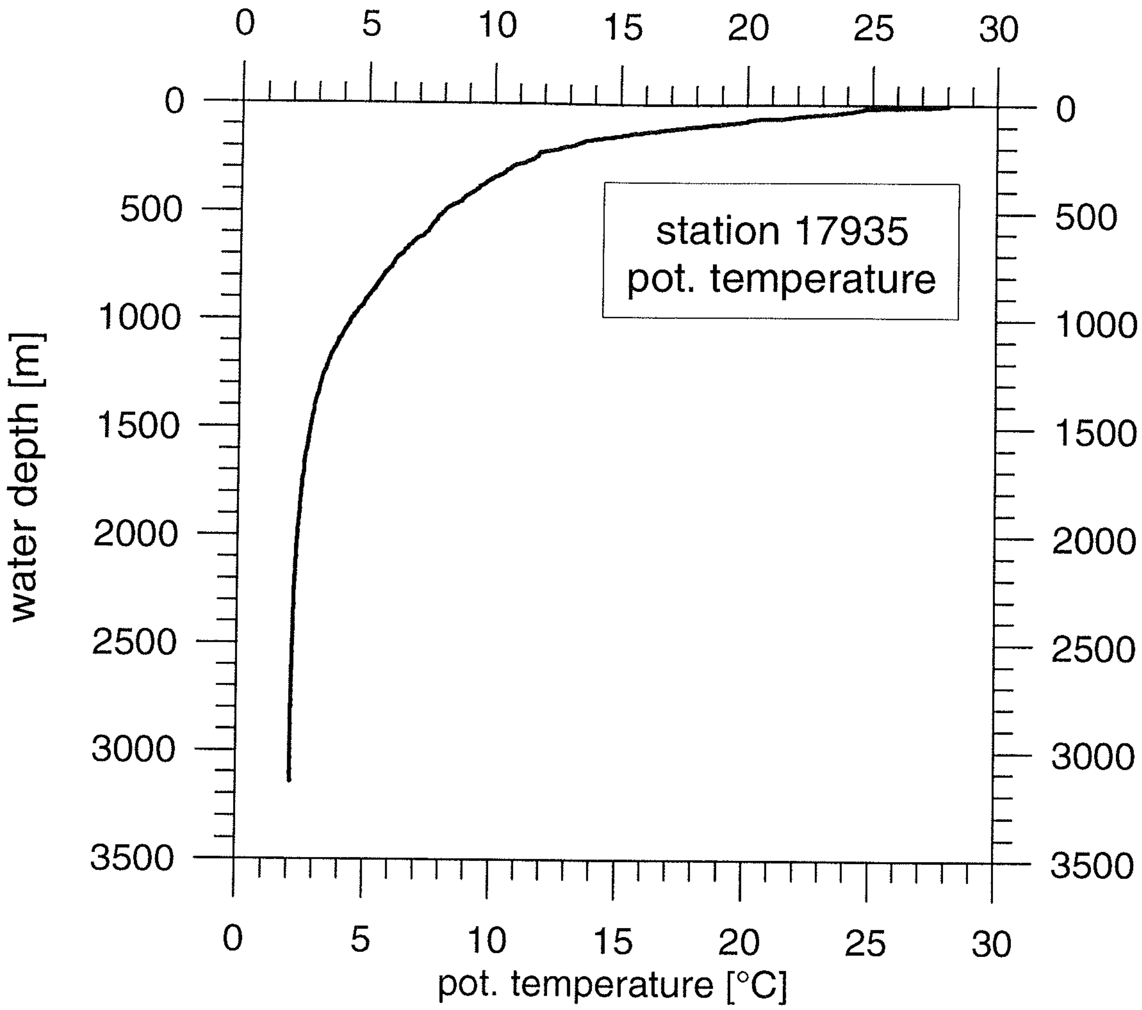

0 5 10 15 20 25 30
0 500 1000 1500 2000 2500 3000 3500
water depth [m]
station 17935
pot. temperature
pot. temperature [°C]

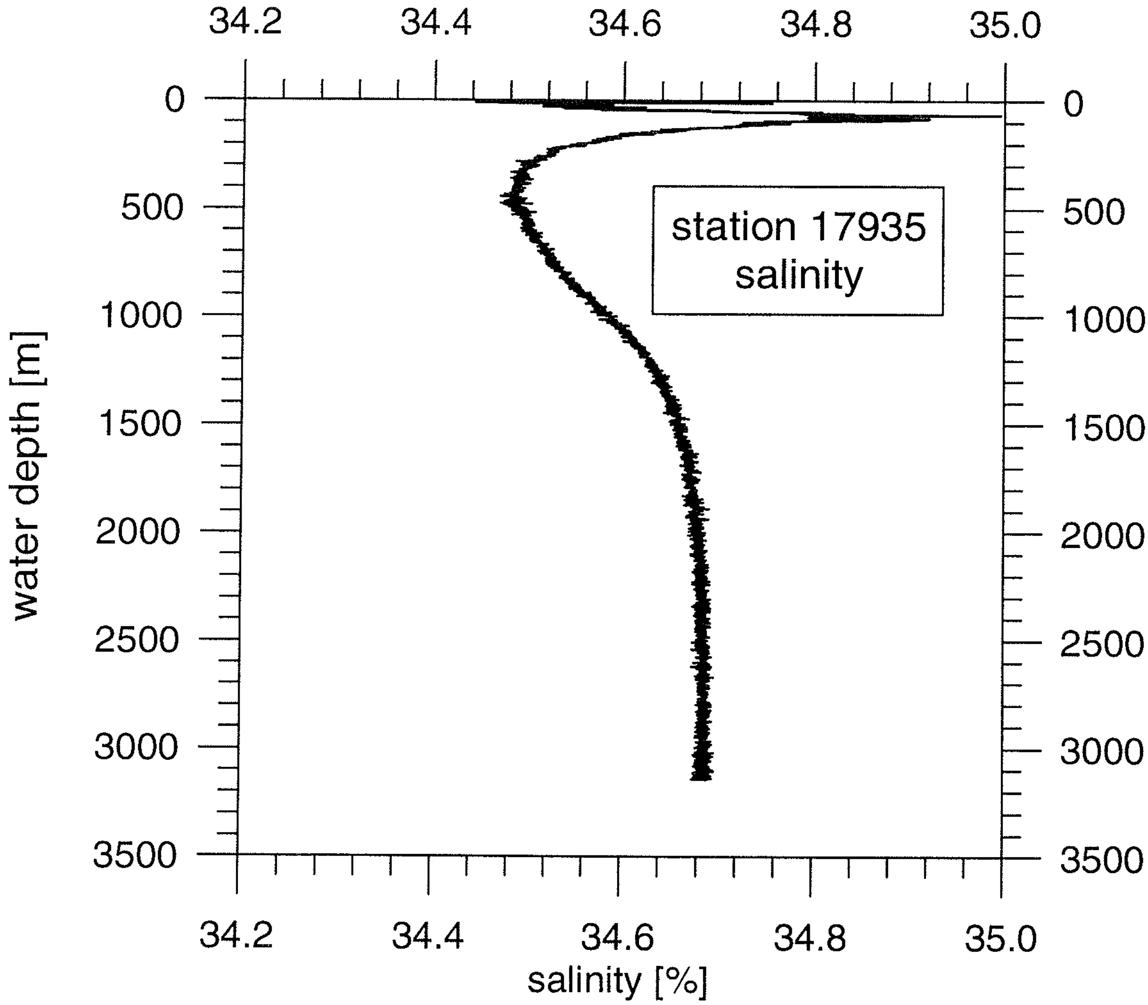

34.2 34.4 34.6 34.8 35.0
0 500 1000 1500 2000 2500 3000 3500
water depth [m]
station 17935
salinity
salinity [%]

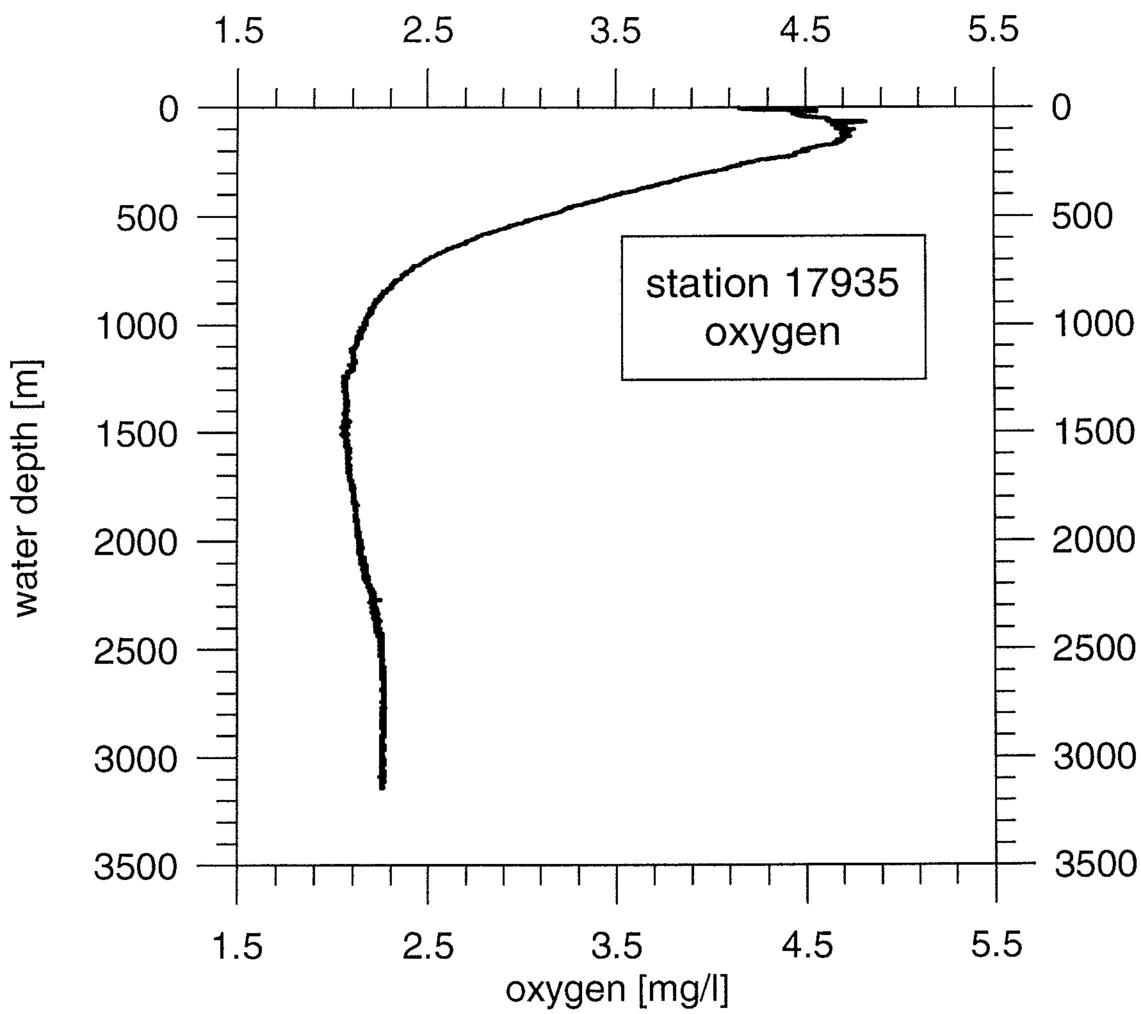

station 17935
oxygen
water depth [m]
oxygen [mg/l]
1.5
2.5
3.5
4.5
5.5
0
500
1000
1500
2000
2500
3000
3500

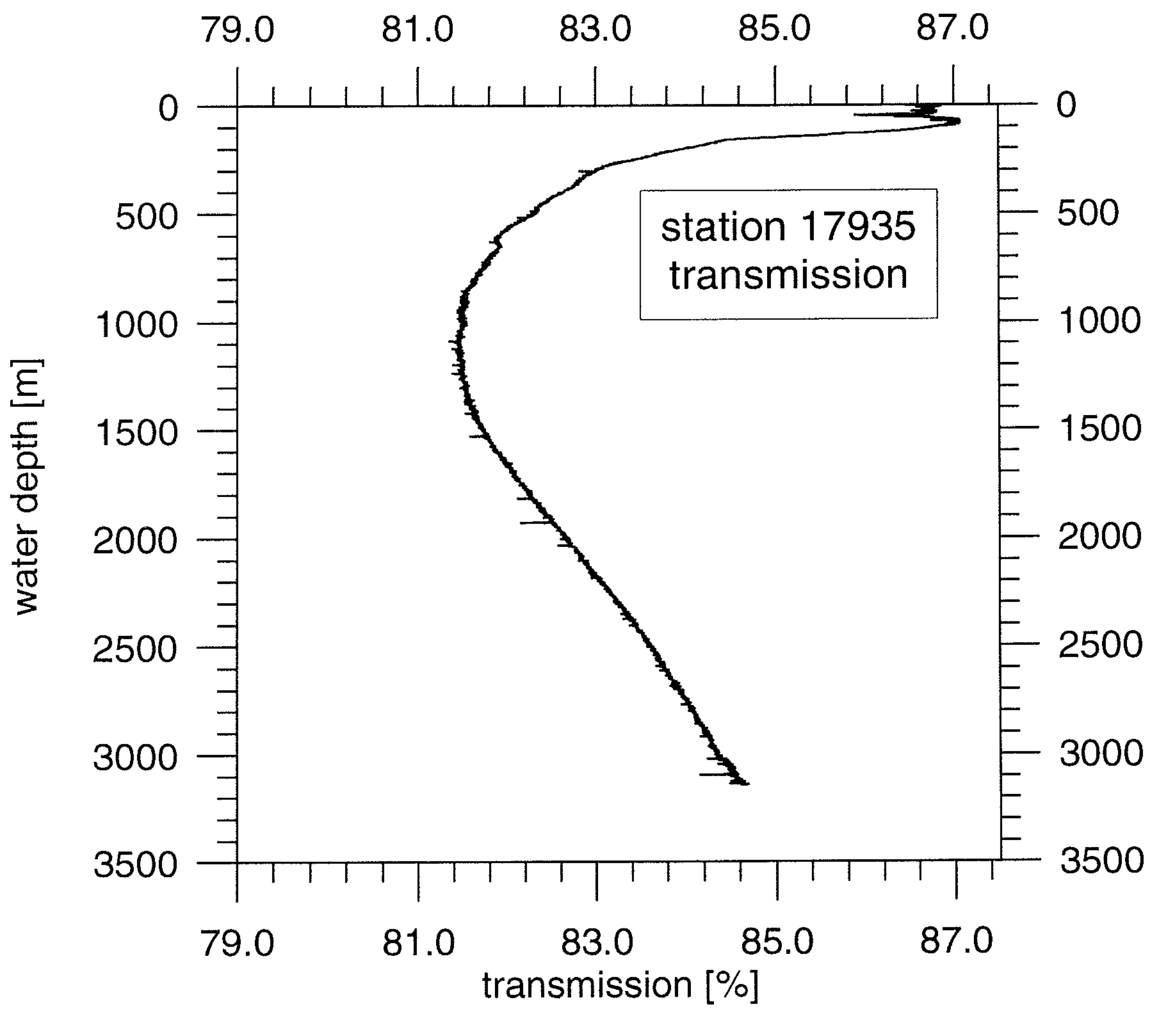

station 17935
transmission
water depth [m]
transmission [%]
79.0
81.0
83.0
85.0
87.0
0
500
1000
1500
2000
2500
3000
3500

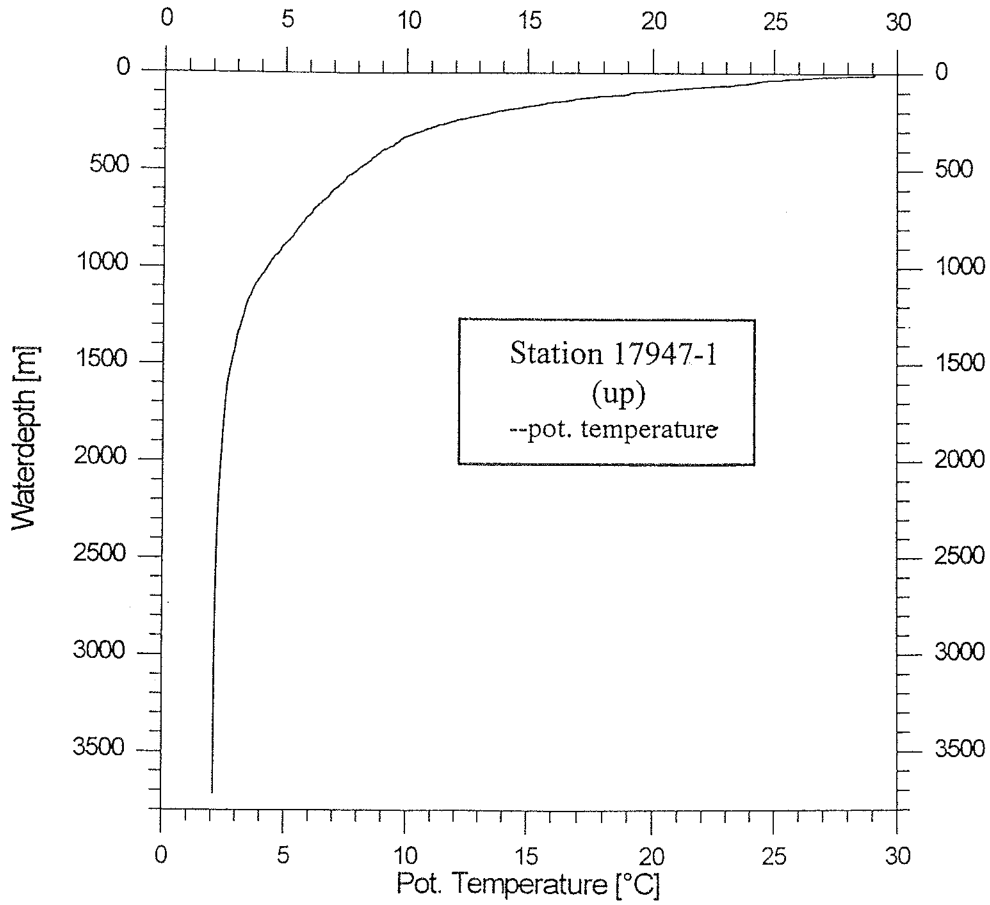

Station 17947-1
(up)
--pot. temperature
Waterdepth [m]
Pot. Temperature [°C]

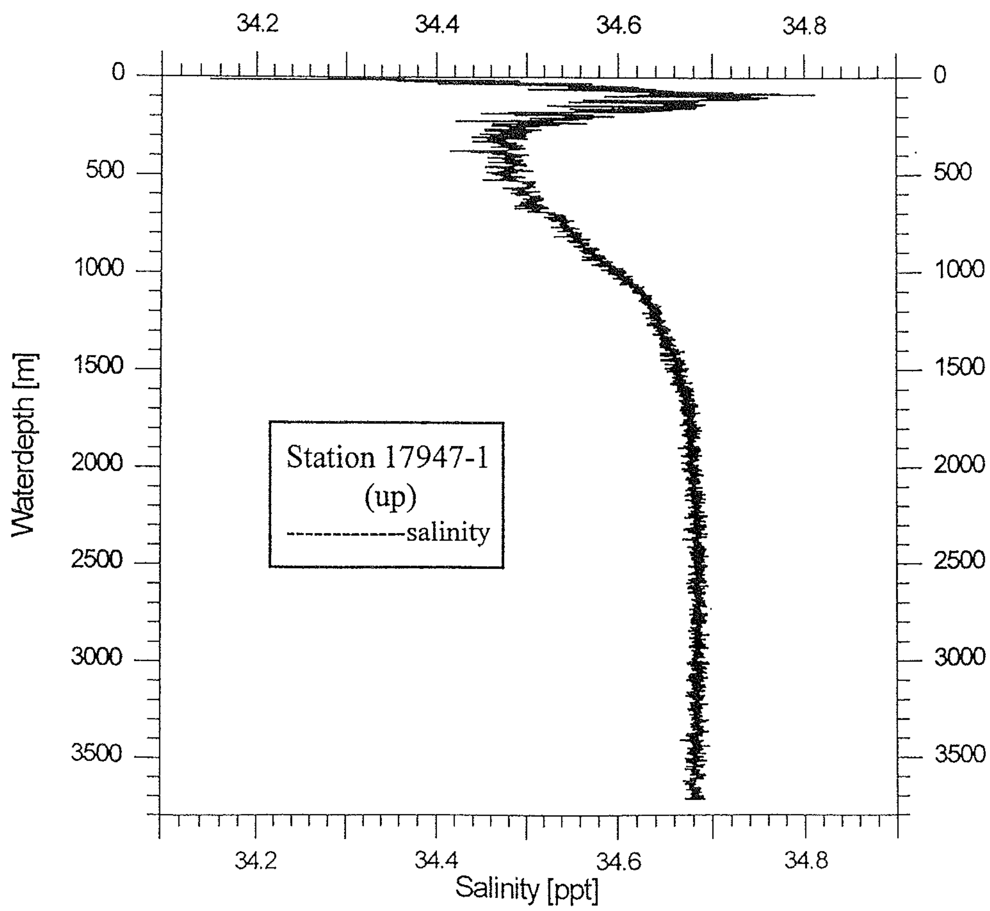

Station 17947-1
(up)
------------salinity
Waterdepth [m]
Salinity [ppt]

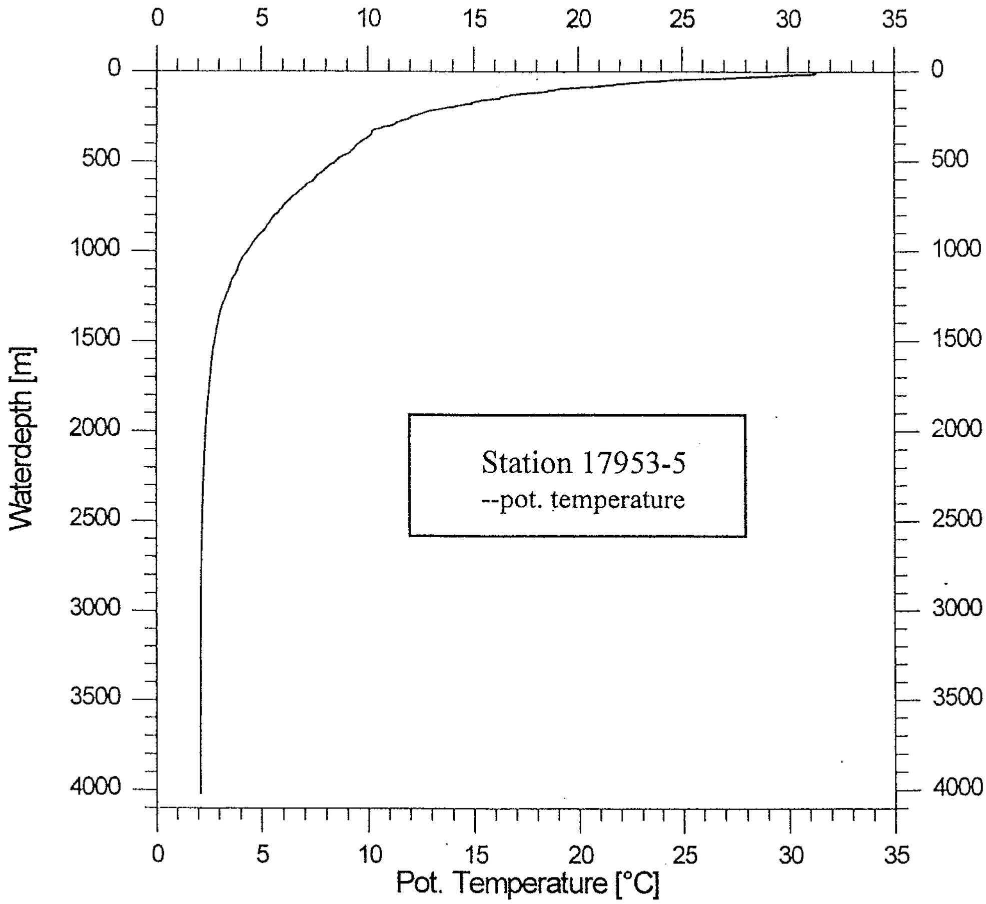
0 5 10 15 20 25 30 35
0 500 1000 1500 2000 2500 3000 3500 4000
Waterdepth [m]
Station 17953-5
--pot. temperature
Pot. Temperature [°C]

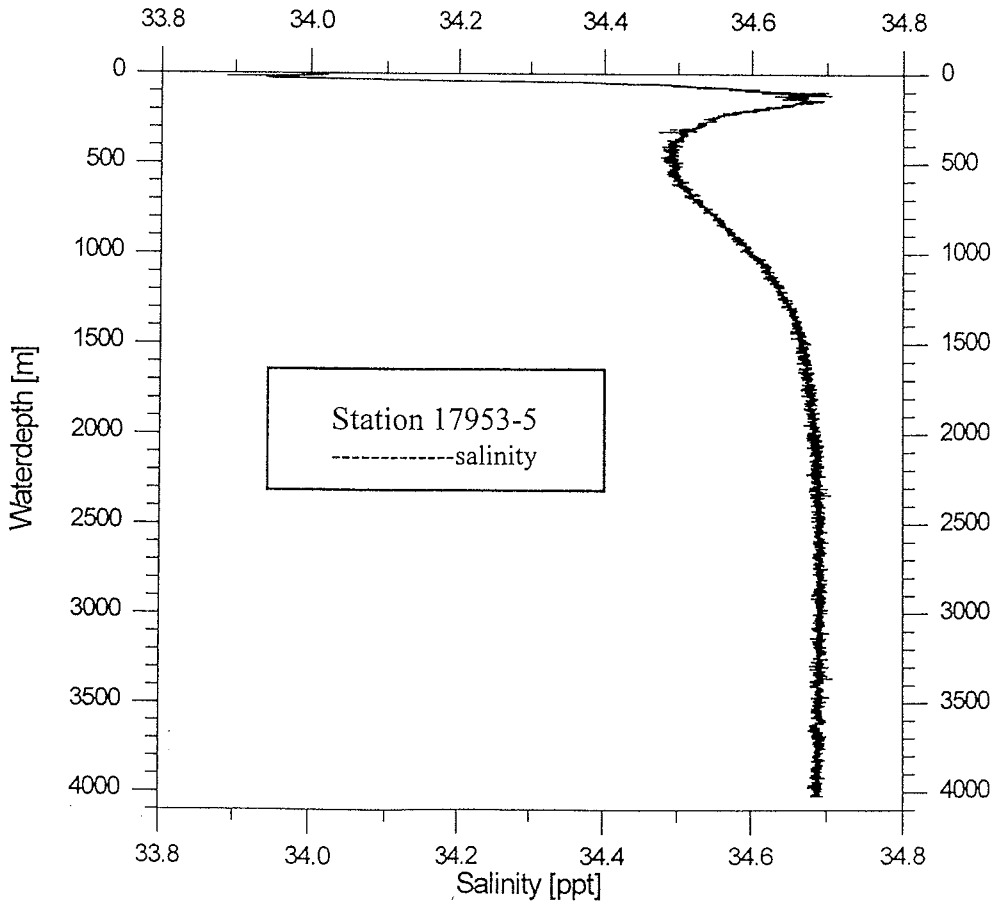
33.8 34.0 34.2 34.4 34.6 34.8
0 500 1000 1500 2000 2500 3000 3500 4000
Waterdepth [m]
Station 17953-5
------------salinity
Salinity [ppt]

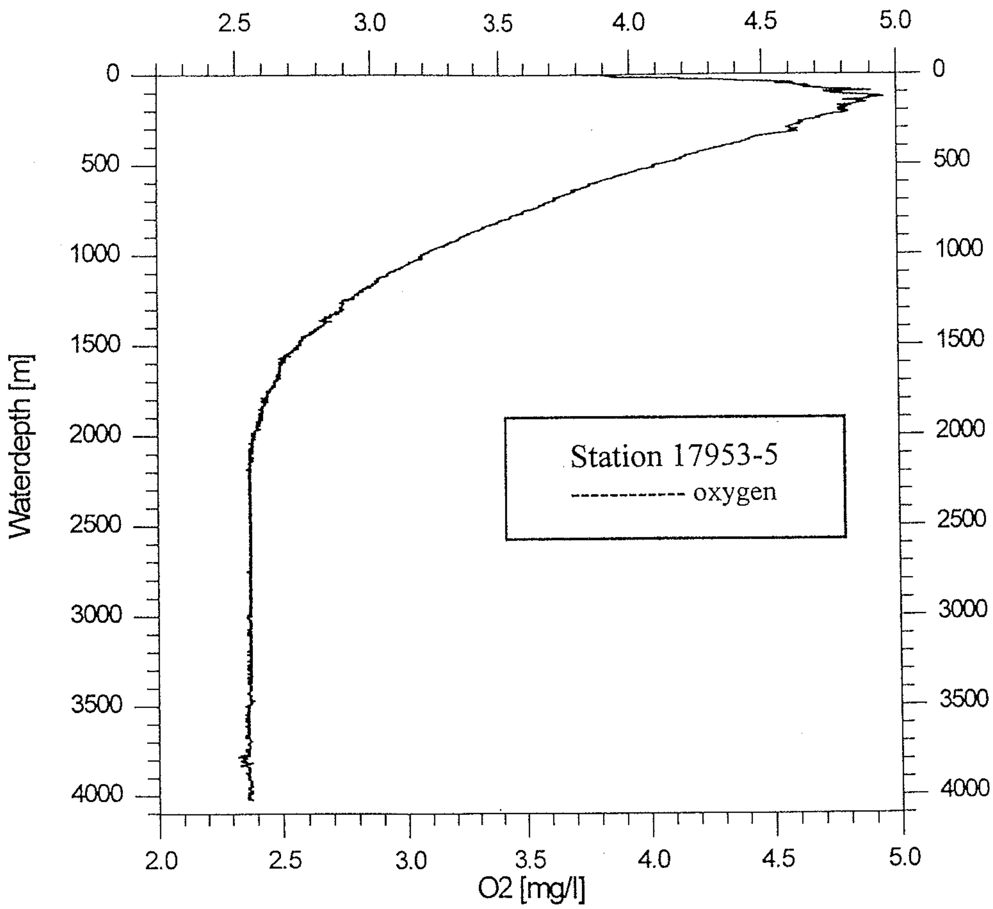

2.5
3.0
3.5
4.0
4.5
5.0
0
500
1000
1500
2000
2500
3000
3500
4000
Waterdepth [m]
Station 17953-5
------------ oxygen
2.0
2.5
3.0
3.5
4.0
4.5
5.0
O2 [mg/l]

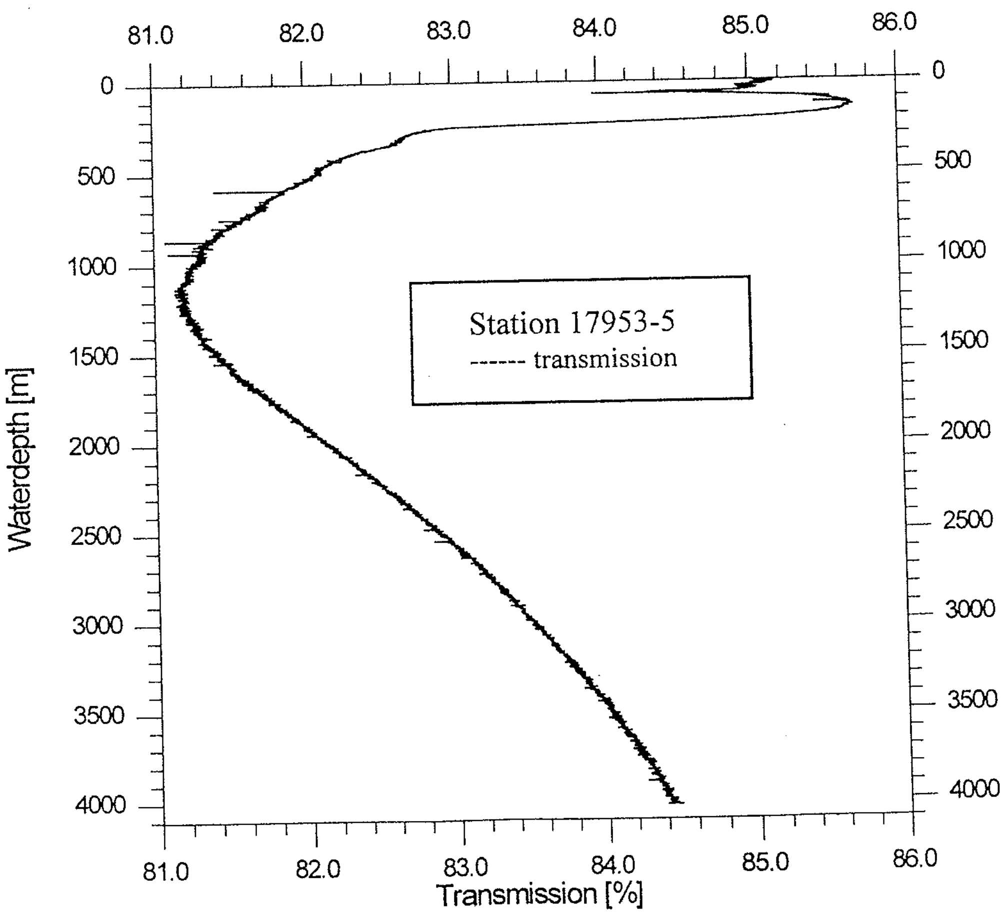

81.0
82.0
83.0
84.0
85.0
86.0
0
500
1000
1500
2000
2500
3000
3500
4000
Waterdepth [m]
Station 17953-5
------ transmission
Transmission [%]

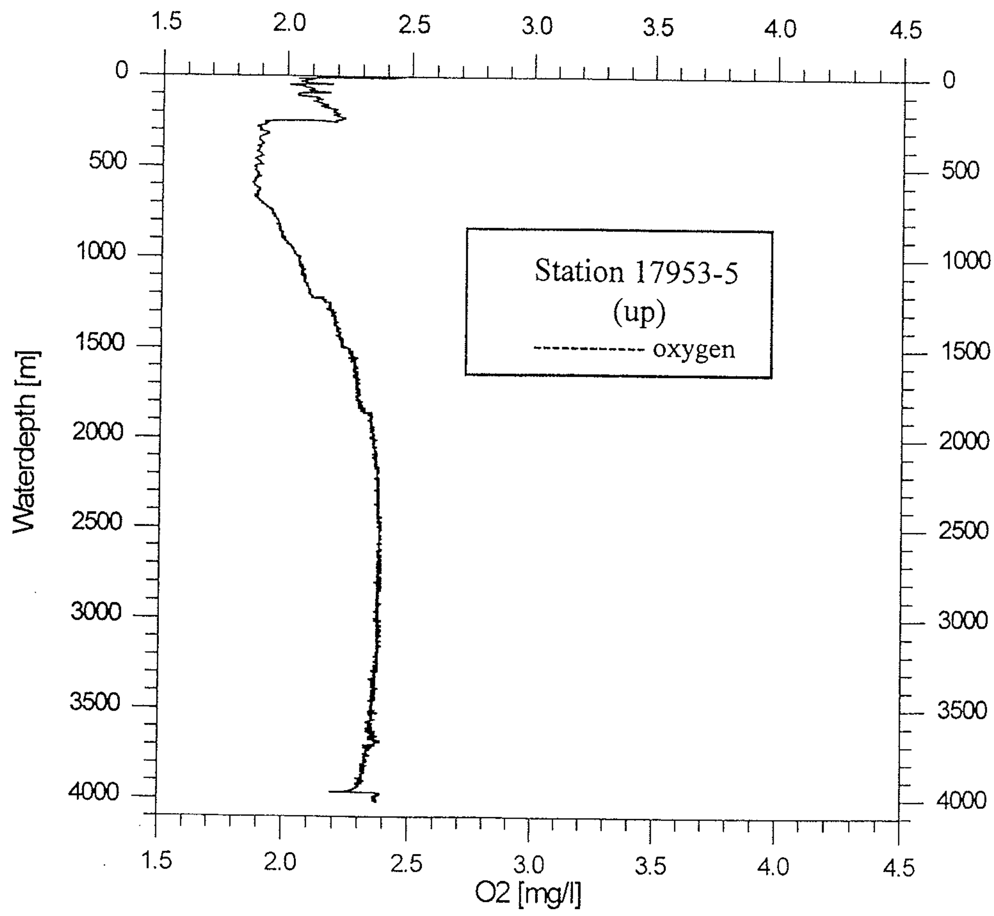
Station 17953-5
(up)
oxygen
Waterdepth [m]
O2 [mg/l]
1.5
2.0
2.5
3.0
3.5
4.0
4.5
0
500
1000
1500
2000
2500
3000
3500
4000

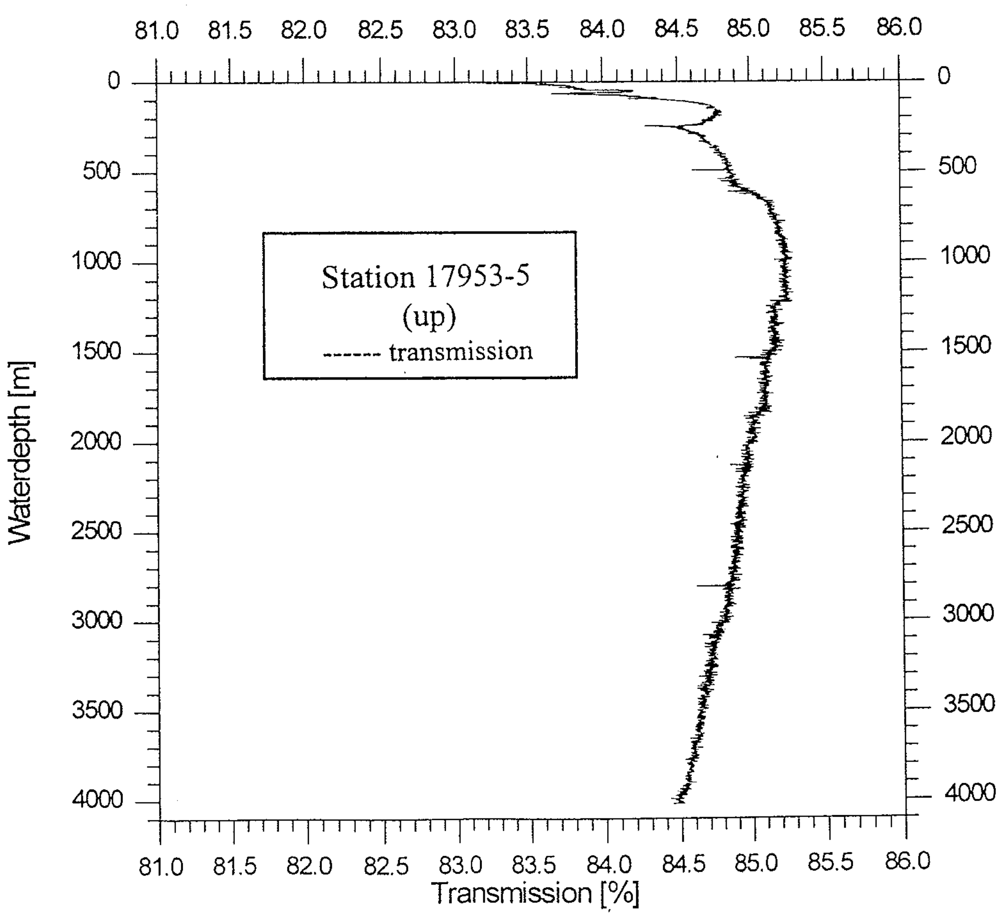
Station 17953-5
(up)
transmission
Waterdepth [m]
Transmission [%]
81.0
81.5
82.0
82.5
83.0
83.5
84.0
84.5
85.0
85.5
86.0
0
500
1000
1500
2000
2500
3000
3500
4000

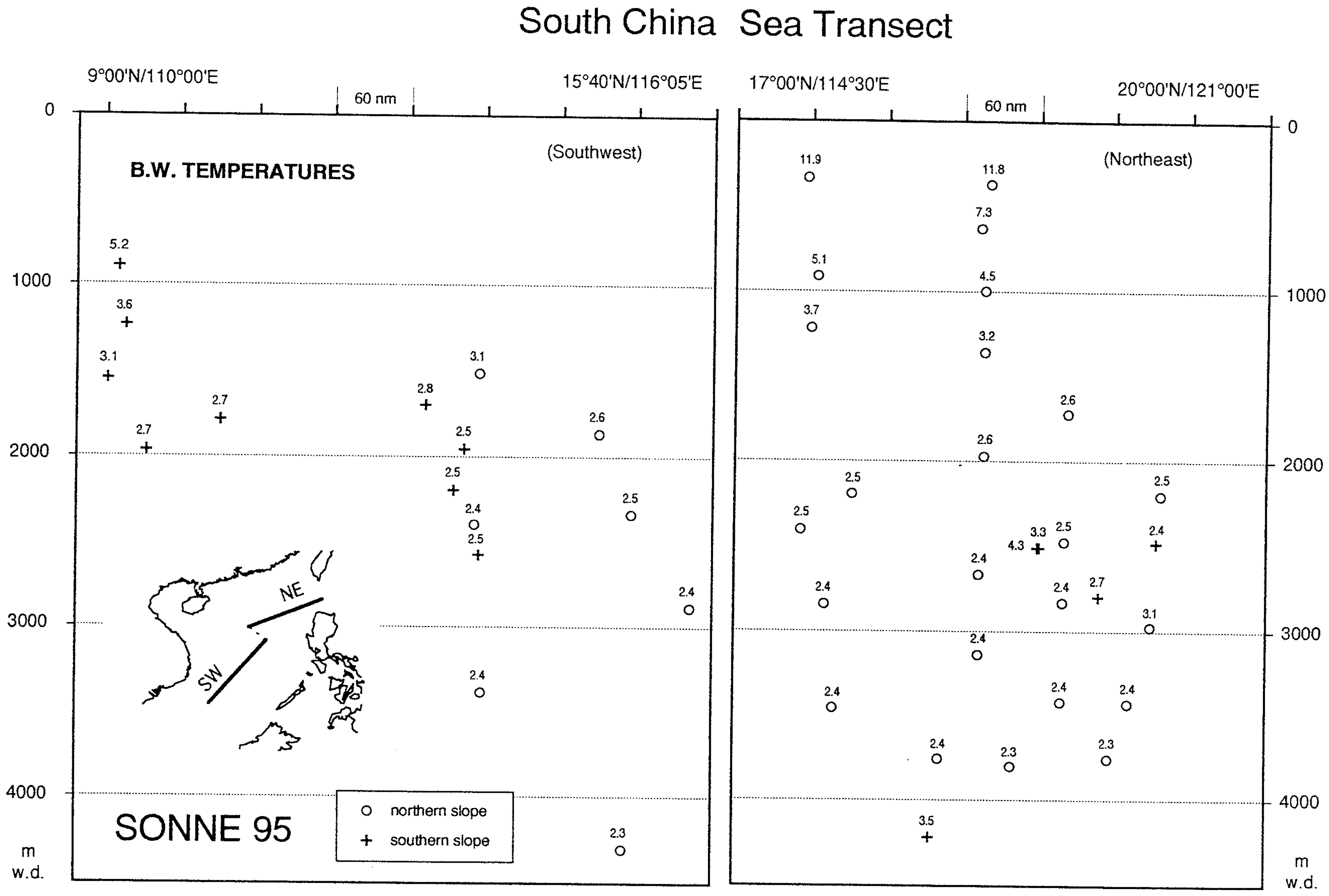

Figure 6. Transect of bottom-water temperatures in the South China Sea, as measured 5 cm below the sediment surface of box cores.

3.9 ASH LAYERS IN THE SOUTH CHINA SEA (SONNE-95 CRUISE)

M.G. Wiesner, Y. Wang and H.K. Wong (Institute of Biogeochemistry and Marine Chemistry, University of Hamburg.)

INTRODUCTION

Volcanic dust is one of the major components of atmospheric particulate matter in deep-sea sediments. The prime source of these particles is island-arc volcanism due to the highly explosive nature of the associated eruptions: massive quantities of pyroclasts are ejected into the upper troposphere and the stratosphere where high-velocity winds induce strong meridional dispersal creating global ash falls (e.g. Kennett 1981). These events may be recognized in the stratigrahic record either by the occurrence of finely disseminated volcanogenic particles (e.g. glass shards) or as discrete layers of tephra. The latter are of particular importance because they represent highly reliable isochronous horizons for stratigraphic intercore correlation. Moreover, they may provide a basis for the reconstruction of upper atmospheric wind regimes and transportation mechanisms to the interior of the oceans.

In the sedimentary sections of the South China Sea, volcanic particles are common constituents and are particularly abundant in the central part of the basin. Here the relative percentage of glass shards and pumice increases from west to east (Wang et al., 1992) indicating that most of this material originates from the Philippine archipelago. It has been argued by Wang et al. (1992) that the distribution patterns of the pyroclasts reflect the tracks of typhoons and the NE trade wind flow. However, satellite data which have documented the interaction of typhoon Yunya with the major eruption cloud of Mt. Pinatubo (Luzon Island, Philippines) emitted on June 15, 1991, showed clearly that the movement of the ash clouds across the South China Sea is governed by upper tropospheric (tropical easterly jet) and stratospheric winds (ESCAP/WMO Typhoon Committee Annual Review 1991; Koyaguchi and Tokuno 1992).

Core studies in the northern and central South China Sea revealed the widespread occurrence of three distinct ash beds (henceforth referred to as layer L, M and U); the base of L, M and U was dated by oxygen isotope curves to be about 64 ka (L), 43 ka (M) and 15 ka (U) in age respectively (Chen and Zhou 1992). Another layer of ash was expected to be present in the uppermost cm of the surface sediments linked to the eruption of Mt. Pinatubo in 1991 (referred to as layer P) (Wiesner et al. 1994).

MATERIALS AND METHODS

Macroscopically visible ash layers were sampled from the gravity and piston cores as well as spade box corer profiles and checked for mineral composition using standard microscopy techniques. A complete section of each individual ash bed was taken out of the cores by plastic boxes for further analyses in Hamburg (BMFT Project 03G0095A). Unfortunately, sampling of the box grab material was not ideal for our study of the Pinatubo ashes because of the sampling scheme adopted for this cruise.

PRELIMINARY RESULTS

All ash beds encountered (L, M, U and P) are pale greyish in color and are usually normally graded. The thickness increases from west to east. The base of the ash layers generally displays a sharp contact to the underlying pelagic muds whereas the top boundary is irregular and appears to be strongly bioturbated. The major component of all ash beds is volcanic glass (glass shards and pumice). Shards are predominantly colorless in M, L and P and brownish in U. The phenocrysts consist of subhedral feldspar, amphibole and biotite flakes. For P the crystal assemblages (plagioclase and hornblende) are closely comparable to the airfall tephra of the June 1991 eruption of Mt. Pinatubo collected by the sediment traps in the central South China Sea (Wiesner et al. 1994). Moreover, in layer P many of the phenocrysts have a coating of vesicular glass attesting to their juvenile origin.

REFERENCES

Chen, W. and F. Zhou (1992): A study of volcanic glass in northern South China Sea during the last 100 ka. In: Jin, X., H.-R. Kudrass and G. Pautot (eds) Marine Geology and Geophysics of the South China Sea. Proc. Symp. Recent Contributions to the Geological History of the South China Sea. (China Ocean Press, Hangzhou), 174-178.

ESCAP/WMO Typhoon Committee Annual Review 1991, Manila, 120 pp.

Kennett, J.P. (1981): Marine tephrochronology. In: Emiliani, C. (ed), The Sea. Vol. 7. The Oceanic Lithosphere. (Wiley and Sons, Chichester), 1373-1436.

Koyaguchi, T. and M. Tokuno (1992): Origin of the giant eruption cloud of Pinatubo, June 15, 1991. - J. Volc. Geotherm. Res., 55, 85-96.

Wang, H., F. Zhou and Z. Lin (1992): Volcanic clasts in the periplatform carbonate ooze near Zhongsha Islands and their bearing on paleoenvironment. In: YE Z. and P. WANG(eds) Contributions to Late Quaternary Paleoceanography of the South China Sea (Qingdao Ocean Press, Qingdao), 42-55 (in Chinese).

Wiesner M.G., Y. Wang , L. Zheng, H.K. Wong and K. Arikas (1994): Massive fallout of volcanic dust to the deep South China Sea. - Deep-Sea Res. (subm.).

3.10 SEDIMENT - TRAP EXPERIMENTS IN THE SOUTH CHINA SEA (SONNE-95 CRUISE)

M.G. Wiesner[1], H.K. Wong[1], L. Zheng[2], Y. Wang[1] and P. Joehrendt[1]

[1] Institute of Biogeochemistry and Marine Chemistry, University of Hamburg; [2] Second Institute of Oceanography, State Oceanic Administration, Hangzhou.

INTRODUCTION

The vertical flux of particles has been sampled by time-series sediment traps in various ocean basins. Most of these studies show that particle fluxes to the deep sea are related to surface processes and primary productivity (e.g. Honjo and Manganini, 1993). Sediment trap studies carried out for more than one year have documented that considerable interannual variations in the flux rates of particulate matter as well as their seasonality can occur (e.g. Haake et al., 1993). Therefore, long-term studies can help to identify anomalous years and allow a comparision of trap-measured particle fluxes to recent sediments. In the tropical seas of southern Asia, strong interannual fluctuations in the strength of the monsoon winds, reflected in the amount of monsoon rainfall and wind speed, clearly affect upper ocean processes (Parthasarathy et al., 1992). Hence, studying the influence of monsoon strength on sedimentation is of special interest as average monsoon intensity has varied in the recent geological history in response to glacial-to-interglacial climatic changes (Sirocko et al., 1991).

In the South China Sea strong winds blowing from the SW (June to September) and the NE (November to February) cause a semiannual reversal of the surface water circulation from roughly clockwise to anti-clockwise. During the NE monsoon, which has generally higher wind speeds than the SW monsoon, upwelling occurs along the coast of Vietnam (LaViolette and Frontenac, 1967). Outside the upwelling areas wind-induced mixed layer deepening accompanied by entrainment of nutrients into the euphotic zone is responsible for enhanced productivity (Jennerjahn et al, 1992; Wiesner, Zheng et al., 1994a). Furthermore, the intensity of the monsoons determines the input of allochthonous material to the South China Sea. The major supply of this (mostly lithogenic) material occurs as dust from mainland China (Wiesner, Zheng et al., 1994) and through the rivers Mekong, Zhujiang and Hunghe (360 x 106 t of suspended matter per year; Milliman and Meade, 1983). Aeolian particles may be also supplied from the Indonesian archipelago during the SW monsoon and from the Philippines during the high season of typhoons (August-September). However, little information on the significance of these sources is available. Another important, though episodic contributor are the volcanoes of the Philippine island arc (Wiesner, Wang et al., 1994).

MATERIALS AND METHODS

The sediment trap program of Hamburg University (BMFT Project 03G0095A) was carried out during leg 3 of cruise SO-95 of the R/V *SONNE* (May-June 1994). Originally it was planned to reactivate the sediment trap station SCS-N in the northern part of the basin at 18°28'N, 116°01'E. This station was operated in 1987-1988 (Jennerjahn et al., 1992) and has documented the importance of the NE monsoon as a trigger for enhanced vertical fluxes of particulate matter in this area. The deployment of a one-trap mooring system at SCS-N, however, failed because of the breakage of one of the wire ropes, and the whole system had to be recovered. The release was lost due to entanglement of the lowermost wire rope with the anchor.

The sediment trap system in the central South China Sea (SCS-C), operated since 1991 at 14°36'N, 115°06'E (Fig. 1), was successfully recovered (SCS-C-03) and redeployed (SCS-C-04). The station was chosen on the basis of high resolution pinger subbottom profiles. One of these profiles shows a wedge-like sedimentary structure leeward of an elongated ëridgeí which is part of the acoustic basement (Fig. 2). These sediments, interpreted to be drift deposits, are the youngest in the area, because they overlie unconformably the stratified sequence which represents normal pelagic strata. The ridge is approximately 1 nm to the north of the mooring and stands about 300 m above the surrounding sea floor.

All data on the recovery and redeployment activities, mooring components, schedule input and retrieval, and the position of the systems are given in Figures 3 and 4 and Tables 1 to 12. Due to limitations in time during legs 3 and 4, SCS-C-03 had to be recovered prior to the closing of cup 13. The configuration of the two-trap system recovered was changed into an array consisting of three Mark VI time-series sediment traps fixed at 1210, 2240 and 3770 m depth below sea level. The total length of the system is 3134 m. Total water depth is 4306 m. Sampling cups were filled with sea water from the respective trap depths with 33.3 g l^{-1} NaCl and 3.33 g l^{-1} $HgCl_2$ added to reduce diffusion and biological activity. The traps were programmed to collect particulate matter at intervals of 28 days from June 1, 1994 to May 31, 1995.

PRELIMINARY RESULTS

Visual examination of the SCS-C-03 trap samples (in total covering the time span from May 1993 to May 1994) revealed considerable variations in bulk particle flux rates. Comparision of the quantities of particulate matter collected by the shallow and deep trap corroborates our earlier findings that one of the major factors influencing sedimentation in the central (and northern) part of the basin is lateral advection (Wiesner, Zheng et al., 1994).

REFERENCES

Haake, B., V. Ittekkot, T. Rixen , V. Ramaswamy, R.R. Nair and W.B. Curry (1993): Seasonality and interannual variability of particle fluxes to the deep Arabian Sea. - Deep-Sea Res., 40, 1323-1344.

Honjo, S. and S. J. Manganini (1993): Annual biogenic particle fluxes to the interior of the North Atlantic Ocean; studied at 34°N, 21°W and 48°N, 21°W. - Deep-Sea Res., 40, 587-607.

Jennerjahn, T.C., G. Liebezeit , S. Kempe , L. Xu, W. Chen and H.K. Wong (1992): Particle flux in the northern South China Sea. In: Jin X., H.-R. Kudrass and G. Pautot (eds) Marine Geology and Geophysics of the South China Sea. Proc. Symp. Recent Contributions to the Geological History of the South China Sea (China Ocean Press, Hangzhou), 228-235.

LaViolette, P.E. and T.R. Frontenac (1967): Temperature, Salinity and Density of the World's Seas: South China Sea and adjacent Gulfs. - Informal manuscript No. 67-2, (U.S. Naval Oceanographic Office, Washington D.C.), 1-134,

Milliman, J.D. and R.H. Meade (1983): World-wide delivery of river sediment to the oceans. - J. Geol. , 91, 1-21.

Parthasarathy, B., K. Rupta Kumar and D.R. Kothawale (1992): Indian summer monsoon rainfall indices: 1871-1990. *Meteorol. Mag.* , 121, 174-186.

Sirocko, F., M. Sarnthein, H. Lange and H. Erlenkeuser (1991): Atmospheric summer circulation and coastal upwelling in the Arabian Sea during the Holocene and the last glaciation. - Quaternary Res., 36, 72-93.

Wiesner, M.G., L. Zheng, H.K. Wong , Y. Wang , S. Zheng and S. Reschke (1994): Particle fluxes in the South China Sea. In: Ittekkot, V.(ed.) Particle Flux in the Ocean (Wiley and Sons, Chicester), (subm.).

Wiesner, M.G., Y. Wang, L. Zheng, H.K. Wong and K. Arikas (1994): Massive fallout of volcanic dust to the deep South China Sea. - Deep-Sea Res. (subm.).

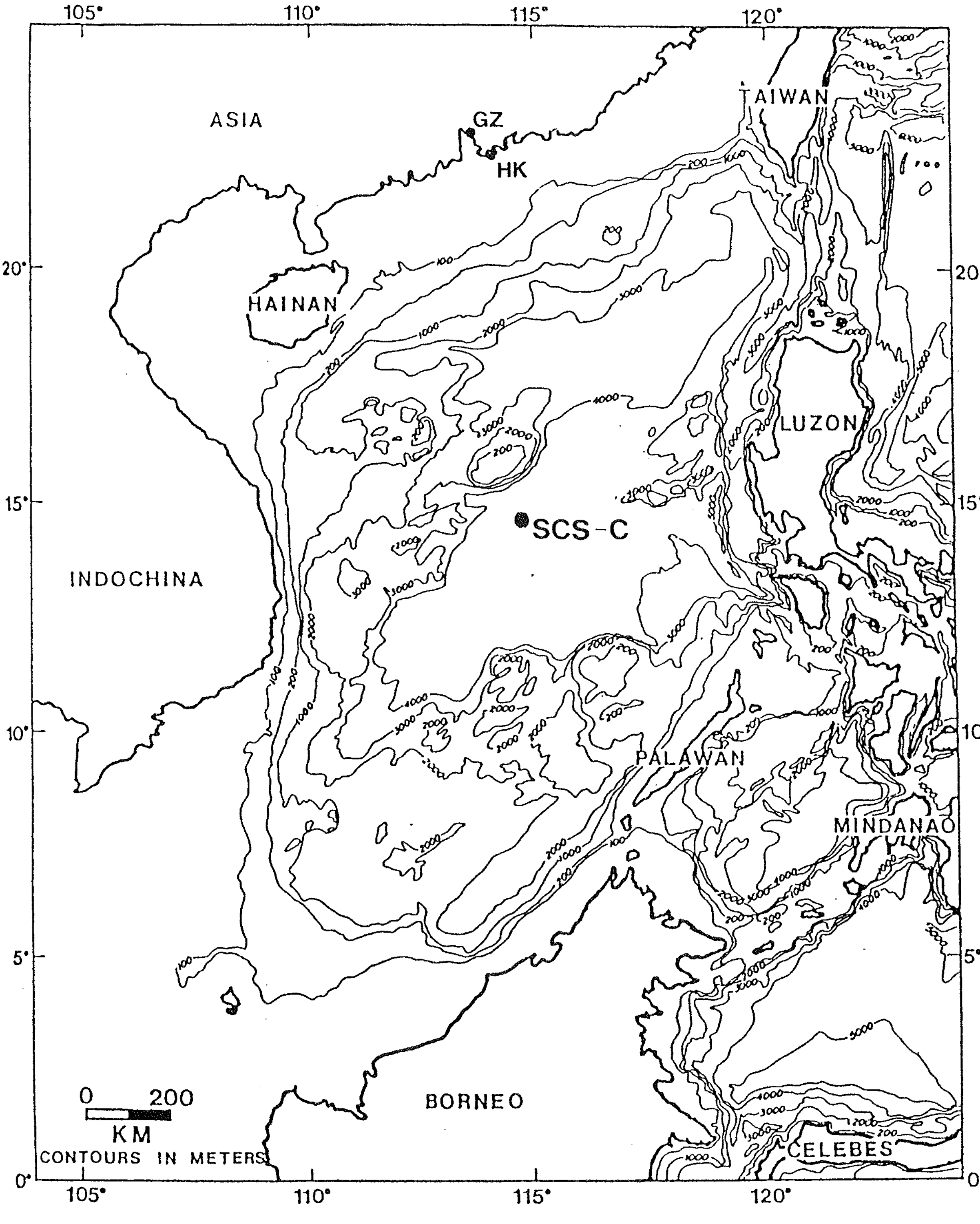

Fig.1: Location of the sediment trap system SCS-C in the South China Sea.

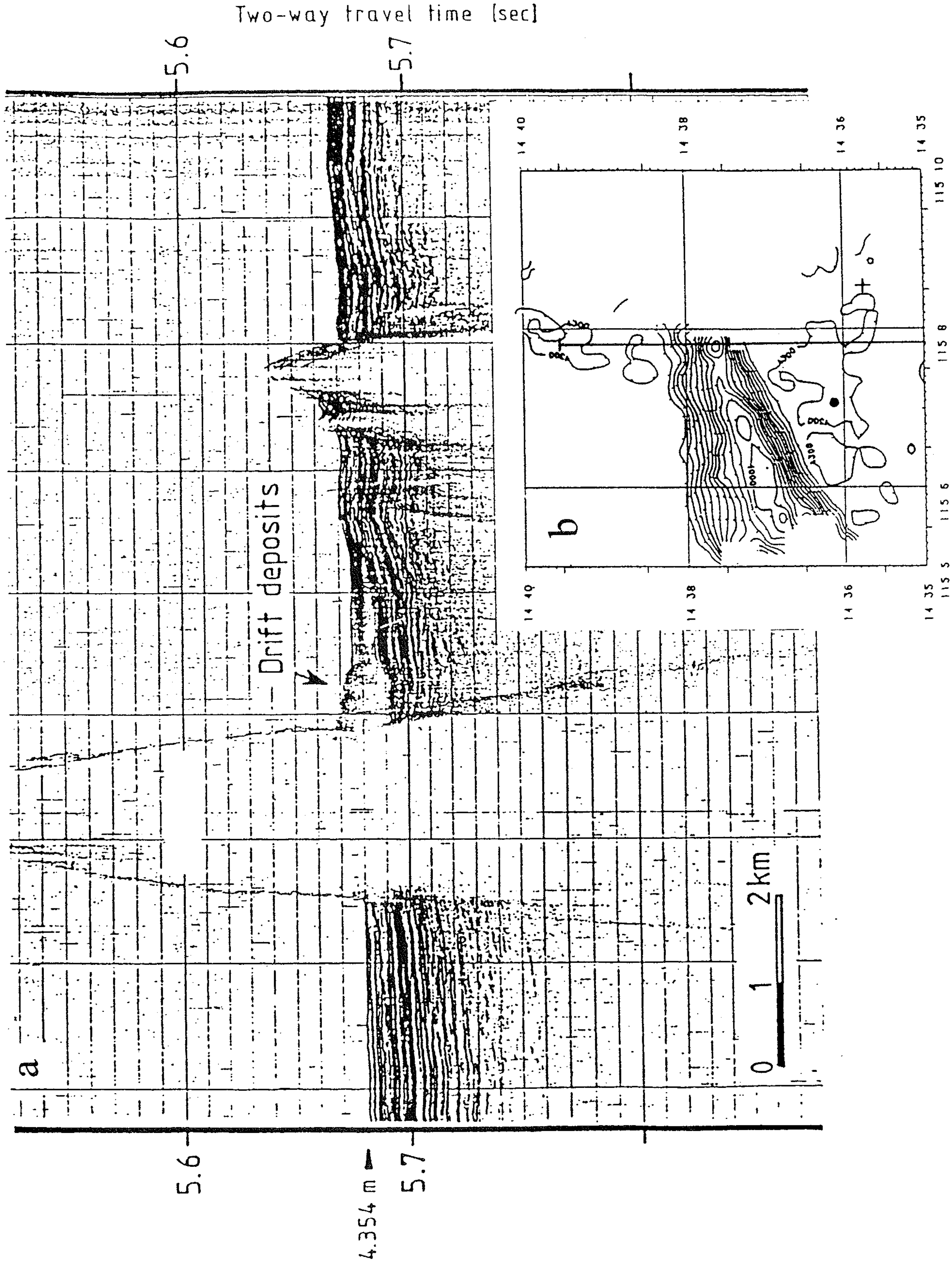

Fig. 2: a) 3.5 kHz pinger profile of 'drift deposits' on the edge of a ridge-like structure recorded during cruise 50B of R/V Sonne. b) SEABEAM bathymetric map of the area around the sediment trap station in the central South China Sea showing the track of the pinger profile and the sites of SCS-C-03 (cross) and SCS-C-04 (dot).

Mooring I.D.: SCS-C-03, Institute of Biogeochemistry and Marine Chemistry, Hamburg

Anchor Drop:

Deployment: 25.05.1993
Recovery: 25.05.1994

Mooring m.a.b.	Depths m.b.s.	Mooring Components	Deployment/Recovery Time out	on Deck
3121	1189	(1) 3 Ball Radio Float + Strobelight	06:38	10:23
		2 m Chain		
		(16) 17′ Glass Balls (20 m)		
		20 m Nylon + Wire Rope		
		2 m Chain		
3075	1235	Mark VI Sediment Trap I.D. 163	07:13	10:45
		2 m Chain		
		500 m Wire Rope	07:30	11:10
		500 m Wire Rope	07:38	11:39
		500 m Wire Rope	07:50	11:59
		500 m Wire Rope	08:10	12:25
		500 m Wire Rope	08:30	12:52
		(10) 17' Glass Balls (10 m)	08:50	
		20 m Nylon Rope		
		2 m Chain		
539	3771	Mark VI Sediment Trap I.D. 136	09:05	13:11
		2 m Chain		
		500 m Wire Rope	11:25	13:28
		(6) 17' Glass Balls (10 m)		
		2 m Chain		
25	4285	Benthos Release	11:30	13:35
		2 m Chain		
		20 m Nylon Rope		
0	4310	Anchor	11:35	

Fig. 3 : Mooring diagram of SCS-C-03 and deployment/recovery operations.

Mooring I.D.: SCS-C-04, Institute of Biogeochemistry and Marine Chemistry, Hamburg

Anchor Drop:	14°36.0' N 115°07.5' E	Deployment: 26.05.1994 Recovery:

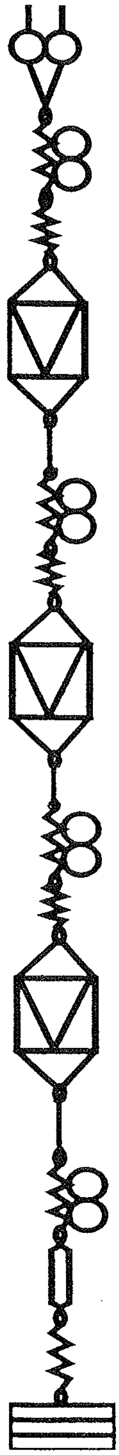

Mooring m.a.b.	Depths m.b.s.	Mooring Components	Deployment/Recovery Time out	on Deck
3134	1172	(1) 3 Ball Radio Float	06:19	
		2 m Chain		
		(14) 17' Glass Balls (10 m)		
		2 m Chain		
		20 m Nylon + Wire Rope		
		2 m Chain		
		Mark VI Sediment Trap	06:32	
		I.D. # 163		
3098	1208			
		2 m Chain		
		500 m Wire Rope	07:01	
		500 m Wire Rope	07:30	
		(12) 17' Glass Balls (9 m)		
		20 m Nylon Rope		
		2 m Chain		
		Mark VI Sediment Trap	07:42	
		I.D. # 178		
2063	2243	2 m Chain		
		500 m Wire Rope	08:11	
		500 m Wire Rope	08:39	
		500 m Wire Rope	09:14	
		(7) 17' Glass Balls (5 m)		
		20 m Nylon Rope		
		2 m Chain		
		Mark VI Sediment Trap	09:21	
532	3774	I.D. # 136		
		2 m Chain		
			09:45	
		500 m Wire Rope		
		(4) 17' Glass Balls (3 m)		
		2 m Chain		
25	4281	Benthos Release	09:50	
		2 m Chain		
		20 m Nylon Rope		
		2 m Chain		
0	4306	Anchor	09:57	

Fig. 4: Mooring diagram of SCS-C-04 and deployment operations.

	Deployment	Recovery
Date	25.05.1993	25.05.1994
Ship, Cruise No.	RV Xiangyanghong-14, XYH-93-1	RV Sonne, SO 95
Captain	Su L.	H. Bruns
Chief Scientist	Chen W.	M. Sarnthein
First Mate		G. Oellerich
Bosun	Guo K.	K.-H. Hartwig
Mooring Master	M.G. Wiesner	P. Jöhrendt
Recorder	Zheng S.	Y. Wang
Crew Hands	Ouyang D., Huang L., Ke Q., Wang T., Huang P., Cai Y.	D. Mahlmann, W. Reichmacher, H. Krüger, G. vom Berg, H. Röpti, G. Stängl
Scientific Hands	P. Jöhrendt, Wang X., Zhang P., Chen W., S. Reschke, Y. Wang, C. Gerbich	M.G. Wiesner, Y. Wang, M. Woll-schläger, R. Botz, M. Staubwasser
Weather Conditions	sea state 3-4	sea state 3-4
Release Model	Benthos 865A, SN 526 (13.5 V)	
Enable Code	2 D	
Release Code	2 A	
Mooring Top	3-Ball Radio Float (red) with Light	
Radio Type and Frequency	RF 700A-1, 156.425 Mhz, CH 68	
Type of Strobe Light, Fls/min	ST 400A Xenon, 40	
Release Armed	09:45	
Witnessed by	P. Jöhrendt, M.G. Wiesner, S. Reschke	
Mooring Position	14°35.80'N, 115°08.55'E	
Water Depth	4310 m	

Tab. 1: 1993 deployment and 1994 recovery of mooring system SCS-C-03.

Trap Depth (m)	1191
Frame No.	163
Rotator No.	163
Timer No.	178
Stepping Motor No.	178
Cup Type	Nalgene, 250 ml
Number of Cups; Code	13; SH
Type of Cupwater, Depth, Station	Seawater, 1000 m, classified
Poison Type, Concentration	Mercury Chloride, 3.33 g/l
NaCl, Concentration	33.33 g/l
Cups Proper Number	1-13, OK
Cups Proper Position	OK
Cups Proper Direction	OK
Deployed on Cup Number	Open Hole
Recovered on Cup Number	13
Timer Battery Voltage Check	
Deployment	External: 28.6 V, Internal: 2.95 V
Recovery	External: 28.0 V, Internal: 2.94 V

Tab. 2: Information on sediment trap 163 deployed and recovered on mooring system SCS-C-03.

Trap Depth (m)	3728
Frame No.	136
Rotator No.	136
Timer No.	163
Stepping Motor No.	163
Cup Type	Nalgene, 250 ml
Number of Cups; Code	13; DP
Type of Cupwater, Depth, Station	Seawater, 1000 m, classified
Poison Type, Concentration	Mercury Chloride, 3.33 g/l
NaCl, Concentration	33.33 g/l
Cups Proper Number	1-13, OK
Cups Proper Position	OK
Cups Proper Direction	OK
Deployed on Cup Number	Open Hole
Recovered on Cup Number	Open Hole
Timer Battery Voltage Check	
Deployment	External: 29.0 V, Internal: 2.95 V
Recovery	External: 28.6 V, Internal: 2.93 V

Tab. 3: Information on sediment trap 136 deployed and recovered on mooring system SCS-C-03.

Schedule Input	Schedule Confirmation	Schedule Retrieval
----SCHEDULE DATA----- Created 05/24 19:52 "SCS 93; 28 DAY " Events= 17 ----------------------- EVENT DATE TIME # 0 05/25 05:00 # 1 05/25 05:30 # 2 05/25 06:00 # 3 06/01 00:00 # 4 06/29 00:00 # 5 07/27 00:00 # 6 08/24 00:00 # 7 09/21 00:00 # 8 10/19 00:00 # 9 11/16 00:00 # 10 12/14 00:00 # 11 01/11 00:00 # 12 02/08 00:00 # 13 03/08 00:00 # 14 04/05 00:00 # 15 05/03 00:00 # 16 05/31 00:00 -----End Of Data------	----RETRIEVAL DATA---- Created 05/24 19:52 "SCS 93: 28 DAY " Retrieved 05/24 20:10 Events= 17 ----------------------- EVENT DATE TIME STEPS STATUS # 0 05/25 05:00 0 80 # 1 05/25 05:30 0 0 # 2 05/25 06:00 0 0 # 3 06/01 00:00 0 0 # 4 06/29 00:00 0 0 # 5 07/27 00:00 0 0 # 6 08/24 00:00 0 0 # 7 09/21 00:00 0 0 # 8 10/19 00:00 0 0 # 9 11/16 00:00 0 0 # 10 12/14 00:00 0 0 # 11 01/11 00:00 0 0 # 12 02/08 00:00 0 0 # 13 03/08 00:00 0 0 # 14 04/05 00:00 0 0 # 15 05/03 00:00 0 0 # 16 05/31 00:00 0 0 -----End Of Data------	----RETRIEVAL DATA---- Created 05/24 19:52 "SCS 93: 28 DAY " Retrieved 05/25 18:04 Valid Data Events= 17 ----------------------- EVENT DATE TIME STEPS STATUS # 0 05/25 05:00 88 F0 # 1 05/25 05:30 90 F0 # 2 05/25 06:00 90 F0 # 3 06/01 00:00 90 F0 # 4 06/29 00:00 89 F0 # 5 07/27 00:00 91 F0 # 6 08/24 00:00 89 F0 # 7 09/21 00:00 91 F0 # 8 10/19 00:00 89 F0 # 9 11/16 00:00 91 F0 # 10 12/14 00:00 89 F0 # 11 01/11 00:00 91 F0 # 12 02/08 00:00 89 F0 # 13 03/08 00:00 91 F0 # 14 04/05 00:00 89 F0 # 15 05/03 00:00 90 F0 # 16 05/31 00:00 0 90 -----End Of Data------

Tab. 4: 1993-1994 schedule input and retrieval for the shallow water sediment trap 163 on mooring system SCS-C-03.

Schedule Input	Schedule Confirmation	Schedule Retrieval
----SCHEDULE DATA----- Created 05/24 19:52 "SCS 93; 28 DAY " Events= 17 ---------------------- EVENT DATE TIME # 0 05/25 05:00 # 1 05/25 05:30 # 2 05/25 06:00 # 3 06/01 00:00 # 4 06/29 00:00 # 5 07/27 00:00 # 6 08/24 00:00 # 7 09/21 00:00 # 8 10/19 00:00 # 9 11/16 00:00 # 10 12/14 00:00 # 11 01/11 00:00 # 12 02/08 00:00 # 13 03/08 00:00 # 14 04/05 00:00 # 15 05/03 00:00 # 16 05/31 00:00 -----End Of Data------	----RETRIEVAL DATA---- Created 05/24 19:52 "SCS 93; 28 DAY " Retrieved 05/24 20:58 Events= 17 ---------------------- EVENT DATE TIME STEPS STATUS # 0 05/25 05:00 0 80 # 1 05/25 05:30 0 0 # 2 05/25 06:00 0 0 # 3 06/01 00:00 0 0 # 4 06/29 00:00 0 0 # 5 07/27 00:00 0 0 # 6 08/24 00:00 0 0 # 7 09/21 00:00 0 0 # 8 10/19 00:00 0 0 # 9 11/16 00:00 0 0 # 10 12/14 00:00 0 0 # 11 01/11 00:00 0 0 # 12 02/08 00:00 0 0 # 13 03/08 00:00 0 0 # 14 04/05 00:00 0 0 # 15 05/03 00:00 0 0 # 16 05/31 00:00 0 0 -----End Of Data------	

Tab. 5: 1993-1994 schedule input and retrieval for the deep water sediment trap 136 on mooring system SCS-C-03.

	Deployment	Recovery
Date	26.05.1994	
Ship, Cruise No.	RV Sonne, SO 95	
Captain	H.Bruns	
Chief Scientist	M. Sarnthein	
First Mate	G. Oellerich	
Bosun	K.-H. Hartwig	
Mooring Master	P. Jöhrendt	
Recorder	Y. Wang	
Crew Hands	D. Mahlmann, W. Reichmacher, H. Krüger, G. vom Berg, H. Röpti, G. Stängl	
Scientific Hands	M.G. Wiesner, Y. Wang, M. Woll-schläger, R. Botz, M. Staubwasser	
Weather Conditions	sea state 4-5	
Release Model	Benthos 865A, SN 526 (13.5 V)	
Enable Code	2 D	
Release Code	2 A	
Mooring Top	3-Ball Radio Float (red) with Light	
Radio Type and Frequency	RF 700A-1, 156.425 Mhz (CH 68)	
Type of Strobe Light, Fls/min	ST 400A Xenon, 40	
Release Armed	09:47	
Witnessed by	P. Jöhrendt, M.G. Wiesner, M. Wollschläger, Y. Wang	
Mooring Position	14°36.2'N, 115°07.1'E	
Water Depth	4306 m	

Tab. 6: 1994 deployment of mooring system SCS-C-04.

Trap Depth (m)	1208
Frame No.	163
Rotator No.	136
Timer No.	178
Stepping Motor No.	178
Cup Type	Nalgene, 250 ml
Number of Cups; Code	13; SH
Type of Cupwater, Depth, Station	Seawater, 1250 m, 17953-5 GIK
Poison Type, Concentration	Mercury Chloride, 3.33 g/l
NaCl, Concentration	33.33 g/l
Cups Proper Number	1-13, OK
Cups Proper Position	OK
Cups Proper Direction	OK
Deployed on Cup Number	Open Hole
Recovered on Cup Number	
Timer Battery Voltage Check	
Deployment	External: 28.6 V, Internal: 2.95 V
Recovery	

Tab. 7: Information on sediment trap 163 deployed on mooring system SCS-C-04.

Trap Depth (m)	3774
Frame No.	136
Rotator No.	136
Timer No.	163
Stepping Motor No.	163
Cup Type	Nalgene, 250 ml
Number of Cups; Code	13; DP
Type of Cupwater, Depth, Station	Seawater, 4000 m, 17953-5 GIK
Poison Type, Concentration	Mercury Chloride, 3.33 g/l
NaCl, Concentration	33.33 g/l
Cups Proper Number	1-13, OK
Cups Proper Position	OK
Cups Proper Direction	OK
Deployed on Cup Number	Open Hole
Recovered on Cup Number	
Timer Battery Voltage Check	
Deployment	External: 28.5 V, Internal: 2.93 V
Recovery	

Tab. 9: Information on sediment trap 136 deployed on mooring system SCS-C-04.

Trap Depth (m)	2243
Frame No.	178
Rotator No.	178
Timer No.	136
Stepping Motor No.	136
Cup Type	Nalgene, 250 ml
Number of Cups; Code	13; MW
Type of Cupwater, Depth, Station	Seawater, 2000 m, 17953-5 GIK
Poison Type, Concentration	Mercury Chloride, 3.33 g/l
NaCl, Concentration	33.33 g/l
Cups Proper Number	1-13, OK
Cups Proper Position	OK
Cups Proper Direction	OK
Deployed on Cup Number	Open Hole
Recovered on Cup Number	
Timer Battery Voltage Check	
Deployment	External: 28.6 V, Internal: 2.94 V
Recovery	

Tab. 8: Information on sediment trap 178 deployed on mooring system SCS-C-04.

Schedule Input	Schedule Confirmation	Schedule Retrieval
-----SCHEDULE DATA----- Created 05/18 10:56 "SCS-C SH 94/95 " Events= 16 ------------------------ EVENT DATE TIME # 0 05/25 19:05 # 1 05/25 23:55 # 2 06/01 00:01 # 3 06/29 00:01 # 4 07/27 00:01 # 5 08/24 00:01 # 6 09/21 00:01 # 7 10/19 00:01 # 8 11/16 00:01 # 9 12/14 00:01 # 10 01/11 00:01 # 11 02/08 00:01 # 12 03/08 00:01 # 13 04/05 00:01 # 14 05/03 00:01 # 15 05/31 00:01 -----End Of Data------	----RETRIEVAL DATA---- Created 05/18 10:56 "SCS-C SH 94/95 " Retrieved 05/25 19:27 Valid Data Events= 16 ------------------------ EVENT DATE TIME STEPS STATUS # 0 05/25 19:20 90 E0 # 1 05/25 23:55 0 80 # 2 06/01 00:01 0 0 # 3 06/29 00:01 0 0 # 4 07/27 00:01 0 0 # 5 08/24 00:01 0 0 # 6 09/21 00:01 0 0 # 7 10/19 00:01 0 0 # 8 11/16 00:01 0 0 # 9 12/14 00:01 0 0 # 10 01/11 00:01 0 0 # 11 02/08 00:01 0 0 # 12 03/08 00:01 0 0 # 13 04/05 00:01 0 0 # 14 05/03 00:01 0 0 # 15 05/31 00:01 0 0 -----End Of Data------	

Tab. 10: 1994-1995 schedule input for the shallow water sediment trap 163 on mooring system SCS-C-04.

Schedule Input	Schedule Confirmation	Schedule Retrieval
----SCHEDULE DATA----- Created 05/18 10:56 "SCS- 94/95 " Events= 16 ---------------------- EVENT DATE TIME # 0 05/20 17:00 # 1 05/20 17:25 # 2 06/01 00:01 # 3 06/29 00:01 # 4 07/27 00:01 # 5 08/24 00:01 # 6 09/21 00:01 # 7 10/19 00:01 # 8 11/16 00:01 # 9 12/14 00:01 # 10 01/11 00:01 # 11 02/08 00:01 # 12 03/08 00:01 # 13 04/05 00:01 # 14 05/03 00:01 # 15 05/31 00:01 -----End Of Data------	----RETRIEVAL DATA---- Created 05/18 10:56 "SCS- 94/95 " Retrieved 05/20 10:22 Events= 16 ---------------------- EVENT DATE TIME STEPS STATUS # 0 05/20 17:00 0 80 # 1 05/20 17:25 0 0 # 2 06/01 00:01 0 0 # 3 06/29 00:01 0 0 # 4 07/27 00:01 0 0 # 5 08/24 00:01 0 0 # 6 09/21 00:01 0 0 # 7 10/19 00:01 0 0 # 8 11/16 00:01 0 0 # 9 12/14 00:01 0 0 # 10 01/11 00:01 0 0 # 11 02/08 00:01 0 0 # 12 03/08 00:01 0 0 # 13 04/05 00:01 0 0 # 14 05/03 00:01 0 0 # 15 05/31 00:01 0 0 -----End Of Data------	

Tab. 11: 1994-1995 schedule input for the mid-water sediment trap 178 on mooring system SCS-C-04.

Schedule Input	**Schedule Confirmation**	**Schedule Retrieval**
----SCHEDULE DATA----- Created 05/18 10:56 "SCS-C DP 94/95 " Events= 16 ----------------------- EVENT DATE TIME # 0 05/25 23:00 # 1 05/25 23:55 # 2 06/01 00:01 # 3 06/29 00:01 # 4 07/27 00:01 # 5 08/24 00:01 # 6 09/21 00:01 # 7 10/19 00:01 # 8 11/16 00:01 # 9 12/14 00:01 # 10 01/11 00:01 # 11 02/08 00:01 # 12 03/08 00:01 # 13 04/05 00:01 # 14 05/03 00:01 # 15 05/31 00:01 ------End Of Data------	----RETRIEVAL DATA---- Created 05/18 10:56 "SCS-C DP 94/95 " Retrieved 05/25 22:03 Events= 16 ----------------------- EVENT DATE TIME STEPS STATUS # 0 05/25 23:00 0 80 # 1 05/25 23:55 0 0 # 2 06/01 00:01 0 0 # 3 06/29 00:01 0 0 # 4 07/27 00:01 0 0 # 5 08/24 00:01 0 0 # 6 09/21 00:01 0 0 # 7 10/19 00:01 0 0 # 8 11/16 00:01 0 0 # 9 12/14 00:01 0 0 # 10 01/11 00:01 0 0 # 11 02/08 00:01 0 0 # 12 03/08 00:01 0 0 # 13 04/05 00:01 0 # 14 05/03 00:01 0 # 15 05/31 00:01 0 ------End Of Data------	

Tab. 12: 1994-1995 schedule input for the deep water sediment trap 136 on mooring system SCS-C-04.

3.11 FIRST OBSERVERVATIONS ON PLANKTONIC FORAMINIFERA

U. Pflaumann (University of Kiel)

In 22 samples of cores 17939 and 17940 the planktonic foraminiferal species were counted to obtain a first confirmation of lithostratigraphy. The technical procedure followed Pflaumann (1986): Washing over a 63 mm sieve, splitting the residuals to a suitable sample size of > 200-300 specimens by an OTTO microsplitter, dry sieving into grain size fractions >150 mm, 200 mm, 250 mm, 315 mm, 500 mm, and 630 mm, and counts of all subfractions.

The samples of cores 17939 and 17940 (Fig. 1) contain mainly tropical/ subtropical species, though in the deeper parts of the cores also cold species such as *Neogloboquadrina pachyderma* (right) and occasionally *Globigerina quinqueloba* occur. Following Li BH (1994) we plotted the percentages of *Pulleniatina obliquiloculata* and *Globorotalia inflata*. In core 17940 these fluctuations of percentages closely parallel the curves published from SOA core 255 from the Okinawa Trough, East China Sea. Based on an oxygen isotope record of the South China Sea core RC12-350 (Zhimin, 1992), both the decline of cool temperate *G. inflata* and the onset of a high abundance of the tropical species *P. obliquiloculata* in South China Sea core TSTD 12G (Rottman, 1979) match the beginning of stage 1. In core 17940 this level occurs at 700 cm core depth, in core 17939 somewhat less distinct between 600 and 800 cm depth. These age estimates lead to preliminary estimates of the local sedimentation rate in the range of more than 50 cm/1000 years on that part of the South China continental margin. These values are in good accordance with values derived from $CaCO_3$ curves (see Section on Carbonate Records, etc., this vol.).

REFERENCES

Jian, Zhimin, 1992, Sea surface temperatures on the southern continental slope of the South China Sea since the last Glacial and their comparison with those on the northern slope. - in: Zhizheng, YE and Wang PX, eds.: Contribution to late Late Quaternary Paleoceanography of the South China Sea (Qingdao Ocean Univ. Press), 78-87.

Li BH, 1994, Paleoceanographic records in the southern Okinawa trough since the last 20,000 years. - M.sc. Thesis Tongji Univ. Shanghai, 51 pp.

Pflaumann, U., 1986, Sea-surface temperatures during the last 750,000 years in the eastern equatorial Atlantic: Planktonic foraminiferal record of 'Meteor' cores 13519, 13521, and 16415. - 'Meteor' Forschungsergebnisse C40, 137-162.

Rottman, M.L., 1979, Dissolution of planktonic foraminifera and pteropods in the South China Sea sediments. - J. Foram. Res. 9, 41-49.

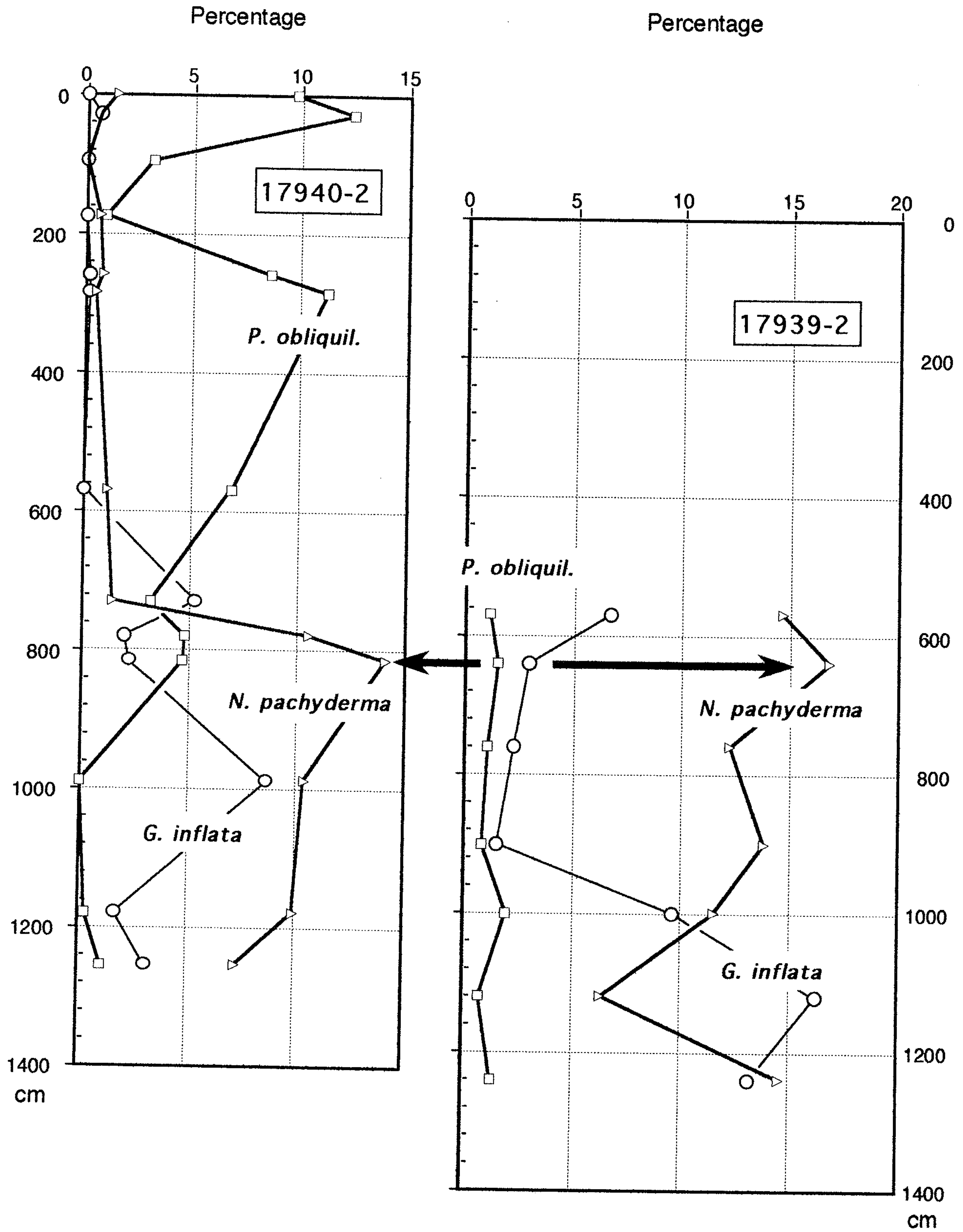

Figure 1. Percentages of planktonic foraminifera species in cores 17939 and 17940, which are indicative of warm (*P. obliquiloculata*), intermediate (*G. inflata*), or cool (*N. pachyderma* d.) sea surface temperatures.

3.12 BENTHIC FORAMINIFERA (SONNE-95 CRUISE)

W. Kuhnt and S. Hess (University of Kiel)

BENTHIC FORAMINIFERAL ECOLOGY (SURFACE DISTRIBUTION)

Objectives:

- Observation of distribution patterns, feeding strategies, and population dynamics of benthic foraminifera at the sediment-water interface and in the uppermost part of the sediment column
- Examination of patchiness of benthic foraminiferal communities in surface sediments
- Correlation of benthic foraminiferal distribution patterns to small scale changes in sediment substrates and microenvironment (i.e., areas with a thick fluff layer above depressions in the sediment surface vs. winnowed areas on small scale sediment ridges)

Sample material:

- Surface water sucked out of the box corer. This water contained benthic foraminifera living in the fluffy layer above the sediment water interface, occasionally komokiaceans (at deeper stations) and other epifaunal benthic foraminifera.
- Macroscopically visible larger agglutinated foraminifera that were collected from the box core surface (mainly species of the genera *Saccorhiza, Astrorhiza, Rhizammina* and *Rhabdammina* as well as rare Komokiacea).
- Standard surface sediment samples (0-1cm and 0-3 cm) of all box cores
- Multiple surface samples of high quality box cores, where no significant washout of the sediment/water interface was observed. Samples were taken with 100 cm^2 gridnets at four different positions on the box core surface to observe patchiness in the surface distribution of benthic foraminifera.

All surface samples were immediately preserved in a methanol-Rose Bengal solution and stored away for identification and counts of of living (stained) vs. dead specimens.

In some well preserved deep-water box cores observations of epifaunal suspension feeders and detritus feeders (i.e., agglutinated foraminifera of the komokiacea and astrorhizidae groups) in life position were possible.

Benthic foraminifera from different substrates were sampled in box cores with a distinct and well preserved small scale surface morphology. In these cases the benthic foraminiferal samples were carefully placed to obtain a wide range of micro-environments and the surface morphology and sample position was documented by sketches and photographs (fig. 1).

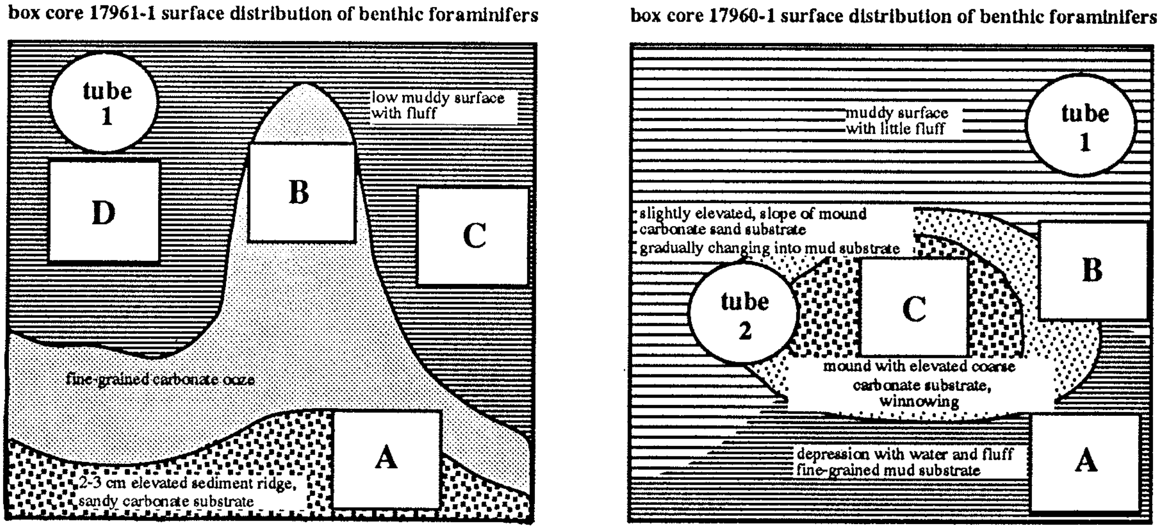

Fig.1: Sampling strategy of box core surfaces with variable micro-environments.

A preliminary shipboard examination of surface samples from 18 selected boxcores led to the following (very preliminary) observations:

1. Agglutinated foraminifera generally dominate the benthic assemblages. Indicator species of oligotrophic environments such as komokiaceans and *Karrerulina apicularis* occur in unusually shallow water depths (up to 2000 m) in the northern and central part of the south China Sea, indicating extremely low export fluxes of organic material which serves as food for benthic foraminifers.

2. Characteristic "high productivity" (HPR) benthic foraminiferal assemblages seem to be restricted to shallow sites were the redox line is close to the sediment surface, but may also occur at deeper stations in the southern part of the South China Sea (fig.2). These assemblages are characterized by common *Uvigerina* spp. Additionally other elongate infaunal calcareous benthic foraminiferal morphotypes occur (i.e. *Bolivina, Globobulimina,* and *Bulimina*) that have been identified as indicators of high organic flux and low oxygen conditions in the North Atlantic (Altenbach, 1988). Such areas with higher organic flux rates are located along the Sunda slope (stations 17963, 17965, and 17960) and at the shallowest part of the transect southwest of Hongkong (station 17929).

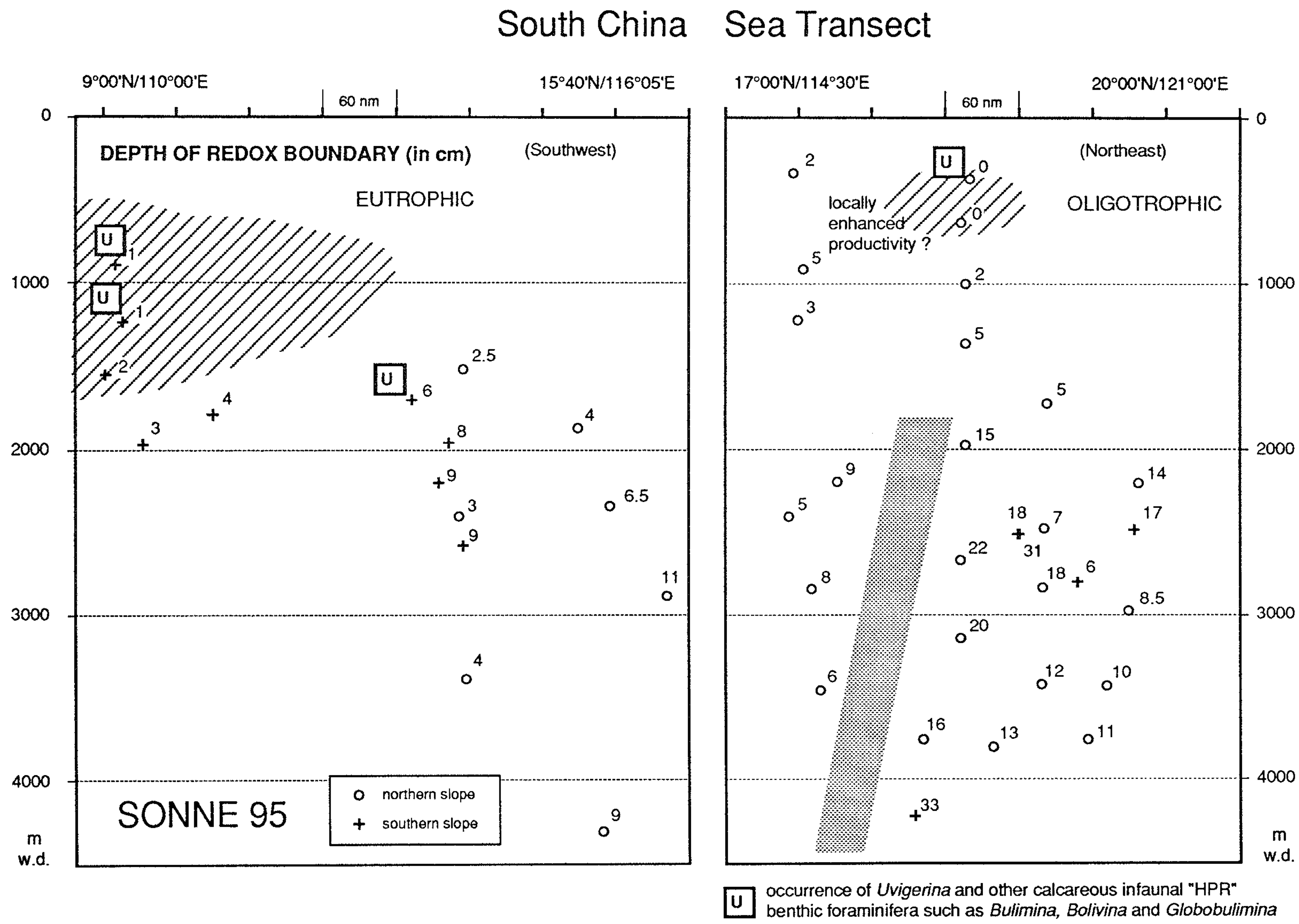

Fig.2: Export flux of OM estimated from depth of redox boundary and benthic foraminiferal assemblages in surface sediments. Hatched areas indicate potential oxygen minimum zones.

BENTHIC FORAMINIFERAL MICROHABITATS (DOWNCORE DISTRIBUTION)

Objectives:

- To record the microhabitat of benthic foraminiferal species in various bathymetric and paleoceanographic settings.
- To examine possible correlations between the distribution of infaunal species and redox conditions. Check for an abundance maximum near the redox boundary.
- To record possible changes in distribution patterns across the upper and lower boundaries of the oxygen minimum zone.
- To test the correlation of microhabitat groups and the flux of organic matter to the sea floor.
- To utilize the microhabitat distribution of benthic foraminifera as a monitor of seasonal (pulsed) organic flux.

Sample material:

- Depending on the position of the redox line, water depth, and sedimentation rate the upper 10 to 20cm of the sediment column were extruded from 10cm diameter pushcores, cut into 1 cm slices and preserved in a methanol - Rose Bengal solution. Each slice represents an 81 cc sediment volume and foraminiferal abundances can be easily normalized to either sediment volume or weight once the physical properties data (water content, bulk density) are available.

RECOLONIZATION OF DISTURBED ASHFALL SUBSTRATES BY BENTHIC FORAMINIFERS

One of the most exciting findings of Sonne 95 cruise are several box cores that contain modern ash layers, most probably resulting from the 1991 eruption of Mount Pinatubo, Philippines. The presence of these layers offers the unique opportunity to study the recolonization of a catastrophically disturbed deep sea substrate by benthic foraminifera. A first shipboard census count of Rose bengal stained benthic foraminifera from a 20 square centimeter surface area on top of the more than 6 cm thick ashfall layer at GIK station 17920 shows the following assemblage composition (fig. 3):

The total number of benthic foraminifers (124 specimens) is extremely low and the ratio of living individuals (43) to empty tests (81) is unusually high. This is an indication of a "young", recently immigrated population. Specific diversity is low, with a significant dominance of two species of the genus *Reophax* (*R. scorpiurus* and *R. bilocularis*).

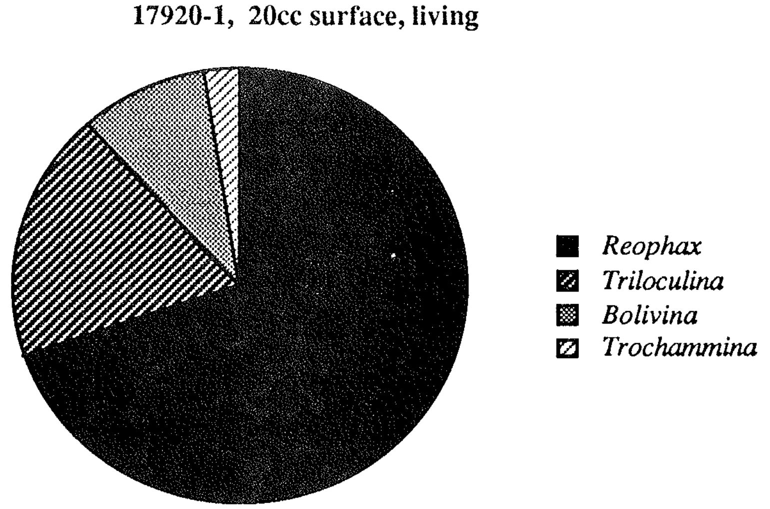

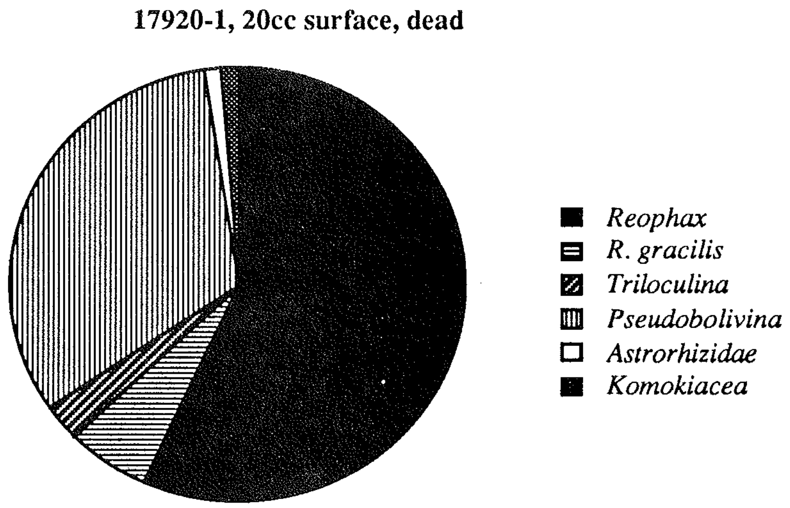

Fig. 3: Benthic foraminiferal community composition of the surface sample of box core 17920 (Philippine margin), above a > 6cm thick ash layer.

With more material examined it may be possible to biometrically distinguish macrospheric and microspheric (sexually reproduced) tests and thus learn more about migration processes of deep water benthic foraminifera. Interestingly enough the genus *Reophax* has been reported among the first recolonizers of destroyed substrates at the HEBBLE site in the Northwest Atlantic (Kaminski, 1985) and in a recolonization tray experiment in the Panama Basin (Kaminski et al., 1988). Moreover, significantly increased numbers of *Reophax* occur in sediments immediately overlying the K/T boundary layer in the Gubbio section (Central Italy) and along the Basque coast (Kuhnt, 1990; Kuhnt and Kaminski, 1993). The material recovered during the Sonne 95 cruise will thus serve as base for a recolonization study which may allow to recognize spatial recolonization patterns, reconstruct the succession of recolonizers and enable a precise timing of the recolonization process.

TAPHONOMY OF AGGLUTINATED BENTHIC FORAMINIFERA

Objectives:

- To observe early diagenetic changes in agglutinated foraminiferal tests within different microenvironments.
- To examine the fossilization potential of different groups of agglutinated foraminifera as related to different sedimentary facies.
- To compare the species composition of Holocene fossil assemblages with the community structure of living populations.

Sample material:

Box core subsamples (push cores) of the uppermost 40-50 cm of the sediment column (this sampling program was combined with the microhabitat studies, i.e., the methanol-preserved samples of the uppermost 10-20 cm of each push core will be used for both projects). The lower part of the pushcore was subdivided into 1 cm and/or 2 cm slices; the subsamples were sealed in plastic bags and stored for laboratory processing.

Laboratory analysis will include SEM studies of the wall structure of agglutinated foraminifera in different stages of preservation (living-dead-early diagenetic overprint). With these studies we shall try to relate the degree of decay of organic cement of agglutinated foraminifera to various wall structure types and to different environmental/early diagenetic conditions.

REFERENCES

Altenbach, A.V. (1988): Deep-sea benthic foraminifera and flux rate of organic carbon. - Revue de Paléobiologie , 2, 719-720.

Kaminski, M.A. (1985): Evidence for control of abyssal agglutinated community structure by substrate disturbance: Results from the HEBBLE Area. - Marine Geology, 66, 113-131.

Kaminski, M.A., J. F. Grassle and R. B. Whitlatch (1988): Life History and Recolonization among Agglutinated Foraminifera in the Panama Basin. In: Gradstein, F. M., and F. Rögl(eds.), Second International Workshop on Agglutinated Foraminifera, Vienna 1986, Proceedings. - Abh. geol. Bundesanst. Wien, 41, 229-244.

Kuhnt, W. (1990): Agglutinated foraminifera of Western Mediterranean Upper Cretaceous pelagic limestones (Umbrian Apennines, Italy, and Betic Cordillera, Spain). - Micropaleontology, 36/4, 297-330.

Kuhnt, W. and M. A. Kaminski (1993): Changes in the community structure of deep-water agglutinated foraminifers across the K/T boundary in the Basque Basin (Northern Spain). - Rev. Española de Micropaleontologia, 25, 57-92.

3.13 NANNOPLANKTON SAMPLING ON SONNE-95 CRUISE

P-X. WANG (Tongji University, Shanghai)

The distribution of calcareous nannoplankton in surface sediments has been repeatedly studied (Chen and Shien, 1982; Chen, 1992 a, b), but its distribution in water has only been mentioned in a general study of nannoplankton in the West Pacific marginal seas (Okada and Honjo, 1975). Further studies of nannoplankton in water samples are essential for any improvement of our paleoenvironmental interpretation of nannofossils.

Therefore, surface water from 39 stations of the cruise has been sampled to investigate the distribution of calcareous nannoplankton in the South China Sea. The water samples have been taken from 6 m below the sea surface at each station, and in most cases, 1500cc water has been filtered immediately on board using filters with a 0.45 micron diameter. The filters will be examined for coccoliths in Shanghai.

REFERENCES

Chen, M.-P. and K.-S. Shieh (1982): Recent nannofossil assemblages in sediments from Sunda Shelf to abyssal plain, South China Sea. - Proc. Nat. Counc. China (A), Taipei, 6(4), 250-285.

Cheng, X.-R. (1992a): Calcareous nannofossils in surface sediments of the central and northern parts of the South China Sea. - J. Micropaleontology, London, 11(2), 167-176.

Cheng, X.-R. (1992b): Distribution of calcareous nannofossil abundance in late Quaternary sediments from central and northern parts of South China Sea: a preliminary study. In: Ye,, Z. and P. Wang (eds.), Contributions to Late Quaternary Paleoceanography of the South China Sea. (Qingdao Ocean University Press), 274-282 (in Chinese, with English abstract).

Okada, H. and S. Honjo (1975): Distribution of coccolithophores in marginal seas along the Western Pacific Ocean and in the Red Sea. - Marine Biology, 31: 271-285.

3.14 AIR - DUST SAMPLING ON SONNE-95 CRUISE

P-X WANG (Tongji University, Shanghai)

Eolian dust in sediments provides direct evidence for paleo-atmospheric circulation. Moreover, information about the modern air dust is needed for evaluation of its variations in the past. In view of the absence of modern air dust data from the South China Sea area, an experiment has been made to collect air dust during the cruise.

An air sampling pump (KB-120E type) set up on the upper front deck of the ship was used for this purpose, and a total of 30 samples were collected by the end of the cruise. For each sample, about 28 to 172 cubic meter of air (4 to 24 hours of pumping with 120 liter per minute) were filtered. Probably because of the low content of air dust in the South China Sea area, the weight of the dust samples is below the sensitivity of the balance available on board.

3.15 EARLY DIAGENESIS IN SEDIMENTS OF THE SOUTH CHINA SEA (SONNE-95 CRUISE)

R. Botz (University of Kiel)

General

Marine sediments that contain in- and metastable primary minerals such as volcanic glass, opal-A, high-magnesian-calcite, or aragonite and reactive organic matter are particularly subject to diagenetic alteration. Diagenetic reactions may include both aerobic and various anaerobic degradation mechanisms of organic matter frequently linked to authigenic mineral formation. These minerals may form a major constituent in the sediment. Hence the study of authigenic mineral formation may provide both important information on postsedimentary processes and, perhaps more importantly, insights into the fluxes of sediment particles and their environmental control.

Sediments from the South China Sea contain organic carbon contents reaching up to 2.2 % (Calvert et al., 1993). Moreover, volcanic ashes, primary opal-A (diatom and radiolarian shells) and / or metastable carbonate minerals such as aragonitic pteropod shells are common. Hence we can expect a broad spectrum of early diagenetic reactions.

Samples

Gravity and piston core sections of SONNE-95 cruise contain at many depths (semi-) consolidated "concretion-like" particles of cm-size and irregular shape (compare core descriptions). The particles are medium to dark greenish. Apparently they are carbonate-cemented. Occasionally the concretions are aggregated to cm-thick layers. Based on their green color and their carbonate content these particles may originate from both diagenetic Fe-reduction and carbonate cementation processes (using dissolved pteropode carbonate and oxidized organic matter as probable carbon sources). Potential iron sources are volcanic ash particles such as basaltic glass, amphibole, pyroxene and detritic material. Although we do not know the relative importance of the various diagenetic processes within South China Sea sediments Fe-reduction follows aerobic oxidation-, denitrification- and Mn-reduction (in order of the electron acceptors used up during the oxidation of organic matter). Diagenetic carbonates may possibly have formed due to an increase in carbonate alkalinity caused by primary dissolution of aragonite and / or early anaerobic oxidation of organic matter during SO4--and CO2 reduction processes. Although these processes were not investigated during our cruise biogenic methane formation is likely to occur at sites 61 to 65 with extreme sedimentation rates of 15 to 30 cm/ka (Sarnthein pers. comm.). Stable carbon isotope analyses of diagenetic carbonate minerals indicate the (various) carbon sources used for diagenetic mineral formation (Irwin et al., 1977). Accordingly, the stable carbon isotopic composition of diagenetic carbonate minerals from South China Sea sediments could show a wide range of 13C values from approximately -25 to +20 %o depending on the carbon source used.

Pore water samples were obtained from sediments in both the box corers (GKG; approx. 40 cm d.b.s.) and gravity and piston core catchers (approx. 700 cm to 1300 cm d.b.s.) for oxygen isotope analyses to relate the 18O values of diagenetic carbonate minerals to the 18O content of the pore water. From these values we plan to calculate the precipitation temperatures of diagenetic minerals.

REFERENCES

Calvert, S.E., T.F. Pedersen and R. C. Thunell (1993): Geochemistry of the surface sediments of the Sulu and South China Seas. - Mar. Geol., 114, 207-231.

Irwin, H., C. Curtis and M. Coleman (1977): Isotopic evidence for source of diagenetic carbonates formed during burial of organic rich sediments. - Nature, 269, 209-213.

4. GENERAL EXPERIENCES - ACKNOWLEDGMENTS

The SONNE-95 cruise had the rare opportunity to sail in the South China Sea during the optimum weather window of the spring saison, after the end of winterly monsoon winds and well before the typhoon season. The only exception was one single typhoon cell we encountered immediately prior to the final port call in Hongkong. As a result of the excellent weather conditions we were able to obtain outstanding core recovery with regard to numbers of stations, core length, and core quality. Additionally, the deployment of sediment traps and all sorts of valuable shipboard observations were significantly facilitated during the optimum weather window. We like to gratefully acknowledge the *German Bundesminister für Forschung und Technologie (BMFT)* in Bonn for providing the optimum shiptime on board of RV SONNE and for generously funding this cruise. In particular, we acknowledge the special care of the *project managers at BEO* Rostock-Warnemünde. The *Tongji University*, Shanghai, and the *State Oceanography Administration of China (SOA)* helped funding the Chinese members of this cruise.

We owe our cordial thanks to captain Bruns and his crew for their great sympathy and extreme readiness to assist our projects on board. These thanks especially apply to boatswain Hartwig and his seamen for their assistance with coring and deployment of sediment traps, furthermore, to the electronicians and the other members of the Scientific-Technical Survey (WTD).

The SONNE-95 cruise strongly benefitted from the international composition of the scientific shipboard party and the cordial and fruitful cooperation between the scientists and technicians, many of them providing an interesting specialized knowhow in the field of marine sciences and contributing to a multidisciplinary approach of this project. 7 and 15 scientists came from Hamburg and Kiel, 7 scientists from the mainland of China (from three institutions), 2 scientists from two institutions on Taiwan, 1 scientist from Canada, and 1 scientist from Spain (supported by the European Human Mobility Program).

The cruise operated in an area of multiple complex national interests. We acknowledge with thanks the readiness of the various ambient states of the South China Sea to provide us with working permissions and last not least, the help of the German Foreign Office in procuring these permissions. Finally, we like to emphasize that we won't forget the friendly welcome party given by the State Oceanography Administration of China (SOA) during our port call in Guangzhou.

Michael Sarnthein and the Shipboard Scientific Party

Geol.-Paläont. Inst. Univ. Kiel, Berichte-Reports

Nr. 68

Editors: Sarnthein, M. (Chief Scientist);
Pflaumann, U.; Wang, P. X.; Wong, H. K. (Senior Scientists)

PRELIMINARY REPORT ON SONNE-95 CRUISE
"MONITOR MONSOON" TO THE SOUTH CHINA SEA

Erratum

1) Please add the following address to the list of participating institutions:

SCSI
South China Sea Institute of Oceanology
Academia Sinica
164 West Xingang Road, Guangzhou
Guangdong 510301/China
FAX: 0086-20-4451672

2) Please replace the following figures in §3.7 :

- Figure 1. 17924,
- Figure 2. 17931,
- Figure 3. 17933,
- Figure 7. 17964.

Kiel, Mon. Aug. 15, 1994

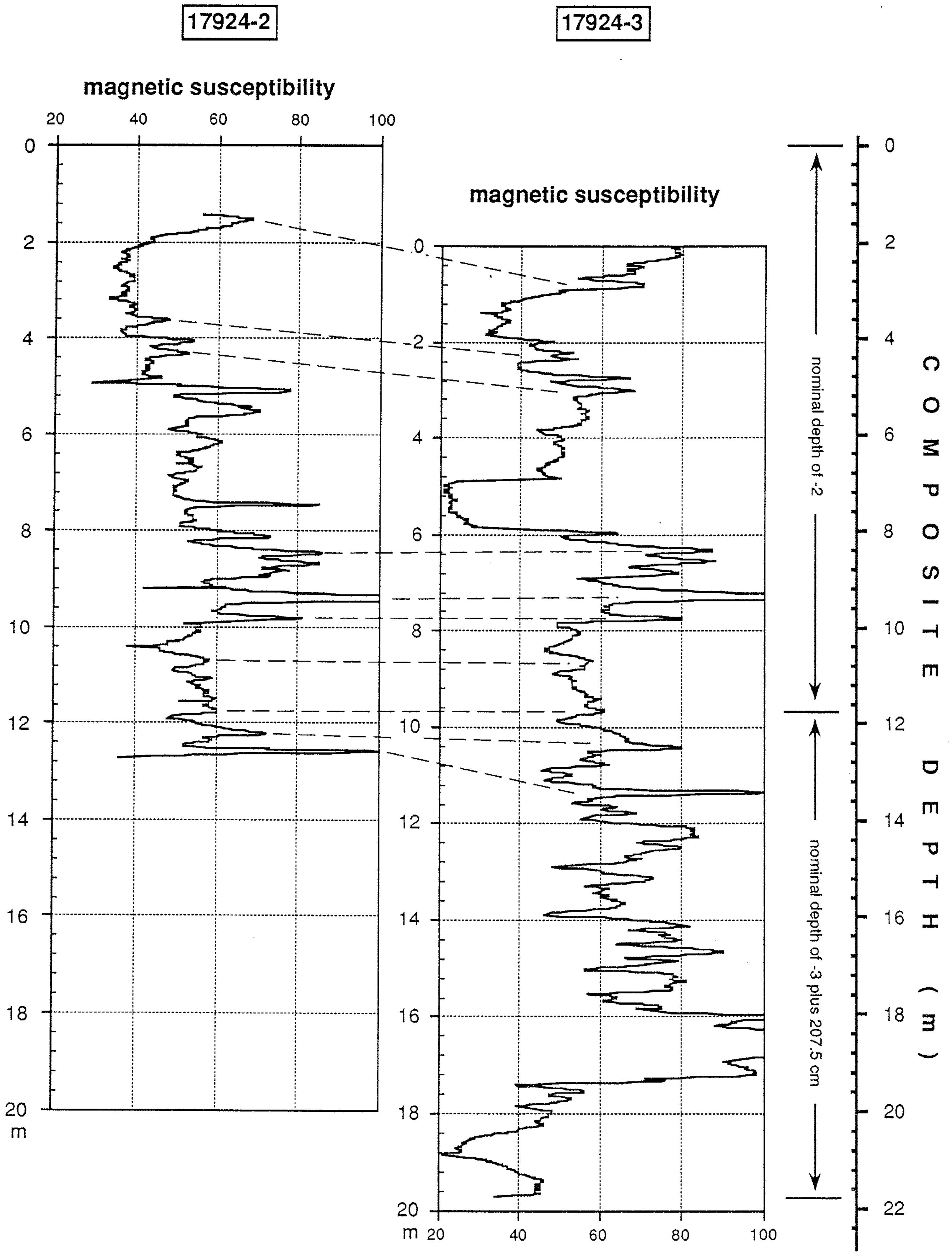

17924-2
17924-3
magnetic susceptibility
magnetic susceptibility
nominal depth of -2
nominal depth of -3 plus 207.5 cm
COMPOSITE DEPTH (m)
m

§3.7, Figure 1.

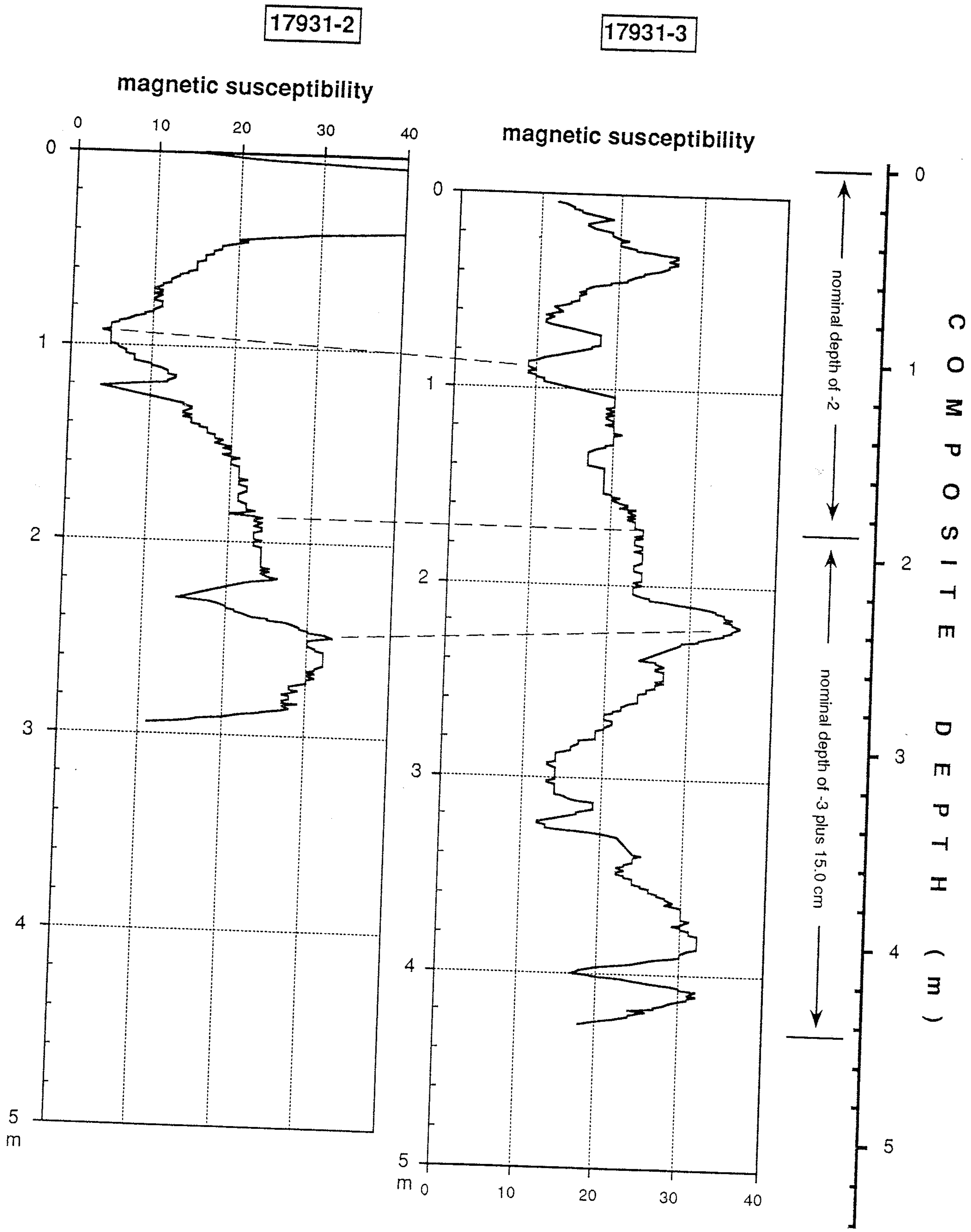
17931-2
magnetic susceptibility
17931-3
magnetic susceptibility
0
10
20
30
40
0
1
2
3
4
5
m
nominal depth of -2
nominal depth of -3 plus 15.0 cm
COMPOSITE DEPTH (m)

§3.7, Figure 2.

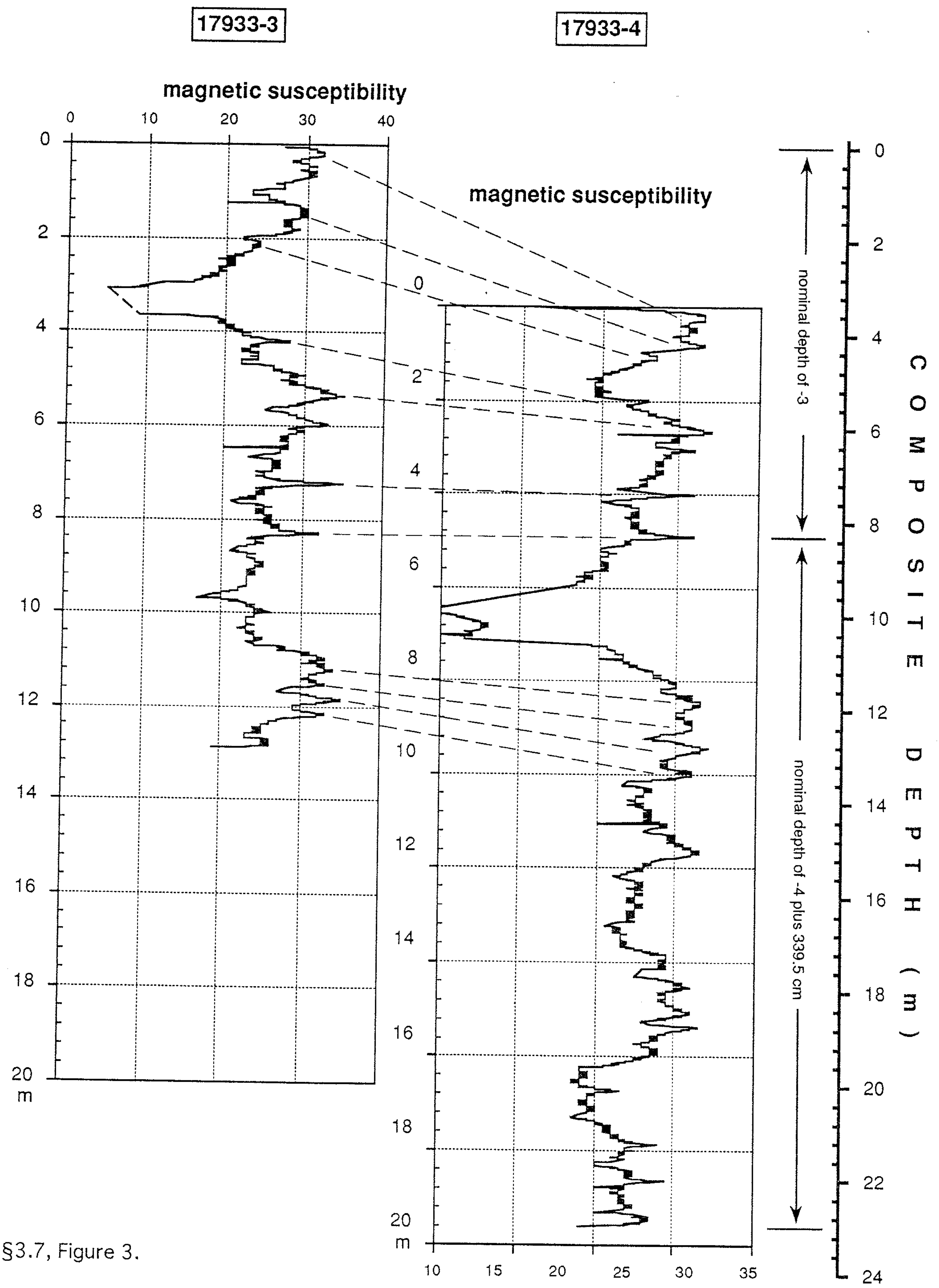

17933-3
17933-4
magnetic susceptibility
0
10
20
30
40
0
2
4
6
8
10
12
14
16
18
20
m
magnetic susceptibility
0
2
4
6
8
10
12
14
16
18
20
m
10
15
20
25
30
35
nominal depth of -3
nominal depth of -4 plus 339.5 cm
COMPOSITE DEPTH (m)
0
2
4
6
8
10
12
14
16
18
20
22
24

§3.7, Figure 3.

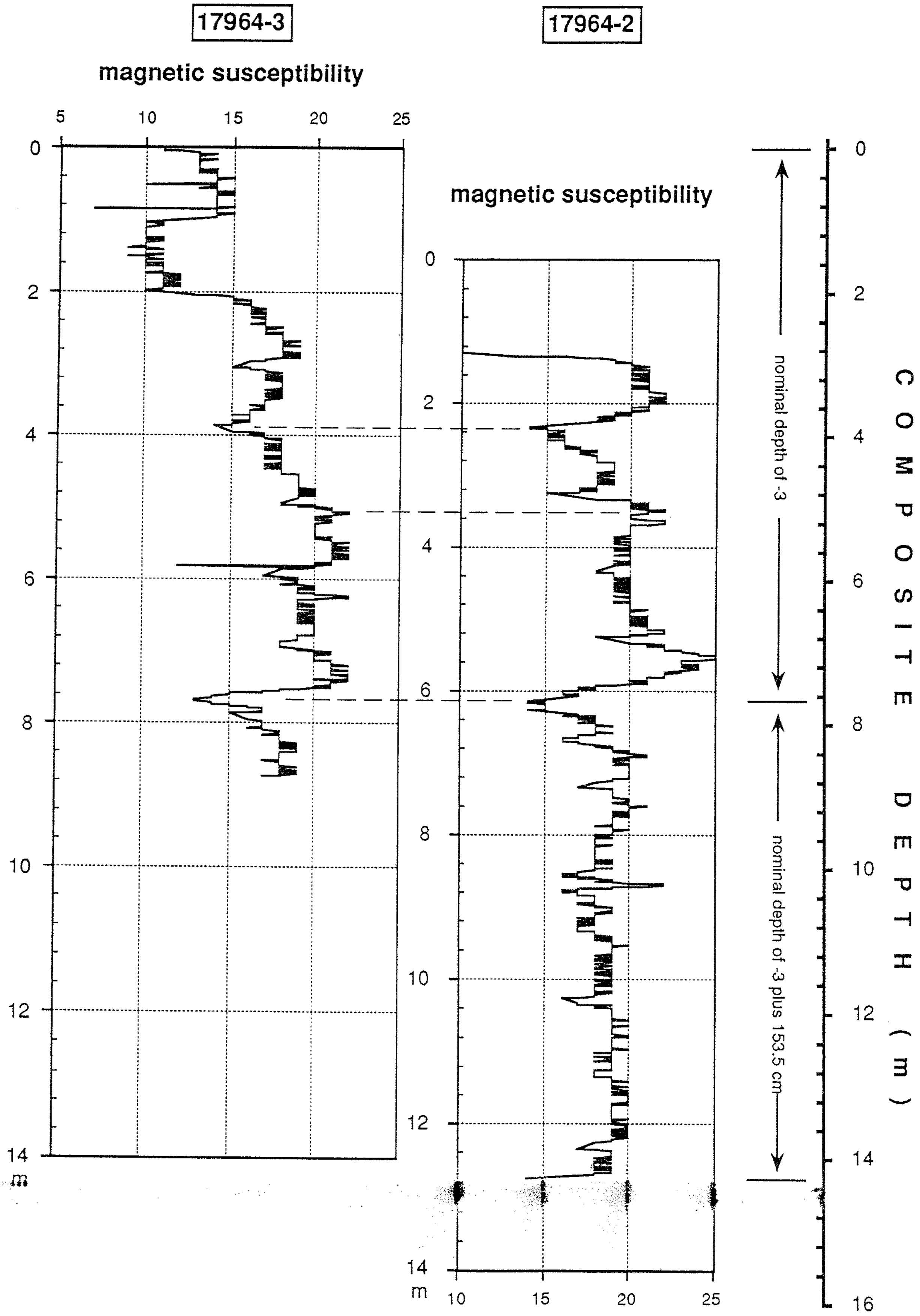
17964-3
magnetic susceptibility
5
10
15
20
25
0
2
4
6
8
10
12
14
m
17964-2
magnetic susceptibility
0
2
4
6
8
10
12
14
m
10
15
20
25
nominal depth of -3
nominal depth of -3 plus 153.5 cm
COMPOSITE DEPTH (m)
0
2
4
6
8
10
12
14
16

§3.7, Figure 7.